

**BONE MARROW-DERIVED CELLS CONTRIBUTE TO MULTILINEAGE
RECONSTITUTION AND BLASTEMA STAGE-SPECIFIC
UPREGULATION OF A TRANSIENT SCAFFOLD IN REGENERATING
MOUSE DIGIT TIPS**

AN ABSTRACT

SUBMITTED ON THE 15th DAY OF APRIL 2014

TO THE DEPARTMENT OF CELL AND MOLECULAR BIOLOGY

IN PARTIAL FULFILLMENT OF THE REQUIREMENTS

OF THE SCHOOL OF SCIENCE AND ENGINEERING

OF TULANE UNIVERSITY

FOR THE DEGREE

OF

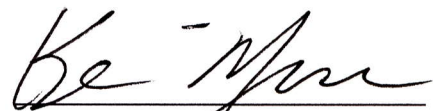
DOCTOR OF PHILOSOPHY

BY



Luis José Marrero

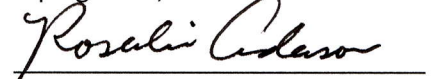
APPROVED:



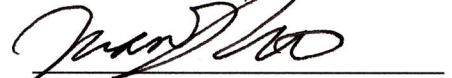
Ken Muneoka, Ph.D.
Director



Yiping Chen, Ph.D.



Rosalie Anderson, Ph.D.



Manjong Han, Ph.D.

ABSTRACT

In 2005, 1.6 million Americans lived with a debilitating amputation and this figure is predicted to double by 2050 (1). But the ability of a mammal to recapitulate a complex limb structure is not impossible. Evidence of children and mice re-growing digit tips following amputation midway through the terminal phalanx (P3) exists. The hallmark of this phenomenon is development of a blastema housing undifferentiated cells capable of being re-programmed to replicate the missing part. Our central goal is to understand specific components of this process for application into pro-scarring injuries.

The mouse digit anatomy is prominently outlined by microfilaments containing ER-TR7, and antigen derived from fibroblast reticular cells (FRCs) of the thymus shown to facilitate intercellular communication to promote lymphoid organogenesis. A unique blastema characteristic is the upregulation of an ER-TR7+ scaffold stemming from half of the blastema population which reverts to its pre-existing pattern after regenerate differentiation concludes. We measured a correlation between ER-TR7 and type III collagen (COL3) at the transcriptional and protein levels both *in vitro* during induction of ER-TR7 in primary P3 cells and throughout digit regeneration. Co-expression with COL3 sheds light on ER-TR7 identity and allows testing various approaches to manipulation of the scaffold through the better understood mechanism of COL3 regulation. Furthermore, we aimed at determining the origin of ER-TR7+ blastema FRCs.

Using bone marrow (BM) transplantation, we generated eGFP+ BM chimeras to study the fate of BM-derived cells (BMDCs) after amputation based on the hypothesis that in the regenerate, multipotent BMDCs contribute to various cellular phenotypes including FRCs. So we tested co-immunolocalization of eGFP with antigens particular to fibroblastic, hematopoietic, endothelial, osteoblastic, and mural cells. Many BMDCs homed to the injury throughout regeneration. But hematopoietic BMDCs were limited to inflammation whereas mesenchymal BMDCs expanded and were primed as ER-TR7+ FRCs in the P3 BM niche prior to homing to the blastema site, where they amounted to nearly 50% of cells. Moreover, BMDCs differentiated into endothelial, osteoblastic, and smooth muscle subpopulations and although diluted by pre-existing progenitors by the endpoint of regeneration, BMDCs persisted as part of various structures thus contributing to long-term function.

**BONE MARROW-DERIVED CELLS CONTRIBUTE TO MULTILINEAGE
RECONSTITUTION AND BLASTEMA STAGE-SPECIFIC
UPREGULATION OF A TRANSIENT SCAFFOLD IN REGENERATING
MOUSE DIGIT TIPS**

A DISSERTATION

SUBMITTED ON THE 15th DAY OF APRIL 2014

TO THE DEPARTMENT OF CELL AND MOLECULAR BIOLOGY

IN PARTIAL FULFILLMENT OF THE REQUIREMENTS

OF THE SCHOOL OF SCIENCE AND ENGINEERING

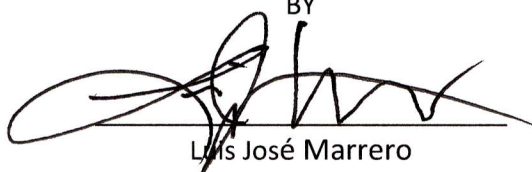
OF TULANE UNIVERSITY

FOR THE DEGREE

OF

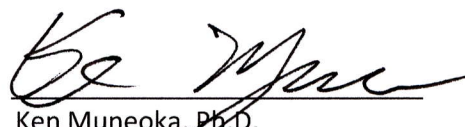
DOCTOR OF PHILOSOPHY

BY

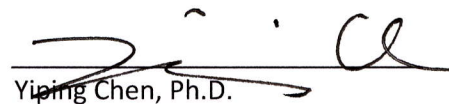


Luis José Marrero

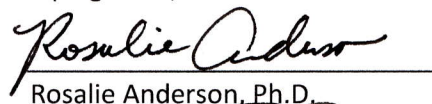
APPROVED:



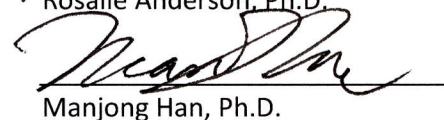
Ken Muneoka, Ph.D.
Director



Yiping Chen, Ph.D.



Rosalie Anderson, Ph.D.



Manjong Han, Ph.D.

© Copyright by Luis José Marrero, 2014
All Rights Reserved

DEDICATION

To my beloved wife, Marcy, and my beautiful children Kiki and Niño

ACKNOWLEDGEMENT

I would like to express my profound gratitude to Dr. Ken Muneoka for allowing me to conduct this research under his wing and presenting me with the opportunity to grow as a scientist and as a person. I would also like to thank my dissertation committee members, Drs. Yiping Chen, Rosalie Anderson, and Manjong Han for providing me with the guidance and support throughout my work and members of the Muneoka lab at Tulane and the labs of Drs. Ed Grabczyk and Yan Cui at LSU Health Sciences Center for their unconditional support and critical thinking. Finally, I would like to thank members of the Morphology and Imaging Core at LSU Health Sciences Center for their helpful input and technical assistance over all these years.



TABLE OF CONTENTS

ACKNOWLEDGEMENT.....	iii
TABLE OF CONTENTS	iv
LIST OF TABLES.....	vii
LIST OF FIGURES.....	viii
CHAPTER I: GENERAL INTRODUCTION AND SPECIFIC AIMS	1
1.1 MAMMALIAN REGENERATION AND DIGIT TIP AMPUTATION	1
1.2 THE WOUND HEALING CASCADE	4
1.3 FIBROBLASTS AND DERIVATIVES.....	8
1.4 COLLAGEN TYPES RELEVANT TO CUTANEOUS INJURIES.....	12
1.5 THE MICROFIBRILLAR ANTIGEN ER-TR7	16
1.6 BONE MARROW-DERIVED CONTRIBUTORS TO INJURY REPAIR.....	19
1.6 SUMMARY AND RATIONALE	24
1.7 SPECIFIC AIMS	27
CHAPTER II: <i>IN VIVO</i> EXPRESSION AND REGULATION OF A NOVEL EXTRACELLULAR MATRIX COMPONENT DURING REGENERATION OF AMPUTATED RODENT DIGITS	30
2.1 INTRODUCTION	30
2.2 MATERIALS AND METHODS	33

Mice and tissue harvest	33
Fluorescence immunohistochemistry on thin paraffin sections.....	33
Primary cell isolation and tissue culture	35
ER-TR7 induction.....	36
RNA extraction and Quantitative RT-PCR	36
Immunocytochemistry	37
Imaging.....	37
Statistical Analysis	38
2.3 RESULTS.....	38
ER-TR7 outlines tissue compartments of the neonatal and adult digit anlagen	38
ER-TR7 is dynamically regulated during digit tip regeneration.....	42
ER-TR7+ cells are growth responsive particularly around the blastema stage.....	47
ER-TR7 can be induced in fibroblast cell lines.....	53
ER-TR7 expression and regulation correlates with COL3+ reticular fibers <i>in vivo</i>	60
2.4 DISCUSSION.....	69
CHAPTER III: CONTRIBUTION OF BONE MARROW DERIVED CELLS TO THE ER-TR7+ REPAIR SCAFFOLD AND OTHER TISSUE LAYERS DURING REGENERATION	79
3.1 INTRODUCTION	79
3.2 MATERIALS AND METHODS	83
Mice and tissue harvest	83
Bone marrow transplants	83
Immunohistochemistry	84
Imaging and morphometry	86
Statistical analysis	86
3.3 RESULTS.....	86

The BM chimera model of digit amputation.....	86
BM-derived hematopoietic progenitor cells (HPCs) are mostly limited to inflammation	97
Differential survival of BMDCs in the regenerate	103
BMDCs differentiate into FRCs and participate in blastema scaffold engineering and long-term structural support of regenerated structures	109
BMDCs remodel bone and integrate into phalangeal membranes	115
BMDCs actively participate in transient blastema contraction and angiogenesis but are limited in permanent vascular layers.....	120
3.4 DISCUSSION.....	127
CHAPTER IV: DISSERTATION SUMMARY, CONCLUSIONS, AND FUTURE DIRECTIONS.....	142
4.1 SUMMARY	142
4.2 CONCLUSIONS.....	151
4.3 FUTURE DIRECTIONS	156
REFERENCES.....	163

LIST OF TABLES

Table 2.1: Selective factors modulated following ER-TR7 induction.	58
---	----

LIST OF FIGURES

Figure 2.1: ER-TR7 delineates tissue compartments of the digit anlagen and its cellular sources can be identified by high resolution confocal microscopy.	40
Figure 2.2: ER-TR7+ cells outline structures with diverse phenotypes, function, and differentiation markers.	42
Figure 2.3: ER-TR7 is discreetly expressed in unamputated neonatal and adult digits but overexpressed in the mature blastema of regenerates.	44
Figure 2.4: ER-TR7 labels an organized network of reticular fibers in the blastema.	46
Figure 2.5: The neonatal stages of digit tip regeneration can be defined by upregulation of proliferation around the blastema stage and decreasing apoptosis after the resolution of inflammation.	49
Figure 2.6: Quantitative analysis of Ki67+ and ER-TR7+/- coexpression in regenerating digit tips with post-natal (PN) day-matched unamputated controls at selected days post amputation (DPA) provides evidence that ER-TR7+ FRCs are growth responsive.	52
Figure 2.7: NIH-3T3 cells can be manipulated to synthesize and secrete ER-TR7+ microfilaments.	54
Figure 2.8: Similar to freshly plated blastema cells, primary fibroblastic cells isolated from the P3 phalanx synthesize the ER-TR7 framework in a pattern that resembles the blastema <i>in vivo</i>	56
Figure 2.9: ER-TR7 staining correlates with COL3 expression following induction of 3T3 and P3 primary cell lines.	59
Figure 2.10: ER-TR7 and COL3 signals in control and regenerating digits yield strong correlation measurements in agreement with <i>in vitro</i> experiments.	61

Figure 2.11: ER-TR7 is co-regulated with COL3 and FN1 in control and regenerating digits but only COL3 mimics its expression pattern.....	68
Figure 3.1: Quantitative and cytological analysis of BMDCs in control digits and regenerates harvested from eGFP BM chimeras yields progressive cellular contribution peaking at the blastema timepoint with regression after differentiation but endpoint counts significantly higher than baseline.....	90
Figure 3.2: BMDCs contribute and localize to diverse tissue layers in regenerating digits.	95
Figure 3.3: Quantitation and localization data of the CD45+ HPC subset of BMDCs following amputation demonstrate it is restricted to the inflammatory phase.	99
Figure 3.4: The co-expression of CD45 with eGFP+ BMDCs was dynamically and differentially regulated between digit BM and CT compartments and throughout regeneration timepoints.	101
Figure 3.5: Sections of control and amputated digits at defined timepoints were stained for Ki67 and cleaved-Caspase-3 (C3) to show that apoptosis is restricted to the early stages of repair, proliferation of eGFP+ cells in the BM precedes blastema formation, and BMDCs in the blastema are progressively diluted by proliferating local cells.	108
Figure 3.6: Immunohistochemical co-expression and quantitation of eGFP with ER-TR7 indicate that BMDCs differentiate into FRCs in the BM and these FRCs and expression are propagated to the wound site to initiate blastema growth and scaffolding.....	112
Figure 3.7: A major source of blastema cells is the P3 BM and these occupy the blastema site along the proximodistal axis towards the wound epithelium as FRCs.	114
Figure 3.8: A fraction of BMDCs in the blastema actively participate in bone remodeling as osteoblasts.....	119
Figure 3.9: Detection and quantitation of total and eGFP+ subpopulation of FVIII+ and SMA+ cells in representative unamputated control, DPA14, DPA21, and DPA35 regenerating digit tips show reasonable contribution of these cells during the blastema and early regenerate differentiation stages but limited persistence by the endpoint of regeneration.....	123

LIST OF ABBREVIATIONS

3T3	3-Day Transfer, Inoculum 3×10^5 Cells
ACTA2	Actin, Alpha 2, Smooth Muscle
BM	Bone Marrow
BMDC	Bone Marrow Derived Cell
BMT	Bone Marrow Transplantation
CB	Cortical Bone
CCD	Cooled-Coupled Device
CMV	Cytomegalovirus
COL1	Collagen Type I
COL3	Collagen Type Iii
CT	Connective Tissue
CTRL	Control
CXCR4	Chemokine (C-X-C Motif) Receptor 4
DAPI	4',6-Diamidino-2-Phenylindole
DBM	Dorsal Blastema Mesenchyme
DBM	Distal Blastema Mesenchyme
DDBL	Dorsodistal Blastema
DDCT	Dorsodistal Connective Tissue
DM	Dorsal Mesenchyme

DMSO	Dimethyl Sulfoxide
DNA	Deoxyribonucleic Acid
DPA	Day Post Amputation
ECM	Extracellular Matrix
EDS	Ehler-Danlos Syndrome
EGF	Epidermal Growth Factor
eGFP	Enhanced Green Fluorescent Protein
EMT	Epithelial Mesenchymal Transition
ER-TR7	Erasmus Of Rotterdam Thymic Reticulum 7
FGF-2	Fibroblast Growth Factor 2
FN-1	Fibronectin
FRC	Fibroblast Reticular Cell
FSP-1	Fibroblast Specific Protein 1
FVIII	Factor 8
GFAP	Glial Fibrillary Acidic Protein
GM-CSF	Granulocyte Macrophage Colony Stimulating Factor
GP36	Glycoprotein 36
GP38	Glycoprotein 38
HB	Heparin Binding
HE	Hematoxylin & Eosin
HGF	Hepatocyte Growth Factor
HIV	Human Immunodeficiency Virus
HPC	Hematopoietic Progenitor Cell

IFN- γ	Interferon-Gamma
IGF	Insulin-Like Growth Factor
IHC	Immunohistochemistry
IL-6	Interleukin 6
IL-8	Interleukin 8
IVC	Inferior Vena Cava
JT	Joint
KGF	Keratinocyte Growth Factor
LT	Lymphotoxin
LTR	Lymphotoxin Receptor
LT β R	Lymphotoxin T-Beta Receptor
MAP2	Microtubule Associated Protein 2
MCP-1	Macrophage Chemotactic Protein-1
MPC	Mesenchymal Progenitor Cell
MSC	Mesenchymal Stem Cell
NB	Nail Bed
NCAM	Neuronal Cell Adhesion Molecule
NEUN	Neuronal Nuclei
NG2	Neuron-Glial Antigen 2
NF κ B	Nuclear Factor-Kappa-Light-Chain-Enhancer Of Activated B Cells
OC	Osteocalcin
OCT	Optimal Cutting Temperature
P2	Second Phalanx

P3	Terminal Phalanx
PBS	Phosphate-Buffered Saline
PCC	Pearson's Correlation Coefficient
PDGF	Platelet Derived Growth Factor
PN	Postnatal
RBC	Red Blood Cell
RNA	Ribonucleic Acid
RT-PCR	Reverse Transcription Polymerase Chain Reaction
SDF-1	Stromal Derived Factor 1
SE	Standard Error
SMA	Smooth Muscle Actin
TB	Trabecular Bone
TBST	Tris-Buffered Saline
TGF	Transforming Growth Factor
TGF β -1	Transforming Growth Factor-Beta 1
THBS1	Thrombospondin 1
TNFR1	Tumor Necrosis Factor Receptor 1
TNFR2	Tumor Necrosis Factor Receptor 2
TNF- α	Tumor Necrosis Factor-Alpha
VE	Ventral Epithelium
VEGF	Vascular Endothelial Growth Factor
VIM	Vimentin
VM	Ventral Mesenchyme

VSMC	Vascular Smooth Muscle Cell
VWF	Von Willebrand Factor
WE	Wound Epithelium

CHAPTER I: GENERAL INTRODUCTION AND SPECIFIC AIMS

1.1 MAMMALIAN REGENERATION AND DIGIT TIP AMPUTATION

There is substantial evidence that not only invertebrates, but both lower and higher vertebrates are able to restore shape, pattern, and function to lost body parts. We have been aware for quite some time that many organisms, including some described in Greek mythology, have the potential to regenerate. Thanks to pioneers in the fields of entomology, zoology, and reproductive biology dating back to the early to mid-eighteenth century such as René-Antoine Ferchault de Réaumur (crayfish limb regeneration), Abraham Trembley (hydra regeneration from its polyps), and Lazzaro Spallanzani (first vertebrate studies) is that regenerative medicine has captured the interest of many and advanced to the level of understanding that we have about it today. Modern science has adopted many model organisms which undergo regeneration to some extent such as hydra, planarians, annelids, frogs, and urodeles (e.g. axolotl, newt) to understand this biological process.

More recently, attention has been focused on studying regenerative potential at various levels of the adult urodele limb (2, 3), embryonic avian limb bud (4), and neonatal mammalian digit tip (5-7) model systems. Studies involving these models agree on three fundamental milestones that must be met to deviate from conventional wound healing and acquire regeneration status. The first one involves wound closure through formation of an epithelial cap over the underlying inflammatory and connective tissue milieu. The second is the controlled migration of a mesenchymal cell population that aggregates into an undifferentiated cell mass,

otherwise known as the blastema, which is rich in positional information at the anatomical level and interacts with adjacent tissue layers through time and concentration-dependent cross-talk between numerous growth factors, chemokines, cytokines and their receptors. Finally, maturation and patterning of this blastema lead to a functional equivalent of the pre-existing appendage (8, 9). However, in the urodele model, this post-amputation phenomenon yields a complete recapitulation of limb architecture and function to include proper skeletal segmentation and elongation along with restoration of attached vasculature, nerve, connective tissue, muscle, and skin. It is still unclear whether the mammalian model of regeneration makes an attempt to mimic events and production of factors that lead to re-development of a missing appendage in some lower vertebrates like the urodele.

Although regeneration competency in a mammal may be restricted to the level of the digit tip, this model is of great importance due to its relevance in the treatment of human injury. Numerous cases of regenerating fingertip injuries in children have been reported in the clinical literature (10, 11). In most cases, the regenerating tip involves regrowth of the skin over the cut surface, its underlying connective tissue and vasculature, and nail. Just a fraction of those injuries have involved disruption and severing of part of the terminal phalanx, which eventually also takes part in the growth and differentiation mechanics of a regeneration event. Regeneration of this bone rudiment occurs through the process of direct ossification (12, 13). For the most part skeletal development occurs through endochondral ossification, the process by which a cartilage template with a bone collar precedes mature and mineralized bone segments. It is thus possible that the regeneration of a missing part in higher vertebrates such as mice and humans skews from the developmental program through a secondary mechanism that attempts to replicate development using an alternate subset of genes that compensate for the ones that have been rendered inactive after birth.

This study will focus on the events and key molecules that attempt to mimic the regulators of limb growth and development and lead to restoration of the amputated mouse digit tip with focus on the extracellular matrix and cell population dynamics. Both the adult and neonatal mouse digit tip is composed of diverse cell populations organized into compartments of bone (terminal phalanx), cartilage, marrow, skin, and tendon integrated within bundles of vasculature, nerves, and connective tissue. The latter is rich in immune cells and fibroblasts, which organize and produce the extracellular matrix that provides structural integrity to the organ. When the digit tip is amputated midpoint through its phalanx, the system undergoes an inflammatory response, wound re-epithelialization, and growth of a blastema. Events and cues within this blastema lead to migration, proliferation, and differentiation of precursor cells within specialized compartments leading to development and recapitulation of the missing part.

It has been extensively documented in the urodele limb regeneration literature that fibroblasts migrate towards an injury site, lose any specialized phenotype through de-differentiation, and expand as stem cell-like units to form the blastema. To that effect, it is possible that fibroblasts may be the precursor cells that lead to blastema formation in the mouse digit tip following amputation. However, the urodele limb regeneration potential is mainly characterized by the re-programming of differentiated cells into embryonic-like progenitor cells that eventually contribute, not only to specialized mesenchyme, but also ectodermal components (8). Whether the mammalian digit tip regeneration mechanism parallels the events leading to urodele blastema formation, progress, and differentiation is currently under investigation.

1.2 THE WOUND HEALING CASCADE

Wound healing mechanisms are often referenced to with regards to tissue restoration following a cutaneous injury. Although many of the processes involved in this complex and dynamic cascade have been examined at the level of the skin, its key factors, cellular regulators, and sequence of events also apply following injury to other organs. Even though many of steps which define wound healing also take place throughout regeneration, the key distinction between both responses is that wound healing closes, protects, and often restores damaged tissue layers but at the end, it may not necessarily reestablish function. There is much parallelism on how wound healing and regeneration manipulate the wound microenvironment. Hence it is important to understand the sequence of events and factors involved in wound healing in order to dissect any subtle variations which make regeneration such a special phenomenon.

The wound healing process requires the coordinated effort of various cell populations to release factors during specific times and at precise concentrations to initiate activation, proliferation, migration, and differentiation of other cell types. The local release of growth factors, cytokines, and chemokines may proceed in an autocrine or paracrine fashion. But all phases of wound healing are in some way controlled by the cytokines. It is the balance, and not the mere presence or abrogation of these small immunomodulators, which decides the behavior of the wound microenvironment and the final outcome of the site (14). In addition, other dynamics such as the intercommunication between cells and the extracellular matrix through various cell surface adhesion molecules are also critical for a successful repair. The conventional sequence of wound healing involves a conserved series of events which overlap in time. These

include clot formation; inflammation; epithelialization; neovascularization; granulation tissue formation; and matrix remodeling.

Immediately after injury, hemostasis occurs by means of a clot that aids in minimizing blood loss due to vascular disruption. This blood clot is composed of platelets dispersed within a provisional network of cross-linked fibrin strands derived from thrombin-mediated cleavage of fibrinogen, fibronectin, vitronectin, and thrombospondin (15). In addition to plugging the wound, the clot functions as a medium for cell migration and as a reservoir of growth factors and cytokines released by degranulating platelets. Examples of these factors include TGF (transforming growth factor) α and β , EGF (epidermal growth factor), PDGF (platelet derived growth factor), and IGF (insulin-like growth factor) -1. These promote initial chemotaxis and proliferation of inflammatory and connective tissue cells (15).

Chemotactic cues such as TGF β -1 cause circulating neutrophils and monocytes to extravasate and home to the wound site (16). Additional chemoattractants include peptides cleaved from bacterial proteins and the by-products of matrix proteolysis. The initial role of neutrophils, which arrive to the wound immediately, is to clear contaminating pathogens and release the first surge of pro-inflammatory cytokines which may serve as the earliest activators of local fibroblasts and keratinocytes (17). After a few days, the short-lived neutrophils cease to infiltrate and are phagocytized by activated macrophages. Macrophages accumulate at the wound site to resume phagocytosis and coordinate the progression of repair by secreting a battery of cytokines and growth factors which amplify the initial response from neutrophils and activated platelets (18).

Initiation of wound re-epithelialization occurs shortly after injury and is marked by alteration of the epithelial cells (keratinocytes) and their underlying basal lamina. Progression of

this step requires the binding of keratinocytes to laminin in the connective tissue basal lamina by means of integrins. Integrins are transmembrane heterodimers of α and β subunits that become tethered to the extracellular matrix through a large extracellular domain. The integrins establish intercellular links with the keratin cytoskeleton of the epithelium. The keratinocytes at the edge of the wound dissolve this attachment using collagenases and trigger expression of other integrin types that are more adaptable to the changing wound microenvironment and allow easier motility of the epithelium onto the healing wound. Migration of then epithelial cells is driven by chemotactic factors and contact guidance. Once the epithelial cells cover the wound, the components of the basal lamina are deposited underneath. The main factors which stimulate keratinocyte growth are EGF, heparin-binding (HB) EGF, hepatocyte growth factor (HGF) and keratinocyte growth factor (KGF) (15, 18). TGF- β on the other hand, has been known to suppress this growth (19).

Concurrent with the inflammatory phase, around four days after injury, the connective tissue in the wound appears red and granular with invading capillaries (20). Therefore, this area is referred to as granulation tissue. These capillaries are critical for the metabolic balance and growth of this unpatterned connective tissue layer. Initiation of angiogenesis at the wound site is triggered by the release of basic fibroblast growth factor (FGF-2) and vascular endothelial growth factor (VEGF). VEGF is induced by epithelial cells at the edge of the wound and activated macrophages (15). Macrophages also stimulate the microenvironment by releasing FGF-2. Other non-angiogenic factors such as integrins and fibronectin receptor must be upregulated to permit endothelial response to the vascular growth factors and allow the movement of endothelial precursors through the tissue via extracellular fibronectin (21, 22). Following exposure to FGF-2 and TGF β -1, fibroblastic cells fabricate rods with a lumen which aid in migration of endothelial precursors along the interior of the tubes and pericytes along the

outside of the endothelial layer (23, 24). Secretion and activation of proteases such as collagenase by plasminogen activator also aids in neovascularization by degrading extracellular matrix and thus releasing its peptide byproducts which induce recruitment and activation of macrophages and fibroblasts (25). Disruption of basement membranes and fibers by these enzymes also facilitate migration of various cell types (20).

Once the wound granulation compartment fills with fibroblasts supported by capillaries, angiogenesis halts and cells which formed the new vessels undergo apoptosis upon upregulation of anti-angiogenic factors (e.g. endostatin, angiostatin) and matrix molecules such as the thrombospondins (26). The fibroblasts in this newly formed granulation stroma synthesize the extracellular matrix necessary to support numerous types of invading cell precursors and acts as a conduit for cell migration. Aside from matrix components such as fibronectin and hyaluronic acid, many secreted cytokines and growth factors remain tethered to this provisional matrix to induce chemotaxis, proliferation, and other modulatory functions (18). Some of the key growth factors upregulated in this stroma include PDGF and TGF β -1, both of which stimulate fibroblasts to proliferate and express integrin receptors to migrate (27, 28). Since fibroblasts typically reside in collagen-rich matrices, their integrin receptors must be differentially expressed prior to collagen synthesis to favor adhesion to the macromolecules available at the time within the non-collagenous matrix (28). Type III collagen synthesis is initiated shortly after the first wave of fibroblast migration and adhesion, at which time the microenvironment becomes interconnected with a mixture of non-collagenous macromolecules and a type III collagen-based “provisional matrix” (29). Although fibroblasts are responsible for matrix deposition, factors which bind to the matrix itself can have a positive or negative effect on their ability to fabricate, remodel, and interact with it (30). The movement of fibroblasts within a tightly woven extracellular matrix is also achieved by the upregulation of enzymes derived from fibroblasts

such as collagenases and matrix metalloproteases (MMPs). The type of enzyme produced at any given point can act as a determining factor in whether the wound heals properly or becomes ulcerated (31). Following activation of pro-collagen genes, in part triggered by the variable synthesis of different TGF β 's, the provisional matrix is replaced by collagen fibers (18, 30, 32, 33). Once the matrix becomes collagen-rich, specifically with type I collagen, many of the fibroblasts undergo apoptosis through a signaling mechanism that remains unclear and the site becomes a relatively acellular scar (34).

Overlapping with the process of granulation tissue formation is the remodeling of the extracellular matrix. The fibroblasts in the granulation tissue layer undergo terminal differentiation into myofibroblasts, a process which is well known to be modulated by TGF β -1 (35) and PDGF(28), to initiate contraction of the wound (36). Contraction also occurs by attachment of fibroblasts to the collagen matrix through collagen-specific integrin receptors with associated cross-links (36). During the granulation stage of wound repair, fibrillar collagen accumulates quite rapidly in the form of type III collagen at which point the wound achieves 20 percent of its ultimate strength (29, 37). It is the degradation, synthesis, deposition, and cross-linking cycle of collagen by fibroblasts and a milieu of growth factors and enzymes that is responsible for the ultimate tensile strength of the wound. Along with collagen-stimulating factors such as the TGF β 's, there is also an assortment of MMPs and tissue inhibitors of metalloproteases (TIMPs) which contribute to this dynamic cycle (38).

1.3 FIBROBLASTS AND DERIVATIVES

Fibroblasts are conventionally defined as specialized mesenchymal cells involved in the synthesis of extracellular macromolecules, thus providing stromal integrity, basement membrane support, and compartmental definition to all organs. They are also responsible for

secreting a series of proteases and growth factors that aid in definition of the extracellular matrix and affect the dynamics of other cells in their surroundings (39). They are derived from the primitive mesenchyme, thus expressing Vimentin (40), and evidence suggests that there is phenotypic heterogeneity once they mature, even within the same organ and injury state (41-43). There is also evidence that fibroblast subtypes are unique to their host tissue by activating gene subsets specific to that region (41).

These connective tissue cells are highly motile due to enhanced filopodial activity and are typically spindle-shaped with speckled nuclei containing one or two nucleoli. The fibroblast has been proven critical from embryonic development to adult wound repair in providing various amounts and types of ground substance and fibers to layout specific structural frameworks in all organs depending on microenvironmental conditions and function of the site. These extracellular matrix (ECM) components conventionally include collagens, glycosaminoglycans, reticular and elastic fibers, and glycoproteins. However, the existence of additional fibroblast-specific ECM components cannot be ruled out. Even though synthesis of these molecules is one of their primary functions, fibroblastic populations cannot specifically be characterized on this attribute alone.

Fibroblasts can also be defined morphologically by the physical appearance of their organelles. For example, an activated fibroblast exhibits an extensive rough endoplasmic reticulum. Otherwise, it resides as an inactive fibrocyte. Fibroblasts can also be subdivided by their cellular phenotype in conjunction with any specific ground substances being synthesized at a particular time and its physical relation to other cell populations and tissue compartments. It is also possible to further define fibroblasts by their state of proliferation during normal conditions and disease state. Finally, even though fibroblast phenotyping has been widely

studied in the literature, there is no reliable specific marker that generally defines them. So far, markers such as the calcium-binding protein S100A4 (also known as fibroblast-specific protein 1 (FSP-1)), found mostly in cutaneous and cardiac fibroblasts (44, 45), have been used in conjunction with markers of the various collagens and associated molecules such as prolyl-4-hydroxylase (46) to phenotype them. Taken together, all these characteristics can segregate fibroblasts from other cell populations but may not fully set apart, for example, blastema fibroblasts from pro-scarring myofibroblasts. Since myofibroblasts are largely found during the granulation and endpoint stages of conventional wound healing, it is of importance to differentiate regeneration competent blastema fibroblasts from this subpopulation.

Myofibroblasts are large contractile cells with a well-defined cytoskeleton expressing high levels of smooth muscle actin (SMA). The content of actin and myosins in this population is largely different from that of typical fibroblasts (47). They are characterized by large bundles of actin microfilaments arranged in a linear fashion along the cytoplasm and membrane and between cell-matrix and intercellular links. Myofibroblasts expand in wounded areas undergoing fibrosis where they produce large amounts of type I collagen (COL1), which along with increased formation of the actin-myosin complex also defines them as the fibroblast subtype of pro-scarring microenvironments. Eventually these cells will trigger apoptosis and get resorbed in the wound. But in all cases in which the outcome of healing is scar, such as in chronic liver injury and fibrosis, they fail to follow this path and persist (48). The survival of these cells at this point depends on the amount and influence of transforming growth factor (TGF- β), which is very high in fibrotic lesions. Evidence suggests that the consequence of stimulation with TGF- β not only leads the fibroblast to become a myofibroblast, but also allows for an increase in COL1 production (35). Conversely, if SMA expression is suppressed, COL1 expression becomes reduced (49). The same principle applies to fibrosis of the lung (50) and

scarring cutaneous wounds (15, 18). Similar to the way the conventional fibroblast can be manipulated and driven into an even more specialized phenotype such as that of the myofibroblast, it can also be stimulated to a phenotype known to contribute to a bone regeneration process.

Osteoblasts are bone-forming cells of mesenchymal origin which are almost indistinguishable from fibroblasts. These cells play a critical role in bone remodeling and participate in a tight control of this process with osteoclasts, which resorb the bone matrix. Most genes expressed in fibroblasts are also expressed by osteoblast with the exception of the transcription factor Cbfa1 (51) and Osteocalcin (OC), a secreted factor that regulates the function of the osteoblast by inhibiting bone formation demonstrated by an increase in the rate of bone growth in OC gene-deficient mice (52). Cbfa1 acts as the activator of osteoblast-specific genes in both fibroblasts and myoblasts. Mice deficient in Cbfa1 lack osteoblasts and albeit developing normal skeletons, show a delay and lack of ossification (53, 54).

As a final note, just like fibroblast derivatives such as the myofibroblast and osteoblast that are morphologically similar to the fibroblast can be found in the blastema, there are also structures populated by fibroblasts that can resemble the blastema. During wound healing, all injuries, regardless of anatomical site, undergo an event concurrent with inflammation termed the granulation stage. During this stage, new stroma composed of macrophages, transient blood vessels, and fibroblasts migrate into the wound space. Platelet-derived growth factor (PDGF) and TGF- β 1 are produced by both activated macrophages and early fibroblasts. These growth factors, along with their regulation at the extracellular matrix level, are the main stimuli for the fibroblast population to proliferate and mobilize into the injury (14, 28). In turn, fibroblasts that aggregate in this area are induced to secrete a provisional or transient matrix

that can serve as a conduit for further cell migration and either a promoter or repressor of differentiation depending on its mechanical properties and the factors that tether to it (28, 30). This matrix is composed of fibronectin, hyaluronic acid, fibrin, laminin, and collagen and can be altered by collagenases, gelatinases, and matrix metalloproteases also produced by fibroblasts (18, 30, 55). As the wound matures it becomes acellular and fibrous. The matrix is eventually replaced by COL1 and the cells responsible for its deposition, myofibroblasts, undergo apoptosis (34).

The events leading to granulation of the injury which leads to scar formation during wound healing resemble the steps that give rise to initiation and growth of the blastema. Even though the fibroblast subpopulations found during both stages may have some of the same phenotypic characteristics, the outcomes are clearly different. It is possible that the regulation and timing of microenvironmental cues at the extracellular level guide the fibroblastic components to regeneration competency.

1.4 COLLAGEN TYPES RELEVANT TO CUTANEOUS INJURIES

Collagens are extracellular matrix macromolecules found in connective tissue and bone. They are the most abundant proteins in the body. Their main role is to preserve structural integrity and tensile strength in most tissue compartments. Their functionality is based on the precise formation and organization of a meshwork. Such network of fibers is often organized to permit tissue flexibility but also to limit the movement of other tissue components. Collagens also have many other biological functions such as providing cell attachment; facilitating chemotaxis; and differentially aggregating agonists and repressors secreted by cells into the extracellular space (56). They are subdivided as fibril and non-fibril forming. Some of the collagens relevant to cutaneous wound repair are part of the fibrillar category which is

composed of type I, II, III, V, and XI collagens. These are translated as individual precursor α -chains composed of a globular N-terminus with a short triple helical sequence, an uninterrupted triple helical domain of 1000 amino acids, and a globular C-terminal domain. After final assembly and enzymatic cleavage of the propeptides at both termini, these collagens assemble as homotrimers with three equivalent α -chains or heterotrimers made of two or three different α -chains. Each α -chain molecule has an uninterrupted triple helix about 300 nm long and 1.5 nm in diameter flanked by short extra-helical telopeptides or cross-linking sites (57). The lateral interaction of the homologous regions within the triple helical domains initiates fibrillogenesis. Of great importance is the removal of the N- and C-terminus propeptides from the precursor molecules by peptidases prior to fibril formation. It has been suggested that these free propeptides aid in regulation of collagen biosynthesis in fibroblasts by interfering with its post-transcriptional machinery and/or fibril assembly (58).

The biosynthesis of collagens involves a great number of post-translational modifications. These modifications occur at the intracellular level along with synthesis of the α -chains, to form the triple-helical pro-collagen molecules, and outside the cell to incorporate these chains into stable fibrils (59). There are several enzymes which aid in this process such as prolyl 4-hydroxylase and lysyl hydroxylase in hydroxylation of residues; transferases for glycosylation; N- and C-terminal peptidases to remove the propeptides at the extracellular level; and lysyl oxidase for cross-linking (56).

Several cytokines and growth factors can promote or inhibit the synthesis of the fibrillar collagens. The main inducer is Transforming Growth Factor β (TGF- β), which has been shown to trigger transcription of various ECM macromolecules in fibroblasts and also disrupt the activity of matrix-degradation enzymes by allowing for the production of Tissue Inhibitors of

Metalloproteinases (TIMPs) (60). Tumor Necrosis Factor α (TNF- α) on the other hand, inhibits COL1 production *in vivo* and *in vitro* (61-63). Interferon γ (IFN- γ) also inhibits collagen gene transcription by interfering with TGF- β stimulation (64). Even though the major fibrillar collagens share structural similarities and regulatory dynamics, the main ones being actively remodeled at the site of a cutaneous injury and that have a significant impact on the endpoint phenotype are COL1 and COL3. These particular collagens have been widely studied in the context of wound healing and fracture repair and how their deposition and persistence help define the extent of fibrosis and scar. Myofibroblasts that accumulate in the wound as early as the granulation stage of wound healing are responsible for the contraction of the site to facilitate closure and also manipulate the behavior of other cells through both direct contact and the extracellular deposition of these macromolecules.

COL1 is a heterotrimeric fibrillar protein and the most abundant collagen in all mature tissues. It is mostly found in bone and tendon but also in large quantities around blood vessels, the dermal layer of the skin, and lung (65). COL1 can facilitate the adhesion and migration of hepatocytes, keratinocytes, and fibroblasts (66). COL1 gene expression can be found throughout most wound healing stages but its synthesis is most prominent as the wound matures, where it replaces other collagen types and forms an acellular fibrous scar (67).

Normally, COL3, a homotrimeric collagen, is more sparsely distributed COL1 throughout soft connective tissues. It typically coexists within the same regions where COL1 is expressed except for bone matrix, in which it is expressed at an almost negligible rate (68). However, higher concentrations of COL3 are found in distensible connective tissue elements such as blood vessels (69). It is also found in abundance in fetal tissue when compared to adult organisms, hence it is also called embryonic collagen (70, 71). In fact, it has been reported that the total

quantity of COL3 decreases as tissues age (72). The disparity of the ratio of COL1 to COL3 in fetal versus adult tissues has led to the belief that the increased availability of COL3 can be attributed to the scarless phenotype that results in fetal cutaneous wounds (71, 73-76). The expression of COL3 is also increased at the early stages of wound healing, where it fabricates the provisional matrix or scaffold during the stage of granulation tissue formation (65, 71). Eventually this matrix is proteolytically degraded and replaced by COL1 as part of the dynamic extracellular matrix remodeling that occurs throughout wound healing.

Evidence regarding the overexpression of COL3 in fetal tissue that heals without scar and the lower ratio of COL3 to COL1 in aging subjects which are more prone to scarring sheds new light into the potential role of COL3 in promoting a regeneration competent environment and modulating factors in the repair cascade. The impact of COL3 overexpression and persistence is currently under study using *in vitro* and *in vivo* models of cutaneous injury. Research on COL1 and COL3 patterns in wound repair suggest that the organization and diameter of their fibrils can affect cellular migration, proliferation, and signaling. But newer evidence suggests that collagen type-specific domains exist that can modulate tethering of factors to the ECM and thus manipulating their ability to induce or repress various signaling cascades (77). Firstly, it has been found that one of the main roles of COL3 is to regulate the diameter of collagen fibrils, including those of COL1, which in turn affects the arrangement of tissue layers and compartments (78, 79) and thus having an effect on scar appearance. There is also some evidence suggesting that COL3 modulates integrin expression thus affecting myofibroblast differentiation. COL3 $-/-$ mice serve as a model of vascular Ehler-Danlos Syndrome (EDS, type IV); a disease characterized by impaired synthesis of COL3, which results in fragile vascular walls and impaired wound healing. Fibroblasts isolated from COL3 deficient mice have been reported to have lower $\alpha 5\beta 1$ (fibronectin receptor) and $\alpha 2\beta 1$ integrin

expression, the former of which is critical for inducing a myofibroblast phenotype along with $\alpha v \beta 3$ (vitronectin receptor) (80).

1.5 THE MICROFIBRILLAR ANTIGEN ER-TR7

In 1984, Els Van Vliet and colleagues at the Erasmus University of Rotterdam successfully isolated seven hybridoma cell lines that produced a panel of monoclonal antibodies with selective immunoreactivity against targets in both lymphoid and non-lymphoid cells of the mouse thymus (81). These were synthesized with the intention of identifying the heterogeneity and complexity of the thymic stroma and its interaction with lymphoid progenitors to promote maturation and differentiation of T-cells. The antibodies were denominated ER-TR (Erasmus of Rotterdam Thymic Reticulum) 1 through 7. Following immunohistological staining of mouse thymus sections with all antibodies, the bulk of the expression was represented as fine reticular patterns in different regions of the tissue depending on the clone number. The first group of clones, ER-TR1 through 3, bound to thymic cortex, medulla, and B-cells. A positive co-localization pattern was measured when co-labeling of these clones was performed with an antibody against the major histocompatibility complex I (H2) in thymus sections. ER-TR4, 5, and 6 respectively were shown to target cortical epithelia, medullary epithelia, and medullary interdigitating (dendritic) cells of the thymus. The last antibody, ER-TR7, specifically detected reticular fibroblasts of the thymus and the support wall of blood vessels (81). Over the years, ER-TR7 has become a very useful marker of the complex network of fibrous extracellular meshwork and as an identification tool of reticular stromal cells or fibroblasts not only in the thymus, but also the spleen and lymph nodes.

Even though the full purpose for the synthesis of the ER-TR7 meshwork by reticular fibroblasts is unknown, let alone its origin and induction mechanism *in vivo*, some studies have

suggested that its function in lymphogenesis is to provide a paracortical chord or conduit for cell-cell interactions (82, 83). This conduit acts as a “road system” for T-cells, for example, to adhere and move depending on factors such as chemokines tethered to it such as CCL19 and CCL21. These ligands are produced by fibroblast reticular cells and interact with the CCR7 receptor in naïve T-cells and activated dendritic cells to influence cell motility (84). The physical mechanism of these interactions has been observed by multiphoton microscopy *in vivo* and *in vitro* (85-87), by which the network allows enough space for microchannels to form through which T-cells can migrate.

No reports exist of *in vivo* manipulation of the ER-TR7 antigen and hence the network it labels. This is mainly due to the fact that to this day its genetic origin remains unknown. However, a potential mechanism of induction has been proposed *in vitro* on reticular fibroblasts isolated from murine lymph nodes (88). By themselves, these cell lines do not secrete the ER-TR7+ meshwork when unstimulated under normal culture conditions. Once they are co-cultured with activated helper T-cells (CD4+), the fibroblasts synthesize large amounts of filaments which assemble in a network and react to the ER-TR7 antibody. Following isolation of the soluble factors produced by the CD4+ cells under these conditions, it was determined that the combinatorial effect of lymphotoxin (LT) and TNF- α ligands on the lymphotoxin beta receptor (LT β R) and TNF receptor, respectively, of the fibroblasts stimulated this response and is critical for proper network formation. Downstream, this co-triggers the canonical and alternative nuclear factor kappa-light-chain-enhancer of activated B cells (NF κ B) pathways to activate gene transcription (88). On the other hand, neutralizing the LT β R with an LT β R-Ig in diabetic CXCL13-RIP mice decreased the amount and efficiency of network formation by fibroblasts within pancreatic infiltrates (89). The importance of stimulating the LT β R with respect to meshwork synthesis has also been demonstrated when indirectly, the loss of LT due

to a depletion of T-cells in HIV infection correlates with lower numbers of reticular fibroblasts and inadequate network synthesis (90).

Deviations from the normal ER-TR7 expression pattern and amount have been implicated in lymphoid organ disorders, architectural anomalies, and diminished efficiency of immune-derived signaling mechanisms, especially those involving dendritic or T-cell interactions (83, 91). There is also evidence of network dysregulation in several models of infectious disease including HIV, which leads to lymphoid organ fibrosis (92). Furthermore, overexpression of the ER-TR7 meshwork and increased invasion by reticular fibroblasts *in vivo* has been demonstrated in models of cancer immunosuppression (93).

The reactivity of this clone has been also described in a limited fashion within the structural framework of non-lymphoid organs (94). In these characterization studies, the immunoreactivity of ER-TR7 was sparsely confined to connective tissue elements of many organs including, but not limited to the dermal layer of the skin; tendon fibers; lining of liver cords; and all blood vessel walls. *In vitro*, ERTR-7 can be detected within the cytoplasm of several fibroblast cell lines but remains unreactive to endothelial or glomerular epithelial cell lines stained through immunocytochemistry (81). Even though the ER-TR7 staining of cultured fibroblasts yields an intracytoplasmic pattern, ER-TR7 expression has been mostly observed as membranous and extracellular filaments within the compartments where the same fibroblast cell lines exist *in vivo*. Moreover, although its labeling pattern suggests similarities and potential reactivity with reticulin in all tissue types, it proved unreactive to purified laminin, fibronectin, collagens I-IV, heparan sulfate proteoglycan, nidogen, and entactin (94). Nonetheless, the fibrous morphology of the ER-TR7 expression pattern is confined to the extracellular space and

any association or reactivity with a portion of well-known matrix components cannot be ruled out.

1.6 BONE MARROW-DERIVED CONTRIBUTORS TO INJURY REPAIR

Repair of an amputated limb involves many of the conventional wound healing stages observed during cutaneous injury. The bone marrow facilitates the inflammatory, mesenchymal, and endothelial progenitor cells necessary to move this cascade forward. Following migration to the injury and initiation of the inflammatory phase, these bone marrow derived cells release cues into the local microenvironment that allow for the mobilization and guidance of epithelial and mesenchymal precursors to remodel the wound (20).

The bone marrow (BM) is composed of two areas within the endosteum of most bones: the *medulla ossium rubra* (red marrow) and the *medulla ossium flava* (yellow). The latter is mostly composed of fat. The red marrow contains a milieu of cells produced through hematopoiesis which include erythrocytes, platelets, and leukocytes. There is also another population of cells which indirectly supports hematopoiesis by producing growth colony stimulating factors (GCSFs), facilitating entry into the circulation, and delivering iron. This population makes up or resides in the stroma of the red marrow. These cells include fibroblasts, macrophages, osteoblasts, osteoclasts, and endothelial cells. But the BM stroma also houses multipotent cells within defined niches that can differentiate into hematopoietic and mesenchymal lineages (95). Due to their capacity for self-renewal, these cells were first referred to as BM-derived stem cells (BMSCs) and further divided into hematopoietic and mesenchymal stem cells, or HSCs and MSCs. In the marrow however, both subtypes can be found as a mixture of progenitors at different stages of commitment to the hematopoietic or mesodermal lineage. In other words, they may not be as naïve as part of the definition of a stem cell suggests.

Regardless, it is now accepted to still refer to them as HSCs and MSCs. The largest amount of these progenitor cells can be found in the femur, pelvis, and sternum and may be also isolated from umbilical cord blood (96).

HSCs are known to reconstitute erythrocytes, platelets, myeloid (e.g. macrophages, dendritic cells), and lymphoid (e.g. T- and B-cell) subtypes. Although under debate, there is also some evidence that suggests their potential role in contribution to non-hematopoietic organ reconstitution such as differentiation into hepatic, skeletal (97), endothelial, and cardiac lineages (98). All HSCs express the leukocyte common antigen CD45 and only a subset express another cell surface marker, CD34. Due to the potential of these cells to exist at various stages of hematopoietic progenitor phenotypes, it is often difficult to measure the full extent of their contribution to repair if only using the CD45 and CD34 markers to label them. Depending on their bias to a hematopoietic lineage, HSCs can be subtyped as myeloid, lymphoid, and balanced with the lymphoid subtype lacking the capability of self-renewal (99).

MSCs, or multipotent mesenchymal stromal cells, are a heterogeneous cell population which can self-renew and has been described as fibroblastic because of its morphology, colony formation dynamics, and capability to adhere to plastic *in vitro*. MSCs can differentiate to osteoblasts, chondrocytes, adipocytes (100), fibroblasts (101), cardiomyocytes (102), lung pneumocytes (103), hepatocytes (104), and skin (105). Although originally derived from BM (106), MSCs have also been isolated from other tissue types such as adipose, respiratory, hepatic, and musculoskeletal (107-110). In the mouse, and unlike HSCs, there is a general consensus that MSCs are negative for CD45, CD11b (myeloid), and CD34 (endothelial) and positive for Sca-1 (stem cell antigen 1) and CD106 (111). Aside from their capability to differentiate into various cell populations, evidence exists that MSCs support the HSCs niche in

the BM; repress proliferation; and control innate and adaptive immune responses at tissue sites compromised by injury or infection.

Together, both progenitor cell subtypes can reconstitute the bone marrow and contribute to repair of non-lymphoid organs (95, 97, 112, 113). Several experimental models, especially those of cardiac injury, suggest that all BMDSCs are able to leave the bone marrow, circulate, and migrate across the endothelium to injured sites (114-117). HSCs have been collected from peripheral blood, expanded, and mobilized by factors such as granulocyte macrophage colony stimulating factor (GM-CSF), thrombopoietin, and interleukin-8 (IL-8) to treat a number of malignancies and non-malignant diseases such as myocardial infarction (98). In the latter however, transdifferentiation into cardiomyocytes has not been observed (118, 119), which suggests a different mechanism of repair and/or influence of these cells on the local progenitor population. A progenitor lineage derived from HSCs, the endothelial progenitor cells (EPCs) are CD34+ and have been implicated in repair of ischemic sites (114, 120).

The capability of MSCs to circulate and migrate to injury sites has also been addressed. Secretion of the small cytokine stromal cell derived factor-1 (SDF1) or CXCL12 is induced as a result of pro-inflammatory stimuli in most injuries. Since MSCs express its corresponding receptor, CXCR4, on their surface, it has been proven that most of the migration of MSCs to the injury site is dependent on the SDF1/CXCR4 axis (121). Infusion of MSCs into animals suffering from strokes, lung fibrosis, and cardiac infarction has improved the outcome of the injury by contributing to the neuronal population as NeuN+, MAP2+, and GFAP+ cells (122); modulate the inflammatory reaction to bleomycin treatment (123); and differentiating into cardiomyocytes (115), respectively.

Many studies on cutaneous wound repair have not only demonstrated that BMDCs contribute to a large percentage of skin cells under normal circumstances but also that many of these cells, which are CD45-, are actively involved in the regeneration of skin (124, 125). A fraction of these cells have been detected in the bulge of the hair follicles within the epidermis, thus suggesting a contribution to an epithelial phenotype (124). This is supported by evidence *in vitro* which shows that differentiation of MSCs into keratinocytes can be achieved after being co-cultured with lung airway epithelia (126). But the most compelling evidence about the migration and differentiation of MSCs within different skin compartments comes from studies involving enhanced green fluorescent protein (eGFP) chimeric mice. The BM of C57BL/6 mice is ablated by lethal irradiation and then reconstituted with BMDCs from eGFP+ transgenic mice. This donor population would include both HSCs and MSCs (124, 127). Following recovery, 15-20% of the eGFP+ BMDCs in the skin were found as cells with a fibroblastic phenotype. Using this same approach on a mouse model of skin fibrosis, a significant percentage of eGFP+ spindle-shaped cells have been found expressing type I collagen within fibrotic lesions (128).

Based on observations from the skin of the eGFP chimera model of BM transplantation, several studies have suggested that, other than their differentiation potential, BMDCs play various roles in cutaneous wound healing and regeneration. In addition to proliferating and localizing to known niches such as the bulge of hair follicles (124), engraftment of BMDCs is increased in wounded skin (129). In the wound, EPCs release protective angiogenic factors to the local endothelium such as vascular endothelial growth factor (VEGF), platelet derived growth factor (PDGF), and GM-CSF (130). In addition to pro-angiogenic factors such as VEGF, MSCs also release basic fibroblast growth factor (FGF-2); pro-inflammatory interleukin-6 (IL-6); and chemoattractants such as macrophage chemotactic protein (MCP-1) (131). In another study, mesenchymal stem cell (MSC) conditioned medium has been found to aid in proliferation

and migration of endothelial cells in a dose-dependent manner; enhance blood flow and tissue remodeling in a mouse hind limb ischemia model; and modulate healing by recruiting inflammatory cells (132). Due to their differentiation potential into fibroblasts and adipocytes, MSCs may also regulate re-epithelialization of the skin and the proper dynamics between epidermis and the underlying dermal integumentary tissue. Co-incubation of mesenchymal cells with keratinocytes promotes survival of the latter and formation of epidermal ridge-like structures (133).

In the same manner by which BMDCs, specifically MSCs, contribute to cutaneous injury repair, they may also play a critical role in coordination of growth and patterning of the digit tip following amputation. Studies addressing this phenomenon would likely focus on the role of BMDCs with respect to the local mesenchymal cells arising from the injured site. Organ-specific mesenchymal cells are those derived from the embryonic mesoderm and contribute to a great majority of the cells in the adult connective tissue. Many of these cells are lineage committed but there is still a fraction of them that remains as progenitors. Precursors such as the skeletal muscle satellite cells and pre-adipocytes presumably participate in repair and regeneration. Following isolation, endogenous organ-specific uncommitted mesenchymal cells have been found to produce other types of tissues such as skeletal muscle (109) and bone (134) around their vicinity *in vitro* hence their potential to contribute to that organ's repair. In a similar fashion to BM-derived MSCs, MSCs isolated from the skin have shown a potential to contribute to repair and regeneration by demonstrating a capability to differentiate into chondrocytes, osteoblasts, adipocytes, and GFAP+/NCAM+ neuronal precursors (135). Furthermore, cutaneous MSCs express the same surface markers as BM-derived MSCs. Whether the BM is the original source of these region-specific MSCs under normal circumstances; the BM-derived MSCs directly or indirectly aid in regeneration; and/or the local MSCs constitute the bulk of the repair

population, strong evidence exists of their shuttling; homing to injury; control of the immune response; and plasticity.

1.6 SUMMARY AND RATIONALE

The number of individuals living with any given sort of amputation is estimated to reach 3.6 million by the year 2050 (1). In many cases, extension and renewal of lost limb components from a stump would aid in restoring conventional form and function. But as opposed to many invertebrates and lower vertebrates such as the salamander, mammals are unable to regenerate missing organs and limbs. Exceptions to conventional mammalian wound healing exist, specifically with respect to turnover of cutaneous injuries; sloughing and renewal of intestinal epithelia; and compensatory hyperplasia of the liver following partial resection (136). An amputated digit tip also undergoes an unconventional repair mechanism that involves various tissue compartments including marrow, bone, peripheral nerve, and vasculature with surrounding connective tissue and skin. This level specific regeneration, starting with formation of a blastema, is limited to amputations at the distal half of the terminal phalanx (6, 7, 12) in both adult and neonatal subjects.

Following inflammation and concurrent with the granulation phase of conventional wound healing (20), fibroblasts migrate and expand to populate the bulk of the blastema after amputation of adult mouse digit tips (6, 137). The fibroblast provides various types of ground substance and fibers to layout specific structural frameworks in all organs. These ECM components include collagens, glycosaminoglycans, reticular and elastic fibers, and glycoproteins. Historically, some of these have been utilized to engineer treatment scaffolds designed to house cells contributing to fracture repair (138, 139), angiogenesis (140), and whole organ development (141). Depending on their location, function, and substances they produce,

fibroblasts can be subdivided into several phenotypes. The major subtypes of fibroblasts which exist in the mouse digit include myofibroblasts, adventitial fibroblasts of the vasculature, and fibroblastic reticular cells which also exist in the stroma of the BM (142). General detection of these different phenotypes is mostly based on cytology combined with histological analysis of compartment-specific localization. More specific detection is hampered by the lack of specific probes against the few proteins, and thus their regulation, which make them different from each other.

In 1984 however, Els Van Vliet and colleagues at the Erasmus University of Rotterdam isolated seven hybridoma cell lines that produced a panel of monoclonal antibodies immunoreactive to non-lymphoid cells of the mouse thymus in an effort to characterize by immunolocalization the fibroblasts which build the lymphoid stroma (81). The antibodies were designated Erasmus of Rotterdam thymic reticulum (ER-TR) 1-7. ER-TR7 detects reticular fibroblasts of the thymus and the support wall of blood vessels (94) and since then, has been used to study numerous lymphoid organ disorders, architectural features, and signaling mechanisms, especially those involving dendritic or T-cell interactions in the spleen and lymph nodes(83). ER-TR7 is unreactive to ECM molecules such as laminin, fibronectin, collagens I-IV, heparan sulfate proteoglycan, nidogen, and entactin (81). Preliminary studies in our lab indicate that ER-TR7 is also expressed by reticular fibroblasts of the mouse digit, where it outlines tissue compartments.

During repair of an amputated neonatal digit tip, ER-TR7 is overexpressed as a scaffold that holds together the blastema region of the regenerating structure. At the endpoint of regeneration it regresses to an outlining expression pattern. These observations give rise to the hypothesis that during the early stages of neonatal or adult mouse blastema formation, a

scaffold is induced by local fibroblasts to serve as a supportive structure that may facilitate the migration, adhesion, and positioning of regeneration-competent precursor cells. Since the development of the blastema occurs around the same time as granulation tissue would develop in a regeneration-incompetent wound and that stage of conventional wound healing is characterized by upregulation of collagen type III over type I (29, 71), we also hypothesize that ER-TR7 expression in the blastema is the counterpart of collagen type III expression in granulation tissue. Moreover, since the granulation or proliferative phase of wound healing is characterized by the migration of fibroblasts into the wound to further expand, we hypothesize that even though blastema cells have been shown to proliferate at the wound site (137), the initial precursors to the blastema at its onset migrate from BM-derived precursors to directly or indirectly repair wounds as shown previously in simple models of cutaneous injury (124, 125, 143).

Many studies have confirmed that the bone marrow (BM) houses both hematopoietic and mesenchymal cells that give rise to a variety of tissues including bone, cartilage, muscle, vessels, and fat. The self-renewal and plasticity of these cells has been examined within the context of tissue repair in models of cardiac restoration (141); bone fracture fusion (139); liver regeneration (144); pancreatic beta cell renewal (145, 146); cystic fibrosis (112); and cutaneous injury (147, 148). The origin, contribution, and plasticity of BM-derived progenitors into the mammalian digit blastema have never been studied. We have performed digit tip amputations on adult chimeric mice of C57BL/6 background reconstituted with enhanced green fluorescent protein (eGFP)-positive BM cells. A time-course analysis of eGFP expression following amputation was performed coupled with detection of the CD45 surface antigen. Consistent with the wound healing cascade, circulating BM-derived hematopoietic cells (CD45+) begin infiltration shortly after amputation as part of hemostasis and early inflammation. However,

preliminary data reflect that starting at 14 days post amputation (DPA), and concurrent with the onset of blastema formation in this strain, 45-50% of the blastema cells express eGFP with only a small fraction co-expressing CD45. These data are consistent with the hypothesis that many BM-derived cells colonize the injury site as inflammatory cells of hematopoietic lineage, but at the onset of blastema formation most of the population is composed of cells from the mesenchymal lineage. Therefore we propose that some of these BM-derived cells may be responsible for engineering the transient blastema scaffold that we observed labeled with ER-TR7 and will incorporate into the final stages of the regenerated site as functional components of various tissue layers as ER-TR7+ cells or other cellular phenotypes.

1.7 SPECIFIC AIMS

A small fraction of tissues in the mammalian system such as liver, epidermis, intestinal epithelium, and fingertips can undergo renewal. Amputated human or rodent digit tips experience a level-specific response that results in a fully functional replica of the damaged region. This response has been compared to the regeneration sequence followed by amphibians such as the salamander with respect to a mass of progenitor cells supported by a loose connective tissue network which together mold the precursor of the regenerate, the blastema. This project targets analysis of the identity, origin, and function of a blastema extracellular matrix (ECM) network component which may serve as a conduit for migration, positioning and/or differentiation of regeneration competent cells. We believe this macromolecule complex plays a role in mammalian digit tip regeneration but its expression and dynamics can only be studied via an antibody derived from reticular fibroblasts named ER-TR7.

Preliminary data support that the ER-TR7 antigen is a filamentous extracellular protein that compartmentalizes the digit anlagen. If the regeneration blastema is populated either by

mass migration or in situ expansion of fibroblastic progenitors, we hypothesize that ER-TR7 will be transiently overexpressed at that stage. Once differentiation and patterning of the renewed structure progresses, we predict ER-TR7 expression will regress to basal levels. There is a temporal similarity between the onset of the blastema and the proliferative phase of wound healing which is known to transiently express various matrix macromolecules. We will address any correlation which ER-TR7 may have with other extracellular proteins regulated during that phase in an attempt to find the identity and potential association of ER-TR7 with other extracellular components of the blastema.

We also aim at addressing the cellular origin of this scaffold *in vivo*. Circulating bone marrow (BM) cells home to cutaneous injuries. We will use a BM transplantation approach to test if the primary role of homing BM cells is immunological (hematopoietic) or structural (mesenchymal). Since we have found that half of the fibroblast-rich blastema is composed of BM-derived cells, we will prove that the majority are non-hematopoietic and participate in engineering of the ER-TR7 positive matrix template as reticular cells of mesenchymal origin. Furthermore, using this same approach, we will also test for various tissue specific differentiation markers to assess if the contribution of BM-derived cells is limited to the blastema phase and engineering of the scaffold or if they expand their potential for plasticity in the regenerate as components of different structures with a long-term fate.

Fibroblasts subpopulations have been found to possess variable genetic activity depending on anatomical origin. So finally, as an introduction and preliminary data to our future work, we hypothesize that the synthesis and organization of the ER-TR7 framework following activation of the TNF and LT β receptors in fibroblasts isolated from terminal (P3) and second (P2) phalangeal elements of the same adult mouse digit will vary. We expect fibroblasts

isolated from the regeneration competent region around P3 to organize a scaffold that mimics the spatial and architectural organization of the distal P3 post-amputation blastema following induction of ER-TR7 microfilament production *in vitro*. On the other hand, we predict P2-derived fibroblasts will respond differently to the same induction regimen by secreting an ER-TR7 positive, but densely packed and diffuse extracellular matrix consistent with that seen in granulation tissue. We have begun testing this hypothesis and will report preliminary findings as one of the foundations for future directions. In additional regard to proposing that P3 and P2 cells are programmed to respond differently to ER-TR7 induction cues, we have observed consistently different structural organization of regenerating P3 and pro-scarring P2 wounds by routine histopathology particularly with respect to extracellular matrix fiber density and cellular components within that matrix. Therefore, we also hypothesize that different temporal and organizational dynamics of ER-TR7 positive microfilament deposition exist between P3 and P2 amputation sites only to corroborate distinct responses of P3 and P2 cells to our *in vitro* induction approach and this can be initially tested by the same means as those applied to characterize the P3 regenerate-specific events presented in this dissertation.

CHAPTER II: *IN VIVO* EXPRESSION AND REGULATION OF A NOVEL EXTRACELLULAR MATRIX COMPONENT DURING REGENERATION OF AMPUTATED RODENT DIGITS

2.1 INTRODUCTION

The mouse digit tip consists of a diverse group of cells and extracellular components organized in tissue compartments such as bone, articular cartilage, marrow, tendon, blood vessels, and nerve surrounded by connective tissue, epidermis, and a nail rudiment. The main difference between this region and other similar mammalian extremities is that the digit tip can regrow following amputation midway through its terminal phalanx (5-7). This phenomenon has been observed in neonatal and adult mice (12, 137) as well as in humans, which makes it of significant clinical relevance (5, 11). Similar to the epimorphic regeneration that occurs in an amputated urodele limb, a severed digit tip will undergo a cascade of events leading to replication of damaged tissue layers. Following clotting and concurrent with the inflammatory cascade and re-epithelialization of the epidermis, the wounded digit tip will become populated with a dense mass of propagating spindle-shaped cells whose genetic profile resembles that of the developing embryonic digit (149) to form a blastema (137, 150). At the cellular level in this mammalian system, this structure parallels the blastema that forms at the early stages of urodele limb regeneration. In the urodele, the cells responsible for this site of regenerative activity have been described as de-differentiated fibroblasts.

The process of mammalian regeneration in this particular model is different from typical wound healing. It is a level specific response that cannot be replicated by neighboring segments as close as the second phalanx, which resolves amputation by activating the typical wound healing approach to become a stump. The conventional repair process involves a series of highly specific cues involved in preventing blood loss; addressing invasion of pathogens and gathering information from infectious agents; protecting the site with an adequate epidermal layer; restoring blood flow; and re-establishing neural cues. However, the scar that accompanies all these different repair events is not suitable to form a replica of the pre-existing part (3). In order for a regeneration competent event to take place, a complex set of microenvironmental factors must be present at both the cellular and extracellular level. The system must be provided with both regeneration-competent cells that are capable of expanding and the proper cues in a time and concentration dependent fashion to position and differentiate themselves. This concerted effort must be in the presence of an extracellular environment that is devoid of cues that will inhibit a regenerative response. Ironically, some of these regeneration inhibitory cues may be found as driving forces of the wound healing cascade and in deep association with the extracellular matrix.

The role of fibroblasts in the mammalian regenerative and wound healing response has been underestimated, especially when it comes to their capability of synthesizing and sustaining the extracellular microenvironment. During the proliferation stage of tissue repair, fibroblasts invade the wound in overlap with the initial inflammatory response. Their participation in matrix remodeling begins at this time, when they synthesize a transient matrix mostly composed of collagen type III (COL3) (20, 29, 71). The matrix has been long viewed as a reticular network of fibers that allows for adhesion and motility of other cell types mainly including those with immunological activity. Due to the wound tissue gritty, soft, and red appearance at this

point, this particular event has been also denominated as the granulation phase of wound healing. This matrix is eventually replaced by a dense fiber network made of collagen type I (COL1) macromolecules which becomes the hallmark of scar tissue formation. At the granulation stage, this same reticular network produced by a subset of fibroblasts has been linked to T-lymphocyte interactions with their surrounding stroma (83, 151, 152) in the lymph nodes and as a template in organogenesis of the spleen (153-155). In this context, the cells responsible for generation of this network are referred to as fibroblast reticular cells (FRCs) (82, 88, 91, 93, 94, 152, 156).

In this study, we would like to address the contribution of FRCs to the regeneration competent environment specifically with respect to their regulation of a transient reticular network thus far observed during lymphoid organogenesis. This ECM component is labeled with an antibody against an unknown antigen cloned from stromal cells of the spleen labeled Erasmus of Rotterdam Thymic Reticulum 7 or ER-TR7. This antibody targets an epitope specific to FRCs and the extracellular meshwork of fibers they secrete (88, 94). One the main aims of this study was to analyze the expression of this framework in a complex non-lymphoid organ. We achieved this by labeling neonatal and adult mouse digit tips with an ER-TR7 antibody by indirect immunofluorescence which enabled analysis of its content, organization, and regulation at different timepoints throughout the regeneration process following a level-specific amputation. Cutaneous sites have been described to contain FRCs which produce reticular fibers (reticulin) similar to those in lymphoid organs (94, 157, 158). Since the connective tissue content around the terminal phalanx of the digit is nearly identical to the one in most cutaneous sites, we expected anti-ER-TR7 to bind targets associated with FRCs throughout the uninjured digit connective tissue mesenchyme to prominently define its various tissue layers and structures. Furthermore, since blastema formation parallels in many regards

the events that define granulation tissue such as fibroblast accumulation, limited capillary formation, and synthesis of a transient matrix (20, 137), we hypothesize that the FRCs endogenous to the digit expand to form the blastema and engineer the reticular framework that can be detected by immunolocalization of ER-TR7.

2.2 MATERIALS AND METHODS

Mice and tissue harvest

All neonatal and adult subjects consisted of outbred CD1 mice supplied by Charles River Laboratories (Wilmington, MA). Post-natal day 3 (PN3) neonates and 8 week old adults were anesthetized with an intraperitoneal injection of Ketamine and Xylazine at 80 and 8mg per kg of body weight, respectively, followed by distal amputation of digits 2 and 4 from each hind limb using microdissection scissors (neonate) or a scalpel (adult) under a stereomicroscope. The distal amputation target region was measured at midpoint of the clearly visible terminal phalangeal (P3) element so approximately 50% of the bone remained in the proximal stump after transection. Digit tissues were harvested for histological, immunohistochemical (IHC), and whole mount analysis at day post amputation (DPA) 0, 4, 8, 12, and 16 for neonate and 0, 5, 10, 14, 21, 28, and 35 in adults. Procedures for care and use of mice for this study were performed in accordance with standard operating procedures approved by the Institutional Animal Care and Use Committee of Tulane University and LSU Health Sciences Center in New Orleans, LA.

Fluorescence immunohistochemistry on thin paraffin sections

Tissues were collected in zinc-buffered formalin (Anatech Ltd, Battle Creek, MI) to fix no longer than 48 hours, decalcified in formic acid-based solution (Decal II; Surgipath, Richmond, IL) for paraffin histology and thin section IHC staining and analysis. Serial tissue sections were collected at 5µm onto charged, glass slides and heated for 45 minutes at 60°C. One set of slides

was chemically treated to stain for reticular fibers by the modified Gridley reticulin method (159) or hematoxylin and eosin staining. The remaining slides were deparaffinized in xylene and rehydrated through an ethanol series to distilled water. All washes were performed with Tris-buffered saline (TBS). Depending on the antigens to be detected, sections were pre-treated with either enzymatic (Proteinase K) or heat induced epitope retrieval (Citrate buffer, pH 6.0) and washed. This was followed by blocking for non-specific protein binding with 5% goat serum diluted in 1% bovine serum albumin. It should be noted that if using a primary antibody derived from mouse for subsequent tagging with an anti-mouse secondary antibody, an additional goat anti-mouse Ig Fab fragment (Jackson ImmunoResearch, Westgrove, PA) was added to the protein block step at a 1:100 dilution to bind endogenous immunoglobulins. Sections were further treated with sodium borohydride (0.5 mg/mL in PBS) to limit autofluorescence from red blood cell porphyrins and elastic fibers for example. Following washing, sections were single or co-incubated overnight at 4°C with a variety of primary antibodies: anti-ER-TR7 (5µg/mL; Abd Serotec, Raleigh, NC), anti-SMA (2µg/mL; Dakocytomation, Carpinteria, CA); anti-VWF (1µg/mL; Dakocytomation); anti-Osteocalcin (1µg/mL Takara, Otsu, Shiga, Japan); anti-Ki67 (2µg/mL; Labvision, Fremont, CA); anti-Caspase-3 (5µg/mL; Cell Signaling, Danvers, MA); anti-Vimentin (Labvision, Fremont, CA); anti-COL1A1 (1µg/mL; Novus Biologicals, Littleton, CO); anti-COL3A1 (2µg/mL; Abcam, Cambridge, MA); anti-FSP1 (1µg/mL; Abcam); anti-Fibronectin (2µg/mL; Abcam); and anti-gp38 (5µg/mL; Abcam). Labeling of antibodies bound to their targets was achieved by indirect immunofluorescence using secondary antibodies against the primaries' host species conjugated to Alexa dyes (Molecular Probes, Eugene, OR) at a concentration of 4µg/mL each. All preparations culminated in several washes followed by nuclear counterstaining with 4', 6-diamidino-2-phenylindole, otherwise known as DAPI, (300mM;

Molecular Probes), and mounted under a coverslip with Prolong Gold Antifade (Molecular Probes) for epifluorescence deconvolution or confocal microscopy.

Primary cell isolation and tissue culture

Adult male (8 week) CD1 (Charles River, Wilmington, MA) or C57BL/6-TGN(ACTB-eGFP) transgenic (The Jackson Laboratory, Bar Harbor, Maine) mice for untagged or eGFP-tagged lines, respectively, were euthanized and hind digits collected in 30mm dishes with 1 ml of 20% (v/v) fetal bovine serum (FBS) in Dulbecco's modified Eagle's medium (DMEM) supplemented with 60% glucose, 40% Ham's F12, 250µg/mL Amphotericin B, and 1X Zonker (penicillin, neomycin, bacitracin, HBSS). The nail, skin, fat pad, blood vessels, nerve, tendons, and ligaments were removed under a stereomicroscope and the denuded terminal (P3) phalangeal elements isolated. The bone segments were treated overnight at 37°C in liberase blendzyme (Roche Applied Science, Indianapolis, IN) followed by removal of the remaining loose connective tissue. The bones were then resuspended in DMEM in fibronectin-coated dishes and re-fed every third day. After 6 days, fibroblast-like adherent cells migrated from the bone segments, at which time the bones were removed from the dish and the cells trypsinized and counted. All cell populations grew at a very slow rate initially and doubling was calculated assuming an initial outgrowth of 250 cells per phalanx. The cells were passaged every 3-5 days at which time the rate of proliferation was relatively fast, especially on those isolated from the second phalanx. Cells originating from the terminal phalanx were labeled P3 and those from the second phalanx P2.

NIH-3T3 fibroblasts (American Type Culture Collection, Rockville, MD) were grown in 100mm dishes with 3mL of DMEM containing 10% (v/v) FBS, 25 U penicillin G sodium, 25 mg streptomycin, and 4mM L-glutamine. Cells were grown to confluency and passaged every third day.

ER-TR7 induction

3T3 and P3 cell lines were plated on fibronectin-coated chamber slides (Corning, Corning, NY) at a concentration of 1×10^5 for primary cells and 1×10^4 for 3T3 per chamber. The 3T3 line was plated at a lower concentration due to their fast proliferation rate and avoiding overconfluency for the extended period of treatment. All cell lines were stimulated according to the procedure described by Katakai et al. (88). Briefly, cells were allowed to adhere and recover from trypsinization for 24 hours at which time they were co-treated with 100 ng/mL of recombinant TNF α (R&D Systems, Minneapolis, MN) and anti-LT β R (R&D Systems) at a concentration of 5 μ g/mL. This treatment was reapplied at days 3, 6, and 9. For concentration-dependent induction assays, all reagents were either diluted 50% or doubled. At day 11, cells were collected for RT-PCR or fixed for immunocytochemistry.

RNA extraction and Quantitative RT-PCR

Total RNA was isolated from control and experimental 3T3, P3, and P2 cells using Trizol Reagent (Invitrogen, Carlsbad, CA). Following DNase treatment, RNA was purified using the Qiagen RNeasy Mini kit (Qiagen, Valencia, CA) and its quality determined using a Nanodrop 2000 (Thermo Fisher Scientific, Inc., Waltham, MA). cDNA was synthesized by RT² First Strand kit (SABiosciences, Frederick, MD) following manufacturer's instructions. Expression profile was assessed using a Mouse Fibrosis RT² Profiler PCR Array and labeled with RT² qPCR SYBR green PCR Master Mix (SA Biosciences, Valencia, CA) according to the manufacturer's recommended protocols. Quantitative PCR was performed with a LightCycler 480 system (Roche Applied Sciences, Indianapolis, IN) and its software used to determine a critical threshold (CT), which was the cycle number where the linear phase for each sample crossed the threshold level. Relative gene expression was determined using CT methods. Data were further analyzed by

SABiosciences PCR array data analysis online tools

(<http://pcrdataanalysis.sabiosciences.com/pcr/arrayanalysis.php>).

Immunocytochemistry

Cell preparations were washed in pre-warmed PBS and fixed in pre-warmed 4% methanol-free formaldehyde (Polysciences, Warrington, PA) and washed in PBS. Samples were permeabilized in acetone at -20°C, washed, and treated with 5% normal goat serum in 1% (w/v) BSA in PBS to reduce nonspecific binding. Subsequently, cells were co-incubated for 3 hours at room temperature with rat anti-ER-TR7 (Abcam; 5 µg/mL) and rabbit anti-COL3A1 (Abcam; 2 µg/mL). After a series of PBS washes, primary antibodies were conjugated by indirect immunofluorescence using goat anti-primary antibody source species conjugated to Alexa dyes (Molecular Probes) all at 4 µg/mL for 45 minutes with added 4'6-diamidino-2-phenylindole, otherwise known as DAPI (Molecular Probes) at 300mM. Samples were mounted under coverglass with Prolong Gold Antifade medium (Molecular Probes).

Imaging

Tissue sections were imaged using a Leica DMRXA upright microscope equipped with a Sensicam QE CCD (Cooke Corporation, Romulus, MI); xyz motorized stage (Prior Scientific, Rockland, MA); an Hg source; and filters suitable for DAPI, Alexa 488, Alexa 568, and Alexa 647 fluorophores. Additional photomicrographs from tissue sections and immunocytochemical preparations were captured with a Fluoview FV1000 laser scanning confocal system (Olympus of America, Center Valley, PA) equipped with Nomarski (differential interference contrast or DIC) and visible excitation light sources including a multi-line Argon laser and diodes covering 405, 561, 592, and 635 nm wavelengths.

No Neighbors and Constrained Iterative deconvolution algorithms were applied to 2D and 3D sets, respectively. Post-imaging measurements included protein expression profiles based on detection areas (both *in vitro* and *in vivo* samples) and cell counts. Area measurements of expression of ER-TR7 and other markers were performed with Slidebook software by masking images with a binary layer encompassing specific minimum and maximum fluorophore detection intensities. The areas were automatically calculated by the software in pixel values and these in turn were divided over the total nuclear area, which was masked using the DAPI intensities. For cell number analyses, events were manually measured with a cell counter and annotated over total nuclei per field. Co-localization analyses including Pearson's and Mander's correlation coefficients were calculated within thresholded areas of co-stained antigens. All renderings and analyses were driven by Slidebook software (Intelligent Imaging Innovations).

Statistical Analysis

Data are represented as means \pm SE. Group differences were determined via the unpaired Student's *t* test. $P < 0.05$ is considered significant.

2.3 RESULTS

ER-TR7 outlines tissue compartments of the neonatal and adult digit anlagen

The terminal phalanx of the mouse digit (P3) is first identified as a chondrogenic skeletal element at E14.5 and ossification initiates at E18.5 (12). By postnatal day 8, the major specialized compartments of the digit tip, such as the skeletal element, the marrow cavity, the proximal growth plate, the ventral tendon, and the joint between the second phalangeal element (P2) and P3 are well defined and remain, aside from growth, unaltered throughout adulthood (Figure 2.1 A). The digit tip is grossly characterized by a nail organ that surrounds the

P3 element dorsally and laterally, and a bulbous ventral pad called the “fat” pad. The nail organ consists of a proximal multi-layered nail matrix that extends distally to a single layer of keratinocytes termed the nail bed underlying the nail plate. The “fat” pad is composed of continuous epidermis, dermal connective tissue and eccrine glands. The interstitial cells of the digit tip appear as a loose mesenchyme primarily composed of fibroblasts with blood vessels coursing throughout the tissue.

Studies of the interstitial or stromal cells of other systems, primarily of lymphoid source, identify a subpopulation of fibroblasts called fibroblast reticular cells (FRCs) (82, 88, 91, 93, 94, 152, 156). One antibody called Erasmus of Rotterdam Thymic Reticulum 7 or ER-TR7 (94) identifies FRCs. It was generated against an antigen exclusively found in splenic stromal cells and is routinely used in studies of organogenesis of lymphoid tissue. This antibody targets the meshwork of fibers secreted by FRCs during lymph node organogenesis that compartmentalizes the organ into distinct zones (82). ER-TR7 immunohistochemical staining of mouse digit tips sections was used to determine whether there is a subpopulation of FRCs in the neonatal and adult mouse digit. ER-TR7 staining identifies a subset of fibroblasts that produce a framework of spindle-shaped cells outlining major anatomical components of the terminal phalanx and surrounding tissues (Figure 2.1B). Cells that secrete the ER-TR7 antigen can be identified because they exhibit moderate cytoplasmic antigen localization as well as well-defined reticular staining (Figure 2.1C).

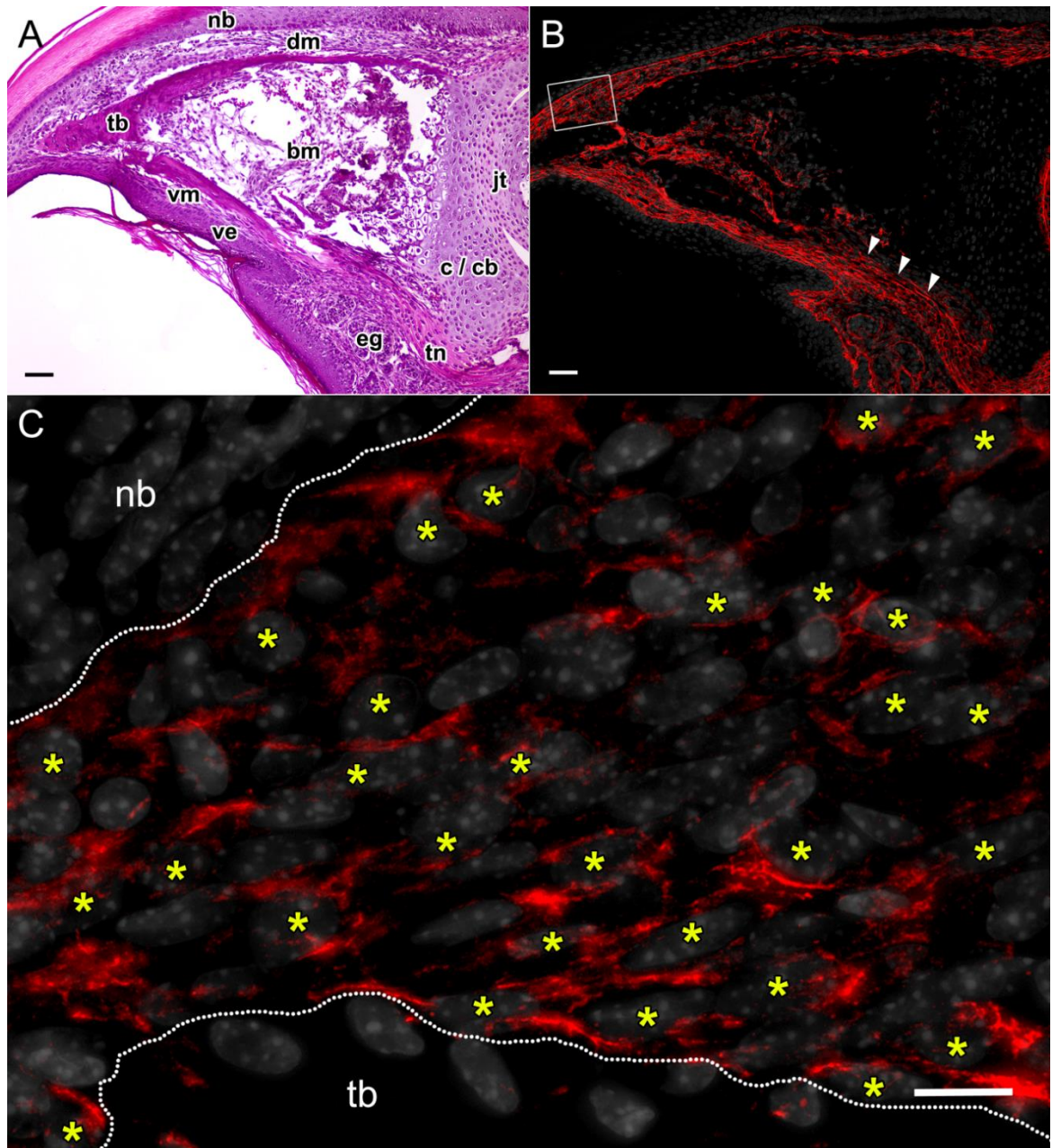


Figure 2.1: ER-TR7 delineates tissue compartments of the digit anlagen and its cellular sources can be identified by high resolution confocal microscopy. (A) Representative section of a PN11 mouse digit tip stained by H&E. Both neonatal and adult digit tips are divided into diverse compartments including a nail bed (nb); ventral epithelium (ve); eccrine glands (eg) inside the ventral fatpad; and a phalanx composed of trabecular (tb) and cortical (cb) bone (adult) or chondrocytes (c; neonate) enclosing the bone marrow (bm) and ending at the synovial joint (jt) area. The phalangeal element (P3) is surrounded by loose dorsal and ventral mesenchyme (dm, vw) mainly composed of blood vessels, immune cells, and connective tissue fibroblasts within a collagen-rich matrix. (B) A serial section through this sample stained against the ER-TR7 antigen reveals that the extracellular macromolecules this protein is related to compartmentalize the digit anlagen. (C) A region of interest captured from panel B (white outlined rectangle) exhibits red fluorescent staining associated with spindle-shaped cells in the connective tissue

layer limited by the nail bed (nb) and trabecular bone (tb) compartments. These cells have been described as fibroblast reticular cells (FRCs) and can be identified (yellow asterisks) by cytosolic, membranous, and extracellular filament expression of ER-TR7. Scale bars (A-B): 50 μm ; and (C): 10 μm .

Prominent ER-TR7 expression lines the interphalangeal joint cavity and extends to the resting zone of articular cartilage where it outlines the lacunae of most chondrocytes (Figure 2.2 A). Upon close examination of the loose connective tissue mesenchyme surrounding the P3 bone, ER-TR7+ cells are closely associated with the vascular endothelium identified by FVIII staining and are also distinct from SMA positive perivascular cells (Figure 2.2 B). A high number of ER-TR7+ cells moderately stratify over OC+ osteoblasts in the periosteum clearly outlining the phalangeal bone (Figure 2.2 C). A similar pattern is seen in the endosteum layer lining the bone marrow cavity (not shown). The second most abundant layer of ER-TR7+ FRCs delineates the boundary between the papillary layer of the loose connective tissue mesenchyme and the stratum basale of the epidermis (Figure 2.1 B). The flexor tendon, which extends ventrally past the sesamoid bone to the proximal end of this phalangeal element, exhibits intercalating staining within tenocyte bundles and more abundantly at the fibrocartilage-rich enthesis (arrow, Figure 2.1B). A similar pattern of ER-TR7 staining is observed in adult digits (see Figure 2.6 J). These observations show that ER-TR7+ FRCs are present in the mouse digit and exist as a subset of mesenchymal fibroblasts that appear to compartmentalize structural components of the digit. Thus, ER-TR7 staining identifies a network of FRCs within the connective tissue stroma of the digit tip that appears analogous to FRCs described during the organogenesis of lymphoid organs (94, 152, 160, 161).

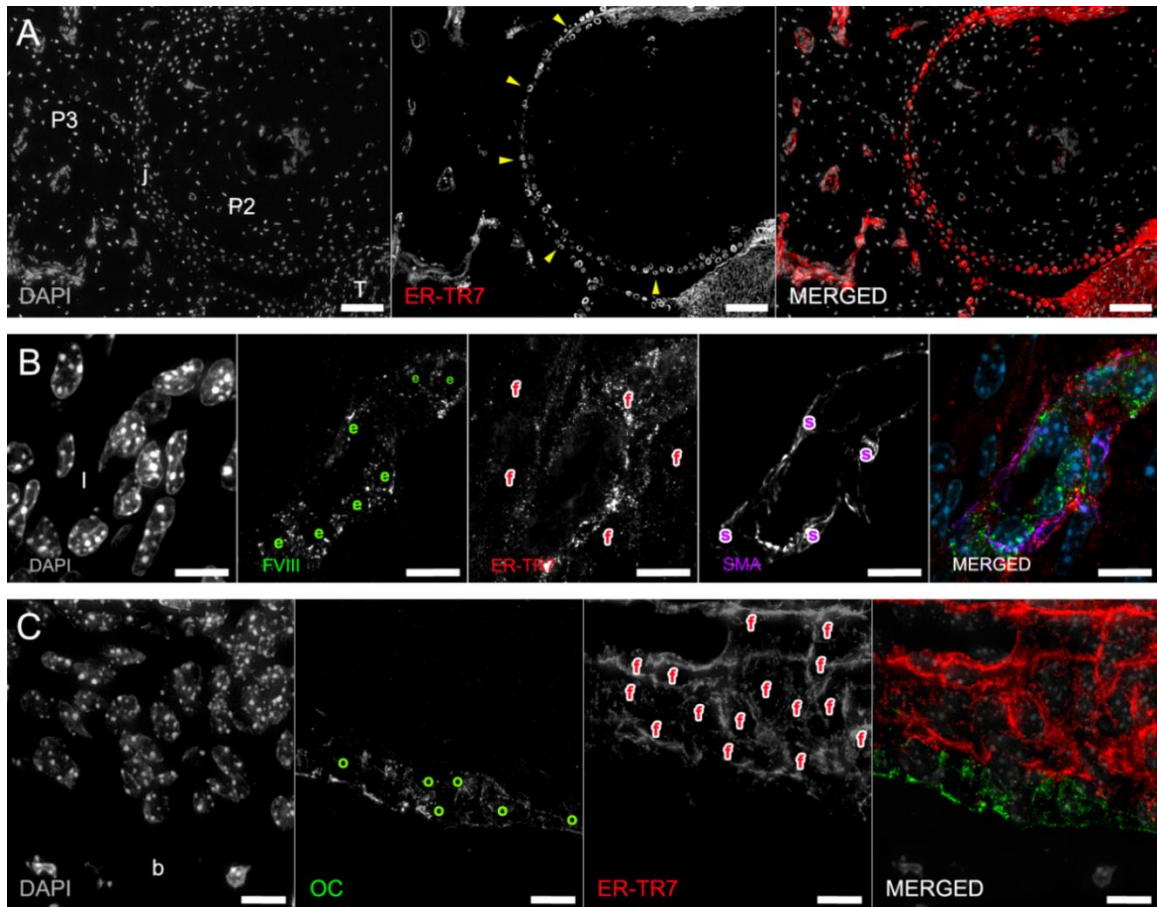


Figure 2.2: ER-TR7+ cells outline structures with diverse phenotypes, function, and differentiation markers. Unamputated neonatal digits at PN11 were co-immunostained for ER-TR7, von Willebrand Factor (FVIII), Smooth Muscle Actin (SMA), and/or Osteocalcin (OC). (A) At the P3-P2 interphalangeal level, ER-TR7 expression can be found outlining the lacunae of most chondrocytes in the resting zone of the joint (yellow arrows); bar = 50 μ m. (B) Supportive ER-TR7+ fibroblasts (f) line the endothelium (e) of blood vessels and intermingle with smooth muscle cells (s); bar = 10 μ m. (C) ER-TR7+ fibroblasts (f) stratify above OC+ osteoblasts (o) at the bone (b) periosteum; bar = 10 μ m.

ER-TR7 is dynamically regulated during digit tip regeneration

One of the values of focusing attention of the mouse digit tip is that it is the only region of the limb that has regenerative capabilities. An amputation midway through the P3 skeletal element in neonates or adults undergoes a healing response that forms a blastema of proliferating cells and these cells eventually re-differentiate to regenerate the pre-existing structure of the digit (12, 137). On the other hand, an amputation through the proximal level of

P3 or any region of the proximal phalangeal elements (P1 or P2) undergoes a healing response that does not involve blastema formation and results in a truncated digit stump. To determine the anatomical differences and expression profile of ER-TR7 during the regeneration response, neonatal and adult mice were amputated and tissues harvested for ER-TR7 immunolocalization at various timepoints during the regeneration response (Figure 2.3). The difference between regeneration of neonatal and adult digits is largely one of timing, neonatal digits are immature and regenerate at a faster rate. What underlies this difference is that mature digits of the adult display a longer period of tissue degradation that precedes blastema formation, and also requires a longer period for the redifferentiation of the larger digit structure.

The maturation of the unamputated neonatal digit is associated with a progressive reduction in the relative amount of ER-TR7 staining in the loose connective tissue from approximately 30-35% of the total area at PN3 to approximately 15-20% at PN19 (Figure 2.3 E). This level of ER-TR7 expression remains stable in adult connective tissue (Figure 2.3 J). In neonates there is a decline in relative ER-TR7 staining during the healing response following amputation that parallels the normal post-natal decline (Figure 2.3 A, B, E), whereas in adult digits this decline is significantly different from unamputated control digits (Figure 2.3 F, G, and J). During blastema forming stages in both neonates and adult digits, there is a dramatic increase in ER-TR7 staining that is not observed in control digits (Figure 2.3 C, E, H, and J). In adult digits this increase is most dramatic and represents a 3-fold increase in ER-TR7 staining. In both neonatal and adult regenerating digits, the relative level of ER-TR7 staining declines from its peak during blastema formation and returns back to control levels as the digit structures redifferentiate (Figure 2.3 D, E, I, and J).

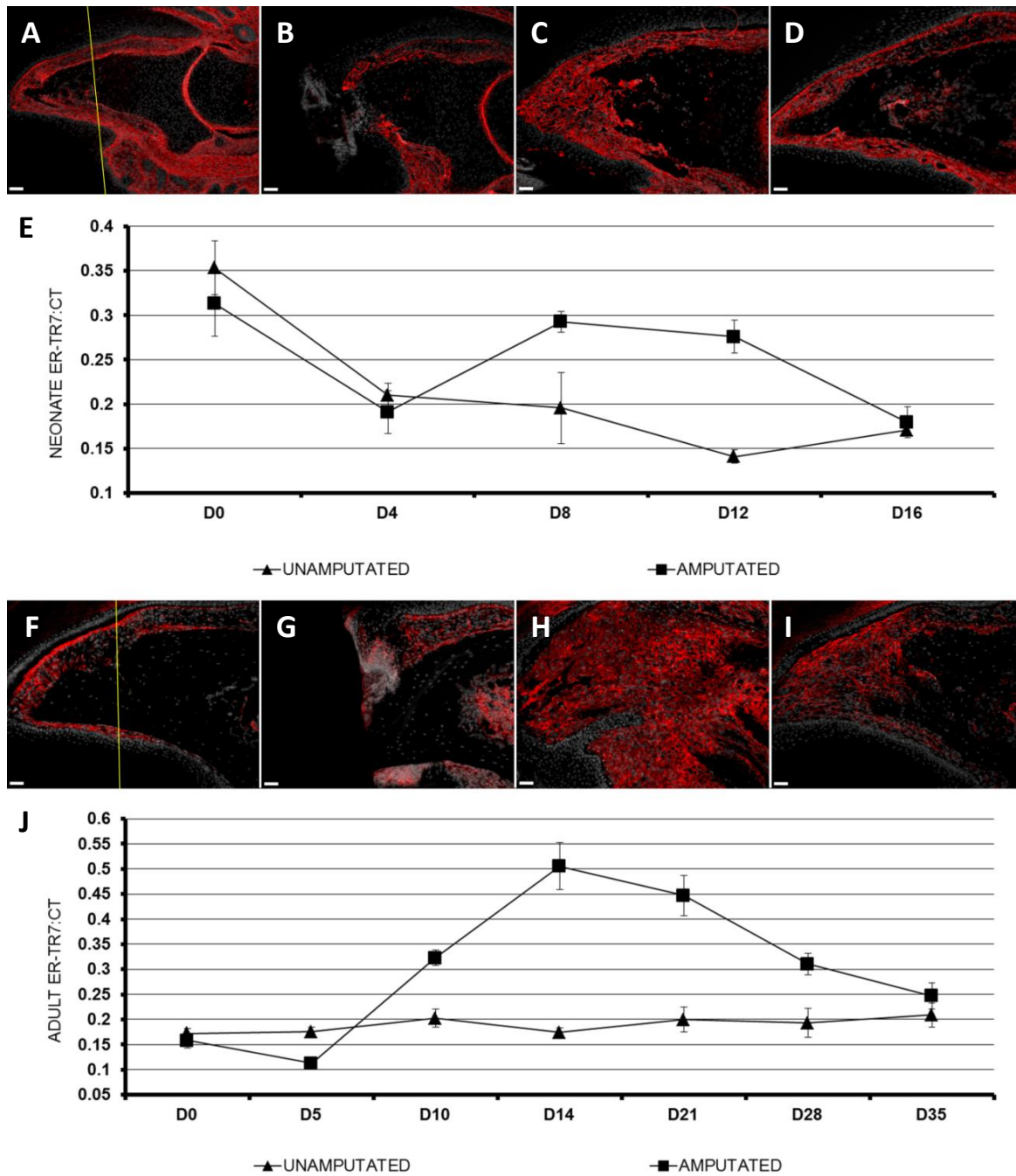


Figure 2.3: ER-TR7 is discretely expressed in unamputated neonatal and adult digits but overexpressed in the mature blastema of regenerates. ER-TR7 (red) expression timeline following neonatal (P3) and adult (8w) distal (P3) digit amputations was detected by indirect immunofluorescence counterstained with DAPI (gray), captured at 100X magnification (bar = 50 μ m), and quantified from selected days. The amputation level for both neonatal and adult digits is marked by a yellow line in the (A and F) unamputated controls at D0. The neonatal amputated digit at (B) D4 shows signs of inflammation and disrupted ER-TR7 pattern at the tip. This is followed by ER-TR7 upregulation within the growing blastema by (C) D8 and regression of ER-TR7 pattern and content by full recapitulation at (D) D16. (E) ER-TR7 expression ratio was quantified from ER-TR7+ area over total connective tissue (ct) around each skeletal

segment. Adult P3 amputations at selected timepoints (F) unamputated control, (G) D5, (H) D14, and (I) D28 demonstrate a steps towards regeneration that are consistent with the neonatal model. In the adult, the peak of ER-TR7 overexpression occurs at D14. (J) The (J) adult regeneration timeline is longer than the neonate's, therefore not only is the initial period of damaged tissue degradation and inflammation longer, but the overexpression of ER-TR7 in the growing blastema is extended well into the period of differentiation and patterning. Data are presented as mean \pm SE (n = 4 per timepoint). Scale bars (A-D) and (F-I): 50 μ m.

During the regeneration response, ER-TR7 staining is most prominent in the blastema.

ER-TR7 staining identifies a loose extracellular framework of fibers produced by a large population of FRCs that are evenly distributed within the blastema (Figure 2.4 A). Differentiated structural components of the digit tip are absent in the blastema and the ER-TR7 staining pattern is relatively uniform. The network of ER-TR7+ fibers appears to be organized along the proximodistal digit axis and parallel to the direction of regenerative outgrowth (Figure 2.4 A). Sections of the blastema stained with the Gomori silver impregnation method (94, 157) for reticular fibers identifies a similar network of extracellular fibers. However, the proximodistal organization of fibers is not evident (Figure 2.4 B). Thus, FRCs represent major cellular constituents of the regenerating digit blastema which appear to produce a prominent extracellular framework associated with the regenerative response.

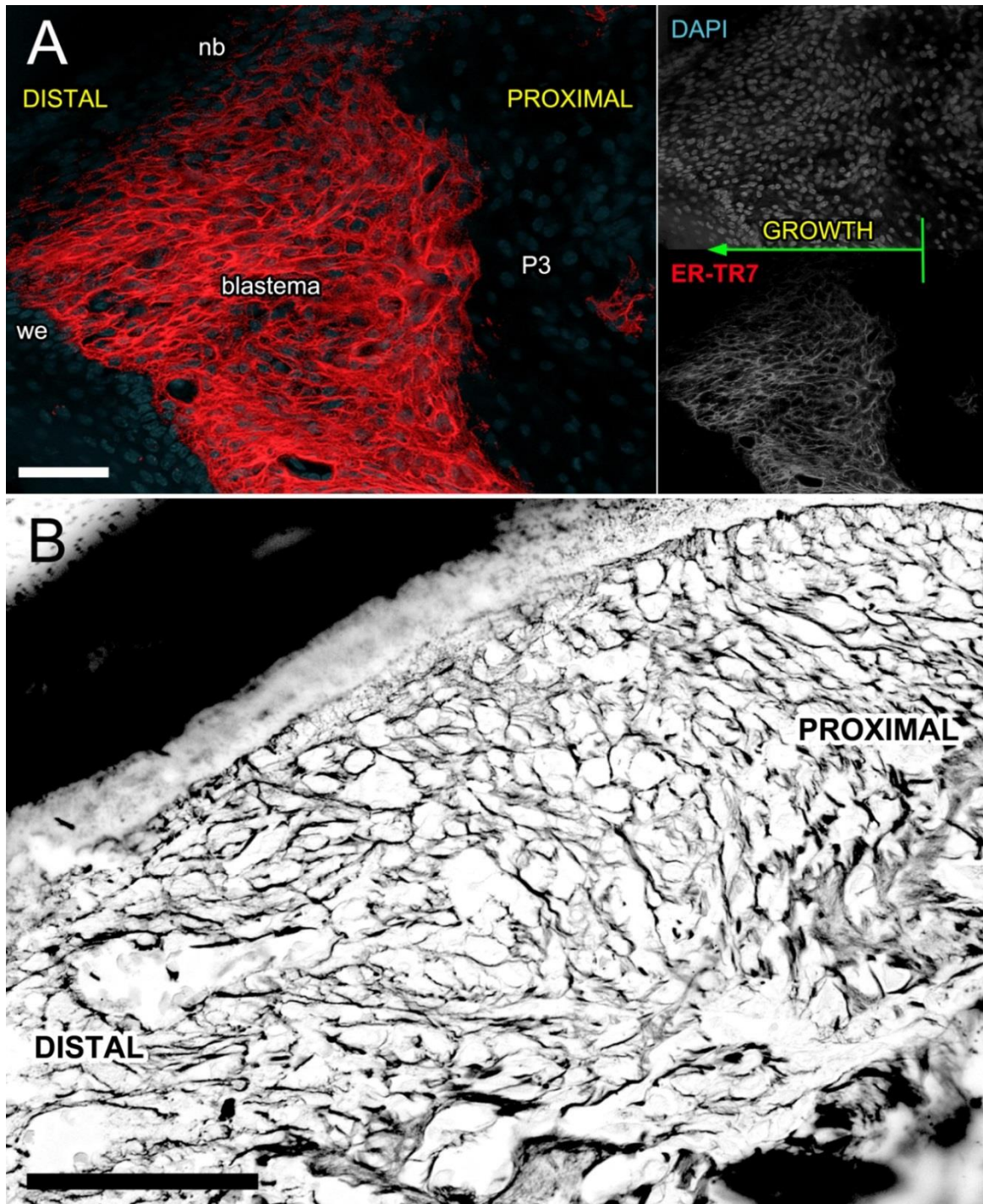


Figure 2.4: ER-TR7 labels an organized network of reticular fibers in the blastema. (A) Following amputation of the neonatal digit tip midway through P3, ER-TR7 is overexpressed in the resulting blastema structure growing distal from the pre-existing phalangeal fragment and underneath the nail bed (nb) by day 8. (A) The 200X projection capture (bar = 50 μ m) of the region stained by indirect immunofluorescence of ER-TR7 (red) and counterstained with DAPI (gray) demonstrates the organization of the ER-TR7+ fiber network. The reticular fibers extend parallel to the proximodistal axis and cell growth is directed towards the wound epithelium (we). (B) The ER-TR7 protein expression in panel A closely

resembles the pattern observed in a serial section stained with the Gomori silver impregnation technique for reticular fibers under 400X brightfield microscopy (bar = 50 μ m).

ER-TR7+ cells are growth responsive particularly around the blastema stage

Differential regulation of cell proliferation and death are typically observed in any injury response. We carried out a quantitative analysis of cell division and apoptosis during neonatal digit tip regeneration using immunohistochemical localization of Ki67 as a proliferation marker and cleaved Caspase-3 (C3) as an indicator of cell death. Tissues were analyzed at 4-day intervals from the time of amputation (DPA0) to include the wound healing period (DPA4), blastema formation (DPA8), and redifferentiation stages (DPA12 and 16). The data are restricted to the loose connective tissue of the unamputated digit and a similar region plus the blastema of the regenerating digit, and normalized to age matched control unamputated digits (Figure 2.5). There are a number of trends that are evident from the data. First, there is a transient rise in apoptosis during the healing period that returns to baseline levels by blastema formation. The rise in cleaved Caspase-3 expression is largely localized to the amputation wound itself, but is also elevated in the proximal digit mesenchyme as well (Figure 2.5 A). Most of the cells expressing cleaved C3 have condensed nuclei and are morphologically indistinguishable from non-expressing cells. We note that there are cleaved C3 positive cells with distinct tri-lobed nuclei indicative of a granulocyte phenotype. The data indicate that apoptosis during digit tip regeneration is transient and largely restricted to the wound healing phase.

Changes in cell proliferation during the regeneration response are more dynamic. During the wound healing phase there is a relative decrease in Ki67+ cells as compared to unamputated controls that is followed by a dramatic rise during blastema formation (Figure 2.5

A, B). The decline in proliferating cells is coincident with the transient rise in apoptosis and the quantitative increase of proliferating blastema cells is similar to previously published studies on regenerating adult digits (137, 162). Following blastema formation there is a gradual decline in cell proliferation associated with the redifferentiation of digit structures. Even though our observations and measurements were focused on the connective tissue mesenchyme, we must note that the leading edges of the wound epithelium retained Ki67+ nuclei at DPA4 (Figure 2.5 D). We also observed that the bone marrow (BM) region becomes hypercellular and displays a high level of Ki67 expressing cells throughout the regeneration process, particularly around DPA8, (Figure 2.5 E) when compared to day-matched controls.

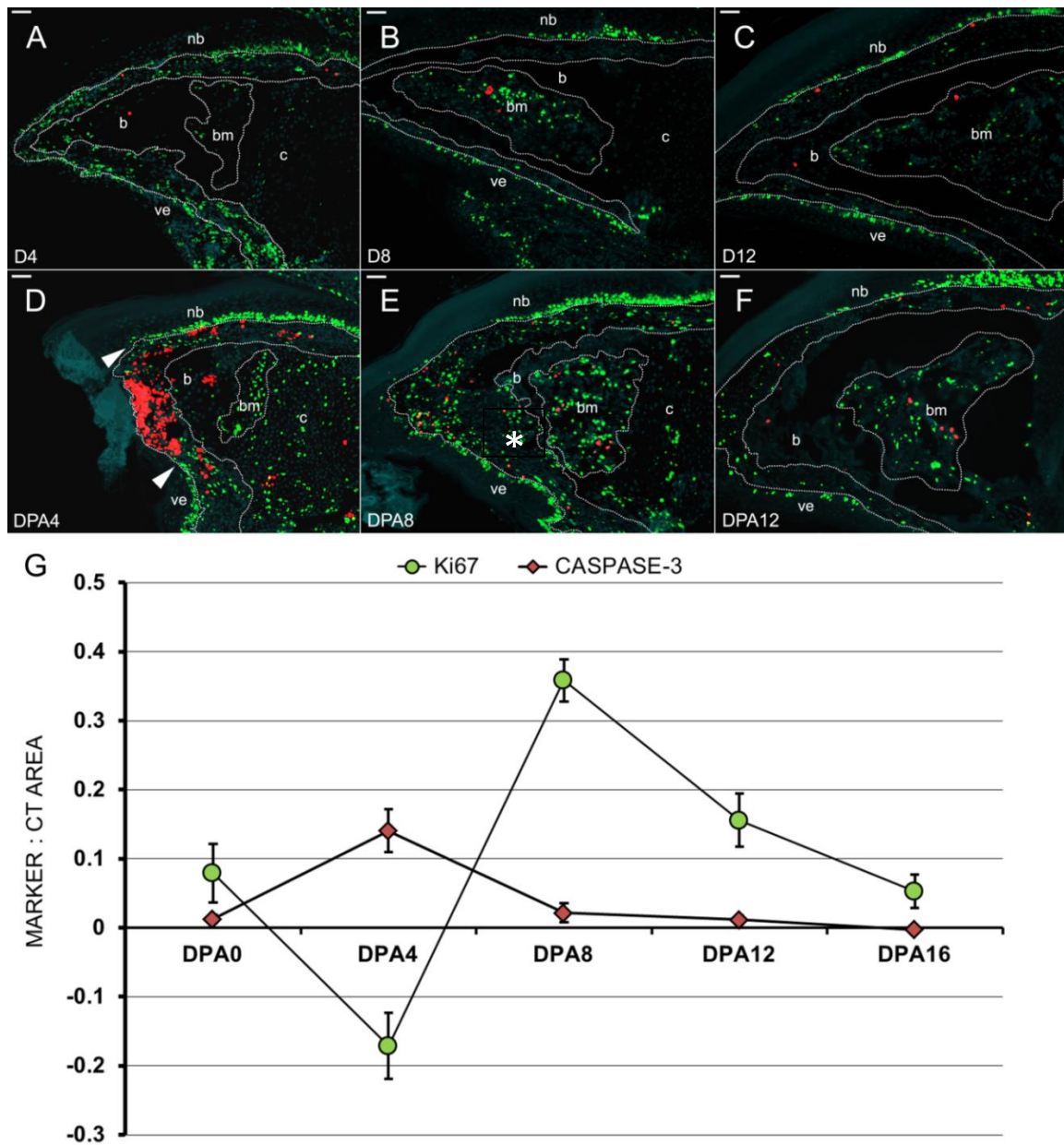


Figure 2.5: The neonatal stages of digit tip regeneration can be defined by upregulation of proliferation around the blastema stage and decreasing apoptosis after the resolution of inflammation. (A-C) Representative control (D0, 4, 8, 12, 16) and (D-F) age-matched amputated digits (DPA0, 4, 8, 12, and 16) were co-labeled with anti-Ki67 (green) and anti-cleaved Caspase-3 (red). Epidermis (e), bone (b), cartilage (c), and bone marrow (bm) are outlined by white dotted lines and bar = 50 μ m. These were discriminated by histological features and anatomical location. Ki67+ and C3+ cells were counted from the mesenchymal area outlined between the basal epidermis and the periosteal/perichondrial layers. (G) The ratios of Ki67+ or C3+ cells to this area were normalized to controls. Data are presented as mean \pm SE (n = 4 per timepoint). Shortly following amputation and by (D, G) DPA4 there is a sharp increase in apoptosis as labeled by cleaved C3. This is especially notable towards the wound epidermis, where damage to the system is more evident. Also at this timepoint, Ki67 staining is below baseline. However, active

proliferation is evident at the (D, white arrows) leading edges of the wound epidermis. (E, G) DPA8 is characterized by growth of the regeneration blastema (white asterisk) and consequentially a significant increase in proliferation in contrast with apoptosis levels reaching baseline. A gradual decrease in proliferation combined with histological evidence of bone formation at the blastema site indicates differentiation and patterning is underway by (F, G) DPA12.

We next addressed the relative proliferation index of ER-TR7+ versus ER-TR7- cells during postnatal digit formation and digit tip regeneration by co-detecting Ki67 and ER-TR7 immunofluorescence of paraffin sections. Regenerating digits were analyzed at DPA 0, 4, 8, 12, and 16 and compared to neonatal stage matched control unamputated digits (PN 3, 7, 11, 15 and 19). This analysis involved direct cell counts of random fields within the connective tissue of unamputated digits and within the connective tissue and blastema of the regenerating digits. Approximately 500 cells were counted per sample. In unamputated control digits the proliferation index steadily declines over the course of this study. At all timepoints the proliferation index of the ER-TR7- subpopulation is significantly higher than the ER-TR7+ subpopulation (Figure 2.6 E). Both subsets display a decline in proliferation rate; ER-TR7- cells decline from 27% at PN3 to 14% at PN19 whereas ER-TR7+ cells decline from 17% at PN3 to 2% at PN19. This study provides evidence that there is a dynamic proliferation profile that is possibly cell type specific during the neonatal development of the mouse digit tip.

During the regeneration response we find that the ER-TR7+ subpopulation of cells at the blastema formation stage appear to be selectively growth responsive (Figure 2.6 C). The proliferation index of the ER-TR7+ cells initially declines from 18% at the time of amputation in parallel with unamputated control digits to 8% during wound healing, but then increases to 28% by the blastema formation stage. At this time (PN 11), control unamputated digits display a labeling index of 5% so the regeneration response is associated with a greater than 5-fold increase in FRC proliferation. This labeling index declines to less than 5% during the

redifferentiation phase, and this level is not statistically different than stage matched unamputated control digits. The ER-TR7⁻ cells display an initial decline in labeling index from 28% at the time of amputation to 20% during wound healing (Figure 2.6 D). This similar decline in the labeling index of stage matched unamputated control digits is also observed. During blastema formation the ER-TR7⁻ cells display a subtle, 1.5-fold increase in labeling index to 25% and this elevated labeling index is maintained during early redifferentiation (DPA12) before it declines to stage matched unamputated control levels by DPA16. The results indicate that a large number of both ER-TR7⁺ and ER-TR7⁻ cells are proliferating during the regeneration response, however there is a dramatic growth response by the ER-TR7⁺ FRCs. Since the ER-TR7⁻ subpopulation of cells is heterogeneous (e.g. endothelial, osteoblastic, ER-TR7⁻ fibroblasts) we cannot determine at this time whether there are additional cell types that display a similar proliferative response.

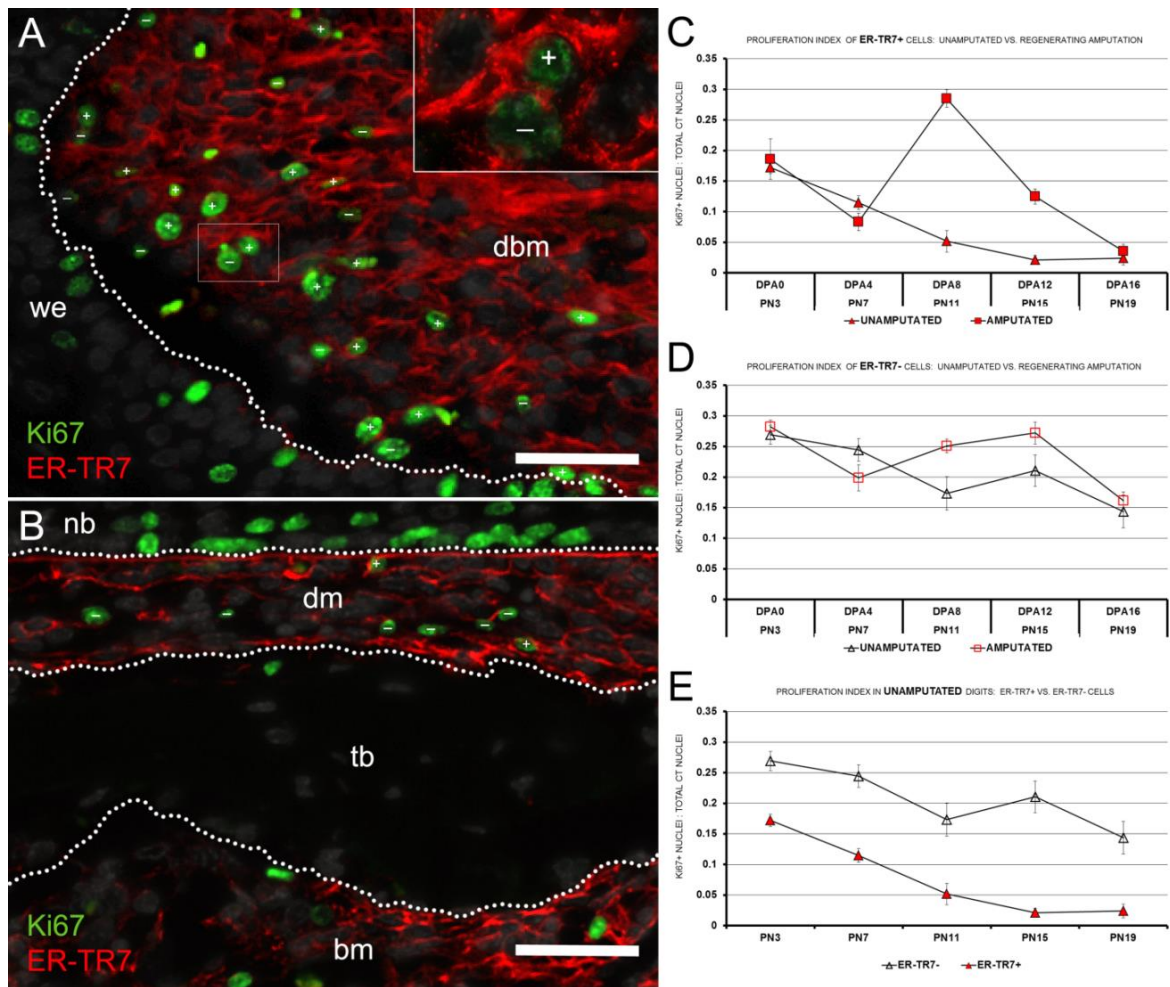


Figure 2.6: Quantitative analysis of Ki67+ and ER-TR7+/- coexpression in regenerating digit tips with post-natal (PN) day-matched unamputated controls at selected days post amputation (DPA) provides evidence that ER-TR7+ FRCs are growth responsive. A total of 500 cells were counted from random fields restricted to the dorsal mesenchyme (dm) or distal blastema mesenchyme (dbm) of controls and regenerates, respectively. These areas are restricted by the nail bed (nb) of the control or wound epidermis (we) of the amputated digits and the trabecular bone (tb) of the P3 phalanx. The bone marrow (bm) was excluded from these analyses. Proliferating (Ki67+) cells were grouped by ER-TR7+ or ER-TR7- expression. ER-TR7+/Ki67+ or ER-TR7-/Ki67+ cell nuclei are labeled with (A, insert) white + and - signs, respectively. (A) In the regeneration blastema at DPA8, there is a significant increase in proliferating cells and most of these cells are ER-TR7+ FRCs (bar = 50 μ m). When compared to (B) age-matched unamputated control connective tissue mesenchyme regions, there is a general decrease in proliferation with both ER-TR7+ and ER-TR7- cells indices significantly lower than in the blastema mesenchyme (bar = 50 μ m). However, (E) the ratio of proliferating ER-TR7- cells to ER-TR7+ cells in the control remains higher throughout all timepoints. Data were segregated by index of proliferation comparison between (C) ER-TR7+ cells in unamputated and regenerating digits; (D) ER-TR7- cells in unamputated and regenerating digits; and (E) ER-TR7+/- cells in unamputated controls. Data are presented as the mean \pm SE (n = 4 per group). (C) The overall ratios indicate a surge in proliferation activity after 8 days of amputation. The mature blastema is evident during this timepoint and expression of Ki67 is the highest in ER-TR7+ cells, thus providing evidence that one of the hallmarks of the regeneration response following an amputation

is expansion of FRCs. (D) ER-TR7- cell proliferation increases shortly after the blastema stage at DPA8 and is concurrent with early redifferentiation and patterning characterized by a more heterogeneous cellular microenvironment. (C) Proliferation at this tissue level is dynamic over the course of development and gradually decreases as the system matures. Overall, a significant portion of dividing cells are ER-TR7-, indicating a population specific expansion.

ER-TR7 can be induced in fibroblast cell lines.

In order to further explore the fibrillar network identified by ER-TR7 immunolocalization *in vivo*, we investigated whether the same ER-TR7+ network could be induced in immortalized and primary fibroblast cell lines. A previous study by Katakai et al (2004) established lymph node stromal cell lines and demonstrated that the ER-TR7+ framework could be induced by treatment with tumor necrosis factor (TNF α) in combination with an agonistic antibody to lymphotoxin-receptor (LT β R) and this induction occurred in a nuclear factor kappa-light-chain-enhancer of activated B cells (NF- κ B) pathway-dependent manner. We used an identical strategy to stimulate NIH-3T3 cells. Cultures of NIH-3T3 cells are minimally reactive to the ER-TR7 antibody (Figure 2.7 A). In the uninduced state, the antigen was detected in a small region of the cytosol close to the nucleus of a small number of cells. However, following treatment with 100 ng/mL of recombinant TNF α and 5 μ g/mL of anti-LT β R, the cultures produced membranous and extracellular ER-TR7+ fibrils which formed a loose network between cells (Figure 2.7 B). The ER-TR7+ network was not uniformly distributed in the culture, but was associated with densely packed cell aggregates that displayed prominent intercellular expression and intense peripheral staining (Figure 2.7 F). ER-TR7 was mostly detected within these aggregates, which increased in size over the induction timeline of 10 days. Not only did the high treatment frequency facilitate aggregate formation with increased ER-TR7 fibril accumulation as shown here and in previous studies (88), but it also promoted a similar response as the reagent concentration was increased (Figures 2.7 C-E). Incubation of 3T3 cultures with half, one, and double the dose of TNF α and

anti-LT β R within the same time period induced changes in aggregate mass and ER-TR7 densities directly correlating with dose and without an adverse effect to the culture. In other words, doubling the induction dose for the same treatment period enhanced the production of the ER-TR7 antigen by 11%.

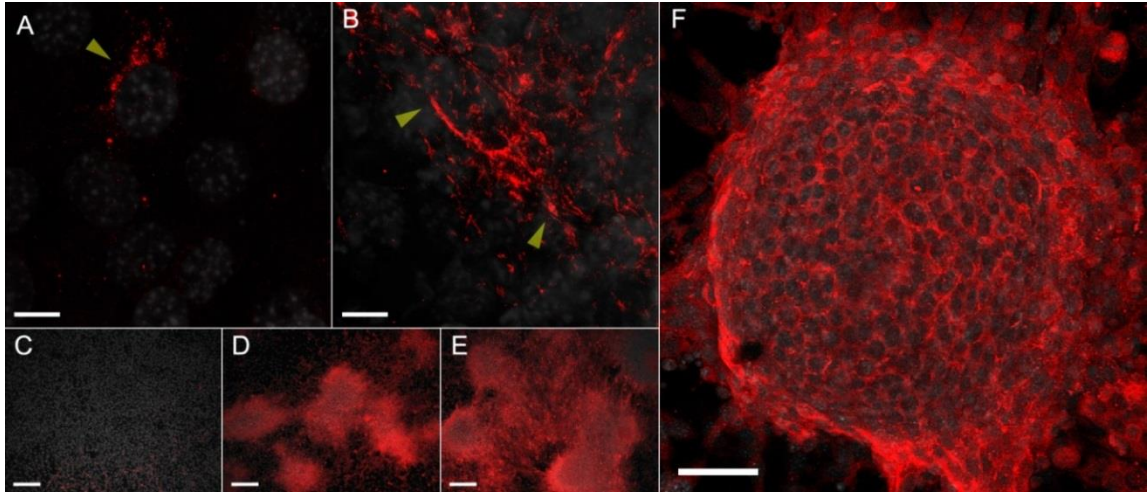


Figure 2.7: NIH-3T3 cells can be manipulated to synthesize and secrete ER-TR7+ microfilaments. (A, B) Confocal microscopy at 1000X magnification (bar = 10 μ m) of uninduced and treated 3T3 cultures demonstrate that (A) a fraction of control NIH-3T3 cells co-stained by indirect immunofluorescence of ER-TR7 (red) and DAPI (gray) express intracellular ER-TR7+ antigen only but can be (B) induced to produce the ER-TR7+ fibrillar network by co-treatment with 100 ng/mL of recombinant TNF- α and 5 μ g/mL of an agonistic antibody against LT β R. (C-E) 3T3 cells were co-incubated with a (C) half, (D) one, and (E) double the dose of induction reagents throughout the 10 day period, labeled with ER-TR7 (red) and imaged at 100X (bar = 100 μ m) magnification to provide evidence of aggregate and protein content changes consistent with a dose-dependent response reported as mean \pm SE (n = 8) fluorescence intensity values of (C) 682.5 \pm 42.9, (D) 880.3 \pm 57.3, and (E) 978.4 \pm 25.5. Regardless of induction time and reagent concentration, the ER-TR7+ extracellular fibrils were never organized in this cell line. (F) Following confocal imaging at 200X (bar = 50 μ m) and optical sectioning over the z-plane of these aggregates and surrounding area increased ER-TR7 expression was found to be prominently and almost exclusively localized to the dense cell aggregates which spread within the horizontal (xy) but also towered over the vertical (z) axis.

Cells derived from the blastema retained membranous and extracellular ER-TR7 fibril formation for one week after isolation for *in vitro* analysis (Figure 2.8 A). The shape of blastema cells during this period ranged from spindle to stellate shape containing large nuclei with

prominent nucleoli. But mostly they were characterized by interconnecting filaments reactive to the ER-TR7 antibody. Since fibroblastic cells derived from the terminal phalanx (P3) of adult mice under normal conditions have been shown to participate in blastema formation (162), we decided to test ER-TR7 induction on this cell line. In order to better characterize cellular morphology, organization, and changes with respect to the treatment, The P3 cell line was derived from the terminal phalanges harvested from mice expressing enhanced green fluorescent protein (eGFP) (Figure 2.8 B). Untreated P3 fibroblast cultures displayed random cells that produced ill-defined ER-TR7+ fibers (Figure 2.8 C-E). Most of these control or uninduced cells portrayed a spindle phenotype with medium sized nuclei and generally grew parallel to each other in confluency to form sheets. However after $TNF\alpha$ /anti-LT β R treatment (Figures 2.8 F-H) many of the cells favored a stellate morphology with larger nuclei and positioned themselves at an angle or perpendicular with respect to one another. In agreement with the progression of treatment and what was reported by Katakai et al. (2004), the ER-TR7 fibrils between these cells grew more intense while maintaining a loose but organized network throughout the culture. At the endpoint of treatment, the induced P3 culture was less cellular than control but the ER-TR7 staining pattern was well-defined and uniform, thus differing from the cell aggregates which progressively formed in NIH-3T3 cultures (Figures 2.7 D-F). Nevertheless, both cell lines could be induced to form the ER-TR7+ network of fibers *in vitro*.

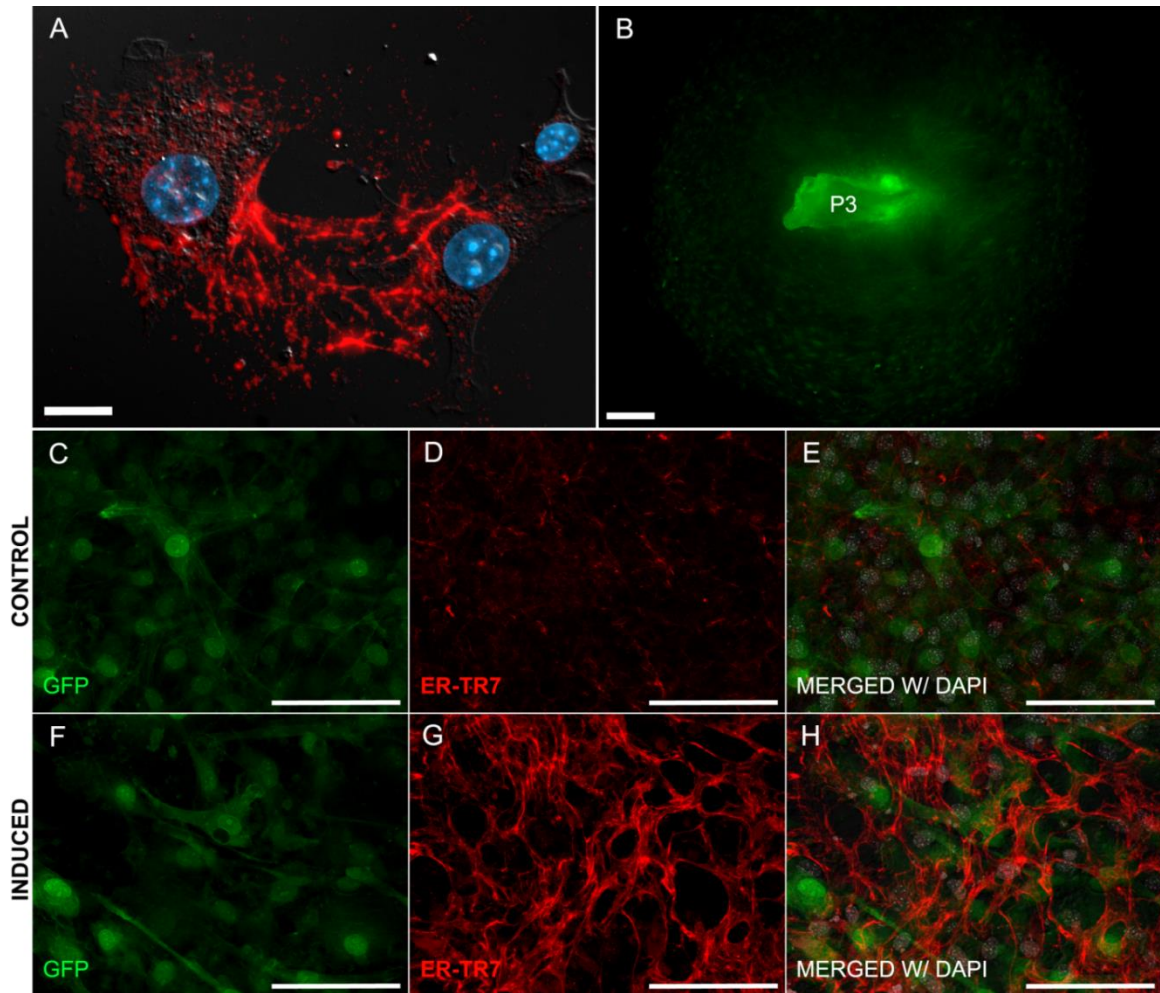


Figure 2.8: Similar to freshly plated blastema cells, primary fibroblastic cells isolated from the P3 phalanx synthesize the ER-TR7 framework in a pattern that resembles the blastema *in vivo*. (A) Blastema cells retain ER-TR7+ expression (red) shown as membrane-bound and intercellular fibrils for up to one week following isolation. Co-staining with DAPI illustrates the nuclear features of these cells while superimposition of differential interference contrast outlines the overall stellate morphology of the cells (630X; bar = 10 μ m). (B) Imaged by stereomicroscopy (bar = 50 μ m), adherent fibroblastic cells (green halo) migrate from a P3 phalanx source harvested from an adult GFP+ transgenic mouse. The GFP label makes cellular features, organization, and changes more prominent as the induction treatment progresses. (C-E) The isolated P3 cells were split into (C-E) untreated control and (F-H) induced line. (C, E) Representative 400X field (50 μ m bar) of control shows a hypercellular culture with cells containing medium sized nuclei (stained with DAPI) growing in parallel. (D) The ER-TR7 (red) expression in controls ranges from focal diffuse at the extracellular level to scarce and ill-defined fibrils extruding from the membrane of some isolated cells. (F, H) The induced population was characterized by cells with stellate appearance and large nuclei. (G) ER-TR7 content following $\text{TNF}\alpha$ /anti-LT β R treatment for 10 days is abundant. Fibrils bundles are dense yet form a loose network with “honeycomb” organization.

Using the induction of ER-TR7 we employed a RT-PCR array to analyze expression of 84 key genes associated with mouse fibrosis (163). Gene expression was analyzed from RNA extracted from lysates of NIH-3T3 and P3 fibroblasts at days 4, 7, and 10 following induction with $\text{TNF}\alpha$ and anti-LT β R. Using the manufacturer's recommended restrictions for analysis and a >2-fold change in expression, we identified 5 genes that were down-regulated and 12 genes that were up-regulated in NIH-3T3 cells at all timepoints (Table 2.1). For P3 fibroblasts, the same array analysis identified 4 down-regulated genes and 4 up-regulated genes at all timepoints. Of particular interest is that there were only 2 genes that were reasonably upregulated in both cell lines at all timepoints and they were *NFkb1* and *Col3a1*. Up-regulation of *NFkb1* was predicted since recombinant $\text{TNF}\alpha$ coupled with anti-LT β R stimulation of lymphoid FRCs induces ER-TR7 in an NF- κ B pathway-dependent manner and this response is completely abrogated by overexpressing I κ B, a dominant inhibitor of this cascade, via retroviral transduction of the cells (88). On the other hand the up-regulation of *Col3a* provides a potential avenue to explore the specific relationship between ER-TR7 staining and ECM production during digit tip regeneration. We also note that only 2 genes were found to be consistently down-regulated in the 2 cell lines and they were *Acta2* or α -smooth muscle actin (SMA) and *Thbs1* (thrombospondin 1).

Gene symbol	Gene description	Fold change from day-matched untreated control					
		3T3 - day 4	P3 - day 4	3T3 - day 7	P3 - day 7	3T3 - day 10	P3 - day 10
<i>Acta2</i>	actin, alpha 2, smooth muscle, aorta	-5.9053	-7.1602	-3.6647	-2.7416	-4.5433	-3.9313
<i>Akt1</i>	v-akt murine thymoma viral oncogene homolog 1	10.112	530.0556	5.8401	-1.6415	7.8571	1.2527
<i>Bcl2</i>	B-cell CLL/lymphoma 2	8.5623	-1.4641	8.0892	1.3708	10.2959	1.5856
<i>Cav1</i>	caveolin 1, caveolae protein, 22kDa	-5.035	-31.125	-2.0195	-8.4269	-1.9132	-2.9794
<i>Col1a1</i>	collagen, type I, alpha 1	-6.0701	-3.2929	-7.4087	-1.2879	-3.62	-2.0755
<i>Col3a1</i>	collagen, type III, alpha 1	3.1188	2.1487	4.9608	6.2856	5.5558	5.9607
<i>Ctgf</i>	connective tissue growth factor	1.4221	2.0279	2.9814	-11.1193	1.6403	-4.6107
<i>Cxcr4</i>	chemokine (C-X-C motif) receptor 4	-1.2159	-10.1261	2.2284	-2.858	3.7166	-2.7992
<i>Dcn</i>	decorin	1.264	81.0084	8.1455	1957.776	5.5558	7206.0852
<i>Il13ra2</i>	interleukin 13 receptor, alpha 2	4.7174	-3.4105	5.4869	1.2614	2.6463	16.6217
<i>Ilk</i>	integrin-linked kinase	2.0534	-1.5583	2.7818	-2.2423	3.9559	-1.0755
<i>Itga2</i>	integrin, alpha 2 (CD49B, alpha 2 subunit of VLA-2 receptor)	100.9852	75.5835	136.8072	125.801	152.6411	81.8551
<i>Jun</i>	<i>jun</i> proto-oncogene	4.8165	-2.4623	10.6001	1.244	7.1801	1.3519
<i>Nfkb1</i>	nuclear factor of kappa light polypeptide gene enhancer in B-cells 1	4.0222	3.1329	3.1733	4.2736	6.0377	2.2423
<i>Smad7</i>	SMAD family member 7	5.61	3.3013	4.426	1.676	3.9917	3.488
<i>Tgfb1</i>	transforming growth factor, beta receptor 1	8.6219	-2.0139	7.0421	-1.3899	8.718	1.3899
<i>Tgfb2</i>	transforming growth factor, beta receptor II (70/80kDa)	4.2222	-2.2038	4.7437	-1.6301	8.421	1.2879
<i>Thbs1</i>	thrombospondin 1	-4.6332	-7.4643	-2.7397	-2.6299	-6.0461	-3.2154
<i>Thbs2</i>	thrombospondin 2	-3.7373	-17.8766	-3.7947	-4.302	-3.6452	1.1134
<i>Timp3</i>	TIMP metalloproteinase inhibitor 3	-11.4082	-5.0982	-2.5562	1.8596	-2.2439	-1.129
<i>Gapdh</i>	glyceraldehyde-3-phosphate dehydrogenase	1.1775	-1.0472	1.1083	-1.0077	1.1813	-1.0389
<i>Actb</i>	actin, beta	1.5454	1.6472	1.3528	1.6077	1.7339	1.0389

Table 2.1: Selective factors modulated following ER-TR7 induction include upregulation of Col3a1

(COL3) and downregulation of Acta2 (SMA). A mouse gene array consisting of 84 fibrosis-related transcripts was used to analyze modulation of gene expression in 3T3 and P3 cell line lysates following treatment with recombinant TNF α and anti-LT β R shortly after days 4, 7, and 10 of the 10 day ER-TR7 induction treatment period. Listed is the subset of genes that yielded >2-fold change from uninduced control cell values. Overall, only two genes were upregulated in both cell lines: Col3a1 and NF κ B1, thus supporting an association of COL3 with ER-TR7 expression and activation of an NF- κ B dependent pathway throughout induction. Conversely, only two genes were downregulated at all timepoints in both lines: Acta2 and Thbs1. Housekeeping genes are listed below the dotted line.

To determine whether there is a relationship between ER-TR7 and COL3A1 we carried out co-immunohistochemical localization studies in TNF α /anti-LT β R treated NIH-3T3 and P3 cell cultures grown and induced at the same time as the samples for RNA isolation and qPCR. Colocalization analysis based on the Pearson's Correlation Coefficient (PCC or r_p) approach over eight high resolution photomicrographs at 400X magnification from each culture was performed. We have evidence indicating that the trends in localization and intensity level for these two antigens in both uninduced (Figures 2.9 A-C, G-I) and treated (Figures 2.9 D-F, J-L) cell lines were almost identical gauged by our qualitative observations and strong pixel correlation measurements with overall mean r_p values above 0.8 on a scale of 1 (perfect correlation) to -1

(perfect but negative correlation) and 0 equal to no relationship. These data support the conclusion that the ER-TR7 antigen is linked either directly or indirectly to the expression of COL3A1 in digit FRCs.

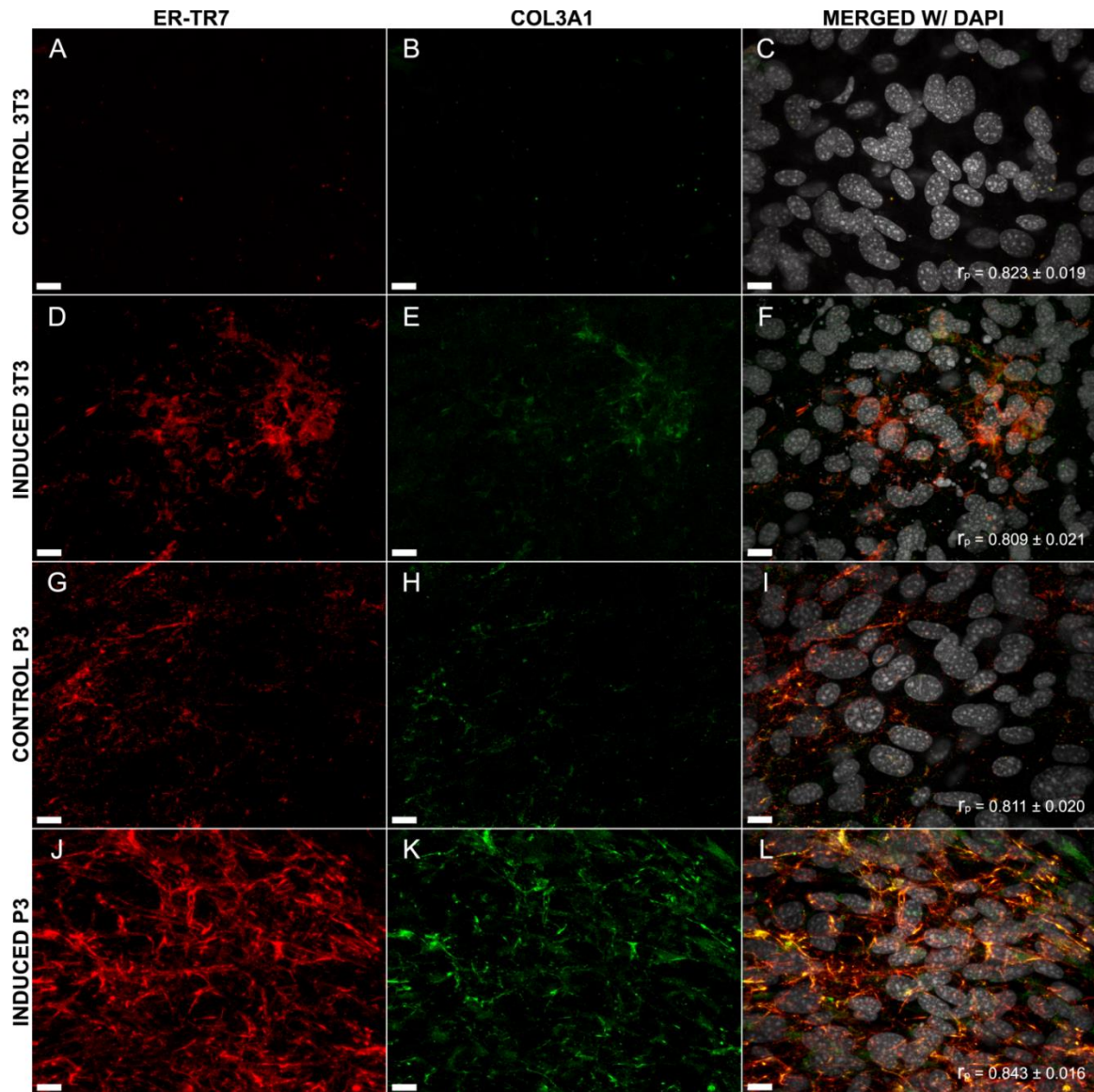


Figure 2.9: ER-TR7 staining correlates with COL3 expression following induction of 3T3 and P3 primary cell lines. (A-L) 3T3 and P3 cells were treated with $\text{TNF}\alpha$ and anti-LT β R over 10 days to stimulate the ER-TR7 network production. At the endpoint of induction, treated cultures and day matched uninduced controls were fixed and co-stained for ER-TR7 (red) and COL3A1 (green) for 2D confocal microscopy imaging at 400X magnification (bar = 10 μm) and colocalization analysis of multiple fields ($n=8$) using a Person's Product Correlation (PPC) calculation (expressed in r_p values \pm SE on merged images). (A-C) Control and (D-F) induced 3T3 cells display the typical ER-TR7 distribution before and after the 10 day

induction treatment with strong correlation between antigens. Although displaying different organization and network engineering dynamics, the colocalization values of P3 cells under either (G-I) control and (J-L) induction circumstances agree with the strongly positive trend between ER-TR7 and COL3A1 in the 3T3 line.

ER-TR7 expression and regulation correlates with COL3+ reticular fibers *in vivo*

To explore the role of fibroblasts in the regeneration response we carried out immunolocalization studies of a number of known fibroblast-specific markers to survey their regulation in unamputated and regenerating digits with respect to the changes observed with regards to ER-TR7 production and organization. We were particularly interested in exploring the relationship between COL3 and ER-TR7 staining based on our *in vitro* studies, so we followed these experiments with co-labeling of ER-TR7 and COL3 on fixed samples of control and amputated neonatal digits. The stained samples were imaged by confocal microscopy and subjected to the non-bias colocalization PCC test applied to the cultured cells. As expected, all sample sets yielded a strong correlation between both antigens, with mean r_p values of 0.845 ± 0.024 and 0.825 ± 0.011 for day 8 control (Figures 2.10 A-D) and amputated (Figures 2.10 E-H) digit tips, respectively, thus serving as supporting evidence that regulatory mechanisms of ER-TR7 and COL3 expression in the regenerating digit are linked.

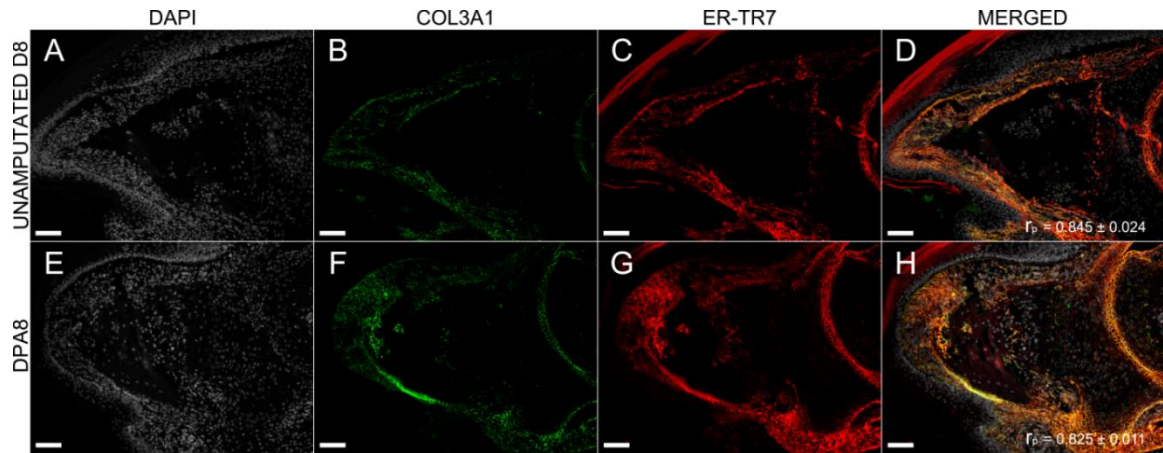


Figure 2.10: ER-TR7 and COL3 signals in control and regenerating digits yield strong correlation measurements in agreement with *in vitro* experiments. Individual fluorescence channels of representative (A-C) unamputated control and (E-G) regenerate at day 8 were co-stained for (A,E) DAPI (gray), (B,F) COL3 (green), and (C, G) ER-TR7 (red) to confirm correlation of the antigens *in vivo* as measured by PCC-based analysis with mean \pm SE values ($n = 4$) shown on corresponding (D,H) merged channel images (bar = 50 μ m).

Since we observe a measured correlation between ER-TR7 and COL3 regulation during regeneration, we decided to investigate if other markers relevant to FRCs and/or proven to be co-regulated with COL3 had a similar relationship with ER-TR7 expression in our model and whether they follow its trend in upregulation. Unfortunately, a majority of these antigens could not be co-incubated on the same sections with ER-TR7 due to conflicting tissue pretreatment requirements. Therefore in these studies, immunolocalization of fibroblast associated markers was carried out in serial paraffin sections of unamputated digits and regenerating blastemas to screen for similarities to the ER-TR7 and COL3 staining patterns (Figures 2.11 A-D, G-H, and Q). A specific area of the dorsal connective tissue mesenchyme from both control and regenerating samples harvested at day 8 was captured at 400X magnification for quantitative analysis based on ratios between each marker and total tissue area housing these proteins (Figure 2.11). Representative serial fields between all markers included the dorsal connective tissue or blastema mesenchyme (dm or dbm), nailbed epithelium (nb), and underlying trabecular bone

(tb) for control (Figures 2.11 C, E, G, I, K, M, and O) and regenerating (Figures 2.11 D, F, H, J, L, N, P). Aside from ER-TR7 and COL3, the panel of markers included Collagen 1a1 (COL1), Fibronectin (FN1), Fibroblast-specific protein 1 (FSP-1), Podoplanin (GP36), and Vimentin (VIM).

VIM is a cytoskeletal protein present in most cells derived from the embryonic mesenchyme such as fibroblasts. Its main function is to provide structural integrity to tissue layers which is the case for most intermediate filaments (164, 165). VIM has been shown to be non-critical for progression of normal development although transgenic VIM knockout mice have been shown to experience inadequate wound healing due to impaired fibroblast contractile function (164). Since VIM is ubiquitously expressed by all cells derived from the mesoderm such as connective, vascular, cartilage, and bone tissue (165), we decided to use it as a housekeeping protein in this assay. VIM abundantly immunolocalized as ultrastructural filaments in the cytosol of all digit cells within the normal connective tissue mesenchyme (Figure 2.11 O) in addition to most non-epithelial or connective tissue digital regions including the phalanx, joint, bone marrow, vascular endothelium, and Langerhans cells of the epidermis. VIM expression in regenerating digits (Figure 2.11 P) increased in unison with the overall connective tissue area as the dorsal blastema mesenchyme expanded, so no significant changes in ratio of marker to connective tissue area were recorded when compared to controls (Figures 2.11 O,P, and Q).

To discriminate the fibroblast population from other VIM+ cells and at the same time screen for changes in regulation of proteins exclusive to fibroblasts such as ER-TR7, we decided to include FSP-1 in our panel. FSP-1, also known as S100A4, belongs to the S100 superfamily of calcium-binding proteins. By subtractive and differential mRNA hybridization, FSP-1 was originally classified as a gene expressed in fibroblasts but not epithelial cells and therefore used

as a marker of epithelial cells undergoing transdifferentiation during epithelial-mesenchymal transition (EMT) events (166). Although mostly expressed at the intracellular level, FSP-1 is also secreted to act as a ligand to an unknown cell surface receptor (167) to promote metastasis (168) and angiogenesis (169) in some neoplasms; regulate apoptosis (170); and induce EMT (166). Moreover, FSP-1 has been found to be expressed and secreted by cell populations other than fibroblasts in normal tissue including macrophages (171), lymphocyte subsets (172), endothelium (173), and smooth muscle cells lining vessels (174) possibly due to potential cross-reactivity of its antibodies to homologous members of the S100 family. Expression in the digit localized to the cytosol of most connective tissue cells including scattered fibroblasts and those lining vessels; macrophages; osteoblasts surrounding the phalanx; and endothelial cells in the lumen of blood vessels in both control and blastema regions (Figures 2.11 K,L). We were unable to observe any differences between extracellular FSP-1 staining between controls and amputated samples. Even though the FSP-1+ fibroblast population gradually increases at the onset of blastema growth, changes from its ratio to connective tissue area compared to control remain insignificant (Figure 2.11 Q) since the connective tissue space grows in tandem with the expanding fibroblasts. Therefore in the context of the regeneration area, FSP-1 only serves as a marker of increased cellularity and due to its non-specificity to FRCs it only resembles a VIM+ type of staining.

In search for additional FRC specific markers to match with ER-TR7+ pattern and regulation, we further dissected studies on stromal contribution to lymphoid dynamics and decided to examine mouse gp38. This transmembrane glycoprotein is also known by different names depending on the cell source where it was extracted from: osteoblasts (OTS-8) (175); kidney podocytes (podoplanin) (176); type I pneumocytes (T1alpha) (177); and peripheral lymphoid tissue from human (gp36) and mouse (gp38) (178, 179). Therefore, depending on the

particular immunogen used to generate the antibody, homologs of this protein could be detected in the ciliary epithelium of the eye, kidney podocytes, alveolar lung cells, osteocytes, osteoblasts, and lymphatic endothelium (180, 181). The gp36/gp38 variant, which is what the antibody we used targets, has been associated with FRCs and/or co-labeled with ER-TR7 only at the lymphoid level (88, 93, 180, 182). In addition to coordination of lymphoid compartment organization from the adjacent stromal layer in several organs (88, 182), it has been characterized in the lymphatic endothelium and demonstrated to have a role in adhesion, migration, and tube formation of lymphatic vasculature in both normal and neoplastic tissue (93, 180, 182, 183). In the non-lymphoid model of the mouse digit tip we found no significant difference between control connective tissue (Figure 2.11 M) and regeneration blastema (Figure 2.11 N). In fact, the expression of gp38 was the most limited in comparison to the other markers. It was diffuse but restricted to the area between the stratum basale and the papillary dermis of the nail bed region (Figure 2.11 M; white arrow) with low cytosolic expression in a low percentage of fibroblastic cells. The strongest staining was observed in osteoblasts lining the periosteum of the P3 trabecular bone (Figure 2.11 M, N; yellow arrows), which indicates that in addition to gp38, the antibody also targets the originally characterized OTS-8 gene homolog (175) of this glycoprotein.

So far we had performed analysis on a subset of fibroblast related markers that seemed to be mostly geared towards portraying an increase in the fibroblast population in the regenerate with the exception of gp38. Even though these proteins may have a role in fibroblast cell structural and motility dynamics during regeneration, the evidence suggests a trend in their expression, localization, and specificity that does not directly correlate with the intracellular and extracellular pattern of ER-TR7 regulation before and after an amputation injury. Therefore we thought about adding to the immunolocalization studies secreted factors

in comparison to ER-TR7 which are well known to contribute to extracellular matrix composition and function during injury repair such as FN1 and COL1 to the previously measured COL3 co-expression study.

FN1 is a glycoprotein secreted by a variety of cell types, mainly fibroblasts, which interacts with fibrin to promote platelet aggregation during clot formation at the early stages of wound healing (184) (158, 185) but also factors into modulation of cell adhesion (186), proliferation (187), migration (188), and apoptosis (189). At the granulation and later stages of tissue repair, the three-dimensional FN1 structural assembly serves as a fundamental building block of the ECM. It has been shown to regulate both composition of the ECM (190) and deposition of macromolecules such as COL1 and COL3 (191-193). Some studies of granulation tissue have demonstrated co-expression of FN1 fibrils with COL3 bundles, otherwise known as reticulin (158). Since ER-TR7 and COL3 had a high correlation of expression, we predicted that FN1 may follow a similar trend in amount of staining of the digit samples. FN1 staining in control digits was diffuse but prominent at the papillary level of the connective tissue (basement membrane) below the stratum basale of the epidermis (Figure 2.11 I, white arrows), which has been previously described (194, 195), and in a layer over the osteoblasts lining the periosteum of P3 (Figure 2.11 I, yellow arrow). These areas are consistent with a larger accumulation of FRCs within the connective tissue mesenchyme layer under normal conditions as we described earlier (Figures 2.1 and 2.2). In between these areas of substantial FN1 staining, we detected isolated cells and focal areas with mild positivity that may have corresponded to fibroblasts outlining endothelium. Following amputation (Figure 2.11 J) a similar blastema area corresponding to the region captured from control exhibited profuse, homogeneous staining throughout, with many of the occupying cells expressing FN1, thus significantly increasing the ratio of FN1 to connective tissue mesenchyme by nearly a 10% mean (Figure 2.11 Q). This

indicates that even though the FN1+ pattern does not correlate with ER-TR7+ fibrils, it is co-expressed around the same regions where ER-TR7+ FRCs are housed and regardless of tissue area expansion, its expression is upregulated in the blastema. This is consistent with wound healing studies showing that during repair, specifically at the granulation stage of wound healing, FN1 is upregulated (14, 22, 55, 158, 196-198).

Along with COL3, COL1 is a fibril-forming collagen mainly synthesized and secreted by connective tissue fibroblasts. It is the most abundant structural protein in higher vertebrates and is found in extensible and non-extensible connective tissue of many organs, tendon, and the organic portion of bone. Many studies have concluded that COL1 fibers can vary in size depending on organ type; throughout development; and during wound healing and in general correlate thinner fibers to less distensible tissues; younger age; and injuries at a stage when they have the least tensile strength (199, 200). It has also been documented that COL3 can copolymerize with COL1 fibers and thus regulate their diameter (78). During embryogenesis, for example, it has been found that the ratio of COL3 to COL1 is higher than in adult organisms and also inversely proportional to the diameter of collagen fibrils (76, 201). This ratio is also very dynamic during wound healing with a higher COL3 to COL1 value around the proliferative phase which then reverses within scar (29, 71, 74, 202). In the unamputated digit, anti- COL1 localizes to the entire bone structure and is moderately expressed in the cytosol of fibroblasts and as extracellular fibrils throughout the connective tissue around it (Figures 2.11 E). Its expression is relatively homogeneous throughout. The corresponding dorsal in the day-matched blastema also shows moderate staining in the cytosol of fibroblasts but the extracellular fibers, although homogeneously spread, are overall thinner than those in the control digit connective tissue (Figure 2.11 F). This observation is consistent to previous findings with regards to smaller COL1+ fibril diameter in areas co-expressing COL3. Taken together, even though COL1 is highly

expressed in the blastema mesenchyme, the difference in ratios of COL1 expression to total connective tissue area between control and blastema soft tissue is insignificant due to larger COL1+ fibrils occupying less connective tissue area in the control and a larger amount of smaller fibrils occupying more total blastema area in the regenerate (Figures 2.11 E-F, Q). Incidentally, COL1 is co-expressed within the location range of ER-TR7 and COL3 staining. However, the similar expression patterns of ER-TR7 and COL3 do not match the anatomical immunolocalization of COL1 and its uneven fibrillar arrangement between control and amputated digits.

Of the marker proteins that show prominent staining in the blastema, most of the fibroblast-related proteins displayed quantitatively similar levels of staining when comparing the connective tissue of unamputated control digits to regenerating digits at the blastema formation stage, whereas ER-TR7 staining displayed a significant enhancement during regeneration (Figures 2.11 B, D). Quantitation of the ratio of protein expression of the various markers versus connective tissue area revealed that COL3 and FN1 share overexpression dynamics with ER-TR7 (Figures 2.11 C-D, G-J, and Q). These data provide further evidence that the ER-TR7 antigen and COL3 are similarly regulated during postnatal digit development and digit blastema formation. In addition, these data suggest interplay between ER-TR7, COL3, FN1, and COL1 in a bed of VIM+/FSP-1+ FRCs with positive coexpression of COL3 and ER-TR7 in amount and spatial arrangement; a positive correlation with FN1 potentially facilitating their overexpression in the blastema based on previous studies; and a negative proportionality with respect to the size of COL1+ fibrils and the amount of COL3 and ER-TR7 macromolecules.

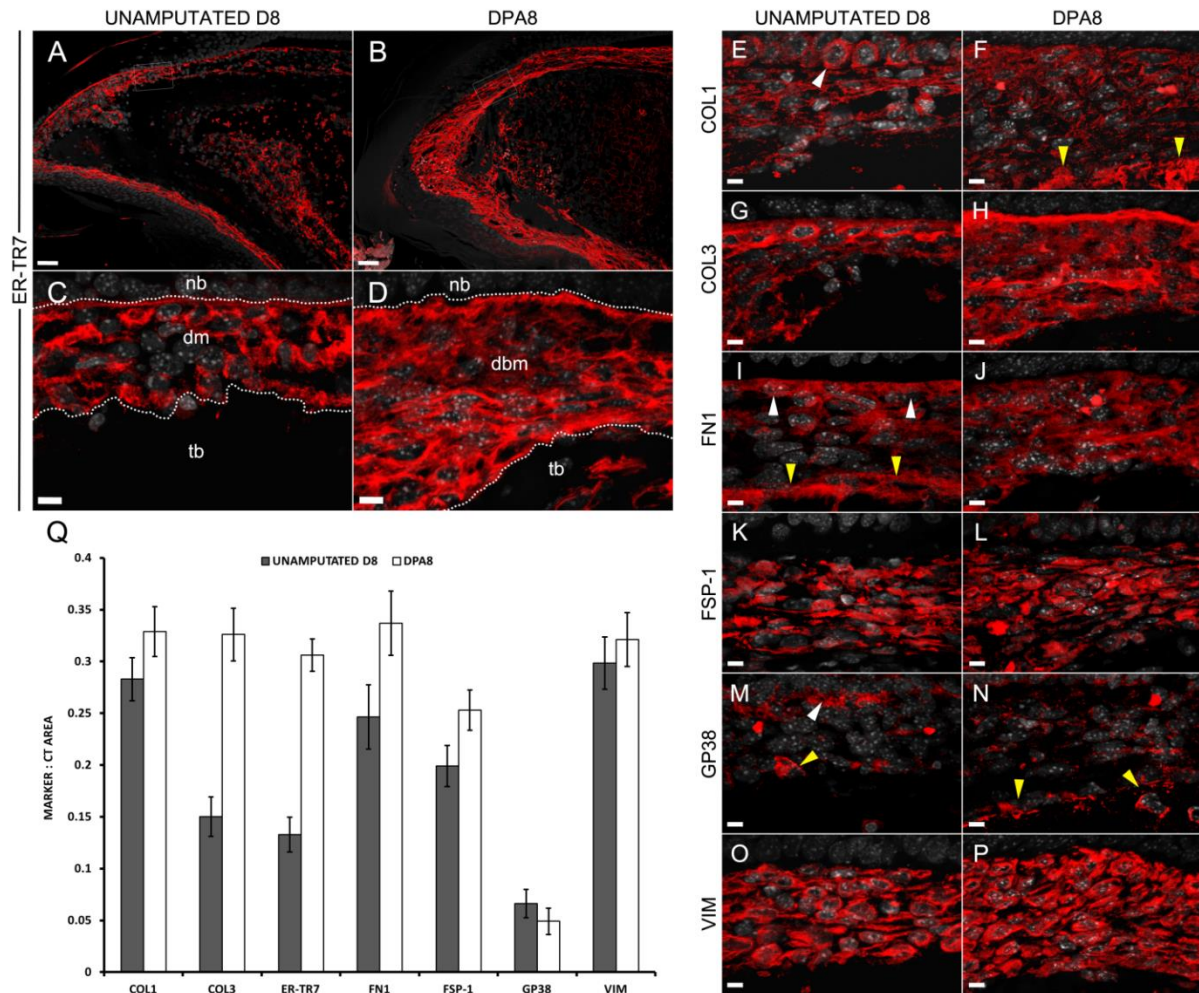


Figure 2.11: ER-TR7 is co-regulated with COL3 and FN1 in control and regenerating digits but only COL3 mimics its expression pattern. Various antibodies against macromolecules and cytoskeletal proteins relevant to injury response from fibroblasts were tested on serial sections of day 8 (A, C, E, G, I, K, M, and O) unamputated control (D8) and (B, D, F, H, J, L, N, P) amputated digit tips (DPA8). The targets were labeled by indirect immunofluorescence using a secondary antibody conjugated to Alexa 594 (red) followed by DAPI counterstaining (gray). At 100x magnification, (A) unamputated controls and (B) regenerating digits express a dynamic regulation of the ER-TR7 antigen with an increase in staining particularly at the blastema site (bar = 50 μ m). Regions between the trabecular bone (tb) of P3 and the nailbed (nb) (white outlined rectangle on A-B) were captured at (C-P) 630x magnification (bar = 10 μ m) for analysis of pattern and localization in addition to (Q) non-biased quantitation of marker expression per total connective tissue area (n=3 per marker). Representative images from the dorso-distal portion of the samples, there is (Q) significant upregulation of ER-TR7 (D) at the dorsal blastema mesenchyme (dbm) when compared to (C) the control dorsal mesenchyme (dm). The discreet ER-TR7 staining in the (A, C) controls mostly outlines vessels and basement membranes as opposed to the (B, D) regenerate, which shows a ubiquitously dispersed network between blastema FRCs. Regardless of these differences, the size of ER-TR7+ fibers remains unchanged. The only two markers that show direct co-regulation with ER-TR7 are (G-H) COL3 and (I-J) FN1 consistent with our *in vitro* and *in vivo* co-expression analysis and the fact that FN1 has been linked to upregulation at sites of fibroblast accumulation and collagen deposition

during injury repair, respectively. However, COL3 regulation and spatial fibrillar expression in both (G) control and (H) blastema is nearly identical to ER-TR7. On the other hand, although (Q) FN1 is significantly upregulated in the regenerate its staining is (J) diffuse at the dbm and (I) below nailbed keratinocytes (white arrows) and over the periosteum (yellow arrow) in controls. We found no significant difference in (Q) COL1 regulation between (E) control and blastema (F) mesenchyme other than an overall decrease in the size of its fibers in the regenerate. This indirect regulation is consistent with cited evidence indicating that COL3 co-polymerizes with COL1 fibers thus limiting an increase in their diameter. The smaller but expanded expression of COLI+ fibers in the (F) blastema makes COLI quantitation proportional to the otherwise thicker but more limited COLI+ fibrils in the (E) unamputated samples. Based on fibril diameter alone, the expression of COLI does not resemble that of ER-TR7. Furthermore, in disagreement with ER-TR7 and COL3 expression, COLI staining is heavily localized to the (F) P3 bone (yellow arrow). Since GP38 has been implicated in co-existence with the ER-TR7 antigen, we decided to also detect and measure its expression under these circumstances. GP38 staining mostly exists around isolated fibroblasts throughout the mesenchyme and at the base of the nailbed in both (M) dorsal control and (N) blastema mesenchyme. Its minimal expression, localization, and (Q) insignificant difference between groups makes it ineligible for pursuing a direct correlation with ER-TR7. (K-L) FSP-1 and (O-P) Vimentin were also analyzed and provide evidence that these proteins are expressed on a bed of cells derived from the mesoderm. Since FSP-1 is mostly expressed by fibroblasts as the name implies, we measured a (L, Q) small but significant increase in its ratio with respect to the dbm of the regenerate. This correlates with the evidence that there is an increase in FRCs at the blastema site and thus FSP-1 positive cells must increase compared to (K, Q) control.

2.4 DISCUSSION

We have used the model of neonatal and adult mouse digit tip regeneration to initiate characterization and understanding of the ECM macromolecule dynamics that participate in this type of repair mechanism after amputation. In this study we focused on the antigen ER-TR7 which was initially isolated from stromal cells of the spleen (94). The monoclonal antibody against this epitope targets a specific and infrequent population of fibroblasts which are found within areas containing reticular fibers and thus are denominated fibroblast reticular cells (FRCs) (88, 94, 152, 156, 161). In addition to confirming previous observations about the level specific regeneration response that occurs after digit tip amputation in neonatal and adult mice with regards to proliferation, chemotaxis, angiogenesis, direct ossification, and re-epithelialization dynamics (6, 12, 137, 203-206), we have gained additional knowledge about a key extracellular

matrix component specific to FRCs that may act as a platform for these events. First, we demonstrated that ER-TR7 can be detected in a non-lymphoid microenvironment with an expression pattern consistent with the discreet compartmentalization demonstrated in lymphoid tissue. Consistent with our hypothesis, ER-TR7 is upregulated at the blastema stage of digit tip regeneration, thus indicating an underlying function of the target it labels in facilitating a regeneration competent microenvironment. Second, by applying previous *in vitro* experiments performed on stromal cells of lymphoid tissue (88) to immortalized NIH-3T3 cells and primary fibroblasts derived from the P3 region of the digit, we have demonstrated that non-lymphoid stromal cell lines can be induced to produce an ER-TR7+ network of fibers, and thus its function, in an NF- κ B pathway-dependent. In search for the potential target of anti-ER-TR7, we generated evidence that ER-TR7 staining is positively co-expressed with COL3 fibers after induction *in vitro*, thus providing a base for characterization of ER-TR7 and functional and molecular studies revolving around COL3 regulation from the transcriptional to the post-translational stage in gain and loss-of-function wound models. Also, we have confirmed that the *in vitro* co-expression between ER-TR7 and COL3 can also be observed *in vivo* before amputation and throughout the regeneration process and that this expression is directly or indirectly linked to other markers such as COL1 and FN1 to further convey a correlation between ER-TR7 and COL3 in our model.

The most distinguishing feature of the mouse digit tip model of mammalian regeneration is the blastema structure that arises by day 8 in the neonate and day 10 in the adult. The morphology and arrangement of cells distributed in the mammalian blastema mimic those of the blastema in urodele regeneration models and these cells have been considered to be mostly fibroblastic. Whether at a blastema stage of regeneration or granulation phase of wound healing, fibroblasts along with other cells types in this arrangement must be held by a

connective tissue stroma. Under normal circumstances, this stroma is composed of many ground substances. Our goal was to find a subcomponent of the extracellular matrix that was specific to regeneration competent fibroblasts. So we found ER-TR7 as an ECM antigen that was derived from stromal cells of the spleen denominated FRCs and has been documented to participate in organogenesis of lymphoid organs and contribute to intercommunication between stromal and lymphoid cells. ER-TR7 was detected by indirect immunofluorescence in FRCs prominently outlining structures of the digit including the basement membrane of the skin, the intima of blood vessels, the resting zone of chondrocytes at the joint interphase, and a layer of cells over the periosteum of the phalanx. Since FRCs have been documented to be in direct interaction with other cell populations, especially in lymphoid organs (207), the role of FRCs and ER-TR7 under normal conditions is clearly that of preserving structural integrity and boundaries but other functions cannot be ruled out.

Following amputation, ER-TR7 expression regressed at the early stages of wound healing (i.e. clotting and inflammation) but was progressively upregulated to peak at the blastema stage. At this stage, the ER-TR7 antigen was localized to the membrane of a large population of FRCs which also secreted thin and discreet ER-TR7+ fibers arranged in a loose “honeycomb” pattern following the proximodistal axis of the anlagen. Following the onset of direct ossification of the blastema, or the future site of the regenerated P3, ER-TR7 gradually began to recess to basal levels leading to an endpoint replica of the pre-existing structure with discreetly localized ER-TR7 expression. This phenomenon occurred in both neonatal and adult groups, with the adult being delayed by its more prolonged inflammatory response and additional bone degradation mechanics. Otherwise, there is an overall parallelism in structural mechanics and cellular dynamics between adult and neonatal responses as shown by evidence, for example, of the similarities in bone regrowth following injury of adult and neonatal mouse digits (206). In

the neonatal group and parallel to the expansion of the ER-TR7 meshwork, we furnished evidence of an increase in the proliferation of ER-TR7+ cells around the blastema stage. This is an indication of a possible cell type and growth specific response during the window of regeneration which we would expect in the adult model due to its parallelism with the neonatal response and previous reports (137). In lymph node paracortical regions, FRCs have been shown to shape T and B cell morphology; facilitate their motility; and enable migration into the marginal zone, for example, based on the extent and boundaries of the ER-TR7+ network within and between those areas (151). Furthermore, in the spleen, the ER-TR7 network acts as a conduit for factors in the blood to reach the lymphocytes in periarteriolar lymphoid sheaths to allow for growth and preserve homeostasis (91, 152, 208). Because of its loose nature and transient upregulation at a critical stage of regeneration, it is not unlikely to conclude that, similar to lymphoid tissue dynamics between FRCs and lymphocytes, the network labeled by ER-TR7 in the blastema could be serving as a scaffold that facilitates motility, expansion, and intercommunication of various cell populations.

One of the most distinctive features of granulation tissue formation, or the proliferative phase of wound healing, is the expansion of fibroblasts which have been thought to arise from both resident cells and bone marrow progenitors (209, 210). Similar to this phase, one of the hallmarks of the blastema stage of regeneration in both neonatal and adult models is the proliferation of fibroblasts. So we analyzed the Ki67 index of FRCs (ER-TR7+ cells) in our model to not only demonstrate the temporal specificity of their expansion, but to also show where the proliferation of FRCs takes place. During the neonatal timeline of regeneration, changes in cell survival were expected as measured in the connective tissue mesenchyme expression of the proliferation marker Ki67 and the cleaved form of the apoptosis enzyme C3. Cell death was limited to the initial stages of wounding, specifically around the inflammatory phase, prior to the

overexpression of ER-TR7. An initial increase in C3 activity can be mostly contributed by polymorphonuclear lymphocytes or neutrophils which are known to live for a few hours (211) and thus we attributed most of this expression to the inflammatory phase of repair. This also means that since cell death is marginal during later timepoints, patterning of the tissue layers in the regenerate are not sculpted by apoptotic elimination as in the case of embryonic skeletal segmentation or tissue layers and organs with a high cellular turnover such as the skin, intestines, and hair follicles (212).

On the other hand, proliferation events over the course of regeneration were very dynamic. Concurrent with increased C3 activity, the ratio of Ki67 to connective tissue mesenchyme is dramatically lower than baseline age-matched control levels, a change consistent with ongoing wound proteolysis and hypoxia. However, we do not interpret these data as impaired healing, since in contrast, the leading (distal-most) edges of the epithelium in the DPA4 timepoint showed consistent Ki67 activity in agreement with re-epithelialization and initiation of wound closure. Furthermore, we observed an increase in Ki67+ nuclei at the site of the emerging bone marrow cavity, which becomes hypercellular with cells of stromal phenotype by DPA8. Of interest is that many stromal cells in the amputated digit bone marrow that remains open to the wound connective tissue express the receptor CXCR4 for the chemoattractant stromal cell derived factor-1 (SDF-1) found at the edge of the wound (205). It is then possible that the expanded bone marrow stromal cell population is a source of blastema cells. The significant increase in proliferation at the blastema site compared to the control connective tissue mesenchyme is consistent with published results from adult blastemas at DPA10 (137). The gradual decrease in proliferation to nearly baseline levels by DPA16 indicates that a balance between proliferation of progenitors and differentiated cells is being reached at the connective tissue mesenchyme level.

In brief, we found that cells in the connective tissue mesenchyme of the amputated neonatal digit tip undergo an increase in proliferation specifically revolving around the time of blastema formation. By co-staining Ki67 with ER-TR7 we were able to generally segregate proliferating FRCs over the time-course of regeneration hypothesizing that if ER-TR7+ FRCs prepare the ground for invasion of ER-TR7- progenitors and differentiation events in the blastema, then we would see an increasing trend of Ki67+ cells actively expressing ER-TR7. We provide evidence that the proliferation index of FRCs is very dynamic and significantly elevated around the time of blastema formation while continuously expressing the ER-TR7+ framework. Later on, ER-TR7- cells undergo an increase in proliferation consistent with growth and patterning of various organ compartments. This indicates that FRCs are a growth responsive population that acts as the groundwork for patterning and re-differentiation of ER-TR7- populations in the anlagen. Since ER-TR7+ cells begin expansion during the end stages of the initial inflammatory response, growth factors, mitogens, and chemokines at this later phase of conventional wound healing must play a role on the behavior of FRCs.

In vitro studies involving FRCs isolated from lymphoid organs have demonstrated that the ER-TR7 network of fibers can be induced under treatment with $\text{TNF}\alpha$ and an $\text{LT}\beta\text{R}$ receptor agonist antibody. These ligands and their receptors both belonging to the TNF superfamily have been known to trigger a milieu of pro-inflammatory factors during injury and host defense in an $\text{NF}\kappa\text{B}$ -dependent manner (88, 213, 214) as well as stimulating pro-angiogenic factors during tumorigenesis and homeostasis during lymphoid organogenesis (90, 215-218). We found that immortalized embryonic mouse Swiss NIH-3T3 fibroblast cultures can also be induced to synthesize the ER-TR7 antigen using this treatment, which directly or indirectly promoted them to build massive cell aggregates associated with overexpression of the framework. The aggregates are consistent with colony formation reported in various studies involving various

fibroblast and mesenchymal pluripotent stromal cells, especially those derived from the bone marrow (106, 219, 220). On the other hand, we found that primary fibroblasts derived from the P3 region of the mouse digit can also be induced but the endpoint phenotype of the cells is a uniform monolayer with ER-TR7 fibril expression consistent with that found at the blastema site *in vivo*.

The multi-TNF receptor activation in these fibroblast subtypes elicits progression of the canonical (RelA (p65)-p50 complex) and alternative (RelB-p52 (p100) complex) NFκB cascades (88) and we show that even though both cultures synthesized ER-TR7 fibrils, the overall biological response of each cell line to the same induction treatment is unsurprisingly different. The activation of NFκB by any given plethora of stimuli can have a profound effect in a wide variety of physiological processes such as inflammation, proliferation, differentiation, and development (221). However, different NFκB species (e.g. RelA, RelB, cRel) can be highly selective on the target genes they regulate and this can be cell type-specific (222). Upstream from that, the regulation and binding dynamics of a particular TNF receptor type (i.e. TNFR1, TNFR2, or TLR) to TNFα can vary between and within cell types (223, 224). Cytotoxicity, cell growth, apoptosis, upregulation of adhesion molecules, expression of colony-stimulating factors, and activation of NFκB are mainly coordinated by the main effector TNFR1 (225). When co-activated, TNFR2 can either enhance the activity of TNFR1 or exert an opposite mechanism (226). In fibroblasts, the pleiotropic nature of TNF is portrayed by *in vitro* studies which demonstrate opposite phenotypes on the synthesis and regulation of ECM macromolecules following activation of TNF receptor(s) suggesting that these events vary in a cell or tissue specific manner (224). As a justification for further investigation, it is possible that the differences in survival and organizational dynamics between 3T3 cells and primary FRCs can be attributed to their particular sensitivity to certain NFκB species and/or members of the TNFR

superfamily in a fibroblast subtype-specific manner. Regardless, we have managed to upregulate ER-TR7+ fibrils *in vitro* in a manner that is consistent with the pattern and extent that we have documented in the digit blastema and this phenomenon is specific to digit FRCs.

Using the induction protocol on 3T3 cells and primary digit FRCs, we achieved further characterization of the ER-TR7+ network by (1) analyzing the transcription of a group of genes known to be active during tissue repair and (2) comparing the co-expression of targets of anti-ER-TR7 to targets of antibodies against fibroblast specific factors based on our RT-PCR results and evidence found in the wound healing and regeneration literature. Consistent with the results shown by Katakai et al. (2004), induction of FRCs and 3T3 cells to produce ER-TR7 is NF κ B dependent and this is shown by the consistent upregulation of *NF κ B* transcripts on both cell lines at all collected timepoints throughout the 10 day induction treatment. In addition, the only gene that was consistently upregulated throughout induction was *Col3a1* or COL3. Since COL3 is a fibril-forming collagen which is transiently upregulated during repair, specifically at the granulation tissue stage of wound healing, and has been shown to control COL1 deposition and impair myofibroblast differentiation (29, 78, 79) we pushed protein localization assays forward with the idea that if ER-TR7 fibers are directly or indirectly co-regulated during *in vitro* induction and at the blastema site, then both must share pro-regeneration characteristics at the level of the extracellular matrix. Using indirect immunofluorescence co-detection of antibodies against ER-TR7 and COL3 and co-localization analysis of the signals, we provide evidence of a direct, physical relationship and co-regulation of ER-TR7 and COL3 fibers. Furthermore, we demonstrate this positive correlation *in vivo* and relate this expression to additional fibroblast related markers.

FRCs are localized to the pool of VIM and FSP-1 positive cells in the digit connective tissue and their expression is proportional to the area of connective tissue space in unamputated controls and regenerates alike. Given the extended distribution of both markers to other cell types of mesodermal origin and fibroblastic source, we cannot establish a correlation in pattern or amount with ER-TR7. At the other end of the spectrum we have demonstrated that even though expression of GP38 has been reported to co-exist with ER-TR7 in stromal FRCs of lymphoid tissue (88), only a small subset of fibroblastic cells and osteoblasts express this glycoprotein in the digit connective tissue and at the cellular level its pattern is inconsistent with ER-TR7 staining. At the end, we observe co-regulation but not co-expression of ER-TR7 and COL3 to FN1, consistent with other studies regarding the dependency of collagen fibrillogenesis to FN1 and the general role of FN1 deposition during the expansion and migration of fibroblasts within granulation tissue (55, 158, 190, 193, 197). But FN1 has been shown to facilitate transforming growth factor beta-mediated myofibroblast differentiation, survival, and wound contraction mechanics (227). Moreover, myofibroblasts upregulate COL1 but not COL3 (228). If FN1 is overexpressed at the blastema stage along with ER-TR7 and COL3 but COL1 levels are lower in the regenerate, then there must be an antagonistic mechanism that controls the unfavorable factors that myofibroblasts exert on regenerating tissue and this may be a tight control of COL1 fibrillogenesis. If this is true, then we can conclude that wherever ER-TR7 is expressed, incorporation of COL1+ fibrils will be regulated by co-polymerization with COL3 (78) and there will also be regulation of local myofibroblast differentiation and survival (29) which otherwise would heavily contribute to COL1 production, increased tensile strength, and wound contraction (229), all of which are unfavorable to the regeneration process (229, 230). Whether the ER-TR7 and COL3 antigens are related at the amino acid or at the structural level, the better

characterized COL3 protein can be used as a base to pursue gain and loss of function studies about the regeneration competency particulars of the ER-TR7+ blastema scaffold.

CHAPTER III: CONTRIBUTION OF BONE MARROW DERIVED CELLS TO THE ER-TR7+ REPAIR SCAFFOLD AND OTHER TISSUE LAYERS DURING REGENERATION

3.1 INTRODUCTION

During wound repair, the granulation or proliferative phase begins before the initial inflammatory response is resolved and occurs in unison to angiogenesis of transient capillaries (15, 20). This phase is characterized by the accumulation of fibroblasts at the wound site which become the main cell population there (231) to function as the coordinating force behind extracellular matrix (ECM) remodeling and wound contraction (209). These granulation fibroblasts (GFs) were thought to originate from the local recruitment and expansion of connective tissue fibroblasts surrounding the wound (209). However, newer evidence suggests that fibroblast precursors enter circulation from other anatomical sites such as the bone marrow (BM) to home and participate in repair of damaged tissue (232). Regardless of their origin, GFs initiate and upkeep the synthesis of a loose provisional ECM that is transient (209) and resembles the network of fibers that we have observed in the blastema of regenerating mouse digit tips.

In previous studies we demonstrated that the great majority of cells which contribute to growth of the regenerating digit tip blastema are fibroblast reticular cells (FRCs). FRCs maintain a high proliferation index at this stage of regeneration while exhibiting cytosolic expression and secreting fibrils marked by an antigen reactive to a monoclonal antibody called ER-TR7 (94). The

loose ER-TR7+ fibrillar network that is gradually organized by FRCs has been implicated in stromal-immune interactions, homeostasis, and organogenesis of lymphoid organs (83, 88, 151, 152). We have measured this network shows to have a trend in expression over space and intensity with collagen type III (COL3), the main collagen subtype found in granulation tissue. In addition, the transient upregulation of ER-TR7 throughout the regenerating tissue is mostly limited to the blastema stage, gradually regresses throughout re-differentiation, and reaches basal levels once recapitulation of the digit anlagen is complete. This transient scaffold of FRCs with prominent fibers is comparable to the one that forms during the granulation stage of wound healing, with the exception that the digit tip area regenerates while other wounds remain stunted and scarred. We consider FRCs to be one of the hallmarks of growth and maturity of the regenerate and thus would like to investigate their ontogeny and fate once incorporated into the regenerated digit tip cell population with specific emphasis on the contribution of BM-derived cell (BMDC) precursors to FRCs and other populations in a regeneration-competent wound.

The plasticity of progenitors in the pool of BMDCs has been extensively studied in models of cardiac restoration (141); bone fracture fusion (139); liver regeneration (144); pancreatic beta cell renewal (145, 146); cystic fibrosis (112); and cutaneous injury (147, 148). The mammalian digit tip amputation model is a prime example of a complex regeneration-competent injury model that has never been studied with respect to the origin, contribution, and plasticity of these progenitor population(s) and we believe that some of them give rise to mesenchymal FRCs. But the BM of adult animals fosters precursor cells that are able to follow either hematopoietic or mesenchymal lineages (95, 233, 234). Both progenitor subtypes are constitutively present in various niches throughout the body to aid in tissue reconstitution, defense, and healing (97, 235). Following injury, these cells migrate via circulation and arrive to

wound areas to regulate a milieu of processes including differentiation, cell proliferation, and migration of other immunological, epithelial, and mesenchymal subtypes (97, 236). BM-derived hematopoietic progenitor cells (HPCs) are most abundantly found as mediators of the immunological response following insult (237). HPCs express the leukocyte surface antigen CD45 and will ultimately differentiate into components of the innate immune response such as neutrophils and macrophages or cells with phenotypes characteristic of the adaptive immune response such as T-lymphocytes and dendritic cells (237, 238). CD45⁺ HPCs have also been shown to transdifferentiate into other immune cell subtypes (237, 239) and even contribute to non-immunological phenotypes, such as vascular cells (240) and fibrocytes (241). For example, during the first week of wound healing, an endothelial precursor subset of HPCs initiates angiogenesis as CD34⁺ cells to vascularize the mass of repair fibroblasts that originates during the granulation stage (120, 242). Although the fibrocyte has been characterized as an important bm-derived cell acting on ECM remodeling, similar to fibroblasts, and serving as professional antigen presenting cells, just like CD45⁺ dendritic cells and macrophages, their surface CD45 expression can only be detected when in circulation and is lost in culture and after they extravasate into tissue (243). Otherwise in general, non-hematopoietic BM-derived precursors or mesenchymal progenitor cells (MPCs) are CD45 negative throughout their lifetime (244) and have been implicated in differentiation into cells of mesodermal lineages, mostly *in vitro*, such as osteoblastic, chondrocytic, tendon, muscle, peripheral nerve, endothelial, and fibroblastic (113, 210, 245-247). Fairly recently, the identification of MPCs and their plasticity has propelled research on their role in homing, engraftment, and participation in sites of injury as cells whose phenotype goes beyond the differentiation range of the hematopoietic precursors. The ability of MPCs to enter circulation and engraft into layers of radiation damage-induced bone, cartilage, and lung airway has also been demonstrated (248).

We employed a chimeric mouse model in which normal C57BL mice BM is replaced with the BM of enhanced green fluorescent protein (eGFP) transgenic mice (127) to investigate the contribution of MPCs to the adult mammalian digit blastema and their fate as either FRCs or cells with vascular, osteoblastic, or myofibroblastic phenotype. Using antigen coexpression techniques, we demonstrate that much of the eGFP⁺ population of cells invading the wound during the inflammatory phase of repair is hematopoietic. However, by the time the blastema peaks in growth, half of the cells that occupy the site are eGFP⁺ spindle-shaped cells lacking CD45 expression and are thus related to BM-derived MPCs. We also discovered that many of the CD45⁻/eGFP⁺ cells which occupy the blastema contribute to deposition of a rudimentary but organized ECM scaffold which expresses ER-TR7 consistent with the upregulation of ER-TR7 by FRCs in our previous studies. Finally, following analysis of lineage-specific markers throughout the repair timeline, we provide evidence that MPCs have a long-term presence at the endpoint of regeneration. Together we propose that in addition to participation in the early inflammatory phase and temporary angiogenic response during the proliferative phase as hematopoietic lines (124), BM-derived progenitors significantly contribute to the regenerating microenvironment of the amputated digit tip by expanding a subpopulation of MPCs that migrates to the blastema site as differentiated FRCs. In agreement with other studies regarding the fate of mesenchymal cells of various phenotypes in cutaneous wounds and bone fractures (124, 139, 143, 210, 248, 249), we also propose that MPCs that enter the digit tip wound participate in long-term reconstitution of various tissue layers of the regenerate as resident fibroblasts, vascular, and/or osteoblast cells.

3.2 MATERIALS AND METHODS

Mice and tissue harvest

BM donors consisted of six-week-old male GFP-transgenic (C57BL/6 background) mice purchased from The Jackson Laboratory (Bar Harbor, Maine). In this strain, control of eGFP transcription is mediated by a chicken β -actin promoter and a CMV enhancer. Outbred female C57BL/6 mice supplied by Charles River Laboratories (Wilmington, MA) served as BM recipients. Eight week old BM chimera mice were anesthetized by intramuscular injection of Ketamine and Xylazine at 80 and 8mg per kg of body weight, respectively, followed by distal (P3) amputations of digits 2 and 4 from each hind limb using a straight-edge scalpel blade under a stereomicroscope. The amputation target region was measured at midpoint of the clearly visible terminal phalangeal (P3) element so approximately 50% of the bone remained in the proximal stump after transection. Digit tissues were harvested for histological, immunohistochemical (IHC) analysis at day post amputation (DPA) 0, 5, 7, 10, 14, 16, 21, 28, and 35. Procedures for care and use of mice for this study were performed in accordance with standard operating procedures approved by the Institutional Animal Care and Use Committee of Louisiana State University Health Science Center in New Orleans, LA.

Bone marrow transplants

Four week old C57BL/6 mice underwent bone marrow transplant (BMT) one month prior to digit amputation in order to create chimeric animals with marked (eGFP) bone marrow cells. Recipient female wild type C57BL/6 animals were conditioned by whole body irradiation at a rate of 139cGy/min using a ¹³⁷Cs source for a total dose of 1000cGy. This is a lethal dose without BMT. Bone marrow cells were harvested by the centrifugation technique as described previously (145) from male eGFP-transgenic mice with a C57BL/6 background. Briefly, donors

were anesthetized with Ketamine/Xylazine then the fur saturated with 70% alcohol. The peritoneal cavity was opened & the animal exsanguinated via IVC transaction. The femur & tibia were removed by blunt dissection and BM cells extracted from the medullary cavity by centrifugation. After rbc lysis and filtering using Ficoll-Paque Plus (GE Healthcare, Pittsburgh, PA), 1×10^7 BM donor cells mixed with 1×10^6 splenocytes (adoptive transfer) were administered via tail vein injection into recipients in 300 μ L saline under isofluorane anesthesia. Following recovery, a group of recipients were set aside to monitor BM reconstitution percentage fluctuations once a week for five weeks (end of regeneration timeline following amputation). The percentage of eGFP+ BM cells from all recipients undergoing amputations and the group set aside for reconstitution standardization was measured by fluorescence activated cell sorting (FACS) analysis using a FACSCalibur controlled with CellQuest software (BD Pharmingen, Franklin Lakes, NJ).

Immunohistochemistry

Adult digits were harvested in zinc-buffered formalin (Anatech Ltd, Battle Creek, MI) to fix no longer than 48 hours for paraffin histology and thin section IHC analysis. Fixation was followed by pretreatment in Decalcifier II (Surgipath, Richmond, IL) solution for 8 hours and processing for paraffin embedding. Serial tissue sections were collected at 5 μ m onto charged, glass slides and heated for 45 minutes at 60°C. Slides were deparaffinized in xylene and rehydrated through an ethanol series to distilled water. All washes were performed with 0.05% Tween-20 in Tris-buffered saline (TBST). Depending on the antigens to be detected, sections were pre-treated with either enzymatic or heat induced epitope retrieval and washed. This was followed by blocking for non-specific protein binding with 5% goat serum diluted in 1% bovine serum albumin in PBS (w/v). It should be noted that if using a primary antibody derived from mouse for subsequent tagging with an anti-mouse secondary antibody, an additional goat anti-

mouse Ig Fab fragment (Jackson ImmunoResearch, Westgrove, PA) was added to the protein block step at a 1:100 dilution to bind endogenous immunoglobulins. Sections were further treated with sodium borohydride (0.5 mg/mL in PBS) to limit tissue autofluorescence. Following thorough washing, sections were co-incubated overnight at 4°C with chicken anti-eGFP (Novus Biologicals, Littleton, CO) and a variety of lineage-specific primary antibodies. For contribution to vascularization, smooth muscle support, and myofibroblasts, samples were co-incubated with chicken anti-eGFP, anti-SMA (2µg/mL; Dakocytomation, Carpinteria, CA) and anti-VWF (1µg/mL; Dakocytomation, Carpinteria, CA) followed by washing and treatment with goat anti-chicken IgG(H+L) Alexa 488 (Molecular Probes, Eugene, OR), goat anti-mouse IgG(H+L) Alexa 647 (Molecular Probes), and goat anti-rabbit IgG(H+L) Alexa 568 (Molecular Probes), at 4µg/mL each for 45 minutes at room temperature. Chicken anti-eGFP co-incubation with anti-ER-TR7 and anti-Osteocalcin (1µg/mL Takara, Otsu, Shiga, Japan) followed by goat anti-rat IgG (H+L) Alexa 568 (Molecular Probes), goat anti-rabbit IgG (H+L) Alexa 647 (Molecular Probes), respectively, and goat anti-chicken IgG (H+L) Alexa 488 (Molecular Probes) for anti-eGFP detection was applied to ECM and osteogenesis-related analyses. Rat anti-CD45 (2µg/mL; Biolegend, San Diego, CA) and chicken anti-eGFP followed by goat anti-rabbit IgG (H+L) Alexa 568 (Molecular Probes) and goat anti-chicken IgG (H+L) Alexa 488 (Molecular Probes) were co-incubated to determine HPCs vs. MPCs lineage ratios. Anti-Ki67 (2µg/mL; Labvision, Fremont, CA) and chicken anti-eGFP followed by goat anti-rabbit IgG (H+L) Alexa 568 (Molecular Probes) and goat anti-chicken IgG (H+L) Alexa 488 (Molecular Probes) were co-incubated to assay proliferation. All preparations culminated in washing following secondary antibody application, nuclear counterstaining with 4', 6-diamidino-2-phenylindole, otherwise known as DAPI, (300mM; Molecular Probes), and mounted under a coverslip with Prolong Gold Antifade (Molecular Probes) for epifluorescence deconvolution microscopy.

Imaging and morphometry

Tissue sections were imaged at 200X in 2D and 630X in 3D using a Leica DMRXA upright microscope equipped with a Sensicam QE CCD (Cooke); xyz motorized stage (Prior); an Hg source; and filters suitable for DAPI, Alexa 488, Alexa 568, and Alexa 647 fluorophores. No Neighbors and Constrained Iterative deconvolution algorithms were applied to 2D and 3D sets, respectively. Probe signals were measured by ratioing specific marker signals with respect to total nuclear (i.e. DAPI-counterstained) areas within the connective tissue paired with manual counting. All renderings and analyses were driven by Slidebook software (Intelligent Imaging Innovations). For high resolution microscopy, we used a Fluoview FV1000 laser scanning confocal system (Olympus of America, Center Valley, PA) equipped with high end PLAN-FLUOR objectives including a 100X with an N.A=1.38, Nomarski (differential interference contrast or DIC) optics and visible excitation light sources including a multi-line Argon laser and diodes covering 405, 561, 592, and 635 nm wavelengths.

Statistical analysis

Data are represented as means \pm SE. Group differences were determined via the unpaired Student's *t* test. $P < 0.05$ is considered significant.

3.3 RESULTS

The BM chimera model of digit amputation

Four week old C57BL/6 mice were exposed to a lethal dose of gamma irradiation immediately followed by intravenous infusion of 1×10^7 BM cells from eGFP transgenic donor mice. Following reconstitution, we determined the percentage of recovery by eGFP+ cells by means of harvesting bone marrow cells and analyzing single cell suspensions by flow cytometry. We gated the cells by forward scatter and determined the reconstitution average of 78.2 % of

the total preparation. Consistent with similar studies (124), weekly flow cytometry analysis of blood from unamputated chimeras revealed no significant changes in reconstitution percentage throughout the five week experimental timeline. To track the fate of these cells in our amputation models, we generated a total of 35 chimeras with only one death shortly after transplantation. Six weeks after irradiation and donor cell transfer, measurement of circulating eGFP⁺ cells by flow cytometry yielded a range of 65-83%. The animals had normal CD45⁺ cells counts as measured by flow cytometry and did not show any signs of rejection. Consistent with methods described here and in other studies (137), the chimeras were subjected to amputations of digits 2 and 4 at the regeneration-competent level of the mid-terminal phalanx (P3). Digit number three of each hind leg served as the unamputated control. The animals were subdivided into four groups to measure progress at days (D) 0, 5, 10, 14, 21, 28, and 35. The remaining animals were set aside for engraftment efficiency measurements by flow cytometry over the course of the study. During each timepoint, digits from a small group of chimeras (n=3) were imaged under a stereomicroscope for eGFP expression over the course of repair. The digits from these mice were then collected at the 35 day timepoint. All amputated and control digits were eventually harvested for hematoxylin and eosin (HE) staining and immunofluorescence labeling of eGFP co-expressed with other markers.

Cytopathology and quantitation of eGFP⁺ BMDCs was optimized by labeling sections from paraffin processed digits at all timepoints with anti-eGFP indirect immunofluorescence. BMDCs were counted from of a total of one thousand cells found within random connective tissue mesenchyme fields captured at 400X magnification. Since our main goal was to determine the general phenotype of BMDCs once they enter the wound CT microenvironment and their fate outside the BM microenvironment at the endpoint of regeneration, the marrow, mineralized bone, and epidermis were excluded. The results are summarized in Figures 3.1 A-I.

Prior to amputation, eGFP was detected in 3-5% of all CT cells and these were randomly distributed within the stroma engulfing the dorsoproximal axis between the nailbed and P3 (Figures 3.1 A, D). DPA0 samples were collected immediately following injury and prior to visible signs of clotting; therefore the change in eGFP expression was insignificant when compared to controls (Figure 3.1 D). The eGFP+ population that enters or expands in the wound dramatically increases to 23-27% from DPA0 and accounts for over 43% of the cells in the mature blastema by DPA14 (Figure 3.1 D). This is consistent with previous studies which indicate that between DPA10 and DPA14, the adult P3 blastema is known to experience a substantial increase in cell growth and migration towards the wound epidermis as measured by the Ki67 proliferation index and dynamics of SDF-1 mediated chemotaxis (137, 205). This is an indication that blastema growth is dependent on expansion or migration of BMDCs at the wound site and we observed this to be a heterogeneous population.

Based on their cytological features and location, we were able to segregate the general population of eGFP+ BMDCs into multiple subtypes and all subtypes were present simultaneously during the DPA14 blastema stage (Figures 3.1 B, E-I). We must note that different cellular phenotypes were color coded to mark the location of representative cells in Figures 3.1 and 3.2. Scattered cells with multi-lobed nuclei were found in the same relatively small amounts around the CT of unamputated controls, the blastema of amputated digits, and the endpoint of recapitulation at DPA35 (Figures 3.1 A-C, E white arrows). We also detected small numbers of giant multinucleated cells around the blastema connective tissue but nowhere near the pre-existing phalangeal structure (Figures 3.1 B, F blue arrows). However, intimately associated with the methodical direct ossification distal to the P3 fragment at DPA14 and full regeneration at DPA35 we found large numbers of cuboidal cells, of which a small percentage exhibited diffuse and somewhat granular eGFP signal (Figures 3.1 B, C, and I pink arrows).

Dispersed in the stroma of the blastema and more frequently at its distal end near the wound epidermis, we identified small vessels resembling venules with distinct endothelial, smooth muscle, and fibrous layers. Some eGFP⁺ elongated BMDCs were detected in the periphery of these venules and others of simple squamous appearance lining the vessel lumen (Figure 3.1 B, H red arrows). Although these eGFP⁺ cell types associated with vascular structures were not found in unamputated controls, they persisted as such in the CT of the DPA35 regenerate (Figure 3.1 A, C red arrows). But overall, the bulk of eGFP⁺ BMDCs in the DPA14 blastema was large groups of spindle and stellate-shaped cells (Figure 3.1 G) growing along the proximodistal axis of the CT stroma. Cells with this particular phenotype decreased by the endpoint of recapitulation but were present in larger detectable amounts when compared to the unamputated control and these, along with other eGFP⁺ phenotypes observed at DPA35, account for the significant presence of eGFP⁺ BMDCs at this endpoint (Figures 3.1 C, D). Although we cannot confirm that BMDCs arrive to the injured digit tip through circulation or by expansion and migration of the pre-existing P3 BM, these data indicate that BMDCs actively participate in blastema formation and the development of diverse cellular phenotypes within its immune, bone, vascular, and stromal compartments. Furthermore, these data also demonstrate that even though the percentage of BMDCs significantly increases by the blastema stage only to gradually regress over time, the remaining BMDCs ultimately become part of well-defined structures in the regenerated tip.

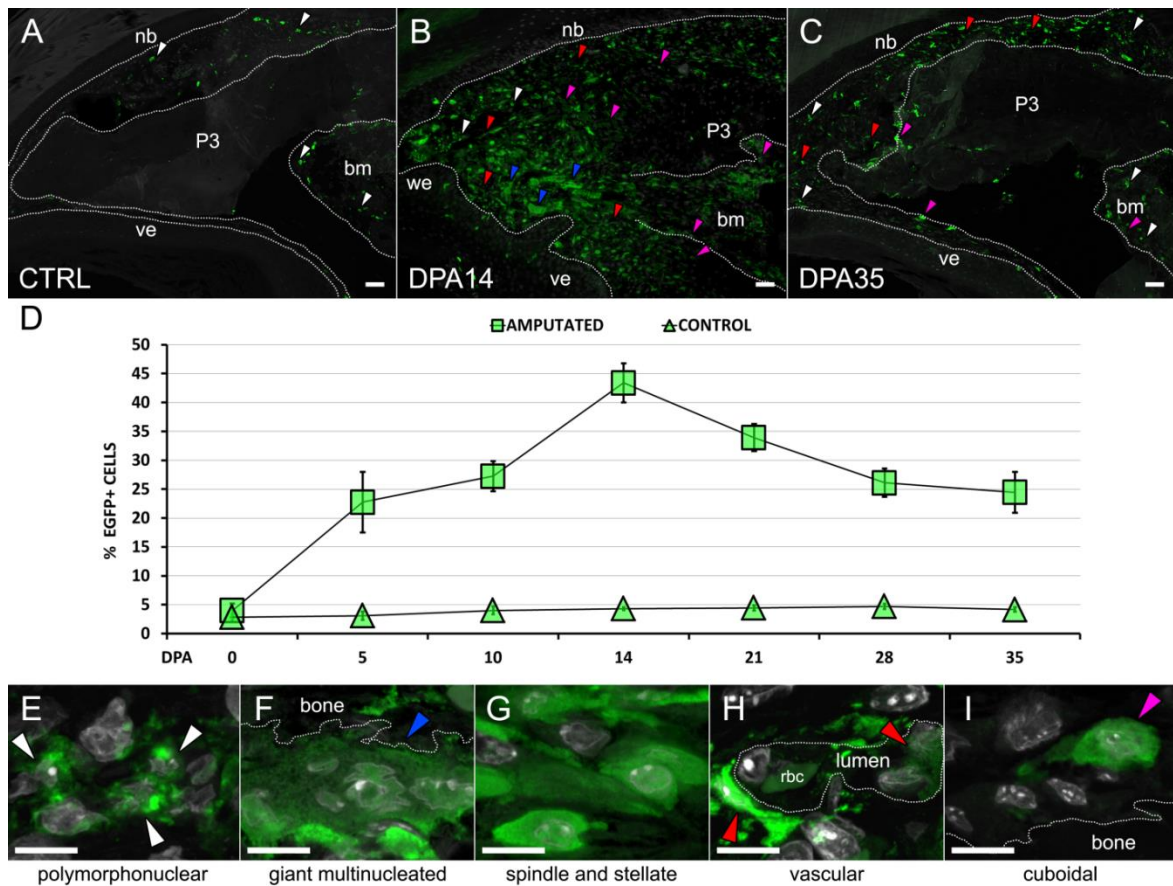


Figure 3.1: Quantitative and cytological analysis of BMDCs in control digits and regenerates harvested from eGFP BM chimeras yields progressive cellular contribution peaking at the blastema timepoint with regression after differentiation but endpoint counts significantly higher than baseline. Representative images were captured by confocal microscopy at (A-C) 100X (bar = 50 μ m) and (E-I) 1000X (bar = 5 μ m) magnification. (D) eGFP+ BMDCs were counted and expressed as a percentage of total connective tissue area (n=4). Several different cellular phenotypes were recorded and representative examples were labeled with color-coded arrows. (A) Day-matched unamputated controls (CTRL) had a hypocellular bone marrow (bm) in P3 mostly composed of eGFP+ cells scattered throughout the bm cavity and tethered to the endosteum. Resident eGFP+ cells outside the marrow compartment of controls were scarce and dispersed throughout the connective tissue layer between the nail bed (nb) epithelium and periosteum of P3. (B) Day post-amputation (DPA) 14 samples encased more eGFP+ cells in the marrow than controls and their blastema regions experienced the largest influx of BMDCs with most of these having a spindle morphology. (C) At the DPA35 endpoint of regeneration the percentage of eGFP+ cells is 2-fold lower than in the blastema stage and the labeled BMDCs appear scattered within most compartments of the regenerate. (D) Quantitative analysis of eGFP+ BMDCs in the connective tissue of amputated digits over time shows a gradual increase in the percentage of eGFP+ cells from DPA0 to the peak of expression at DPA14. This is followed by a steady decline by DPA21 and somewhat of a plateau between DPA 28-35. (E-I) Study on the location, morphology, and occurrence of the general eGFP+ BMDC population at 1000X magnification allowed us to segregate it into different phenotypes and label their location on the 100X magnification views. (E, white arrows) Some BMDCs had multilobed nuclei and were scattered in low amounts throughout the connective tissue and marrow of controls, DPA14, and DPA35 digits. (F, blue

arrows) Particular to the blastema stage, we found giant multinucleated cells distal to the pre-existing P3 fragment. (G, unmarked) eGFP+ spindle cells were more frequently observed in the regenerate when compared to control digits whereas an overwhelming amount populated the blastema. (H, red arrows) At least two different cell phenotypes were in close association with vascular walls in both the DPA14 and DPA35 stages and these were either tethered to the tunica media or inside the lumen of small vessels. (I, pink arrows) Another cell type with cuboidal shape and more granular and diffuse eGFP labeling than others was found in association with areas undergoing direct ossification at DPA14 and in both the periosteum and endosteum of the regenerated P3 at DPA35. This cell type was not observed in controls.

So far we have shown evidence that the BM eGFP chimera model of digit amputation results in recapitulation of the missing segment by means of a blastema intermediary. Some of the BM derived lineages that were observed in the blastema were not detected in unamputated controls but present in at various levels of the DPA35 regenerate and therefore have a long term fate inside repaired tissue. But to record any potential variations at the anatomical and cellular level during specific steps throughout the course of regeneration due to BM depletion by irradiation and cell transplantation and study the structural changes at the pre- and post-blastema stages, we employed stereomicroscopy and careful microscopic analysis of all timepoints (Figures 3.2 A-R) and compared histological changes to similar digit tip amputation models which had not experienced manipulation prior to injury (6, 137, 206). Day-matched unamputated digits appeared anatomically normal under stereomicroscopy with almost undetectable eGFP fluorescence. Histology of these control digits by H&E showed no signs of fracture, inflammation, or any other structural deviation from standard examination (250).

DPA0 digits displayed an immediate response to injury with an increase in eGFP intensity (Figures 3.2 A-C) as a result of rapid clotting and invasion by polymorphonuclear cells (Figure 3.1 E) consistent with hematopoietic BMDCs of granulocyte origin. Most of these eGFP+ granulocytes had multi-lobed nuclei consistent with a neutrophil subtype which infiltrated into the fibrin cap at the wound edge and formed a “plug” between the opposing endosteum layers of the open BM cavity (Figure 3.2 B, C red asterisks). We must note that the eGFP signal

increase was restricted to this fibrin clot at DPA0 and that region was discounted from counts based on CT area. Gross atrophy of the wound edge, cell debris and condensed nuclei characteristic of apoptosis in multiple tissue compartments such as the epidermis, connective tissue mesenchyme, and bone was more evident by DPA5 (Figures 3.2 D-F) and this is consistent with the consequences of platelet derived growth factor release and hypoxia (209). As a result, there was an increased presence of eGFP+ monocytic phagocytes or macrophages which could be somewhat identified by cytological features but confirmed by ingested debris. Along with neutrophils, these infiltrated the proximodistal axis of the connective tissue areas surrounding the damaged P3 (Figures 3.2 E, F), a response consistent with the pro-inflammatory phase of wound healing. Due to the capacity of these hematopoietic BMDCs to migrate and infiltrate within a large radius of the tissue stroma adjacent to the wound, intense eGFP expression accumulated within the entire P3 segment and the distal end of the adjacent phalangeal segment (Figure 3.2 D). The neutrophil “plug” observed in DPA0 became enlarged but was still restricted to the distal opening of the BM cavity (Figures 3.2 E, F red asterisks). Altogether, this means that critical steps which define the inflammatory phase of cutaneous wound healing such as immune cell accumulation and migration in the CT were progressing at a reasonable rate. Interestingly, there was a parallel response in the BM. The BM cavity became reasonably hypercellular with these hematopoietic cells and large multinucleated cells (Figures 3.1 F, 3.2 E, F blue arrows). The features of these giant polykaryons are consistent with bone-resorbing osteoclasts which are known to be a product of the fusion of multiple macrophages stimulated by factors produced by stromal cells (251).

Expansion of a spindle-shaped population of cells in the marrow and a larger accumulation of osteoclasts in both the endosteum and periosteum of P3 characterizes DPA10 (Figures 3.1 F, G and 3.2 G-I, blue arrows). Not surprisingly, extensive bone degradation was

seen midway through P3 and although these changes are delayed by three days, they run parallel to recent published descriptive data on adult digit amputation (137). The extent of bone resorption through the dorsoventral axis of this midline and the amount of abscess at the by the neutrophil “plug” indicate that eventual extrusion of the P3 fragment distal to points of significant degradation is about to occur (Figures 3.2 H, I blue asterisks). Concurrent with these changes we observed a decrease in the immune cell infiltrate in both the CT and marrow, which can be interpreted as a step in resolution of the initial inflammatory cascade (Figure 3.2 I white arrows). On the other hand, we noted the formation of venules scattered mainly along the proximodistal axis of the CT region dorsal to P3 and some of these had eGFP+ BMDCs associated with them (Figures 3.1 H and 3.2 H, I red arrows). These vessels may be the initiation of the transient neovasculature characteristic of the granulation stage of wound healing and may be precursors to the ones observed at DPA14 and previously described (Figure 3.1 B, H and 3.2 L red arrows). Interestingly, at DPA10 and DPA14, most of these structures generally remain proximal to the mass of blastema cells and close to the wound epidermis.

Although mostly composed of a heterogeneous group of cells, the blastema was mostly composed of scattered spindle cells around minute foci of immune cells, small aggregates of leftover osteoclasts, and extravascular space (Figures 3.1 B, E-I and 3.2 J-L). But most importantly, at this stage we described cuboidal cells seated along the endosteum and periosteum of P3 shortly after an evident loss of osteoclast activity (Figures 3.1 B, I). The shape and location of these cells are indicative of an osteoblast phenotype and thus provide the backdrop for direct ossification with a possible shift in a cell ratio that favored bone forming cells to bone degrading cells. By DPA28, the regenerating organ acquired better definition with evidence of a hypocellular BM cavity and distal ossification of the P3 fragment. There was persistence of cuboidal cells, some of which were eGFP+, tethered to the periosteum and

endosteum of P3 and seeded into the mineralized matrix (Figure 3.2 N-O, pink arrows) which began occupying the area formerly populated by blastema cells. It is partly for this reason that detection of eGFP at DPA28 in the whole digit was partially hindered under stereomicroscopy when compared to previous timepoints. Furthermore, we observed that even though the soft tissue area around the bone remained hypercellular by H&E (Figure 3.2 N), eGFP+ cells seemed displaced by eGFP- cells (Figure 3.2 O), which means that the local cell population must be propagating throughout the different tissue layers as well and thus further diluting the eGFP signal. By this timepoint the only prevalent cell types are cuboidal around the bone; vascular related; and spindle throughout thus confirming the end of the inflammatory stage and bone resorption. Patterning and definition are clear by DPA28 and only a small area resembling the undefined blastema remains at the distal tip (Figures 3.2 P-R). We also observed the long term fate of a percentage of eGFP+ BMDCs in contributing to bone, vessels, and stroma of the shaping regenerate as described previously (Figure 3.1 C and 3.2 R, pink and red arrows). Once again, results from eGFP+ cell counts at DPA28 indicate a 2-fold dilution of the eGFP+ population from the blastema stage and 21% over unamputated controls (Figure 3.1 D). This reiterates that invasion of BMDCs reaches a limit shortly after blastema maturity, concurrent with direct ossification and growth of the local cell population which co-occupy the area (137).

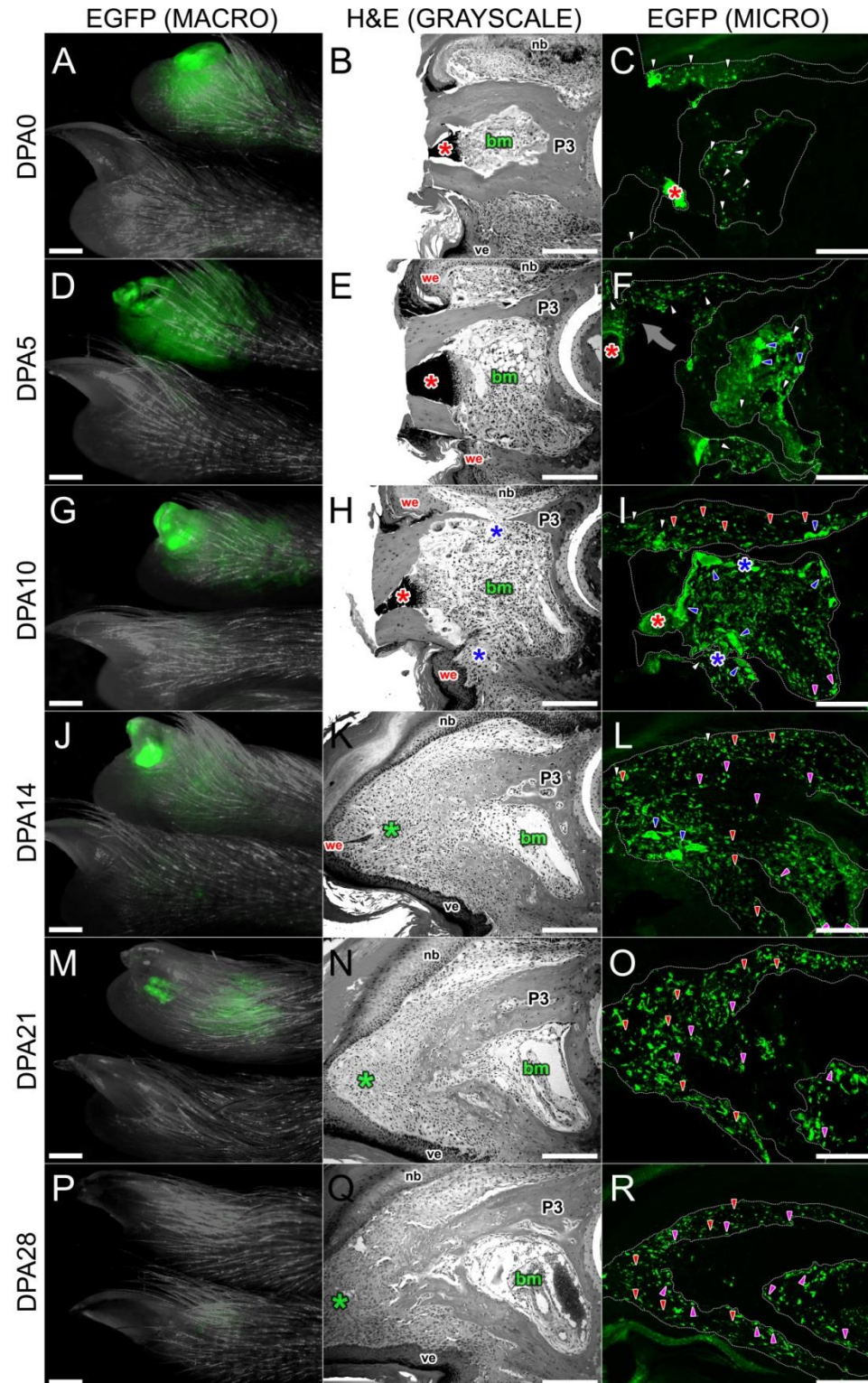


Figure 3.2: BMDs contribute and localize to diverse tissue layers in regenerating digits. Representative timepoints in the adult digit tip regeneration sequence visualized by (A, D, G, J, M, and P) stereomicroscopy (macro view; bar = 1 mm), (B, E, H, K, N, and Q) brightfield microscopy of H&E stained sections (bar = 200 μ m), and (C, F, I, L, O, and R) epifluorescence of anti-eGFP indirect immunolabeling of

adjacent sections (bar = 200 μ m). The eGFP label, nuclear morphology, cell shape, and localization aided in segregating and color-coding various cell phenotypes corresponding to immune (white arrows), bone resorbing (blue arrows), vascular (red arrows), bone-tethered cuboidal (pink arrows), and spindle (unmarked). (A) Immediate inflammatory response of hematopoietic BMDCs to insult at DPA0 caused diffuse eGFP detection throughout the digit with enrichment of polymorphonuclear cells visualized by (B) H&E and (C) epifluorescence in the distal CT and marrow (bm) of the P3 phalanx, which was sealed by a mass of eGFP+ neutrophils (red *) and fibrin clot. (D) DPA5 amputations appeared atrophied at the gross level with a greater influx of eGFP+ signal spreading to the neighboring P2 element. (E) By H&E, The distal nail bed (nb) and ventral epithelium (ve) appeared contracted but viable to become the wound epithelia (we) over the exposed distal portion of P3 which remained plugged by neutrophils. Apoptosis and edema shared the distal CT space with neutrophils and other monocytic phagocytes with ingested debris and basophilic cytosol. The bm cavity at DPA5 was also invaded by immune cells but also marked the initiation of bone resorption with the appearance of a few osteoclasts in the endosteum. (F) Most eGFP+ BMDCs at DPA5 were classified into the hematopoietic lineage for having multi-lobed nuclei, ingested debris, or multiple nuclei consistent with neutrophil, macrophage, and osteoclast differentiation, respectively. BMDCs of hematopoietic phenotype were mostly restricted to the CT stroma below the nb and above the ve. We note that in the representative picture of the eGFP label and most of DPA5 sections pretreated for immunohistochemistry, the dorsal CT was especially susceptible to detaching from the P3 bone (gray curved arrow). The bm at DPA5 becomes hypercellular with the hematopoietic lineages mentioned above. (G) DPA10 has more localized eGFP expression at the digit tip and marks a turning point in the cellular constitution of the regenerating tip. (H) By H&E, there is evidence of bone resorption by osteoclasts around the bone and inside the P3 marrow. Bone degradation is more prominent through the P3 fragment midline (blue asterisks) indicating separation of the distal osseous half of P3 for extrusion. The cellular phenotype of the bm population undergoes a dramatic change with spindle-shaped cells replacing most of the area previously occupied by cells of hematopoietic phenotype. The neutrophil “plug” described in the previous timepoints remains but at a lower density. (I) The serial section stained for eGFP reveals a less cellular CT with scattered venules containing eGFP+ cells closely associated with them (red arrows). On the other hand, the cells derived from the bm compartment are mostly eGFP+ to include osteoclasts, spindle cells, and a few cuboidal cells tethered to the endosteum. (J) The blastema (green asterisk) stage in this model occurs around DPA14 and eGFP expression under stereomicroscopy is more prominent and intense at the tip. (K) The blastema seems to be composed of a homogeneous mass of cells with intercalating zones of mineralization protruding distally and fused with the pre-existing bone leftover after extrusion at DPA10. The bm at DPA14 has more definition and is less hypercellular. (L) eGFP expression in the blastema is high and the cells that express it have the most heterogeneous phenotypes with spindle cells being the most abundant. The other phenotypes exist as either foci leftover from previous timepoints’ hallmark events or arrange in layer-specific fashion. (M) The eGFP signal is gradually diluted by DPA21 and by (N) H&E stain we were able to discriminate patterned zones such as the bm with arterial blood supply; direct ossification of P3 into trabecular bone; and a better organized dorsal stroma below the nb. However the distal most tip of the regenerating structure remains undefined (green asterisk), which means that patterning occurs in a proximodistal fashion. (O) The immunolocalization of eGFP is more scattered throughout the soft tissue at DPA21, indicating the increased presence of eGFP- cells possibly derived from local precursors. Moreover, the cellular phenotypes that could be identified were more restricted to spindle throughout the stroma; cuboidal at the edges of the bone; and vessel-related. This is an early indication that eGFP+ BMDCs have a long-term survival in different tissue layers as patterning occurs. (P) By DPA28, the eGFP signal is almost undetectable by stereomicroscopy which by (Q) H&E seems to be the consequence of increased bone

surface area and co-occupation of eGFP⁻ cells with (R) eGFP⁺ cells still scattered in the stroma and within bone trabeculae.

BM-derived hematopoietic progenitor cells (HPCs) are mostly limited to inflammation

We found that the great majority of BMDCs in the connective tissue of unamputated controls and those that invade the amputation site starting at DPA0 through DPA10 are of hematopoietic phenotype and we determined this by their location, nuclear phenotype, H&E dye uptake, and/or evidence of ingested cellular debris. All hematopoietic immune cells, including their progenitors, are characterized by their expression of surface CD45, which can regulate their maturation (252). Since the cytology of some of these cells may be unclear by standard pathologic observation, we labeled serial sections from all unamputated and amputated digits with anti-CD45 indirect immunofluorescence and counted nucleated objects co-labeled with both CD45 and eGFP (CD45⁺/eGFP⁺) in relation to total eGFP⁺ cells. The purpose of this experiment was to add a more precise level of discrimination between the extent and presence of immune response elements and HPCs in relation to that of mesenchymal components thus initiating proof that the inflammatory phase of wound healing must be resolved prior to blastema growth and for repair to proceed with non-hematopoietic regeneration-competent cells.

When discounting the fibrin clot and neutrophil “plug” at the wound edge, the average percentage difference of CD45⁺/eGFP⁺ cells in CT regions of control and amputated digits was negligible and of no significance (Figure 3.3 E). However, from our selected timepoints, DPA5 experienced an influx of eGFP⁺ cells at the CT level of which 70-80% had prominent membrane expression of CD45 (Figures 3.3 A, B, and E) and many of these fit the earlier cytological description. Also from this point forward, CD45⁺/eGFP⁻ cells were difficult to find and thus we

concluded that pre-existing resident cells do not play a major role in the overall inflammatory process and were not counted. DPA10 marked the turning point in the ratio of CD45+/eGFP+ to CD45-/eGFP+ populations where we observed roughly the same amount of eGFP+ cells in the CT but in average, a decrease in cells that expressed CD45. Even though the difference in the CD45+/eGFP+ percentage of cells between DPA5 and DPA10 is not statistically significant, we must note that, as described previously, a large amount of cells in the periosteum of P3 are large osteoclasts which retain CD45 expression (253) from their macrophage sources and thus may account for a large percentage of the measured CD45 signal in the CT. Regardless, the number of CD45-/eGFP+ cells increases without increase of the hematopoietic marker in this timepoint which we conclude is the initiation of a population shift that favors BM derived MPCs and other non-hematopoietic lineages. Concomitant with the mature blastema stage at DPA14 we have shown a peak in the percentage of eGFP+ cells in the wound and most of these populate the blastema mesenchyme (Figures 3.3 C, E, and F). At the same time, we witnessed a dramatic 58% decrease in the percentage of CD45+/eGFP+ cells from DPA10, especially midway through the blastema, signaling the resolution of the HPCs of healing guided by leukocytes differentiated from BM CD45+ HPCs (Figures 3.3 C, D, E, and F). The remaining cells typically gathered in foci and had the appearance of monocytic phagocytes including macrophages and neutrophils (Figure 3.3 F, white arrows). From DPA21 through DPA35, which are mostly characterized by the presence of differentiating cells and patterning of different tissue layers, we only observed baseline levels of CD45+/eGFP+ cells.

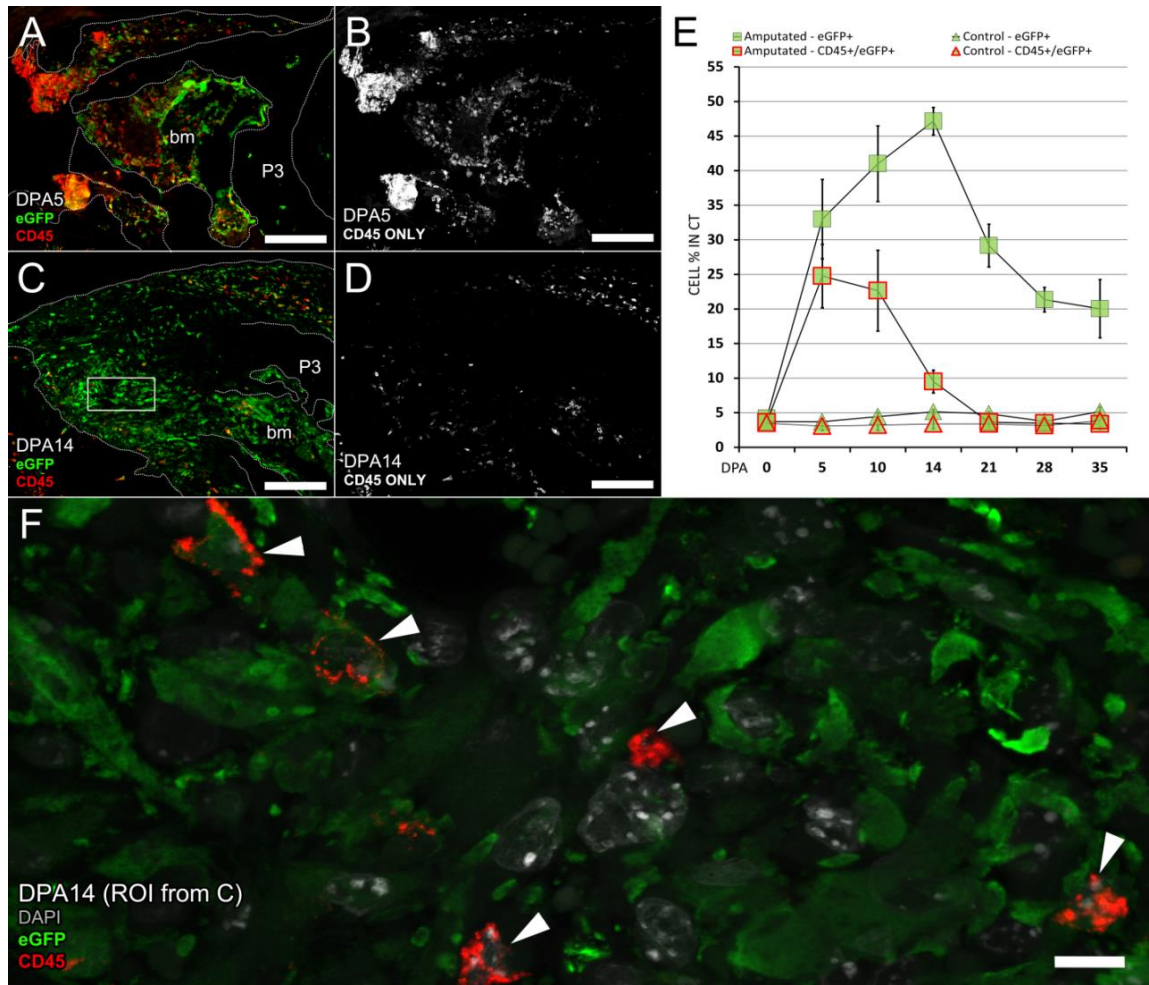


Figure 3.3: Quantitation and localization data of the CD45+ HPC subset of BMDCs following amputation demonstrate it is restricted to the inflammatory phase. Digit sections were co-labeled with anti-eGFP (green) and anti-CD45 (red) immunofluorescence to measure the extent of the hematopoietic fraction of BMDCs involved in regeneration. A strong presence of immune cells was observed during the inflammatory response at (A) DPA5. The involvement of CD45+ cells in the CT and BM compartments can be better observed in the (B) extracted raw CD45 channel. In contrast, the immune response is mostly resolved around (C) DPA14 or mature blastema stage and in contrast with DPA5, (D) the extracted CD45 channel from DPA14 shows the bulk of hematopoietic expression is mostly restricted to the CT proximal to the blastema proper. (E) The entire CT area or blastema mesenchyme were analyzed for percentage of CD45+/eGFP+ versus CD45-/eGFP+ cells and shows that the increasing number of eGFP+ BMDCs up to the mature blastema stage is independent from CD45 expression, which is mostly restricted to the earlier stages of regeneration which fall around the inflammatory phase of healing. (F) A closer view of the DPA14 blastema marked with a rectangle on panel C shows a relatively low number of CD45+/eGFP+ cells surrounded by a greater amount of CD45-/eGFP+ cells with a spindle and stellate phenotype. Data are presented as mean \pm SE (n = 4 per timepoint). Scale bars, (A-D) 200 μ m; and (F) 10 μ m.

Even though our intention was to focus on the changes occurring at the CT level during the regeneration process, we must note that dynamic changes also occurred in the BM with regards to content of HPCs and MPCs which led us to believe that a major part of the mesenchymal component of the blastema is derived from the remaining BM compartment of P3. So we performed a qualitative comparison of cellular changes within dorsodistal regions of interest from the CT or blastema mesenchyme analyzed earlier to those in the BM by capturing the representative ratio of CD45+/eGFP+ versus CD45-/eGFP+ cells over time in both compartments. The individual amount of eGFP and CD45 expression was represented as high (+++), moderate (++), and low (+) scale (Figures 3.4 A-H). As previously described and measured, the CT of DPA0 digit houses a low percentage of eGFP+ cells, most of which are CD45+. The marrow at DPA0 was mostly occupied by a large arterial blood supply with many tunica media (tm) cells under a layer of tunica adventitia (ta) fibroblasts, some of which were negative for eGFP. Alongside the vessel and scattered throughout the BM cavity, we found a similar number and prevalence of eGFP+ cells as in the DDCT that mostly tested positive for CD45 (Figures 3.4 A, E). Both the CT and BM at DPA5 became hypercellular with mostly CD45+/eGFP+ cells which indicates that the BM was not excluded from the inflammatory milieu (Figures 3.4 B, F) which was extensive enough to thwart the architectural definition of the arterial blood supply and occlude visualization of the cells that make up its tm and ta layers. At this point, the ratio of CD45+/eGFP+ cells to CD45-/eGFP+ cells was the highest of all timepoints but began to change, especially in the BM at DPA10.

The CT at DPA10 was enlarged compared to DPA5 and earlier due to sprouting vessels displacing the stroma which caused CD45+/eGFP+ cells to scatter throughout a larger surface area (Figure 3.4 C). We must note that representative cross sections from many of these vessels displayed a one cell thick endothelial layer and were thus mostly labeled as capillaries but we

also observed simple vessels characteristic of venules and arterioles. After discounting the vascular lumina from the total CT area measurements, the percentage of CD45+/eGFP+ cells remained significantly higher than controls and both eGFP and CD45 levels low enough from the DPA5 CT to grant it a moderate (++) amount of expression (Figure 3.3 E). On the other hand, we observed that in the hypercellular BM at DPA10 there was a dramatic shift in expression favoring CD45-/eGFP+ cells suggestive of concurrent expansion of MPCs and resolution of inflammation specific to the BM compartment during this timepoint (Figure 3.4 G). With the exception of the presence of osteoclasts, the overall cellular content and arrangement of the blastema at DPA14, including representative DDBL regions (Figure 3.4 D) resembled that of the BM at DPA10. Notably, we observed that the BM components at DPA14 had already begun patterning better defined subcompartments and this was more evident around the re-emerging large arterial wall which hallmarks the BM vasculature of unamputated controls. In this instance however, the lumen was instead supported by CD45-/eGFP+ cells and some of these cells were arranged in a similar fashion to the prominent CD45-/eGFP- tm and ta cells identified in the early timepoints.

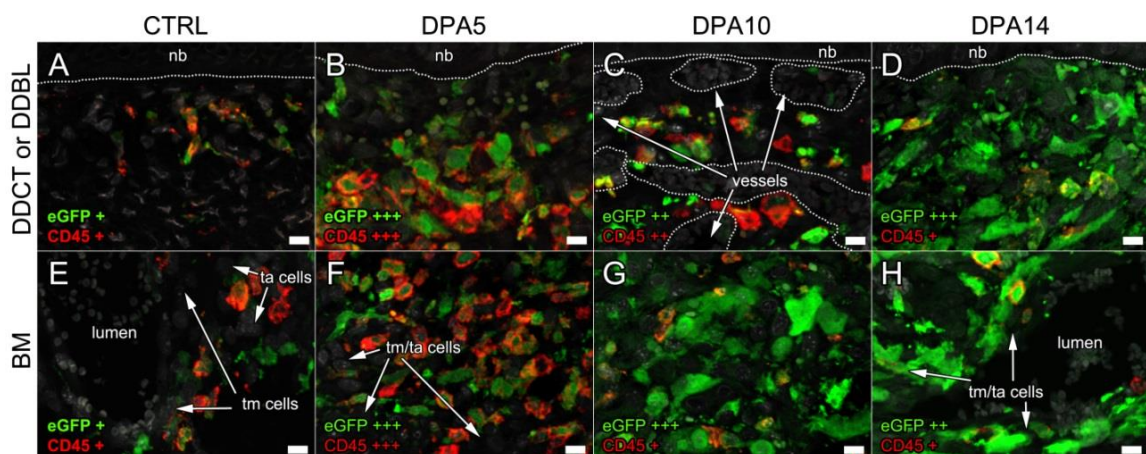


Figure 3.4: The co-expression of CD45 with eGFP+ BMDCs was dynamically and differentially regulated between digit BM and CT compartments and throughout regeneration timepoints. A shift in the ratio of HPCs to MPCs gated by CD45 expression was observed in the (A-D) dorsodistal connective tissue (DDCT)

or dorsodistal blastema (DDBL) below the nailbed (nb) and the (E-H) bone marrow (BM) cavity of D0 controls and regenerating digits at DPA5, 10, and 14. General concentrations of eGFP and CD45 were assigned a qualitative score of low (+), moderate (++), and high (+++). We must note that at DPA10, BMDCs scattered throughout the DDCT as the tissue layer was displaced by small newly formed vessels. Also, the BM cavity in particular was characterized by an arterial blood supply with a large lumen immediately lined by tunica media (tm) and tunica adventitia (ta) cells and both vascular layers were ill defined by the mass accumulation of eGFP+ cells mostly around DPA10 and thus could not be labeled. Definition of these tissue layers re-emerged by DPA14 as BM compartmentalization was underway. Scale bars, 10 μ m.

These data suggest that the fundamental clotting and inflammatory phases of wound healing take place in a regenerating wound and, due to the scarcity of pre-existing resident CD45+/eGFP- cells, these early events are mostly orchestrated by BMDCs that differentiated into monocytic phagocyte lineages. The sudden decrease in CD45+/eGFP+ cells in the mature blastema not only indicate that the bulk of immune responders are limited to the inflammatory phase of repair but also that upkeep of the blastema structure is not dependent on persistence of a large number of immune cells. However, indirect triggering of blastema formation and growth by certain cytokines, chemokines, and growth factors produced by these CD45+/eGFP+ cells cannot be ruled out. Since only baseline percentages of CD45+ cells are measured in the later stages (DPA21-35) of regeneration and CD45- phenotypes prevail, we conclude that factors immediately derived from leukocytes do not have a direct effect in differentiation and patterning of the regenerate. Moreover, we have demonstrated that the turnover of CD45+/eGFP+ to CD45-/eGFP+ cell content in the CT and BM compartments is very dynamic but asynchronous. Although small vessel accumulation in the DDCT may facilitate circulating progenitor with access to the wound site, expansion of MPCs in the BM of P3 by DPA10 prior to blastema growth suggests a direct role of the pre-existing P3 BM as a major source of blastema cells.

Differential survival of BMDCs in the regenerate

So far our findings indicate that BMDCs occupied the wounded digit tip with cells of hematopoietic and mesenchymal features. Not surprisingly, the presence of most HPCs was restricted to the inflammatory phase of repair. Turnover of the cellular population was mostly observed by DPA10, where CD45⁻ BMDCs prevailed, thus changing the ratio of CD45⁺/eGFP⁺ to CD45⁻/eGFP⁺ cells and these BMDCs had spindle morphology. Because of this lack of CD45 expression, we described the bulk of eGFP⁺ spindle-shaped cells as non-immunological and mesenchymal. To begin examining the survival rate and fate of these MPCs over the course of regeneration, we co-labeled control and amputated digits from the defined timepoints by indirect immunofluorescence of Ki67, a nuclear marker present in all phases of the cell cycle except G0 (254), and the executioner of apoptosis, cleaved C3 which localizes to the cytosol (255). The differential expression of each antigen was recorded at the cellular level and the percentage of eGFP⁺ or eGFP⁻ cells expressing either one was calculated from the total CT or BM area and normalized to the almost negligible level of expression in control CT and BM. Emphasis was placed on DPA10, since based on our observations this period marked the turning point in both turnover of general cell phenotypes and enrichment of eGFP⁺ MPCs. We must note that, specifically in the BM of amputated digits, we were able to detect a small percentage of eGFP⁻ cells which expressed either Ki67 or C3 and these eGFP⁻ cells may be either the result of variations in sensitivity of the anti-eGFP staining and detection threshold of the CCD; inclusion of cells belonging to the tunica media of the major artery feeding the BM which survives irradiation and thus was negative for eGFP; or simply not achieving absolute BM reconstitution of the marrow exclusively with eGFP⁺ populations of HPCs and MPCs which can be explained by reports on the radioprotection to γ rays that characterizes a subset of BM stromal components(256, 257).

Expression of Ki67 in unamputated controls was mostly restricted to the proximal nailbed (nb) and ventral epithelium (ve) which were excluded from the analysis (Figure 3.5 A). We were unable to detect but one or two proliferating cells in either the CT or BM of control digits at any given point. Beginning at DPA0 through DPA5, a 3.1% increase of total Ki67 staining was observed in the CT when compared to controls and one fourth of these co-expressed eGFP (Figure 3.5 E). This indicates that during the inflammatory phase of repair during which CD45+ cells comprise the bulk of eGFP+ cells (Figures 3.3 A, B, E and 3.4 B), proliferation in the CT was not completely abrogated and this might have been due to recent evidence showing that accumulation of macrophages in the wound during inflammation is partially due to proliferation of local pre-existing monocytic phagocyte precursors rather than by recruitment of those derived from the BM in circulation alone (258). Cells continued to expand at an increased rate by DPA10 to an average of 13.0% of which 39.5% were eGFP+ (Figures 3.5 B, E, and I). Interestingly, of the total proliferation index peak of 21.2% at DPA14 in the blastema mesenchyme, less than one third of these cells also stained for eGFP (Figures 3.5 C, E, and J), which is consistent with blastema growth but does not explain why the highest yield of CD45-/eGFP+ cells is measured around the mature blastema stage (Figures 3.3 C, D, E and 3.4 D). However at DPA21, we observed a significant 26.5% decrease in total proliferation with a steady percentage of Ki67+/eGFP+ BMDCs compared to DPA14, thus indicating a decrease in proliferation of eGFP- cells (Figure 3.5 E). The total proliferation index decreases 2-fold to 8.4% at DPA28 from DPA21 with a simultaneous 62.9% decrease in Ki67+/eGFP+ cells. By DPA35, Ki67 staining almost reverted to DPA0 measurements and with a similar trend in eGFP and Ki67staining ratio we conclude that terminal differentiation had occurred for most cells (Figure 3.5 E). After the resolution of inflammation based on earlier CD45 expression studies (Figure 3.3), the dramatic deviation of eGFP- cells at the level of the wound CT at DPA14 combined with

the steady state of eGFP+ cells marks a possible support role of BMDCs in the survival of pre-existing local precursors.

The proliferation dynamics in the BM compartment of the regenerating digit portray a different profile. Consistent with BM reconstitution and expression of eGFP on most cells, Ki67 staining was mostly associated with donor BMDCs housed in the marrow cavity throughout the regeneration timeline. No significant deviations from the stable ratio between Ki67 to eGFP staining were detected before DPA21 (Figure 3.5 F). Most of the total Ki67+ fraction of cells was eGFP+ at DPA0 and DPA5, during which a 5.1% increase was measured (Figure 3.5 F) and based on the high expression of CD45 in the BM at this timepoint (Figures 3.3 A, B and 3.4 F) we conclude that these are proliferating monocytic phagocytes as previously observed within the CT of DPA5 amputations. At DPA10, prior to blastema onset in this model, we measured a 24.8% increase of proliferating cells in the bm of which an average 81.9% expressed eGFP (Figures 3.5 B, F, and I). Even though sampling error between total Ki67+ and Ki67+/eGFP+ at DPA10 was insignificant (Figure 3.5 F), we must note that we did find a number of eGFP- cells proliferating in the marrow and these were mostly associated with the endosteum (Figure 3.5 I, arrows). Since we described a drop in CD45 expression in the BM of DPA10 digits (Figure 3.3 G), it is unlikely that this dramatic increase in eGFP staining is due to expansion of the hematopoietic lineage.

By the time the blastema mesenchyme is saturated by an increasing number of actively replicating CD45-/eGFP- cells and CD45-/eGFP+ cells with lower but steady proliferation index, we detected a significant decrease in overall Ki67 reactivity by one third of DPA10 expression in the more patterned BM compartment during DPA14 (Figures 3.4 H and 3.5 C, F, and J). We also measured a significant average increase in the number of Ki67+/eGFP- cells of 32.8% and 43.3%

from the total dividing cells in the marrow at both DPA14 and DPA21, respectively, and these were continually associated with the endosteum layer of P3 (Figures 3.5 F and J, arrows). It is well documented that most cells lining the endosteum are osteoblasts and these undergo cell cycle arrest following marrow radioablation in an NF κ B pro-survival signaling-dependent manner, which protects them from radiation-induced apoptosis and upholds their role as modulators of progenitor niches in the BM (259). Therefore we cannot rule out that the source of the increase in eGFP⁻ cells in the BM at DPA14 and DPA21 is an expanding eGFP⁻ subset of radioprotected osteoblasts from the pre-existing P3 fragment that gradually reconstitutes that tissue layer within the BM of the regenerating P3. The steady decrease in Ki67 expression returned to baseline levels by DPA28 and DPA35 (Figures 3.5 D and F) without significant gaps in the ratio between total dividing cells and those that were eGFP⁺ and this signals the end of growth of the regenerate with a focus on differentiation.

Unlike the index of proliferation, the trend in expression of cleaved C3 was less asynchronous between compartments and timepoints and an almost undetectable fraction of a percentage of cells were positive in unamputated controls. In general, the total number of cells undergoing apoptosis decreases as regeneration progresses with near baseline counts occurring after DPA28 in the CT and BM compartments alike and only significant changes were measured between eGFP⁺ and eGFP⁻ subpopulations (Figures 3.5 G, H). In both the CT and BM there was an overall increase of apoptosis in 7.6% of total cells by DPA5 (Figures 3.5 A, B, G, and H). Since previously we measured that most eGFP⁺ cells in both the CT and BM at DPA5 co-expressed CD45⁺ and conversely very few cells were measured or observed to be CD45⁺/eGFP⁻ (Figures 3.3 A, B, E and 3.4 B, F), we attributed the increase in staining for apoptosis to inflammatory eGFP⁺ HPCs with a short lifespan thus, along with a decrease in CD45 staining, the elevated level of C3 served as an indicator of resolution of the inflammatory phase. Based on this, we report

that while half of the C3+ cells at DPA5 co-expressed eGFP in the CT, 71.3% were eGFP+ in the BM and the difference between total and eGFP+ cells in the BM expressing C3 was insignificant (Figures 3.5 G and H). In both compartments, apoptotic eGFP+ cell content by DPA10 significantly decreased by 2-fold from DPA5 while changes in the total C3+ fraction remained insignificant, indicating an increased amount of apoptotic eGFP- cells (Figures 3.5 B, G-I). We could not rule out that C3+/eGFP- cells up to DPA10 belonged to a pre-existing non-BM derived cell phenotype still responding to death cues brought on by damaged vasculature, inflammation, matrix degradation, or a combination of these events.

Following blastema onset at DPA14, apoptosis remained at an average 2.5% higher than baseline and only a fraction of a percentage of these were eGFP+, especially in the BM compartment. Therefore, at DPA14 the majority of dying cells in both sites were eGFP- and since we ruled out most of these from being of a hematopoietic origin, an alternative is that they were part of short-lived support structures derived from pre-existing compartments similar to the transient sprouts of endothelial cells that arise during the granulation phase of wound healing. Along with a peak in proliferation index measured in the BM prior to that of the CT (Figures 3.5 B-C, E-F, and I-J), the earlier clearance of C3 activity suggests that the BM is one of the first compartments of the regenerate to undergo microenvironmental modifications conducive to increased survival of BMDCs. We were unable to detect significant changes in C3 staining in neither compartment following DPA14 nor a significant difference in apoptosis percentages between eGFP+ and eGFP- cells from the CT in this regard (Figures 3.5 G-H). However C3 staining was still detectable in an average of 1.75% of eGFP- cells in the BM. Along with the proliferation index results of the eGFP- fraction in the BM between DPA14 and DPA21, the moderate presence of eGFP- cells, a fraction of which expresses C3, not only confirms the

ongoing presence of radioprotected cell types in the marrow but also suggests a prolonged turnover of this population in a compartment-specific manner.

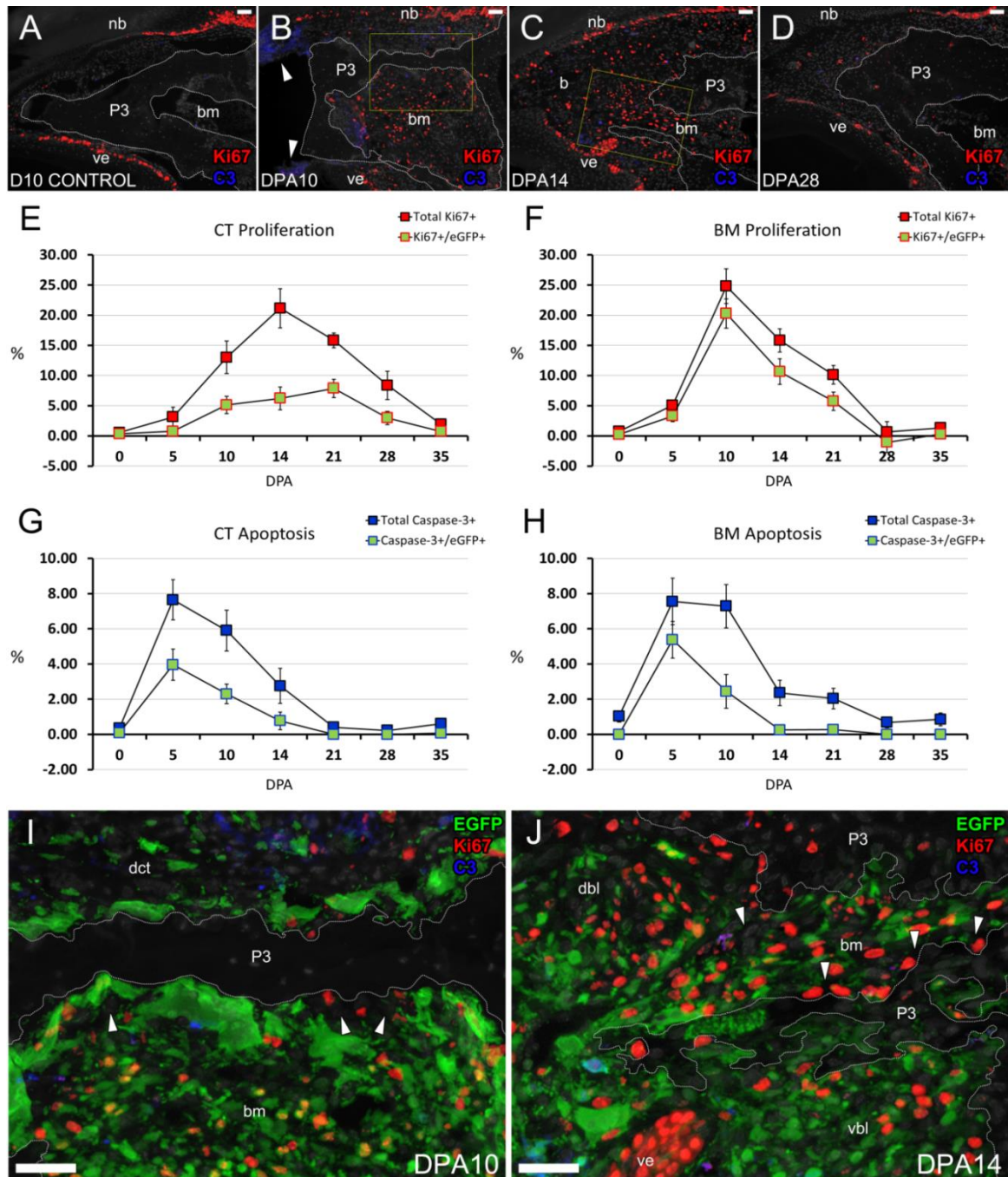


Figure 3.5: Sections of control and amputated digits at defined timepoints were stained for Ki67 and cleaved-Caspase-3 (C3) to show that apoptosis is restricted to the early stages of repair, proliferation of eGFP+ cells in the BM precedes blastema formation, and BMDCs in the blastema are progressively diluted by proliferating local cells. Analyses were restricted to the bone marrow (bm) cavity and the connective tissue (ct) areas between the nailed (nb) or ventral epithelium (ve) and the P3 phalanx. (A-D)

Low magnification (100X) views of unamputated control and DPA10, 14, and 28 timepoints of regeneration co-express Ki67 and C3 with DPA10 and 14 showing the most dynamic differences in survival between timepoints and compartments. Indices of both proliferation and apoptosis returning to baseline levels by DPA28 mark the end of growth and, paired with histological analysis, an ongoing focus on differentiation. (E-H) Cells expressing nuclear Ki67 or cytosolic C3 were counted and graphed as a percentage of total CT or BM area. Data are presented as mean \pm SE (n = 4 per timepoint). (I-J) Higher magnification photomicrographs from DPA10 and 14 regions of interest marked by the yellow rectangle in the (B-C) lower magnification composites to include the dorsal ct (dct) or dorsal and ventral blastema (dbl or vbl, respectively) and bm compartments demonstrate the localization and distribution of proliferating and apoptotic cells. Most eGFP- cells associated with the bm expressing either both or neither marker (white arrows) were localized to the endosteum thus suggesting that a population of pre-bm transplant cells resilient to irradiation undergo dynamic turnover specifically detected throughout bone remodeling but not in the pre, early or post-regenerate bm microenvironment. Scale bars, 50 μ m.

BMDCs differentiate into FRCs and participate in blastema scaffold engineering and long-term structural support of regenerated structures

According to our results so far, amputated digit tips proceed through an initial response that involves an inflammatory phase which is driven by a large number of CD45+ BM-derived HPCs and these cells comprise the bulk of the eGFP+ population of BMDCs in the CT up to DPA10. However, concurrent with a decrease in CD45+ HPCs, a large percentage of eGFP+ cells which tested negative for CD45 aggregate in the blastema at DPA14. Based on the large ratio of proliferation index to apoptosis potential, we concluded that the blastema microenvironment can sustain these cells. We have also demonstrated that a moderate amount of FRCs in the CT of unamputated digits retain exclusive expression of the ER-TR7 antigen and detection of this protein by immunolabeling with a monoclonal antibody results in prominent staining which outlines digit structures such as vessels, bone, and epithelial basement membranes. Moreover, we also measured that along with accumulation of fibroblasts in the blastema comes the overexpression of this antigen at the subcellular level of the cytosol and membrane of FRCs and as secreted filaments in the blastema extracellular space. So we next tested the ER-TR7 antibody in coexpression with eGFP on our control and amputated digits from the BM chimeras

to determine if BMDCs of CD45- and mesenchymal phenotype differentiate into FRCs in the regenerate.

On average, a fourth of total CT cells in controls from all timepoints and digits at DPA0 stained positive for ER-TR7 but consistently less than half a percent of these were eGFP+ (Figure 3.6 F) thus suggesting that under normal conditions the grand majority of eGFP+ cells in the control CT were CD45+ resident cells or non-hematopoietic ER-TR7- cells (Figure 3.4 A). As previously described, ER-TR7+ cells and associated extracellular filaments in the CT are predominantly found tethered to basement membranes of the skin, extravascular linings, and the periosteum of P3. In the BM, ER-TR7 reactivity is limited to the endosteum and tunica adventitia of the main arterial blood supply (Figure 3.6 A). Since most ER-TR7+ cells in sub-compartments of the CT and BM from control digits and DPA0 did not express eGFP, these data also suggest a strong baseline presence of resident FRCs which either experienced a slow turnover frequency or were not derived from the BM after transplantation.

During the inflammatory phase at DPA5, we observed apoptosis (Figure 3.5 G) and indications of matrix degradation mostly at the level of the CT dorsal to P3 with total extinction of FRCs distal from the midline of the pre-existing digit tip thus lowering the percentage of ER-TR7+ resident cells in the total CT over 2-fold from controls (Figure 3.6 A, B, and F). Along with initial enrichment of the BM with CD45+/eGFP+ cells during DPA5 (Figures 3.3 A and 3.4 F), we observed an unexpected increase in ER-TR7 staining beyond the normal endosteum and tunica adventitia layers described earlier therefore potentially identifying the BM as the primary site of homing and/or expansion of blastema FRCs (Figure 3.6 B). By DPA10, the total ER-TR7+ population in the CT dorsal and ventral to the phalanx recovered to levels measured in unamputated and DPA0 digits and 42.61% of these expressed eGFP (Figures 3.6 C and F) which

points to a correlation with the gradual accumulation of ER-TR7+/eGFP+ cells in the BM from DPA5 to DPA10 (Figures 3.6 B and C) along with the displacement of the dorsal CT at DPA10 by newly formed vessels described previously (Figure 3.4 C). This indicates that those vessels, along with the exposed distal BM compartment are facilitating migration of BMDCs to the injury site.

The results from DPA14 regenerating digits in the BM chimeras were consistent with our previous findings indicating that the blastemas of neonatal and adult mice become enriched with ER-TR7+ FRCs around this timepoint. In the present study we measured a 3-fold increase from DPA10 in the amount of FRCs co-expressing eGFP to encompass half the population of ER-TR7+ FRCs in the total CT area of the regenerate at DPA14 excluding the BM (Figures 3.6 D and F). Alongside ER-TR7+ BMDCs, there was also expansion of eGFP negative FRCs, which comprised 41.7% of the total population of ER-TR7+ FRCs in the CT at DPA14, an increase of 1.6 fold from DPA10. But then we measured a simultaneous decrease in both eGFP+ and eGFP- FRC populations beginning at DPA21 with a total decrease of 24.5% of total FRCs and 13.5% from those expressing eGFP+ by DPA28. However, at DPA28 we observed that most of the blastema area is occupied by trabecular bone and many of the cells within the trabeculae are negative for eGFP. Furthermore, we noticed that the eGFP+ population in the remaining soft tissue portion of the blastema was not as prolific, thus indicating that cells which were not derived from the BM progressively diluted the eGFP+ cells (Figures 3.6 E and F). Near the endpoint of regeneration at DPA35, the percentage of total ER-TR7+ cells in the CT approximated control levels and less than half of those remaining cells expressed eGFP and this subpopulation encompassed 10.5% of the total cellular content. Nonetheless, we not only found that many of the remaining eGFP+ cells had active ER-TR7 expression but that they had also become part of basement membranes and supporting stroma. For example, we observed this long-term

presence in the regenerated dorsal CT. Unlike the age-matched control chimeras, which exhibited scarce eGFP+ cells randomly distributed throughout the CT without direct association with structures such as vessels (Figure 3.6 G), similar regions in DPA35 regenerates housed spindle ER-TR7+/eGFP+ cells outlining below the stratum basale of the nailbed and within the tunica adventitia surrounding vessels (Figure 3.6 H).

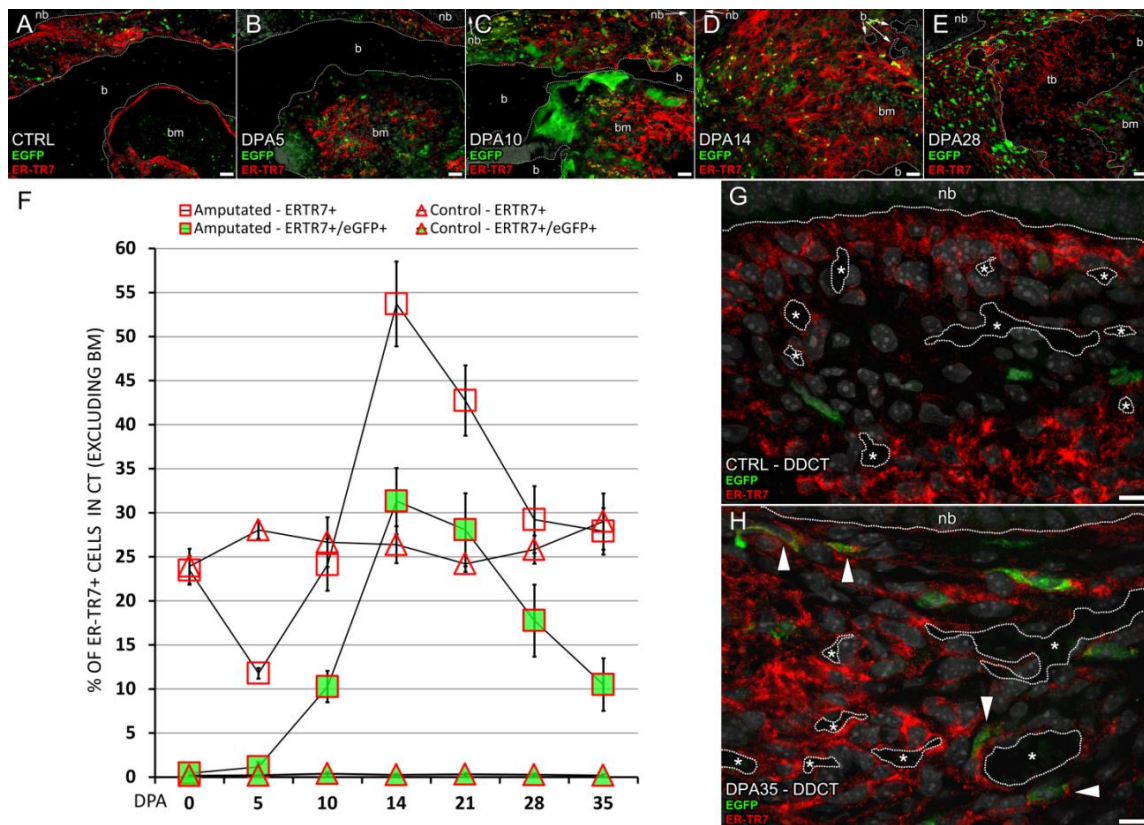


Figure 3.6: Immunohistochemical co-expression and quantitation of eGFP with ER-TR7 indicate that BMDCs differentiate into FRCs in the BM and these FRCs and expression are propagated to the wound site to initiate blastema growth and scaffolding. (A-E) Representative photomicrographs including dorsodistal connective tissue (CT) and marrow (bm) regions encased by the nailbed (nb) or P3 bone (b), respectively, of control (CTRL) and amputated digits at days post amputation (DPA) 5, 10, 14, and 28. Scale bar, 50 μ m. Imaging of stained digit sections (n=4 per timepoint and control) was followed by objective digital quantitation of cells in the CT expressing cytosolic eGFP with membranous and/or cytosolic ER-TR7 staining. The bm was excluded from these measurements. (F) Results were graphed as total ER-TR7+ versus ER-TR7+/eGFP+ subtotal percentages and show that a subset of BMDCs have the ability to synthesize and become part of the majority of the ER-TR7 scaffold by the mature blastema stage at (D, F) DPA14. However, even though the CT area increases over time, the eGFP signal, along with ER-

TR7+ expression becomes gradually diluted in the CT by an increase in eGFP- cells and emerging trabecular bone (tb) more prominent by (E, F) DPA28. Regardless, in comparison with age-matched (G) controls, we observed that eGFP+/ER-TR7+ cells have a long-term presence in the (H) DPA35 regenerate as support cells mainly in the stratum basale of the epidermis and the tunica adventitia of a few vessels (white arrows). (G, H) Scale bar, 10 μ m. Merged with all images is the DAPI nuclear counterstain (gray).

Combined with our regenerating adult BM chimera survival studies (Figures 3.5 C, E, and F) and the proliferation dynamics of ER-TR7+ cells during matched timepoints of neonatal digit tip regeneration (Figures 2.6 A, C, and D), these data so far suggest that enrichment of blastema FRCs is dependent on both expansion of eGFP+ FRCs inside the BM followed by migration towards the distal wound and expansion of eGFP- precursors of FRCs originating from the local CT. Experiments involving digit tip amputations following *in vivo* labeling of P3 marrow cells with Dil *in situ* or engraftment of tagged fibroblasts into the P3 BM provide evidence that cells in that compartment migrate to the blastema site (162). Regardless of eGFP reporter expression, blastema FRCs with secreted and membrane-bound ER-TR7+ fibers (Figure 3.7 B) aggregated and stretched parallel to the proximodistal axis of the DPA14 blastema towards the wound epidermis, which is consistent with prior observations (Figures 2.4 A and 3.7 A). Based on our observations and measurements, we hypothesize that (I) BM-derived mesenchymal precursors of FRCs become enriched and are primed to secrete ER-TR7 in the BM prior to onset of the blastema; followed by (II) distal outflow of FRCs into the immature blastema site with consequential increase in ER-TR7 expression but decreasing BM cellular content; and colonization of the blastema space thus promoting its growth alongside further decellularization and differentiation of the BM compartment (Figure 3.7 C). In other words, initial outgrowth of the blastema structure is directly linked to *in situ* expansion of MPCs in the P3 BM source followed by migration towards the wound epidermis. Circulating BMDs were ruled out from being the primary contributors to the general blastema population since observations at the

level of the dorsoproximal CT which we described as sprouting with young vessels at DPA10 indicate similar availability of eGFP+ cells between DPA10 and DPA21 (Figures 3.7 D-F). On the other hand, in addition to early hypercellularity, more dynamic changes were recorded between DPA 10 and DPA21 in the BM cavity such as decreasing cellularity over time with patterning of structures (Figures 3.7 G-I) and without evidence of apoptosis based on our survival studies, thus supporting that many of the cells which had previously expanded there migrated out.

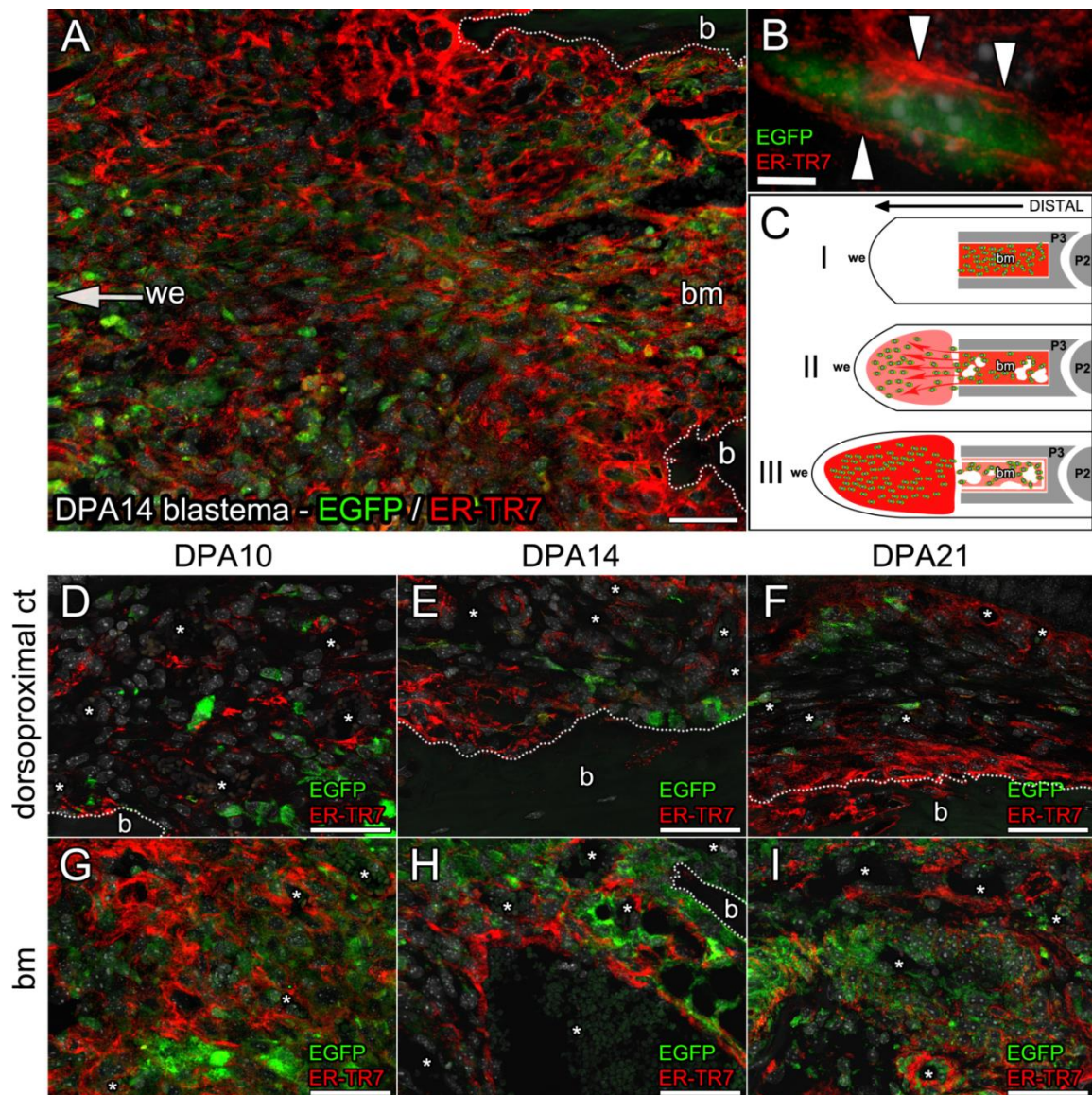


Figure 3.7: A major source of blastema cells is the P3 BM and these occupy the blastema site along the proximodistal axis towards the wound epithelium as FRCs. (A) Further microscopic analysis of DPA14 blastemas reveal ER-TR7+/eGFP+ cells in agreement with following a proximodistal growth pattern from

the marrow (bm) towards the wound epithelium (we). (B) Many eGFP+ cells were encased by ER-TR7+ membranous expression (white arrows) with secreted ER-TR7+ microfilaments into their immediate extracellular space. (C) Hypothetical diagram of the basic steps followed by BMDCs capable of expressing ER-TR7 and colonization of the blastema depicts: I. Ongoing expansion of eGFP+ mesenchymal progenitors primed to become ER-TR7+ FRCs in the bm between DPA5-10; II. Migration of these cells in the immature blastema site with further priming to generate the ER-TR7+ scaffold with initiation of decreasing cellular content of the bm and more patterned ER-TR7 expression between DPA10-14; and III. Colonization and growth of the blastema site with organized but upregulated ER-TR7+ scaffolding and further decellularization and patterning of the bm between DPA14-21. (D-F) We found little evidence of contribution of circulating eGFP+ FRCs to the blastema from the small newly formed vessels in the dorsoproximal region of the CT above the bone (b) during the timepoints in which we had measured the greatest blastema onset and growth. (G-I) On the other hand, qualitative analysis of the bm at the same timepoints demonstrate a gradual decrease in ER-TR7+/eGFP+ cells with increasing evidence of discreet patterning such as the outlining of vasculature within the bm. Scale bars (A): 50 μ m; (B): 10 μ m; and (D-I): 50 μ m.

BMDCs remodel bone and integrate into phalangeal membranes

We have provided evidence that BMDCs of mesenchymal phenotype which expand in the pre-existing BM of regenerating P3 participate in onset and growth of the blastema by differentiating into FRCs and expanding the ER-TR7 network of fibers. Even though an average of over half of the eGFP+ cells housed in the mature blastema at DPA14 were ER-TR7+, there was a large percentage of BMDCs remaining with undetectable ER-TR7 and therefore unknown fate. Since the endpoint neonatal or adult regenerate is largely composed of mineralized bone matrix arising from direct ossification (12, 13) stemming from the pre-existing P3 stump (137) - blastema interface, we decided to employ co-labeling of eGFP and ER-TR7 with Osteocalcin (OC). Quantitation was limited to the CT around the phalanx thus excluding the BM cavity. Assessment of osteoblasts in the endosteum was limited to qualitative observation. Although limited to the periosteum and trabeculae in the remodeled bone of the regenerate, the assay would serve three purposes: (1) to determine if any osteoblasts coordinating bone remodeling are derived from the BM; (2) to demonstrate that potential OC+/eGFP+ cells and ER-TR7+ FRCs follow a pattern consistent with periosteum and endosteum layers described previously (Figure

2.2 C); and (3) to answer if the fate of these OC+/eGFP+ cells is long-term. Since we observed the presence of eGFP+ cuboidal cells tethered to both the endosteum and periosteum of P3 during preliminary analysis of the amputated chimera digits (Figures 3.1 B, C, I, and 3.2 I, L, O, and R) we were inclined to believe that a percentage of total OC+ cells or osteoblasts would stain positive for eGFP.

We were unable to detect definitive OC+/eGFP+ co-expression in the periosteum of age-matched unamputated digits (Figure 3.8 E) and DPA0 samples. However, we do note that in several control samples we were able to find OC+/eGFP+ cells scattered in the endosteum layer of the BM (Figure 3.8 I, white arrows). We attribute this to direct repair after irradiation-induced damage of the marrow and its lining with donor osteoblastic precursors and this was our first indication that the OC+/eGFP+ phenotype and the extended presence of this phenotype after injury were possible. This plausible explanation has been demonstrated in ganciclovir and radiation induced damage of host bone lining followed by engraftment and integration of donor BM-derived osteoblast progenitors from total and calvaria BM to repair the injury (260). On an average, the total number of OC+ cells in the periosteum comprises 5.5 to 6% of the total cell population in the CT space. Along with a gradual decline of half the population originally found in controls and DPA0 digit due to bone resorption and degradation, rare occurrences of OC+/eGFP+ events began to be detected at DPA10, during which roughly one fifth of the osteoblasts expressed eGFP (Figure 3.8 D). And this subpopulation doubled by DPA14, where we also measured overall gradual recovery of OC+ cells as evidence of bone regrowth which was expected around this timepoint consistent with previous studies (137, 261). A significant spike in osteoblast numbers of an average 1.5% above control was measured at DPA21 (Figure 3.8 D). It was during this timepoint in our model that direct ossification and growth of trabecular bone were the most prominent (Figure 3.8 A) and even though there is evidence suggesting that

osteoblasts participating in digit tip regeneration come from lineage-restricted progenitors (261, 262), we were able to detect scattered OC+/eGFP+ cells lining trabeculae and regenerated continuation to the pre-existing endosteum (Figure 3.8 B, C, white arrows). With exclusion of the BM cavity and thus the endosteum OC+/eGFP+ cells added to an average of nearly one third of the osteoblast population and the great majority of these cells were housed within the trabeculae. Consistent with the stratification of neighboring ER-TR7+ and OC+ cell layers which encase the mineralized bone matrix and lines the BM and trabeculae as periosteum or endosteum (Figure 2.2 C), we were also able to identify cells co-expressing ER-TR7 and eGFP in close association and conventional pattern with OC+/eGFP+ cells and the overall osteoblastic linings (Figures 3.8 B, C, yellow arrows).

Overall, these data so far hint at a notable contribution from BMDCs to the osteoblast phenotype during regeneration and their incorporation into patterned subcompartments. Even though the overall OC+ percentage changes are insignificant between after DPA21, the OC+/eGFP+ population counts significantly decrease over 2-fold into DPA28 but plateau near the endpoint of regeneration by DPA35 (Figure 3.8 D). The significant decrease in DPA28 can be attributed to dilution of the OC+/eGFP+ cells by truly fate-restricted pre-amputation niche or lineage (262) and the overall decline in eGFP staining with sudden takeover of eGFP negative cells is most prominent within the direct ossification zone or new forming trabecular bone after DPA21 (Figures 3.6 E and 3.8 A). Nonetheless, the persistence of OC+/eGFP+ cells even at less than one fifth of the total OC+ population excluding the BM compartment alludes to the long-term commitment of BMDCs to regenerated bone and the possibility of an additional lineage restricted population originating from the P3 BM. Events suggestive of the incorporation of OC+/eGFP+ cells in the periosteum of the regenerate were more detectable near the endpoint of regeneration at DPA35 (Figure 3.8 F). We found scattered OC+/eGFP+ cells tethered to the

regenerated trabecular bone of P3 (Figure 3.8 H, white arrows) co-existing with OC+/eGFP- osteoblasts. The same elongated or cuboidal cell phenotype was found in unamputated cortical bone of P3 without evidence of eGFP signal (Figure 3.8 G). Not surprisingly, we were able to observe OC+/eGFP+ cells in the endosteum of the BM in both unamputated and regenerated samples (Figures 3.8 I and J, white arrows) but it was there that we were able to capture an overlying layer of ER-TR7+ cells of which some expressed eGFP (Figures 3.8 I and J, yellow arrows) and thus providing further evidence of multilayer patterning. It has been known that osteoblasts can remain inactive, undergo apoptosis, or slow down matrix production to become embedded in the mineralized bone matrix as osteocytes following bone growth (263). Interestingly, we were also able to observe in the bone underlying both the periosteum and endosteum layers of P3 eGFP+ cells embedded in the trabecular bone matrix of the regenerate only (Figures 3.8 H and J, gray arrows), which only adds to evidence of the long-term commitment and functional preservation of the OC+/eGFP+ lineage derived from the BM.

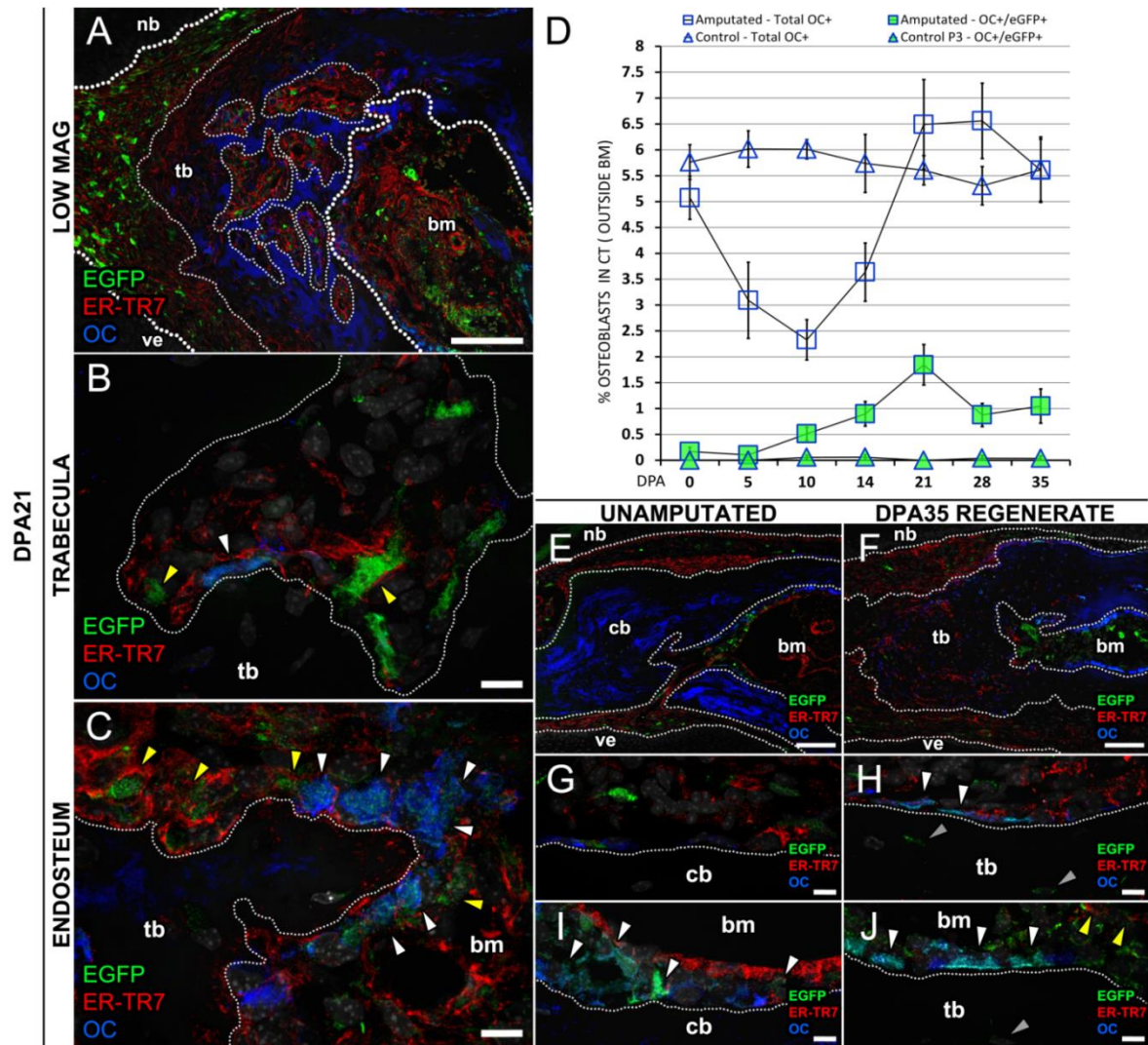


Figure 3.8: A fraction of BMDs in the blastema actively participate in bone remodeling as osteoblasts.

We co-labeled digit sections from age-matched unamputated controls and all regeneration timepoints using antibodies against eGFP, ER-TR7, and OC. The signals were subsequently cross-matched to count eGFP/OC co-localization events and observe if the patterning of OC+ cells with ER-TR7+ cells correlated with conventional architecture following regeneration. (A) The influx of osteoblasts in the regenerate peaked at DPA21 and these are mostly detected outlining the periosteum, endosteum of the marrow (bm), and trabeculae of the regenerating trabecular bone (tb) portion of P3. Scale bar, 50 μ m. (B) The subpopulation of OC+/eGFP+ cells was mostly detected lining the trabecular spaces (white arrows) and co-existing with ER-TR7+ or ER-TR7+/eGFP+ FRCs (yellow arrows). (C) Many OC+/eGFP+ osteoblasts integrated in the endosteum lining of the bm (white arrows) and surrounded by ER-TR7+ or ER-TR7+/eGFP+ FRCs (yellow arrows) in most controls and regenerates, thus indicating a direct participation of eGFP+ donor BMDs in general homing, restoration, and repair of the bm after irradiation damage prior to amputation injury. Scale bars for B and C, 10 μ m. (D) OC+ only and OC+/eGFP+ cells were counted within the connective or blastema tissue area with exclusion of the bm (n=4 each for age-matched control and amputated timepoints) and these data show a progressive percentage of OC+ cells invading the tissue with a peak at DPA21 and insignificant changes from that percentage towards the

endpoint of regeneration. A similar trend was measured with the OC+/eGFP+ fraction with nearly one sixth of the total OC+ population expressing eGFP which means that a long-term presence of a fraction of BMDCs with an osteoblastic phenotype is active in the endpoint regenerate. (E) Age-matched unamputated and (F) DPA35 regenerate low magnification views show direct ossification of the regenerate near completion as tb no longer subcompartmentalized by many trabecular spaces and thus at this point any OC+/eGFP+ events were mainly detected in the periosteum and endosteum. Scale bars for (E-F): 50 μ m. (G) Control cortical bone (cb) and (H) regenerated trabecular bone (tb) periosteum at day 35 is composed of a monolayer of flattened OC+ osteoblasts surrounded by ER-TR7+ FRCs. OC+/eGFP+ co-labeled cells were only detected in the regenerate (white arrows) and some cells embedded in the bone matrix or osteocytes by definition, were also labeled with eGFP in the regenerate only (gray arrows). (I) Day 35 controls and (J) DPA35 regenerates consistently co-expressed OC and eGFP in the bm endosteum (white arrows) in a patterned layer with integrated ER-TR7+ and ER-TR7+/eGFP+ FRCs (yellow arrows) which is one of the main reasons why we excluded it from quantitative analyses. We could not rule out if these events in the regenerate were brought on by pre-amputation radioablation, amputation injury, or both. (J, gray arrow) Similar to the bone matrix areas adjacent to the periosteum, we also noted eGFP+ osteocytes near the vicinity of the bm cavity in the regenerate only which may be an indication of a more prolific eGFP+ osteoblast presence in the regenerate's endosteum thus making eGFP+ osteocyte events more frequently detectable. Scale bars (G-J): 10 μ m.

BMDCs actively participate in transient blastema contraction and angiogenesis but are limited in permanent vascular layers

To study the participation of BMDCs in the regenerate's vasculature, we employed immunohistochemical labeling of age-matched unamputated controls and amputated digits at the specified timepoints with a primary antibody against the blood glycoprotein von Willebrand Factor (VWF) exclusively biosynthesized by endothelial cells and megakaryocytes (264, 265) which forms a complex with a platelet-derived co-profactor glycoprotein Factor 8 (FVIII) to promote platelet adhesion and coagulation in wounds (266). For practical purposes, the VWF-FVIII complex detected in endothelial cells by immunolabeling was labeled and referred to FVIII in this study. In previous studies we co-labeled FVIII with α -smooth muscle actin or SMA, a marker of smooth muscle cells in various organs especially in the tunica media cells and pericytes of the vasculature (267, 268) but also non-smooth muscle cells such as myofibroblasts (269).

As independent markers of the vasculature, FVIII and SMA are specifically localized to the endothelial layer and surrounding tunica media of all vascular subtypes of arteries and veins of the unamputated digit CT and BM with the exception of capillaries, which are one endothelial cell thick and devoid of a defined smooth muscle layer. Only the CT from all samples was analyzed and measured for the labeled markers. Typical FVIII immunolabeling was expressed in a globular pattern within the lumen of most vessels showing portions the tunica intima or endothelium. Only cells with direct membranous and/or cytosolic FVIII signal were counted and these comprise an average 4% of the total population in representative sections. But following analysis of all timepoint-matched unamputated controls, we found no direct correlation between eGFP staining and FVIII within the endothelium (Figures 3.9 A and E). As expected, we measured a sharp 2-fold decrease in FVIII staining following amputation without significant recovery until DPA21 (Figure 3.9 E). Between DPA10 and DPA21 however, we counted an influx of FVIII+/eGFP+ co-labeled cells within the recovering vasculature which amounted to half a percentage of the total CT population and one fourth of FVIII labeled endothelial cells (Figures 3.9 B, C, and E). After DPA21, FVIII+ cells were more detectable and steadily recovering to baseline levels as early as DPA28. Following the co-expression peak at DPA21 on the other hand, the percentage of FVIII+/eGFP+ cells was diluted to control levels (Figures 3.9 D and E). These findings suggest an active role of BMDCs in angiogenesis of the regenerate but this contribution is limited to the initial stages of the process or to the evolution of the transient vasculature which is known to develop between the inflammatory and granulation stages of wound healing in this case to support the bulk of colonizing blastema cells.

Another well-defined layer of the vasculature is the tunica media composed of SMA+ cells but in digit sections careful examination of signal counts were carefully recorded because the interface between SMA+ and FVIII+ cells was complex, especially around tangential cuts of

venules and arterioles and their respective bifurcations and interfaces with major veins and arteries (Figures 3.10 A and B). The SMA+ signal in these cells was observed and measured at 2 to 3-fold stronger arbitrary light units than that in non-vascular SMA+ cells. In general, SMA+ cells in timepoint-matched controls were restricted to the vascular compartments and these accounted for an average 4-5% of the total CT cellular area (Figures 3.9 A and F). Even during the tissue degradation and resorption around the wound that is typically observed at DPA5, we did not record any negative changes in the concentration of SMA signal, which remained at baseline counts. This means that even though we measured a decline in vascular area by FVIII staining, non-vascular SMA+ signal compensates for vascular-related SMA+ staining potentially in the form of early migration of SMA+ cells and this is confirmed by the average increase of this SMA+ subtype of 13% and 20% at DPA10 through DPA14, respectively, from controls (Figure 3.9 F). We observe that non-vascular SMA+ cells permeate the blastema at DPA14 (Figure 3.9 B). And a fraction of these cells expressed eGFP in parallel increase to peak at nearly half of the overall SMA+ population at DPA14 (Figure 3.9 F). So far these data provide evidence of a significant rise in the SMA+ population composed of both BM and non-marrow derived cells which colonize the wound concurrent with blastema growth. Although insignificant, we began measuring an overall decline in SMA staining at DPA21, with signal becoming better defined and distributed (Figure 3.9 C). Progressive and significant decrease to nearly 36% and 60% from the peak of expression followed at DPA28 and DPA35, respectively, with SMA+ cells mostly re-assigned to vascular structures (Figures 3.9 D and F). This means that SMA expression is transient and mostly restricted to the pre-differentiation stages of the regenerate and due to its function in tissue contractility, active molding of the blastema structure. Beginning at DPA21, cells co-expressing eGFP also followed a significant and steady decrease around this period to end at DPA35 with less than half that of the co-expression peak measured at DPA14 (Figures 3.9

D and F). Overall, these data indicate an active multi-tissue compartment role of different subsets of smooth muscle cells in both transient soft tissue contraction between DPA10 and 21 during undefined blastema expansion followed by restructuring of the regenerate's vasculature around the endpoint of regeneration.

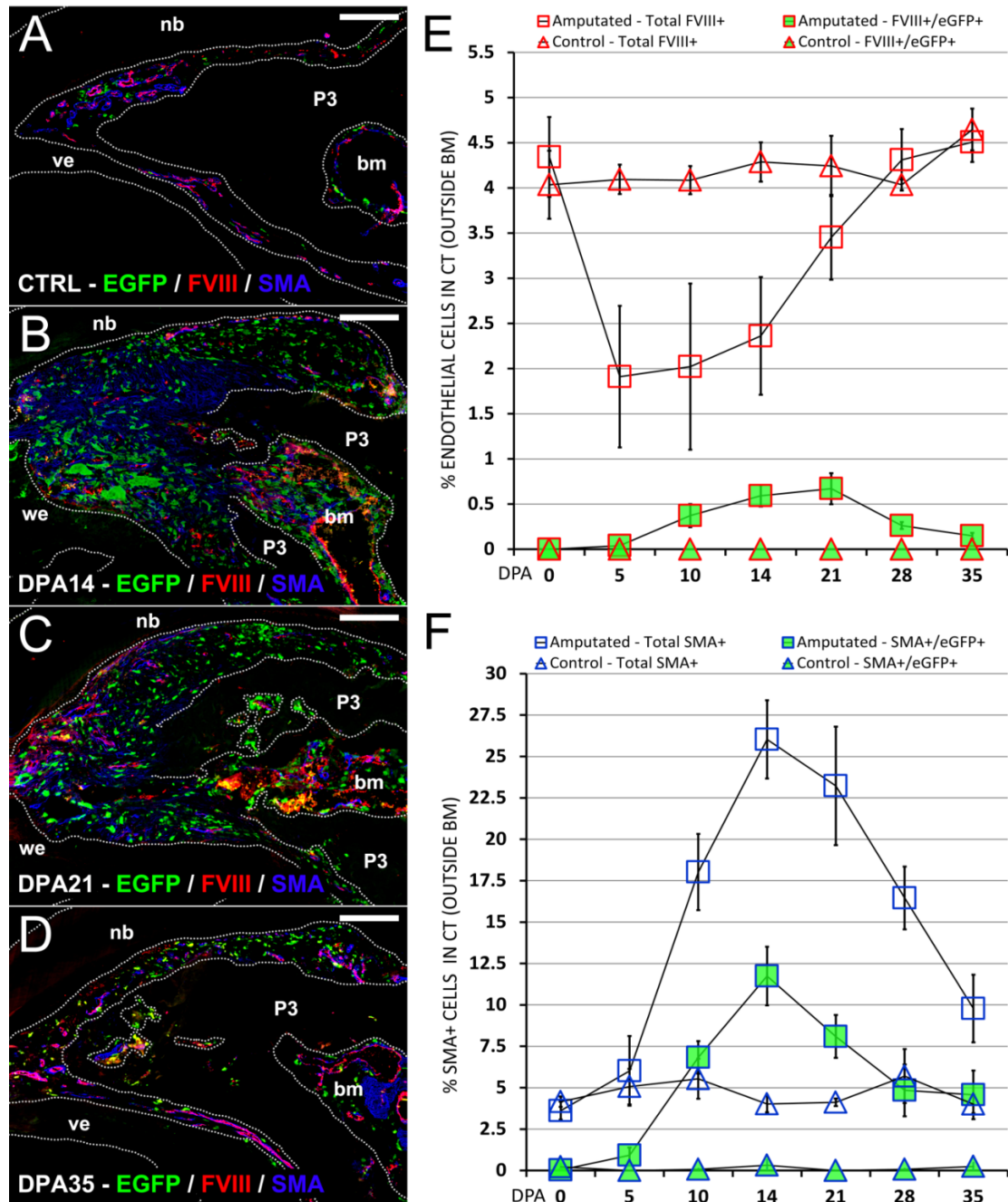


Figure 3.9: Detection and quantitation of total and eGFP+ subpopulation of FVIII+ and SMA+ cells in representative unamputated control, DPA14, DPA21, and DPA35 regenerating digit tips show

reasonable contribution of these cells during the blastema and early regenerate differentiation stages but limited persistence by the endpoint of regeneration. (A-D) 100X magnification photomicrographs of triple immunolabeling of eGFP, FVIII, and SMA. Major tissue compartments such as the nailbed (nb), P3 phalanx (P3), bone marrow (bm), and ventral epithelium (ve) were outlined by dotted lines using histological landmarking with DAPI counterstain which is not shown to enhance multicolor contrast. (E and F) Cell counts expressed as percentage of total CT area graphed as (E) total FVIII+ and FVIII+/eGFP+ co-expression or (F) total SMA+ and SMA+/eGFP+ co-expression in control and regenerating digit tips at all timepoints. (A) Co-expression signals were undetectable in age-matched unamputated controls. Only discreet baseline FVIII and SMA labeling was detected associated with endothelium and smooth muscle layers of vessels. All eGFP+ cells in controls, if any, were negative for the markers. (B and E) The mature blastema at DPA14 marks the beginning of FVIII upregulation with incorporation of cells co-expressing eGFP. (B and F) Many SMA+ cells express eGFP+ in the blastema indicating actin fiber-mediated contraction. (C) The DPA21 regenerate provides evidence of differentiation and patterning by distal remodeling of the P3 bone but also by more defined vascular structures with multicellular endothelium with a (E) higher incidence of incorporated FVIII+/eGFP+ cells and (F) downregulation of extravascular SMA signal in both eGFP+ and eGFP- cells. (D) DPA35 show the end result of the progressive and long-term rescue of the vasculature with (E) a small percentage of integrated FVIII+/eGFP+ cells and (F) a larger percentage of total SMA+ cells mostly restricted to vascular structures and SMA+/eGFP+ cells incorporated within and close to vascular layers. Scale bars (A-D): 50 μ m.

High resolution histological analysis of representative regions of interest from control and regenerating tissue demonstrate that we can identify vascular layer interfaces and further expands insight into the dynamic differentiation and positioning of SMA+ cells along vasculature and non-vascular layers. In general, SMA expression can be attributed to elongated cells with small to medium nuclei within the tunica media of vessels outlining FVIII+ luminal endothelium in tangential and cross-sectional slices of most vessels (Figures 3.10 A and B). As previously described, eGFP+ cells were located in the extravascular space or very close to vessels, indicating a phenotype limited to immune or fibroblastic (Figure 3.10 C, G, K, and O). We also found few instances of SMA+ cells not associated with vascular layers and none of these were labeled positive for eGFP. At the peak of blastema formation at DPA14 we found however more SMA+ cells in the extravascular space than those in the tunica media and many of these tested positive for eGFP (Figures 3.10 D, H, and P). This confirms a large emerging subpopulation of cells in the blastema which are positive for SMA and this overexpression is specific to the

mature blastema. We also observed isolated events of FVIII+/eGFP+ cells in luminal spaces lacking well-defined SMA+ walls (Figure 3.10 D and L) within random blastema regions and these were consistent with capillaries. By DPA21, SMA staining seemed to be downregulated in many cells within the extravascular space yet many of the remaining SMA+ cells retained eGFP labeling (Figures 3.10 E, I, Q). In addition, we were able to find more evidence of well-defined vasculature with eGFP+ cells within both endothelial (Figures 3.10 E, I, M) and smooth muscle (Figures 3.10 E, I, and Q) layers. Similar to unamputated controls, we found very few instances of SMA+ or SMA+/eGFP+ non-vascular cells in the CT of the DPA35 regenerates. Conversely during this timepoint, we were able to detect SMA+/eGFP+ or FVIII+/eGFP+ cells integrated into vascular structures in and around well-defined layers (Figures 3.10 F, J, N, and R). In some cases, SMA+/eGFP+ cells were detected in the tunica adventitia typically composed of fibroblasts and during adventitial remodeling, occasional myofibroblasts with low SMA expression (270) (Figures 3.10 F, J, and R, blue arrow). These data point to additional roles of BMDCs in digit tip regeneration during contraction and vascularization of the injury and these events are more detectable following the onset of blastema formation. We have demonstrated that FVIII+/eGFP+ co-expression is not only limited to transient vascular structures when the abundance of BMDCs in the regenerate is at its peak at DPA14, but that they also remain in the endothelium of more complex vessels in DPA35 regenerates. In addition, we have shown that even though the presence of SMA+ BMDCs increases analogous to growth of the undifferentiated blastema and downregulate SMA during its differentiation, some SMA+/eGFP+ cells experience long-term integration into the tunica media and adventitia of more complex vessels as early as DPA21.

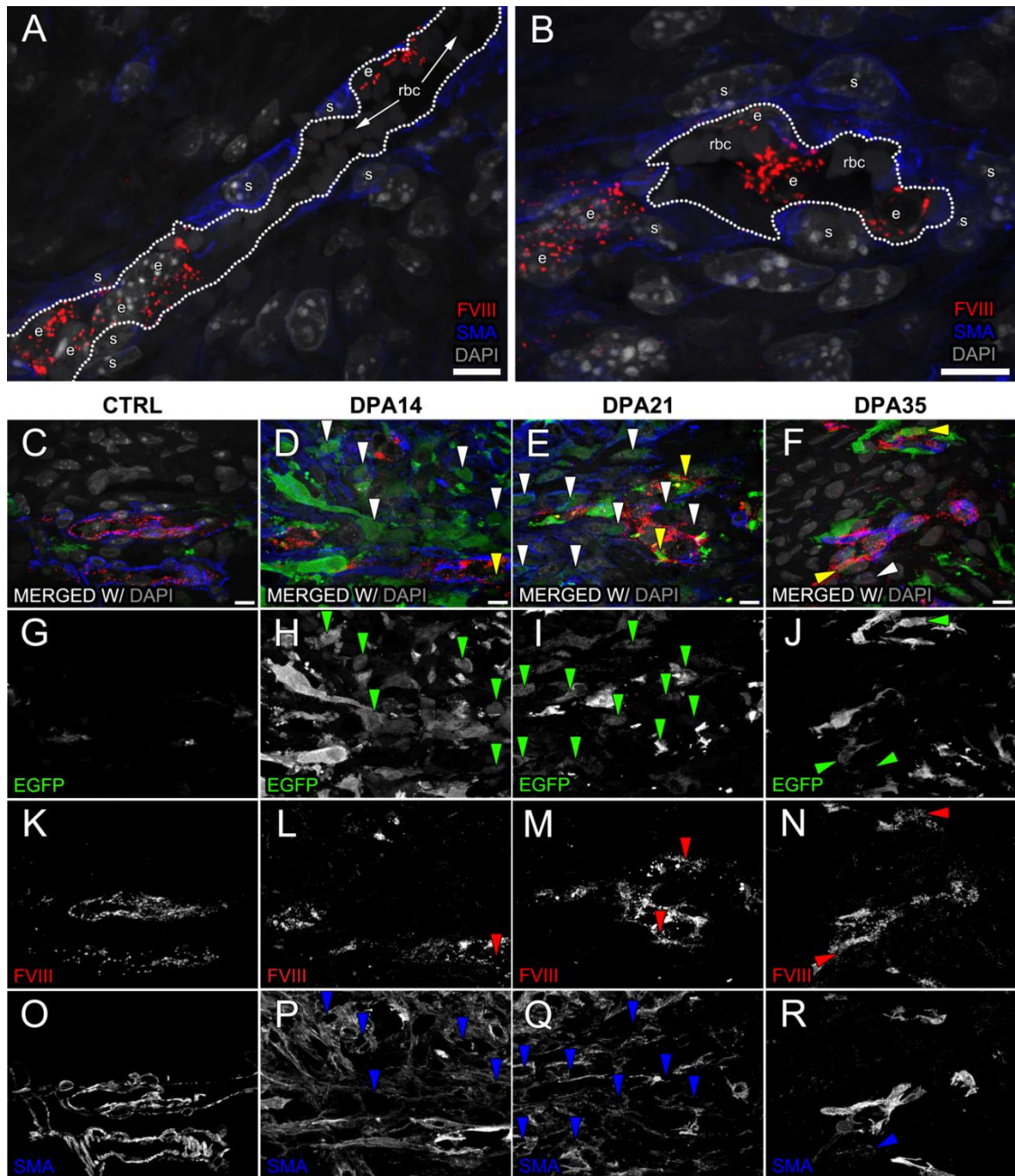


Figure 3.10: The integration of FVIII+ BMDCs is limited in both transient and permanent endothelium and eGFP+/SMA+ events are abundant around the blastema stage but regress to extravascular layers at the end of regeneration. High resolution confocal imaging of CT or blastema regions of interest co-labeled for eGFP, FVIII, SMA, and DAPI and captured at 1000X magnification. (A) Longitudinal and (B) cross-sectional slices of control vessels rendered with FVIII, SMA, and DAPI only show the degree of detail that can be obtained from vascular layer interfaces to show the FVIII+ endothelial (e) cell-lined lumen with red blood cells (rbc) surrounded by elongated smooth muscle (s) cells of the tunica media and fibroblasts or monocytic phagocytes flanking that layer as the tunica adventitia. (C-R) Representative regions of interest from selected control, DPA14, DPA21, and DPA35 timepoints showing quadruple labeling with

eGFP, FVIII, SMA, and DAPI. (C-F) Merged channels with FVIII+/eGFP+ co-expression (yellow arrows) and SMA+/eGFP+ co-expression (white arrows). (G-J) Extrapolated eGFP channel with eGFP+ cells co-expressing either FVIII or SMA in corresponding merged channel marked by green arrows. (K-N) Extrapolated FVIII channel with cells co-expressing eGFP in corresponding merged channel marked by red arrows. (O-R) Extrapolated SMA channel with eGFP+ cells co-expressing eGFP in corresponding merged channel marked by blue arrows. Scale bars (A-R): 10 μ m.

3.4 DISCUSSION

The amputated digit tips of mice undergo a complex process of repair including many stages which mimic, at least chronologically and histologically, steps of the conventional wound healing cascade including clotting, inflammation, re-epithelialization, fibroblast proliferation, matrix reorganization, and angiogenesis. During either process of regeneration or wound healing, and in a stage-specific manner, a diverse number of hematopoietic and mesenchymal precursor and differentiated cells home to sites of injury and participate in their repair in a transient or persistent manner. And one specific step in regeneration in which we observed progressive cellular content is the blastema stage. Even though the blastema resembles the area of granulation tissue in a wound, in which fibroblasts are well known to deposit scarring fibers, its end result is a site continuous with the undamaged tissue and segmented into patterned layers composed of various cell lineages consistent with the lost tissue layers. Based on the numerous reports on the homing, plasticity, and contribution of both hematopoietic and mesenchymal progenitors to organ injury, we hypothesized that the digit tip regenerate is no different and that one of the main sources of these regeneration-competent cells is the BM and these cells can integrate and differentiate inside several tissue compartments with temporal variations in stage of repair and overall lifetime. We thus incorporated the BM transplantation model using transgenic eGFP donors and, combined with immunohistochemical co-expression

technique; we tested and measured the major anatomical source, fate, and persistence of BMDCs during the blastema stage and beyond.

First and foremost, by means of the BM eGFP chimera model, we were able to conclude that the grand majority of eGFP+ cells in the amputation wound were derived from the marrow regardless of migration route. Occurrences of eGFP+ cells increased to nearly 50% of the total cells in the blastema by DPA14 but slowly decreased until the endpoint of regeneration at DPA35. Yet eGFP+ cell counts remained five-fold higher than unamputated controls which we interpreted as part of a long-term commitment from BMDCs to reconstitution of digit structures. Moreover, because we did not achieve absolute reconstitution of the BM after transplantation and recovery, the amount of BMDCs that contribute to the regenerate may be much higher than our data show. Even without the co-expression of phenotypic markers, we were able to measure and observe changes in the amount and cytology of these eGFP+ cells throughout the course of regeneration and these changes correlated with the onset of specific events and resurgence of various structures identified by histopathology. First, we used the cell-surface marker CD45 to tag inflammatory cells and those that conserve it in tissue, mostly in the form of granulocytes and macrophages, which are known to be derived from the BM and initiate the repair process, and most of these tested positive for eGFP. Presumably, these cell types have a relatively short lifetime and either undergo apoptosis or revert back into circulation once chemotactic signals from the wound dissipate. Even without CD45 labeling, many neutrophils and macrophages were detected by either their multi-lobed nuclei or the presence of ingested debris, respectively. However, CD45 staining was instrumental in showing that most eGFP+ BMDCs in normal unamputated digits are CD45+ and therefore integrate as resident immune cells in the steady-state after transplantation. In addition, based on CD45 staining, we are able to conclude that most BMDCs at the early stages of repair are inflammatory and most

CD45+/eGFP+ cells and CD45+ hematopoietic cells in general are restricted to the inflammatory phase and excluded from the site by the time the blastema forms. This means that the persistence of an inflammatory milieu is not necessary to sustain the blastema and this reminds us of how cutaneous wound repair is unaffected in the PU.1 null mouse even though it lacks functional neutrophils and macrophages (271). Therefore, cues to maintain a regenerative response and promote differentiation must be derived from non-inflammatory cells which do not express CD45 in tissue.

Along with the degradation of damaged bone that followed, BMDCs also presented themselves as multinucleated osteoclasts, which we expected since these are believed to be derived from the fusion of macrophages from the BM (251). Simultaneously, we observed the first potential evidence of non-hematopoietic or CD45- cells in the shape of fibroblasts invading the BM cavity and the future blastema space by DPA10, which supports the general consensus that fibroblasts derived from the BM participate in wound repair by promoting fibroplasia during the proliferation stage of healing (124). Some of our CD45/eGFP co-labeling results support that the BM becomes invaded by CD45-/eGFP+ cells prior to any indication of a blastema structure and becomes hypercellular with these cells starting at DPA5. Conversely, the BM becomes more decellularized by the mature blastema stage of DPA14. Based on the asynchronous order of these events we began to label the P3 BM as one of the main sources of blastema BMDCs. But before examining the differentiation phenotype of these cells, we measured the overall survival of BMDCs throughout the regeneration timepoints by dual Ki67 and C3 immunostaining to determine if once inflammation is resolved, the mass of CD45- non-hematopoietic cells which accumulates in the blastema afterwards has a more prolonged presence in the regenerate.

When comparing the survival dynamics of the BM versus the CT or blastema, our data show similar trends between both tissue compartments with regards to apoptosis and between C3+/eGFP- and C3+/eGFP+ cells, which are between one fourth up to one third of the total C3+ population. Total C3 activity increases roughly 8-fold, of which 2 to 4-fold of its signal co-expresses with eGFP, at the early regeneration timepoints and sharply declines to nearly a fourth of that response by DPA14. This indicates that active C3 is mostly limited to the inflammatory phase of repair and its detectability increases due to the high content of damaged soft tissue, degrading bone, and short lifespan of immune responders regardless of local CT or BM origin. The low C3 levels following that, especially in the CT, indicate that blastema cells and those reconstituting various compartments including the BM are protected from tissue reorganization and committed to long-term existence. On the other hand, our proliferation index data does not show a straightforward trend between compartments. The peak of cell expansion arrives first in the BM at DPA10 followed by the CT at DPA14 and while proliferation drops by DPA28 in the BM, it continues nearly 5% above baseline in the CT. Moreover, while most proliferating cells in the BM expressed eGFP, only a fraction were eGFP+ in the CT including only a fourth of total Ki67+ cells during the peak of proliferation at the DPA14 blastema stage. Since proliferation of eGFP+ cells is triggered and peaks in the BM prior to blastema formation then we propose that a BM niche is enriched to be the main source of blastema cells. In addition, since the proliferation rate of eGFP+ cells is significantly lower than the total Ki67+ population in the CT and the blastema, we interpret the colonization of eGFP+ cells in the space outside the BM as a migration event, given that BMDCs can freely travel to and from the BM cavity driven by chemotactic signals such as SDF-1, which in this model is mainly derived from the wound epidermis distal to the BM opening and within the BM itself (205, 272). And a major bulk of these eGFP+ BMDCs which evidently pre-expanded in the BM populated the

blastema only to be subsequently diluted by eGFP⁻ cells dividing nearby throughout the later timepoints, thus adding to the supportive role of eGFP⁺ BMDCs to the rescue of local or non-BM derived cells in the digit capable of expansion and differentiation in the regenerate.

Our current and previous studies show that compartments such as the lining of the terminal phalanx in unamputated digits of the neonatal, adult, and the BM chimera mouse model are outlined by ER-TR7⁺ FRCs also known as reticular fibroblasts. In general, fibroblasts also exist in the BM as reticular and adventitial stromal cells (273) and can be derived from MPCs or a subset of HPCs denominated fibrocytes which are found in the marrow and in circulation (274) and many of these, especially the reticular subtype, are capable of expressing ER-TR7. But we found no evidence of such cells co-expressing eGFP in the CT of the unamputated digit. On the other hand, many eGFP⁺ BMDCs in the regenerating digit begin to overexpress ER-TR7 in the immature blastema site by DPA10. But this overexpression, mainly caused by the mass accumulation of primed FRCs is not restricted to the blastema stage. The first evidence of ER-TR7 microfibril synthesis in the regenerate was observed coming from the hypercellular BM starting at DPA5, which indicates that many cells in the BM compartment are capable of becoming ER-TR7⁺ FRCs and the factors which induce this differentiation affect the BM first. We must note that since the presence of ER-TR7⁺/eGFP⁺ cells in the pre-existing dorsoproximal and dorsoventral CT remained moderate throughout regeneration we ruled out this region as a niche of eGFP⁺ FRCs. Even though we believe the BM is the main niche of FRCs in the blastema, one phenomenon that we still cannot rule out is if many of these BMDCs migrate outside the marrow niche to the blastema site already primed to become differentiated FRCs. This is especially intriguing when observing progressive decellularization of the BM from ER-TR7⁺ cells and ER-TR7⁺ fibers while simultaneously measuring blastema growth with ER-TR7⁺ cells and microfibrils in matched timepoints. We have shown previously that ER-TR7

microfibrils co-express COL3 and there are data in cutaneous wound injuries from BM eGFP chimera models which suggest that COL3 transcription and deposition in wounds is exclusively orchestrated by fibroblastic BMDCs while resident fibroblasts lean more towards production of COL1 (124). Our data supports this evidence since most ER-TR7+ cells counted co-expressed eGFP throughout the regeneration timeline. However, also throughout the regeneration timeline we quantified a progressive number of ER-TR7+ cells which tested negative for eGFP, especially towards the end of repair, where more than half of the ER-TR7+ population were devoid of eGFP. And this indicates that, since the bulk of CD45-/eGFP+ BMDCs are limited to the blastema site between DPA14 and DPA21 and serve as supporting predecessors to the recovering local population which later outnumbers it, pre-existing resident CT FRCs are responsible for the expansion of ER-TR7+/eGFP- cells. ER-TR7 was also instrumental in labeling general areas of patterning and compartmentalization in the regenerate. Not only did some ER-TR7+/eGFP+ FRCs remain in the progressively decellularizing BM cavity to flank the endosteum and encase blood supplies but we also found more evidence of ER-TR7+/eGFP+ cells becoming part of regenerated structures outside the BM such as, for example, the stratum basale of the nailbed and the tunica adventitia of various vessels.

Overall, our data indicate that a major portion of BMDCs differentiates into FRCs which build the blastema extracellular framework through upregulation of ER-TR7+ microfibrils to become intermediary support tissue during the recovery of pre-existing cells. Although an increasing population of FRCs with the same phenotype as those found later in the blastema was detected in the BM and the onset of increased microfibril formation is often associated with BM anomalies and neoplastic disease (273), the hypercellularity and fibrosis of the BM at early timepoints is transient and may be labeled as a contribution to the regenerative response. Moreover, even though this scaffold regresses towards the endpoint of repair, the same BMDCs

also integrate in the regenerate as long-term FRCs to discreetly outline various compartments in a similar fashion as the lost structure and thus can be viewed as functional rather than fibrotic cells. In addition to the differentiation of BMDCs into ER-TR7+ scaffold producing and compartmentalization FRCs, data involving co-expression with other lineage differentiation markers furnished evidence of the multilineage plasticity of BMDCs and integration into the regenerate as other functional cell phenotypes other than FRCs.

Similar to FRCs, another subset of BMDCs which can be derived from subsets of MPCs or fibrocytes are osteoblast progenitors (275-277). In fact, when comparing active genes in human trabecular bone osteoblasts to dental fibroblasts by microarray technique, for example, most transcript levels related to structural and signal transduction processes are the same (278). Since this evidence suggests that both lineages are derived from similar mesenchymal progenitors, we also considered osteoblasts as one of the endpoint cell populations of differentiating BMDCs in the regenerate. We found that the pre-amputated BM cavity of our chimeras was lined with eGFP+ cuboidal cells in direct contact with the mineralized surface of the P3 bone many of which tested positive for OC which means that the endosteum lining is susceptible to radioablation injury and is partially repaired by BM donor cells. Based on this capability, we anticipated renewal of the damaged P3 bone with the aid of BMDCs following amputation. Following the end of bone and rise of the blastema structure between DPA10 and DPA14 (137) we measured a progressive influx of OC+ osteoblasts surrounding mineralized trabeculae as a result of direct ossification of the blastema soft tissue. But onward from the peak of osteoblast counts at DPA21, there was no significant change in osteoblast numbers within areas outside the BM cavity proper and most of these did not express eGFP. A possible explanation to the lower percentage of OC+/eGFP+ cells in the regenerate stems from the recent discovery that the majority of osteoblasts in regenerating P3 trabecular bone are the

descendants of pre-amputation osteoblasts (261). Regardless, we measured that generally one sixth of the total osteoblasts from the blastema stage onward were labeled with eGFP, except for a peak to one third during DPA21, yet we could not determine by our means if the source of OC+/eGFP+ cells was the pre-amputated portions of the BM lining reconstituted with eGFP-labeled osteoblasts or osteoblast progenitors in the general population of BMDCs not localized to the endosteum layer. At the end, eGFP+ osteoblasts reconstitute the lining of trabeculae starting at DPA21 and extend their presence to the periosteum of the regenerated trabecular bone portion of P3 by DPA35. In addition, these cells were consistently localized to the edge of mineralized areas and generally flanked by ER-TR7+ FRCs, thus indicating that not only do these eGFP+ osteoblasts contribute to the regenerating bone, but also promote the normal tissue pattern associated with it. But the integration of BMDCs as osteoblasts around the bone is not limited to the periosteum and endosteum lining. Interestingly, we also observed eGFP+ osteoblasts encased in the mineralized bone matrix, thus suggesting that not only do eGFP+ osteoblasts potentially participate in continuous bone remodeling of the regenerated P3 and release osteoid, but also add functionality to the regenerate as osteocytes, which sense mechanical stress and strain signals and convert them into chemical stimuli to ultimately change and maintain bone structure (279).

In conjunction with the onset of direct ossification of the regenerate following the relatively hypoxic blastema structure, an increase in angiogenesis measured by CD31 staining has been reported (137). Therefore we felt that the abundant population of BMDCs in the regenerate around this period must have some implications into the local sprouting of endothelial cells or extension of the pre-existing vasculature. Following IHC co-staining of FVIII and SMA in the amputated chimera digits, we employed high resolution confocal microscopy to pair the co-expression of these proteins to careful histopathology of vascular structures

throughout the regeneration timeline. The potential participation of circulating BMDCs into neovasculature as EPCs and eventually endothelial cells has been widely documented in models of ischemic repair and tumor growth but recent dispute over the temporal, quantitative, and phenotypic assessment of these events has made this subject controversial (280-283) and focus has been diverted to how BMDCs, mainly from the hematopoietic fraction, exert a paracrine, mainly VEGF-mediated, pro-angiogenic effect on tissues undergoing repair and/or growth (284-286). Our experiments confirm that BMDCs have a limited but direct contribution as endothelial cells in the regenerate but we cannot rule out if other subtypes of BMDCs such as macrophages and fibrocytes derived from HPCs or stromal cells derived from MPCs facilitate elongation of the pre-existing vasculature with paracrine signals. The highest detection of FVIII+/eGFP+ cells clearly within the lumen of vascular structures and therefore in the tunica intima was experienced between DPA14 and DPA21, but these were overall simple vessels mostly one-endothelial cell thick, especially at DPA14, and thus labeled as capillaries. And studies in similar models with healing cutaneous wounds have found that any significant integration of BMDCs in the tunica intima is transient and restricted to the proliferative phase of repair characterized by temporary vascular structures which feed granulation fibroblasts and eventually regress as the wound matures (124, 125). But consistent with the same studies, we were able to measure co-labeling of FVIII and eGFP within the tunica intima of scarce vessels towards the endpoint of regeneration at a rate of less than 4% of the total FVIII population. Therefore, a subset of BMDCs has the ability to differentiate into endothelial cells of the transient vasculature of the blastema at DPA14 but have limited potential towards the long-term contribution in the endothelium of more complex and permanent vessels.

Excluding capillaries, most vasculature in the digit is composed of three tunica layers and we found no evidence of contribution of BMDCs to any of them in unamputated controls,

thus further supporting that resident cells tagged with eGFP in the steady state are of hematopoietic origin and must have an immunological role. Other than the contribution to the tunica intima of transient capillaries and venules during the blastema stage and a more limited incorporation in complex vessels towards the endpoint in regeneration, there is a significant contribution to the tunica adventitia and media. Earlier we demonstrated that during differentiation of the regenerate, eGFP+ spindle cells localize to the perivascular adventitial space and basal lamina of the epithelium. Even though resident macrophages integrate into these regions, we were able to rule out a monocytic phagocyte phenotype because these cells co-expressed ER-TR7. And this not only supports that BMDCs can integrate into the regenerate as functional fibroblastic cells but that they also express ER-TR7 and thus can be included in the pool of FRCs.

From the blastema stage onward in the BM and CT, we also observed BMDCs assimilating in capillary walls and into the tunica media of larger vessels which stain positive for SMA due to their content of vascular smooth muscle cells (VSMCs) and/or pericytes tethered to the abluminal side of the endothelium (287). Both of these cell types have a similar morphology of small prominent nuclei with small cytoplasmic volume and long processes (288); are derived from common mesenchymal precursors in various anatomical niches of diverse developmental origins ranging from the embryonic neural crest to the adult BM (289, 290); and have similar functions in regulation of blood flow, endothelial permeability, vascular stabilization, and basement membrane deposition (288, 291-294). And with the current lack of practical distinguishing markers, VSMCs and pericytes are collectively categorized as mural cells and segregated by location within the vasculature, that is, capillaries versus larger vessels, respectively, and density around the vessel (295). We were able to detect SMA+/eGFP+ BMDCs associated with the outer layer of capillaries mostly within the blastema at DPA14 through

DPA21 and paired with their location in the vasculature and cytology, made an educated decision to label them as eGFP+ pericytes. On the other hand, it was difficult to detect SMA+/eGFP+ mural cells as part of the tunica media of larger vessels in the CT at the later stages and endpoint of regeneration. Interestingly, our combined data on SMA+ cell counts does not follow a trend with the progression of endothelial FVIII expression. Beginning at DPA10 and peaking at DPA14, we measured a significant spike in the total number of SMA+ cells only to undergo sudden regression to nearly baseline percentage by DPA35 and the SMA+/eGFP+ subset also follows this trend. We attribute this to that along with BMDs tethered to the basement membrane of capillaries; we detected a significant number of eGFP+/SMA+ cells in the extravascular blastema space, especially at DPA14. Since we observed that the cytology of cells outside vascular structures contradicts the fundamental morphological description of pericytes, we cannot rule out a myofibroblast phenotype.

Similar to pericytes, one of the primordial markers of the myofibroblast phenotype is also SMA (27). The functional hallmark of myofibroblasts is wound contraction accompanied by deposition of proteoglycans, matrix-remodeling enzymes, and extracellular matrix collagens, mainly COL1 at pathological levels, which can lead to fibrosis (229). Studies on the ontogeny of myofibroblasts are mixed and hypothesize that these fibroblast-like cells are derived from either resident stellate fibroblasts (296, 297), circulating BM-derived fibrocytes (274, 298), mesenchymal BMDs (299), epithelial cells following epithelial-mesenchymal transition (300), endothelial cells following endothelial-mesenchymal transition (301), and/or pericytes (268). Other than promoting fibrosis in the lung (50) and liver (48) for example, myofibroblasts influence the wound environment by coordinating inflammation via IL-6 (229); and inducing proliferation and differentiation through release of TGF- β s (27, 229, 302), keratinocyte growth factor (KGF) (229), and hepatocyte growth factor (HGF) (48, 229) among others. Due to a lack

of better markers, we cannot rule out that the bulk of SMA⁺ cells at the undifferentiated DPA14 stage and differentiating DPA21 is the result of a mass colonization by myofibroblasts. Furthermore, similar to the downregulation we measured in the later stages of our regeneration timeline, SMA in these cells can be downregulated *in vitro* when exposed to TNF- α (303) or FGF-2 (304) by antagonizing TGF- β 1-induced SMA expression. Since both of these proteins are known to participate in blastema scaffold induction and upkeep of Msx1-mediated mammalian blastema growth and differentiation (149), respectively, these are likely active during the blastema stage in our model. But due to their biological function and general propensity in pro-scarring microenvironments, we believe that the enrichment of the blastema with myofibroblasts would be counterproductive to the regeneration process. Moreover, the myofibroblast phenotype is one of terminal differentiation (302) thus making it unlikely for these cells to be a large fraction of SMA⁺ counts that our data yield in the relatively undifferentiated environment of the blastema. Instead, their presence in the steady state in cutaneous and cardiac models has been limited to support and remodeling of the vascular adventitia (270), which is very similar to what we detected in the CT of the late regeneration timepoints.

On the other hand, SMA⁺ pericytes have been shown to give rise *in vitro* to some of the differentiated populations found in the digit not only as vSMCs of the vasculature (287) but also various fibroblast subtypes including myofibroblasts (288), osteoblasts (305, 306) and chondrocytes (307), thus sharing the plasticity of MPCs derived from the BM that we have been referring to all along. SMA expression in pericytes is relative to their differentiation state and similar to myofibroblasts, can be positively modulated by TGF β –1 and conversely, downregulated as a response to FGF-2 or after transdifferentiating into a non-contractile lineage such as the osteoblast (288, 306, 308). Although we did not pursue further assessment of the

large influx of SMA+ cells with additional validated pericyte markers such as NG2, PDGF β , and Desmin (309-311), based on review of the literature, our knowledge of the secreted factors active around blastema formation, and our data we can propose that many cells in both eGFP+ and eGFP- fractions of the transient SMA+ population influx in the blastema at DPA14 and DPA21 are pericytes from a subclass of MPCs which dedifferentiate or transdifferentiate into the other lineages we measured, especially osteoblasts and even FRCs. In addition, we also propose that local pericytes or progenitor cells are responsible for the SMA+ mural cell population in the tunica media of vessels, since we were only able to detect SMA+/eGFP+ cells associated with the outer tunica adventitia in the DPA35 endpoint regenerate and these may be myofibroblasts. We can also hypothesize that regeneration incompetent sites will experience a similar influx of these progenitor cells but only to be surrounded by microenvironmental cues which induce an endpoint myofibroblast phenotype that would promote over deposition of collagen to build scar.

We conclude that both hematopoietic and mesenchymal progenitor pools of BMDCs significantly contribute to digit tip regeneration. The presence of differentiated HPCs is robust but limited to the clotting and inflammatory phases of repair and during this early response we observe the bulk of apoptosis. Overlapping the late stages of inflammation and bone degradation and specific to the onset of the blastema, we measure a massive response from MPCs stemming from expansion in the BM with distal migration towards the wound epidermis. Most cells in the blastema are derived from the marrow and are capable of differentiation into FRCs to build a regeneration competent network of extracellular fibers that may serve to provide structural support, migration pathways, and tethering of various factors in the immature blastema. Furthermore, the invasion of BMDCs is specific to the undifferentiated blastema since along with initial histological evidence of differentiation, we observed an

increasing influx of local precursors which also means that the BMDCs in the blastema act as transient support until the local population is able to take over. Although the content of BMDCs was progressively diluted over the course of differentiation of the blastema, we measured their consistent presence in the regenerate contributing to various extents to the long-term reconstitution and functionality of missing structures. Other than mass differentiation into ER-TR7+ scaffold engineering FRCs with subsequent incorporation into basement membranes, adventitia of vessels, and subperiosteum layers, another major bulk of MPCs expressed SMA mostly at the blastema stage, but this expression was transient and we propose a pre-differentiation pericyte phenotype for these cells. Ultimately, upkeep of SMA expression by BMDCs was restricted to eGFP+ myofibroblasts in the adventitia of vessels and thus most mural cells were derived from the local population. Similarly, we noted a limited contribution to the endothelial phenotype and this may be due to evidence suggesting that the intima or endothelial lining of vessels is mostly derived from circulating EPCs from various sources other than the marrow even though conflicting view exist regarding this matter (282-284). So we do conclude that although limited, BMDCs have the potential of endothelial differentiation in a regenerating environment. Although many BMDCs tested positive for OC in the BM endosteum prior to injury and this phenomenon is likely related to radiation-induced injury, many BMDCs during the regeneration response also tested positive for OC in the periosteum and lining of trabeculae in direct ossification areas of the regenerating P3 bone. And it is possible that many of these OC+ BMDCs were once part of the transient SMA+ pericyte population specific to the earlier stages. Overall, the mouse digit houses all cells capable of reconstituting it after amputation. We must focus our attention then in understanding how to modulate the extracellular factors in a temporal and concentration-specific manner to modify the migration,

differentiation, and positional dynamics of BMDCs in tandem with the local population to promote a similar response in regeneration incompetent sites.

CHAPTER IV: DISSERTATION SUMMARY, CONCLUSIONS, AND FUTURE DIRECTIONS

4.1 SUMMARY

The mouse digit tip undergoes a level-specific regeneration response following amputation midway through its terminal phalanx unlike any other segment of limb. One of the defining features of this response is the progressive accumulation of fibroblasts at the wound site to form an undifferentiated and unpatterned cellular mass referred to as the blastema. In order to understand the ontogeny, differentiation, and function of blastema fibroblastic cells, we labeled digits by indirect immunofluorescence with an antibody against ER-TR7, an antigen derived from splenic stroma FRCs which has been shown to serve as a medium for cell interactions in lymphoid organs. In past studies, ER-TR7 was reported to outline the compartments of multiple lymphoid organs in the steady state and with these data we have demonstrated that it can also outline structures in non-lymphoid organs such as the mouse digit. Baseline localization of ER-TR7 is similar at all stages of postnatal development into adulthood but is more profusely distributed in neonates. Moreover, when comparing the neonatal versus adult regeneration timelines, ER-TR7 regulation is asynchronous. However, its expression trend is consistent following amputation regardless of age.

Since ER-TR7 is produced by a subset of fibroblasts, the blastema is mostly composed of fibroblastic cells, and the endpoint of regeneration yields a functional replica of the missing part, we hypothesized dynamic expression of ER-TR7 during repair with upregulation at the blastema

stage followed by regression concurrent with cellular differentiation and structural patterning of the regenerate. Indeed our data show that ER-TR7 is not only upregulated in the blastema but is arranged as an organized network of microfilaments extending parallel to the growth axis of the regenerate. And at the blastema stage, this growth is mostly associated with proliferation of ER-TR7+ FRCs within this scaffolding matrix without evidence of apoptosis at the increased levels measured in the preceding phases. But similar to the transient upregulation of ER-TR7, proliferation as the scaffold regresses shifts to ER-TR7- cells indicating that both growing FRCs and the ER-TR7 framework prepare the ground for the differentiation and patterning that is known to follow.

Primary adherent cells isolated from the P3 phalanx can be induced *in vitro* to become growth responsive FRCs which produce an ER-TR7+ blastema scaffold through binding of surface TNF and LT receptors in these cells that stimulates downstream activation of the canonical and alternative NF κ B pathways in agreement with studies by Katakai et al (2004) on stromal cells of the lymph node. Primary fibroblastic cells isolated from the terminal phalanx have the capability of becoming ER-TR7+ FRCs and since FRCs comprise most of the population that occupies the immature blastema and blastema cells express ER-TR7 both *in vivo* and *in vitro*, these P3-derived cells can be considered by definition blastema cells. In addition, similar to the blastema scaffold *in vivo*, the induced primary cells engineer a loose arrangement of ER-TR7+ microfibrils with an organized “honeycomb” appearance. Transcriptional analysis of these cells throughout the induction timeline revealed reasonable downregulation of the smooth muscle actin gene *Acta2*, which is considered one of the hallmark cytoskeletal molecules of pro-scarring myofibroblasts. Conversely, we measured consistent upregulation of *Col3a1*, or type III collagen (COL3). Therefore we postulate that treated primary P3 cells lose actin-mediated contractility in

exchange for an FRC phenotype which secretes ER-TR7+ scaffold microfilaments in tandem or association with synthesis of COL3.

Our protein data based on indirect co-immunolabeling of induced cell lines and *in vivo* blastema with primary antibodies specific for ER-TR7 and COL3 further corroborate the co-regulation of these two antigens at the post-translational level. Analysis of additional cytoskeletal and extracellular markers related to fibroblasts were also analyzed and their expression was either proportional to the number of fibroblastic cells in the wound at any given timepoint or remained constant relative to control tissue. Furthermore, trends in localization and concentration of these markers did not match the tight correlation between ER-TR7 and COL3 at the intracellular and matrix levels. Whether the COL3 macromolecule is directly linked to the ER-TR7 antigen or they are simultaneously expressed around the same microfilaments, we are now aware that both outline tissue compartments and their upregulation is an indication that fabrication of a potentially regeneration competent microenvironment is in progress. But along with expansion of the extracellular scaffold in the blastema comes a significant influx of multipotent cells which we hypothesized to be partly derived from the BM niche.

To test if BMDCs contribute to the blastema scaffold and the regenerate as a whole, we infused eGFP transgenic BMDCs into gamma-irradiated wild type hosts to generate BM chimeras with significant reconstitution of all marrow compartments with labeled donor cells. Our data serve as evidence that BMDCs are indeed major contributors to various key events throughout the regeneration process. During the inflammatory phase of healing, BMDCs of hematopoietic origin, or HPCs, present themselves mainly as eGFP+ polymorphonuclear cells, monocytic phagocytes, and osteoclasts. Interestingly, the colonization of the wound by these pro-inflammatory and pro-histolytic subtypes is transient and mostly terminated by the time

initiation of the blastema is observed. And this is an indication that an active presence of cells which promote an innate or adaptive immune response is not necessary to sustain progression and differentiation of the blastema. However, based on these data we cannot rule out if the early blastema is permeated with cytokines, chemokines, and growth factors secreted by the CD45+ inflammatory surge and tethered to the extracellular space to promote blastema-specific responses. CD45+ cells typically encompass most of the cellular area in the unamputated marrow compartment of the P3 phalanx. Changes in the ratio of HPCs and BMDCs of mesenchymal phenotype, or MPCs, are dramatic following the inflammatory phase and we were able to trace a higher content of CD45- MPCs to CD45+ HPCs originating in the P3 marrow compartment extending to the soft tissue space distal to the bone stump.

The shift in a higher cellular ratio favoring MPCs over HPCs based on detection of CD45 prompted us to look at the survival dynamics of BMDCs and location-specific expansion and death profiles of the progressing regenerate. First, by measuring the levels of the apoptosis effector cleaved caspase-3 (C3) we determined that the majority of programmed cell death occurs at the early stages of repair with similar location-based response curves between the BM and CT of the regenerate as well as analogous response curves at the cellular level between BMDCs and local cells. We conclude that apoptosis is mostly limited to hypoxia, shock, and degradation related to tissue damage along with the known fast turnover, short lifespan, and clearance of inflammatory cells. In contrast with apoptosis, the proliferation index throughout regeneration is very dynamic and manifested as Ki67 expression with location and cell type-specific temporal variations. In the BM, proliferation peaks prior to blastema formation in the distal CT space, which indicates that the BM cavity is either protected or recovers earlier from the trauma and is thus able to facilitate expansion of BMDCs. Subsequently, there is a massive colonization of BMDCs in the blastema space, but interestingly we measured a lower index of

proliferation in these cells. Instead at this point, in the blastema CT, the proliferation index of local non-BM derived or eGFP⁻ cells quadruples to that measured during the late inflammatory phase causing a peak in Ki67 expression which is also four times higher than that of eGFP⁺ cells. These data therefore implicates the P3 BM as a niche for contributors to the blastema population which pre-expand in the marrow, home towards the distal wound epidermis, and prime the blastema for future expansion of the recovering local digit soft tissue progenitors. Following the differential proliferation of marrow versus local CT, Ki67 counts become progressively lower overall down to baseline levels near the end of recapitulation, which can be interpreted as a progression into differentiation and patterning of the blastema.

One of the first events that we can truly define as being part of the blastema differentiation process is that of MPCs acquiring a phenotype of FRCs as marked by their membrane expression of ER-TR7 and its secretion as extracellular microfilaments. In the steady state, we found no definitive evidence of eGFP⁺ FRCs in neither the CT or BM compartments of the chimeric digit tips. Interestingly, the initial bulk of BMDCs capable of producing the ER-TR7 network is derived from the BM at its hypercellular state prior to blastema formation and in the blastema; over half of ER-TR7⁺ cells are positive for eGFP and thus derived from the BM. This leads us to conclude that the BM is the primary niche of both differentiated FRCs and progenitors of FRCs in the blastema. Since apoptosis events are rare in this stage and the BM becomes more depleted of FRCs as the blastema becomes enriched with them, we also conclude that BMDCs destined to be FRCs home to the wound regardless of FRC differentiation stage. Once in the blastema, BM-derived FRCs build the ER-TR7 scaffold along with the progressively expanding eGFP⁻ local CT FRCs. And local FRCs continue to become enriched in the regenerate while the presence of BM-derived FRCs becomes more dilute. Overall, from these findings we can conclude several events. First, that many of the eGFP⁺ cells initially

proliferating in the BM and ceasing to expand once they arrive at the wound site are imported FRCs whose role is to initiate the blastema scaffold. Second, those cells that we found proliferating in the blastema which test negative for eGFP are destined to become FRCs which upkeep the scaffold and amplify its growth and that of the blastema in general. Although limited later on during the differentiation and patterning phases many eGFP+ FRCs retain this phenotype and remain long term structural components of the regenerate. Early indications of this phenomenon can be first observed concurrent with blastema growth in the differentiating BM cavity where eGFP+ FRCs allocate to the adventitia of the blood supply and the fibrous layer of the endosteum. As expected, these eGFP+ FRCs are distributed in the tunica adventitia of mature vasculature in the CT and can also be detected around basement layers of the stratum basale of the epidermis and the periosteum around the phalanx in agreement with our characterization of the normal anatomical distribution of FRCs and ER-TR7 fibers secreted by these FRCs.

One of the hallmark events in blastema differentiation is the osteogenesis of the missing P3 fragment by means of direct ossification, which overlaps with continuous lengthening of the distal blastema scaffold thus suggesting that the scaffold is also an active anatomical template of the future phalangeal area. We generated evidence that BMDCs also contribute to the osteoblast lineage in the regenerate and this probability was initially postulated during analysis of unamputated chimeras, whose endosteum was occasionally reconstituted by eGFP+ donor osteoblasts as part of the repair process following irradiation damage. During regeneration, we found evidence of eGFP+ cuboidal cells similar to those found lining the endosteum associated with the trabeculae in areas undergoing direct ossification. These cells tested positive for OC in a similar fashion as eGFP- osteoblasts. However, this eGFP+ phenotype was relatively scarce in both the trabecular lining and the periosteum of the newly formed bone and mostly limited to

DPA21. Altogether these data support that regeneration osteoblasts are mostly derived from pre-existing lineage restricted osteoblast progenitors but nevertheless, to a lesser extent, BMDCs are also capable of incorporating into these regenerating tissue compartments as bone-forming cells. In addition, we observed rare occurrences of eGFP+ osteocytes, indicating that this small percentage of eGFP+ osteoblasts not only contribute to direct ossification but further participate in ongoing functionality of the regenerated P3 by extending their life cycle as osteocytes embedded in the bone matrix to maintain bone structure.

Another example of the added level of persistent functionality that BMDCs provide to the regenerate besides blastema scaffolding with endpoint outlining of structures and basement membrane support and bone growth and remodeling is the multilayered process of vascularization. During digit tip regeneration, we observe anywhere from transient, simple vascular structures that support blastema cells to late stage development of more complex permanent vessels tied to the pre-existing blood supply. We were able to detect BMDCs participating throughout these events at different structural and functional levels. Using co-immunodetection techniques, we were able to measure co-expression of FVIII with eGFP within the lumen of vascular structures as early as DPA10 but most prominently in the mature blastema and during the early differentiation stage of DPA21. During this period, we monitored an increase in the occurrence of eGFP+ endothelial cells but these were mostly associated with capillaries or vessels without complex tunica layers. Towards the endpoint of regeneration however, FVIII+/eGFP+ events were diminished to near unamputated baseline counts and only associated with more complex vessels composed of multiple tunica layers. These data mostly support that even though BMDCs have the ability to persist in the long-term reconstitution of damaged endothelium; their main activity as vascular endothelial cells in the regenerate is to provide functionality to the transient capillaries which are known to feed intermediary

structures such as granulation tissue and the blastema. But generally, vessels are also characterized by a tunica media and adventitia mainly composed of mural cells and fibroblasts, respectively, and we found that the contribution of BMDCs to these layers was limited to adventitial fibroblasts.

In order to further understand the role of BMDCs in angiogenesis of the regenerate, we co-labeled FVIII and eGFP with SMA found in precursor pericytes, mural cells, adventitial fibroblasts, and myofibroblasts. In control tissue, SMA expression is very prominent and mostly restricted to the tunica media of complex vasculature. In the regenerating digit tip on the other hand, we detected a significant rise in SMA⁺ cells from both eGFP⁺ and untagged cell populations beginning at DPA10 and peaking at DPA14, or around the mature blastema stage in this model. But we observed that many of these cells were neither incorporated in vascular layers nor had the morphological characteristics of mural cells. Much like ER-TR7 levels, SMA overexpression is transient and gradually declines and becomes more restricted to the growing vasculature in future timepoints. And based on our survival studies, we can conclude that regression of SMA levels occurred without exclusion of this phenotype by apoptosis.

Other than VSMCs, cells with SMA⁺ phenotype include myofibroblasts, fibrocytes, and pericytes. Since we ruled out that once in the blastema, a marginal number of cells express effector of apoptosis C3 and the SMA⁺ myofibroblast is a phenotype of terminal differentiation, we agree that SMA expression in the blastema is not related to the typical wound contraction which eventually leads to scarring. However, since we learned that SMA expression can be downregulated in cells exposed to FGF-2 *in vitro* and this factor is present in the blastema, we must be open to the possibility that these cells could be myofibroblasts which undergo

dedifferentiation. We demonstrated that many of the cells that home to the blastema site around this stage of SMA overexpression stem from expansion in the BM of P3 and subsequently migrate in the direction of the wound epidermis. Since the fundamental definition of a fibrocyte is that of a CD45+ circulating cell, we are unable to establish a direct connection between the fibrocyte phenotype and this SMA+ pool of cells. At the same time, we cannot rule out that the precursors of these cells were once fibrocytes which circulated to the P3 BM and thus we could state that fibrocytes indirectly contribute to accumulation of SMA+ cells in the blastema. So even though these SMA+ cells do not resemble pericytes, altogether this leaves us with the pericyte as being the phenotype with the most direct, early contribution to this pool of SMA+ blastema cells.

Almost half of the SMA+ cells in the blastema tested positive for eGFP. Therefore the source of the remaining SMA+ population must be derived from local pre-existing tissue compartments. Towards the end of regeneration, many eGFP+ cells mostly persist as subpopulations of FRCs including those incorporated in the tunica adventitia of vessels which also test positive for SMA. Conversely, even though a limited fraction of BMDCs also contribute to the osteoblast and endothelial lineages, the majority of cells with these phenotypes are derived from non-marrow sources including pre-existing tissue compartments and even circulation. We could then postulate that since SMA+ pericytes have been shown to be multipotent, then SMA+ BMDCs in the blastema differentiate to engineer the template and become support cells of regenerating vascular sprouts and local cells are more susceptible to pro-osteogenic cues, therefore acquiring a leading role in regeneration of the P3 bone.

4.2 CONCLUSIONS

Similar to published studies involving organogenesis, compartmentalization, and extracellular dynamics of lymphoid organs, the mouse digit is also divided into specialized structures outlined by FRCs which secrete extracellular microfilaments positive for the ER-TR7 antigen. Following amputation of neonatal or adult digit tips at a specific level which induces a regenerative response, the wound site is populated by numerous FRCs which are growth responsive and progressively upregulate secretion of ER-TR7+ microfilaments arranged in an organized, loose network with a peak of expression during the mature blastema stage. However, this network is transient and quickly replaced by compartment specific differentiated cells and structures discreetly outlined once again by FRCs and ER-TR7 by the endpoint of regeneration which indicates that ER-TR7 can specifically label an intermediate scaffolding stroma around blastema cells that is conducive to a regeneration-competent microenvironment.

Production of the ER-TR7+ microfilaments by stromal FRCs of lymphoid organs has been induced by co-activation of the TNF and LT receptors on the surface of these cells to trigger both canonical and alternative NF κ B pathways. Primary fibroblastic cells derived from the digit tip of mice can also be expanded and treated in a similar manner to promote secretion of ER-TR7+ microfilaments and engineer a scaffold *in vitro* which mimics the organizational distribution of that in the regeneration blastema *in vivo*. Enrichment of ER-TR7 in these cells provides a relevant model for characterizing and manipulating the ER-TR7 antigen. RNA analysis from these cultures following induction we were able to identify dynamic transcriptional expression of genes specific to wounding and fibrillogenesis including the predicted upregulation of NF κ B. But in addition, we found progressive upregulation of COL3 and due to this collagen's participation as the provisional matrix of granulation tissue; its higher proportion over COL1 in scar-free embryonic versus adult pro-scarring wound healing; and involvement in reticular

fibers, data from transcripts were paired with co-immunolocalization studies between COL3 and ER-TR7 in the same cultures and these resulted in a strong correlation between both antigens. To further understand the relationship between these proteins, expression of fibroblast-related markers was measured in serial control and blastema tissue sections to reveal that the only two markers that were significantly upregulated in the blastema and followed a trend in location, pattern, and concentration were indeed ER-TR7 and COL3. Therefore from these data we conclude that ER-TR7 is related to COL3 and this is primordial to explore the specific ties between the ER-TR7 antigen and ECM production during digit tip regeneration by means of loss of function and rescue experiments with models of COL3 deficiency. Moreover, we have gained further understanding that, even in regeneration-incompetent areas, ER-TR7 and COL3 overexpression in sites undergoing repair is an indication of a region with plausible potential for pro-regenerative manipulation at that specific time.

Other than engineering the ER-TR7+ scaffold through FRCs, the regenerate requires an influx of multipotent cells that differentiate to reconstitute the various cellular phenotypes in the digit and many of these cells are imported from the BM. Following distal P3 amputations of eGFP BM transplant chimeric mice, we determined that many BMDCs home to the wound site at various stages of the regeneration timeline. Cells of hematopoietic origin home to the injury as inflammatory cells such as granulocytes and macrophages and are mostly restricted to the immunological component of the repair. This response is shortly followed by a massive accumulation of proliferating mesenchymal cells stemming from the BM cavity of P3. This particular event leads us to believe that the BM is the primary source of the initial influx of blastema cells into the wound. At the blastema stage, the inflammatory milieu is mostly cleared from the wound, yet nearly half the cells in the blastema tested positive for eGFP, so we determined that most of this population is of mesenchymal origin rather than hematopoietic.

Interestingly, we measured that the initial bulk of proliferation occurs in the BM prior to blastema initiation, thus making the BM hypercellular and as expected, most of these expressed eGFP. Proliferation in the CT distal and around the P3 bone progressively increases over the blastema formation period but contrary to earlier events in the marrow, the majority of dividing cells were negative for eGFP. Since proliferation in the BM undergoes a sharp decline following blastema formation and eGFP+ cells in the blastema tissue do not expand as much as eGFP- cells, we conclude that the massive presence of BMDCs in the blastema CT from its initiation forward is due to migration from the BM rather than in situ expansion in the blastema.

A great fraction of the hypercellular BM is composed of FRCs actively producing ER-TR7+ microfilaments and similar to proliferation events in the overall regeneration timeline, ER-TR7 overexpression occurs first in the BM. This indicates that BMDCs capable of differentiation into FRCs are primed in the BM to differentiate into ER-TR7+ FRCs prior to involvement in the blastema CT. Mobilization of the majority of marrow-derived FRCs seems mostly limited to the proximodistal axis running from the BM cavity towards the wound epithelium since only a small fraction of eGFP+ FRCs can be detected along the dorsal and ventral proximal CT flanking the phalanx. The migration of active FRCs into a regeneration competent wound site re-enforces the notion that the ER-TR7 scaffold is a pro-regeneration event which stems from the local BM but is linked and assimilated into the developing blastema. Moreover, ER-TR7 levels begin to regress to baseline and defined structures are more discernible in the BM while blastema growth is underway, which suggests that differentiation of the BM precedes differentiation of the remainder of the regenerate.

Differentiation of the blastema is marked by declining ER-TR7 expression and thus a lower number of activated FRCs. Likewise, BMDCs become diluted with eGFP- precursor cells

which, according to our proliferation studies, progressively expand from local populations. Many of these local precursors have been shown to be lineage restricted and one of these is the osteoblast. And the integration of new osteoblasts immediately around the pre-existing bone and throughout the ER-TR7 framework around this bone is a well-defined differentiation event around this time as well. A subset of BMDCs is evidently capable of progressing into the osteoblast phenotype as a response to damage as that incurred following radioablation of the BM to generate the chimeras or as a response to factors such as bone morphogenetic proteins around the bone matrix which are active during digit tip regeneration. But BMDCs differentiated into osteoblasts remain a small fraction of the total osteoblast population in the regenerate. This also holds true for endothelial cells.

The majority of endothelial cells co-stained for eGFP and FVIII were limited to the transient capillaries which sprout to support the undifferentiated blastema structure. By the endpoint of regeneration, integration of eGFP+ endothelial cells was a rare event. New vessels are known to originate from two sources: the BM and the injured pre-existing vessels, with the latter being the major source. We conclude that this holds true in our model. But in regards to vessel differentiation, we also conclude that even though we counted many BMDCs which expressed SMA, a marker of mural cells, pericytes, and myofibroblasts, the majority of tunica media from mature vessels at the endpoint of regeneration did not include BMDCs. Instead, SMA+ BMDCs were largely found scattered throughout the undifferentiated blastema and integrated within the tunica adventitia of complex vessels in the regenerated digit tip. The large counts of SMA+ BMDCs in the undifferentiated blastema cannot be attributed to a myofibroblast population because this would be accompanied by higher levels of cleaved C3 associated with terminal differentiation in the matched timepoints of our survival study and accumulation of thick collagen fibers at the end of repair, neither of which was observed. Since

the SMA expression in these cells was transient, we must propose that the prevailing phenotype at the undifferentiated blastema stage is the pericyte. And the pericyte has been documented to have additional functions other than becoming peri-endothelial cells and maintain vessel integrity such as differentiating into osteoblasts. Furthermore, the peak of SMA+ expression in both eGFP+ and eGFP- populations precedes the one in OC+ counts. Therefore it would seem reasonable not to rule out that SMA+ cells in this current state, whether derived from the marrow or the local soft tissue population, are part of the lineage-restricted precursor population of new P3 osteoblasts that we observe to take part into most of the direct ossification of the regenerating P3 bone. Otherwise, we conclude that eGFP+/SMA+ cells at the endpoint of regeneration persist only as outer extravascular support cells in the tunica adventitia of complex vessels.

The bulk of the participation of BMDCs in differentiation events such as scaffolding, direct ossification of P3, and formation of layers in neovasculature is restricted to initiating or transient events of the blastema and in the early stages of regenerate differentiation. Nonetheless, subsets of BMDCs have high plasticity and are capable of differentiating into FRCs, osteoblasts, endothelial cells, and support fibroblasts of the regenerating digit structure and their integration in the regenerate, although limited on occasion, persists to provide long-term functional support to its basement membrane, connective tissue, vascular, and skeletal elements.

4.3 FUTURE DIRECTIONS

We plan to expand our studies utilizing the models outlined in this work in order to broaden answers regarding: (1) the identity of ER-TR7 and its relation to COL3; (2) the fate and behavior of BMDCs in the regeneration incompetent P2 following amputation (3) the requirement and function of the ER-TR7+ blastema scaffold with respect to support of the regeneration competent microenvironment and cells in adhesion, migration, survival, and differentiation dynamics; and (4) the potential anti-fibrotic effect of the extracellular microenvironment around the blastema stage and its application to pro-scarring models *in vivo* and *in vitro*.

We have demonstrated that control of the ER-TR7 antigen in the digit tip amputation model is tightly controlled and co-expressed along with COL3. We would like to strengthen these findings by expanding our RT-PCR results to statistically significant figures showing increasing transcriptional levels of COL3 in response to the induction of ER-TR7 in primary fibroblasts *in vitro*. Since the ER-TR7+/COL3+ scaffold can be produced in large amounts following induction, we expect this material to be useful in pairing our co-immunolocalization and transcriptional co-regulation measurements of these two proteins by semi-quantitative western blot analysis under denaturing conditions.

Since we are as interested in the characterization of the interaction between these two proteins as the scaffold which the antibodies against them tag, we also plan *in vivo* gain and loss of function studies using our injury model. Existing evidence suggests that COL3 is critical during wound healing due to its increasing expression early in the process. Other than housing granulation fibroblasts in a wide variety of wounds, COL3 is known to regulate the extent of collagen fibrillogenesis and thus the strength of the resulting fibers. This role in structural

integrity of several organs including the skin and cardiovascular system has been demonstrated in loss of function studies involving COL3 ^{-/-} mice which serve as a model of the Ehler-Danlos syndrome of COL3 deficiency during which, primarily, the vascular system of affected individuals gradually collapses. And this phenotype has also been observed in the skin, which loses integrity when lacking COL3, thus giving rise to studies of healing cutaneous injury which demonstrate that COL3 is not only necessary for proper granulation tissue formation but that a lack of it enhances myofibroblast differentiation and thus endpoint fibrosis. We have also cited studies which implicate COL3 in scarless healing in fetal wounds partly based on evidence that COL3 content is four times higher than COL1 in embryonic and fetal tissues and this ratio is reversed into adulthood. So based on our cited literature in this matter and the upregulation of ER-TR7+ microfibrils in the regeneration blastema, we hypothesize that the ER-TR7+ scaffold although transient and, if related to COL3, similarly engineered during the granulation phase of healing, is a requirement for regeneration and given the potential link that we have established between ER-TR7 and COL3, mice deficient in COL3 production will experience impaired regeneration of the digit tip if none at all. But since COL3 ^{-/-} are embryonic lethal, we would perform digit tip amputations on COL3 +/- heterozygous mice, which have been shown to produce half the amount of COL3 without major pathological conditions (Liu 2007). Since we have shown that prior to blastema formation the P3 marrow becomes hypercellular with fibroblastic cells primed in situ to behave like FRCs secreting ER-TR7+ microfilaments which transfer to the wound site, we postulate that local infusion of primary fibroblasts from age and strain-matched wild-type mice into the BM of COL3 deficient mice will rescue impaired regeneration of the digit tip. The local delivery of cells into the P3 BM has been previously done in our lab (Karen Wang, Muneoka Lab) and briefly, the fibroblasts would be introduced by micro

CT-guided stereotactic injection through the ventral proximal foramen of the amputated P3, which connects the ventrolateral CT to the BM of the digit.

We have also provided evidence that in addition to the FRCs that build the ER-TR7+ scaffold, other cells which are required by the regenerate are available as native progenitors in the BM and local, possibly lineage-restricted cells in the pre-existing soft tissue outside the BM. We hypothesize that in a regeneration incompetent environment such as an amputation midway through the second phalanx, or P2, progenitors participating in the repair response are not level-specific and become as available as in the P3 model but the local microenvironment of the P2 wound is unable to sustain regenerative capability and instead uses alternative stimulation to skew these progenitors into favoring myofibroblast differentiation thus resulting in a scarring wound healing endpoint. Using the same approach as that shown with the BM eGFP chimeras in P3, we have gathered preliminary data indicating that BMDCs and local progenitors in the CT of P2 also contribute to various cellular phenotypes which could possibly participate in a regeneration response. Nonetheless, at the end, our preliminary data also indicate persistent, increased reactivity to CD45 and SMA in P2, the former of which has been duplicated by others (Jennifer Simkin, Muneoka Lab), and thus differences in P2 compared to P3 regeneration may stem from persistence of the inflammatory CD45+ response, enhanced TGF activity by inflammatory cells, and/or repression of TGF inhibitors. And these differences can be tested by harvesting the extracellular matrix from P3 and P2 injuries and measuring the concentration of analytes enzymatically released from these areas and immobilized by protein microarray technology. We believe this to be a positive step towards realizing that many differences between regenerating P3 and scarring P2 amputation sites are not completely cell based. But in regards to different cellular contribution to P2 in contrast with P3 we would also like to elucidate the phenotype of the cells which we have shown to transiently express SMA in

the CT around the blastema stage. We discussed the possibility that these cells could be pericytes building a template and/or acting as predecessors for both differentiated vascular and bone structures. Therefore we propose to label regenerating and non-regenerating P3 and P2 amputations, respectively, around the timepoints of blastema development with establishes markers of pericytes such as NG2 and its co-expression with ER-TR7, OC, and SMA. And this will test the hypothesis that many SMA+ cells in the P3 blastema are reactive to NG2 while SMA+ cells in the P2 granulation tissue are not, and thus assume an earlier role as pro-scarring myofibroblasts during this period.

To rule if the differences between P3 and P2 injury sites are related to alternate responses depending on anatomical origin of the cells, we have gathered preliminary data on the regulation of a subset of transcripts during induction of cell lines derived from the P2 site assayed in tandem with the induced P3 cell arrays. Similar to P3 results, we identified reasonable upregulation of *NFkb1*. However, we did not measure consistent upregulation of *Col3a1*. We also measured downregulation of *Acta2* but this trend did not last towards the end of the induction period. Differences in the regulation pattern of these genes between P3 and P2 cells means that first, even though cells may be responsive to the induction regimen by triggering activation of NFκB, the downstream effect on *Col3a1* production and therefore possibly ER-TR7 is impaired in P2 cultures. Second, the resurgence of *Acta2* after an extensive period of downregulation indicates a higher propensity of the P2 population to have an alternate mechanism for SMA recovery and upkeep following transient repression through a mechanism in need of further investigation. Interestingly, other transcripts of interest that yielded consistent positive fold changes beyond steady state levels in P2 cell lines and not P3 were *Mmp3/13/19* and *Grem1*. Conversely, we measured reasonable downregulation of *Timp2/3/4*, and *Lox*. Based on the function of these genes, the results suggest that, in P2 cells,

MMP-guided extracellular material degradation is enhanced; differentiation into bone cells by paracrine production of BMPs is compromised by upregulation of one of their inhibitors; and the lysyl oxidase-based cross-linking step in collagen fibrillogenesis is potentially hindered. Overall this means that differences in critical genes driving extracellular matrix reorganization and differentiation potentially exist between induced P3 and P2 cells and these differences may negatively impact the ability of P2 cells to fully contribute to the regenerate. But since we cannot assign any significance to any of these results, it is our goal to repeat these experiments in order to decrease variability and strengthen that P3 and P2 subpopulations are segment specific and respond differently to the regeneration scaffold induction process.

Finally, it would be interesting to follow up on our preliminary observation that P3 and P2 cells undergo dramatic changes in phenotype following response to the induction treatment. Following co-immunolocalization of ER-TR7, COL1, and SMA in P3 and P2 induced cell cultures, we counted almost 25% of the cells reacting to SMA and COL1 prior to treatment in both groups. This suggests that following isolation, the cultures are composed of a heterogeneous group of fibroblastic cells. Although stellate and spindle-shaped, cells co-staining for these two markers on average appeared to have larger cytosolic and nuclear areas. Conversely once induction was underway, the cells responsive to the treatment and actively producing ER-TR7+ microfilaments were markedly smaller with a more elongated shape. This phenomenon was more evident in P3 cultures. In addition, even though they also responded to the induction with upregulation of ER-TR7, P2 cultures exhibited a more diffuse and disorganized scaffold pattern and had a higher incidence of SMA and COL positive cells than P3, which mostly correlates with our data indicating higher transcription of genes related to extracellular matrix degradation such as MMPs and late recovery of *Acta2* or SMA activation by an unknown mechanism but one possibly linked to TGF β regulation and bioavailability in each of these cultures. However,

differences in the responses from P3 and P2 cells may stem from differential expression of the receptors responsible for triggering the induction cascade and even those that are required to upkeep integrity and pattern of the scaffold after induction. The agonistic response of TNFRs is required for initiating engineering of the scaffold. However, we do not have any control over which TNF receptor our recombinant TNF α ligand would bind to: TNFRI or TNFRII. These two receptors have been shown to be independently regulated and trigger different cellular cascades and functions. For example, TNFRI has been shown to be an initiator of programmed cell death and TNFRII an inducer of proliferation (312). Differential expression of these receptors may explain the heterogeneous nature of our fibroblastic cultures particularly with regulation of *Acta2* and the responses to TNF in models of fibrosis, specifically regarding its antagonistic effect on TGF β and COL1 synthesis (61, 63, 224, 313-315). So we would like to test the hypothesis that TNFRs may be differentially regulated and thus mediate different phenotypic changes such as TGF β -mediated expression of SMA and scaffold induction responses in P3 compared to P2 cells. In addition, a lower exposure of cells to COL3 has been inversely correlated to myofibroblast differentiation and COL3-driven differential regulation of integrin receptors in fibroblasts has been determined a critical factor in promoting or discouraging a myofibroblast phenotype (29, 80, 316). In lieu of these findings then we would postulate that the reason why P3 and P2 respond somewhat differently to the induction of the ER-TR7 and COL3 positive scaffold is because of the heterogeneity in the fibroblast subpopulations with respect to being primed with differential receptor availability specifically in the integrin superfamily and this receptor distribution may be segment specific.

Taken together, we hope to improve the understanding of how the P3 blastema scaffold can be stimulated to become a regeneration competent microenvironment in otherwise pathological fibrosis and regeneration incompetent wounds. From what we have discovered so

far and what we attempt to pursue in the future, our central aim is to manipulate endogenous populations of progenitor cells derived from the local and BM niches around the wound and in circulation to build, populate, and differentiate this extracellular scaffold in a manner consistent with how the P3 microenvironment behaves and thus translate this response into traumatic limb amputations and general organ disease in humans which conventionally favor the wound healing cascade to culminate in hypertrophic scar deposition and loss of function.

REFERENCES

1. Ziegler-Graham K, MacKenzie EJ, Ephraim PL, Travison TG, Brookmeyer R. Estimating the prevalence of limb loss in the United States: 2005 to 2050. *Arch Phys Med Rehabil*. 2008;89(3):422-9.
2. Gardiner DM, Carlson MR, Roy S. Towards a functional analysis of limb regeneration. *Semin Cell Dev Biol*. 1999;10(4):385-93.
3. Brookes JP. Amphibian limb regeneration: rebuilding a complex structure. *Science*. 1997;276(5309):81-7.
4. Taylor GP, Anderson R, Reginelli AD, Muneoka K. FGF-2 induces regeneration of the chick limb bud. *Dev Biol*. 1994;163(1):282-4.
5. Muller TL, Ngo-Muller V, Reginelli A, Taylor G, Anderson R, Muneoka K. Regeneration in higher vertebrates: limb buds and digit tips. *Semin Cell Dev Biol*. 1999;10(4):405-13.
6. Bоргens RB. Mice regrow the tips of their foretoes. *Science*. 1982;217(4561):747-50.
7. Neufeld DA. Bone healing after amputation of mouse digits and newt limbs: implications for induced regeneration in mammals. *Anat Rec*. 1985;211(2):156-65.
8. Han M, Yang X, Taylor G, Burdsal CA, Anderson RA, Muneoka K. Limb regeneration in higher vertebrates: developing a roadmap. *Anat Rec B New Anat*. 2005;287(1):14-24.
9. Bryant SV, Endo T, Gardiner DM. Vertebrate limb regeneration and the origin of limb stem cells. *Int J Dev Biol*. 2002;46(7):887-96.
10. Stevenson TR. Fingertip and nailbed injuries. *Orthop Clin North Am*. 1992;23(1):149-59.
11. Allan CH, Fleckman P, Fernandes RJ, Hager B, James J, Wisecarver Z, et al. Tissue response and *Msx1* expression after human fetal digit tip amputation in vitro. *Wound Repair Regen*. 2006;14(4):398-404.
12. Han M, Yang X, Lee J, Allan CH, Muneoka K. Development and regeneration of the neonatal digit tip in mice. *Dev Biol*. 2008;315(1):125-35.

13. Casanova JC, Sanz-Ezquerro JJ. Digit morphogenesis: is the tip different? *Dev Growth Differ.* 2007;49(6):479-91.
14. Barrientos S, Stojadinovic O, Golinko MS, Brem H, Tomic-Canic M. Growth factors and cytokines in wound healing. *Wound Repair Regen.* 2008;16(5):585-601.
15. Gurtner GC, Werner S, Barrandon Y, Longaker MT. Wound repair and regeneration. *Nature.* 2008;453(7193):314-21.
16. Reibman J, Meixler S, Lee TC, Gold LI, Cronstein BN, Haines KA, et al. Transforming growth factor beta 1, a potent chemoattractant for human neutrophils, bypasses classic signal-transduction pathways. *Proceedings of the National Academy of Sciences of the United States of America.* 1991;88(15):6805-9. PMID: 52177.
17. Hubner G, Brauchle M, Smola H, Madlener M, Fassler R, Werner S. Differential regulation of pro-inflammatory cytokines during wound healing in normal and glucocorticoid-treated mice. *Cytokine.* 1996;8(7):548-56.
18. Martin P. Wound healing--aiming for perfect skin regeneration. *Science.* 1997;276(5309):75-81.
19. Moses HL, Yang EY, Pietenpol JA. TGF-beta stimulation and inhibition of cell proliferation: new mechanistic insights. *Cell.* 1990;63(2):245-7.
20. Singer AJ, Clark RA. Cutaneous wound healing. *The New England journal of medicine.* 1999;341(10):738-46.
21. Brooks PC, Clark RA, Cheres DA. Requirement of vascular integrin alpha v beta 3 for angiogenesis. *Science.* 1994;264(5158):569-71.
22. Clark RA, Lanigan JM, DellaPelle P, Manseau E, Dvorak HF, Colvin RB. Fibronectin and fibrin provide a provisional matrix for epidermal cell migration during wound reepithelialization. *J Invest Dermatol.* 1982;79(5):264-9.
23. Madri JA, Marx M. Matrix composition, organization and soluble factors: modulators of microvascular cell differentiation in vitro. *Kidney international.* 1992;41(3):560-5.
24. Merwin JR, Anderson JM, Kocher O, Van Itallie CM, Madri JA. Transforming growth factor beta 1 modulates extracellular matrix organization and cell-cell junctional complex formation during in vitro angiogenesis. *Journal of cellular physiology.* 1990;142(1):117-28.
25. Pintucci G, Bikfalvi A, Klein S, Rifkin DB. Angiogenesis and the fibrinolytic system. *Semin Thromb Hemost.* 1996;22(6):517-24.

26. Ilan N, Mahooti S, Madri JA. Distinct signal transduction pathways are utilized during the tube formation and survival phases of in vitro angiogenesis. *Journal of cell science*. 1998;111 (Pt 24):3621-31.
27. Desmouliere A, Geinoz A, Gabbiani F, Gabbiani G. Transforming growth factor-beta 1 induces alpha-smooth muscle actin expression in granulation tissue myofibroblasts and in quiescent and growing cultured fibroblasts. *The Journal of cell biology*. 1993;122(1):103-11. PMCID: 2119614.
28. Xu J, Clark RA. Extracellular matrix alters PDGF regulation of fibroblast integrins. *The Journal of cell biology*. 1996;132(1-2):239-49. PMCID: 2120701.
29. Volk SW, Wang Y, Mauldin EA, Liechty KW, Adams SL. Diminished type III collagen promotes myofibroblast differentiation and increases scar deposition in cutaneous wound healing. *Cells Tissues Organs*. 2011;194(1):25-37. PMCID: 3128157.
30. Clark RA, Nielsen LD, Welch MP, McPherson JM. Collagen matrices attenuate the collagen-synthetic response of cultured fibroblasts to TGF-beta. *Journal of cell science*. 1995;108 (Pt 3):1251-61.
31. Vaalamo M, Mattila L, Johansson N, Kariniemi AL, Karjalainen-Lindsberg ML, Kahari VM, et al. Distinct populations of stromal cells express collagenase-3 (MMP-13) and collagenase-1 (MMP-1) in chronic ulcers but not in normally healing wounds. *J Invest Dermatol*. 1997;109(1):96-101.
32. Welch MP, Odland GF, Clark RA. Temporal relationships of F-actin bundle formation, collagen and fibronectin matrix assembly, and fibronectin receptor expression to wound contraction. *The Journal of cell biology*. 1990;110(1):133-45. PMCID: 2115975.
33. Shah M, Foreman DM, Ferguson MW. Neutralisation of TGF-beta 1 and TGF-beta 2 or exogenous addition of TGF-beta 3 to cutaneous rat wounds reduces scarring. *Journal of cell science*. 1995;108 (Pt 3):985-1002.
34. Desmouliere A, Redard M, Darby I, Gabbiani G. Apoptosis mediates the decrease in cellularity during the transition between granulation tissue and scar. *The American journal of pathology*. 1995;146(1):56-66. PMCID: 1870783.
35. Petrov VV, Fagard RH, Lijnen PJ. Stimulation of collagen production by transforming growth factor-beta1 during differentiation of cardiac fibroblasts to myofibroblasts. *Hypertension*. 2002;39(2):258-63.
36. Montesano R, Orci L. Transforming growth factor beta stimulates collagen-matrix contraction by fibroblasts: implications for wound healing. *Proceedings of the National Academy of Sciences of the United States of America*. 1988;85(13):4894-7. PMCID: 280543.

37. Viljanto J. [Connective tissue regeneration and wound healing]. *Duodecim*. 1967;83(11):625-31.
38. Madlener M, Parks WC, Werner S. Matrix metalloproteinases (MMPs) and their physiological inhibitors (TIMPs) are differentially expressed during excisional skin wound repair. *Experimental cell research*. 1998;242(1):201-10.
39. Souders CA, Bowers SL, Baudino TA. Cardiac fibroblast: the renaissance cell. *Circulation research*. 2009;105(12):1164-76. PMCID: 3345531.
40. Franke WW, Schmid E, Osborn M, Weber K. Intermediate-sized filaments of human endothelial cells. *The Journal of cell biology*. 1979;81(3):570-80. PMCID: 2110384.
41. Chang HY, Chi JT, Dudoit S, Bondre C, van de Rijn M, Botstein D, et al. Diversity, topographic differentiation, and positional memory in human fibroblasts. *Proc Natl Acad Sci U S A*. 2002;99(20):12877-82.
42. Fries KM, Blieden T, Looney RJ, Sempowski GD, Silvera MR, Willis RA, et al. Evidence of fibroblast heterogeneity and the role of fibroblast subpopulations in fibrosis. *Clinical immunology and immunopathology*. 1994;72(3):283-92.
43. Jelaska A, Strehlow D, Korn JH. Fibroblast heterogeneity in physiological conditions and fibrotic disease. *Springer Semin Immunopathol*. 1999;21(4):385-95.
44. Camelliti P, Borg TK, Kohl P. Structural and functional characterisation of cardiac fibroblasts. *Cardiovascular research*. 2005;65(1):40-51.
45. Banerjee I, Fuseler JW, Price RL, Borg TK, Baudino TA. Determination of cell types and numbers during cardiac development in the neonatal and adult rat and mouse. *American journal of physiology Heart and circulatory physiology*. 2007;293(3):H1883-91.
46. Mussini E, Hutton JJ, Jr., Udenfriend S. Collagen proline hydroxylase in wound healing, granuloma formation, scurvy, and growth. *Science*. 1967;157(3791):927-9.
47. Eyden B. The myofibroblast: an assessment of controversial issues and a definition useful in diagnosis and research. *Ultrastruct Pathol*. 2001;25(1):39-50.
48. Brenner DA, Kisseleva T, Scholten D, Paik YH, Iwaisako K, Inokuchi S, et al. Origin of myofibroblasts in liver fibrosis. *Fibrogenesis Tissue Repair*. 2012;5 Suppl 1:S17. PMCID: 3368775.
49. Hinz B, Gabbiani G, Chaponnier C. The NH2-terminal peptide of alpha-smooth muscle actin inhibits force generation by the myofibroblast in vitro and in vivo. *The Journal of cell biology*. 2002;157(4):657-63. PMCID: 2173846.

50. Zhang K, Rekhter MD, Gordon D, Phan SH. Myofibroblasts and their role in lung collagen gene expression during pulmonary fibrosis. A combined immunohistochemical and in situ hybridization study. *The American journal of pathology*. 1994;145(1):114-25. PMID: 1887314.
51. Ducy P, Zhang R, Geoffroy V, Ridall AL, Karsenty G. *Osf2/Cbfa1*: a transcriptional activator of osteoblast differentiation. *Cell*. 1997;89(5):747-54.
52. Ducy P, Desbois C, Boyce B, Pinero G, Story B, Dunstan C, et al. Increased bone formation in osteocalcin-deficient mice. *Nature*. 1996;382(6590):448-52.
53. Ducy P, Geoffroy V, Karsenty G. Study of osteoblast-specific expression of one mouse osteocalcin gene: characterization of the factor binding to *OSE2*. *Connect Tissue Res*. 1996;35(1-4):7-14.
54. Komori T, Yagi H, Nomura S, Yamaguchi A, Sasaki K, Deguchi K, et al. Targeted disruption of *Cbfa1* results in a complete lack of bone formation owing to maturational arrest of osteoblasts. *Cell*. 1997;89(5):755-64.
55. Greiling D, Clark RA. Fibronectin provides a conduit for fibroblast transmigration from collagenous stroma into fibrin clot provisional matrix. *Journal of cell science*. 1997;110 (Pt 7):861-70.
56. Minor RR. Collagen metabolism: a comparison of diseases of collagen and diseases affecting collagen. *The American journal of pathology*. 1980;98(1):225-80. PMID: 1903399.
57. Byers PH, Click EM, Harper E, Bornstein P. Interchain disulfide bonds in procollagen are located in a large nontriple-helical COOH-terminal domain. *Proceedings of the National Academy of Sciences of the United States of America*. 1975;72(8):3009-13. PMID: 432908.
58. Wiestner M, Krieg T, Horlein D, Glanville RW, Fietzek P, Muller PK. Inhibiting effect of procollagen peptides on collagen biosynthesis in fibroblast cultures. *The Journal of biological chemistry*. 1979;254(15):7016-23.
59. Prockop DJ, Kivirikko KI. Collagens: molecular biology, diseases, and potentials for therapy. *Annu Rev Biochem*. 1995;64:403-34.
60. Roberts AB, Heine UI, Flanders KC, Sporn MB. Transforming growth factor-beta. Major role in regulation of extracellular matrix. *Annals of the New York Academy of Sciences*. 1990;580:225-32.
61. Greenwel P, Tanaka S, Penkov D, Zhang W, Olive M, Moll J, et al. Tumor necrosis factor alpha inhibits type I collagen synthesis through repressive CCAAT/enhancer-binding proteins. *Molecular and cellular biology*. 2000;20(3):912-8. PMID: 85208.

62. Kouba DJ, Chung KY, Nishiyama T, Vindevoghel L, Kon A, Klement JF, et al. Nuclear factor-kappa B mediates TNF-alpha inhibitory effect on alpha 2(I) collagen (COL1A2) gene transcription in human dermal fibroblasts. *Journal of immunology*. 1999;162(7):4226-34.
63. Solis-Herruzo JA, Brenner DA, Chojkier M. Tumor necrosis factor alpha inhibits collagen gene transcription and collagen synthesis in cultured human fibroblasts. *J Biol Chem*. 1988;263(12):5841-5.
64. Kahari VM, Chen YQ, Su MW, Ramirez F, Uitto J. Tumor necrosis factor-alpha and interferon-gamma suppress the activation of human type I collagen gene expression by transforming growth factor-beta 1. Evidence for two distinct mechanisms of inhibition at the transcriptional and posttranscriptional levels. *The Journal of clinical investigation*. 1990;86(5):1489-95. PMID: 296894.
65. Liu SH, Yang RS, al-Shaikh R, Lane JM. Collagen in tendon, ligament, and bone healing. A current review. *Clinical orthopaedics and related research*. 1995(318):265-78.
66. Grzesiak JJ, Davis GE, Kirchhofer D, Pierschbacher MD. Regulation of alpha 2 beta 1-mediated fibroblast migration on type I collagen by shifts in the concentrations of extracellular Mg²⁺ and Ca²⁺. *The Journal of cell biology*. 1992;117(5):1109-17. PMID: 2289472.
67. Scharffetter K, Kulozik M, Stolz W, Lankat-Buttgereit B, Hatamochi A, Sohnchen R, et al. Localization of collagen alpha 1(I) gene expression during wound healing by in situ hybridization. *J Invest Dermatol*. 1989;93(3):405-12.
68. Niyibizi C, Eyre DR. Bone type V collagen: chain composition and location of a trypsin cleavage site. *Connect Tissue Res*. 1989;20(1-4):247-50.
69. Sage H, Pritzl P, Bornstein P. Characterization of cell matrix associated collagens synthesized by aortic endothelial cells in culture. *Biochemistry*. 1981;20(2):436-42.
70. Epstein EH, Jr. (Alpha1(3))3 human skin collagen. Release by pepsin digestion and preponderance in fetal life. *The Journal of biological chemistry*. 1974;249(10):3225-31.
71. Merkel JR, DiPaolo BR, Hallock GG, Rice DC. Type I and type III collagen content of healing wounds in fetal and adult rats. *Proc Soc Exp Biol Med*. 1988;187(4):493-7.
72. Takasago T, Nakamura K, Kashiwagi S, Inoue S, Ito H, Takeo K. Analysis of collagen type III by uninterrupted sodium dodecyl sulfate-polyacrylamide gel electrophoresis and immunoblotting: changes in collagen type III polymorphism in aging rats. *Electrophoresis*. 1992;13(6):373-8.
73. Cuttle L, Nataatmadja M, Fraser JF, Kempf M, Kimble RM, Hayes MT. Collagen in the scarless fetal skin wound: detection with picrosirius-polarization. Wound repair and

regeneration : official publication of the Wound Healing Society [and] the European Tissue Repair Society. 2005;13(2):198-204.

74. Goldberg SR, Quirk GL, Sykes VW, Kordula T, Lanning DA. Altered procollagen gene expression in mid-gestational mouse excisional wounds. *The Journal of surgical research*. 2007;143(1):27-34.

75. Whitby DJ, Ferguson MW. The extracellular matrix of lip wounds in fetal, neonatal and adult mice. *Development*. 1991;112(2):651-68.

76. Lovvorn HN, 3rd, Cheung DT, Nimni ME, Perelman N, Estes JM, Adzick NS. Relative distribution and crosslinking of collagen distinguish fetal from adult sheep wound repair. *J Pediatr Surg*. 1999;34(1):218-23.

77. Tran KT, Griffith L, Wells A. Extracellular matrix signaling through growth factor receptors during wound healing. *Wound repair and regeneration : official publication of the Wound Healing Society [and] the European Tissue Repair Society*. 2004;12(3):262-8.

78. Romanic AM, Adachi E, Kadler KE, Hojima Y, Prockop DJ. Copolymerization of pNcollagen III and collagen I. pNcollagen III decreases the rate of incorporation of collagen I into fibrils, the amount of collagen I incorporated, and the diameter of the fibrils formed. *The Journal of biological chemistry*. 1991;266(19):12703-9.

79. Liu X, Wu H, Byrne M, Krane S, Jaenisch R. Type III collagen is crucial for collagen I fibrillogenesis and for normal cardiovascular development. *Proceedings of the National Academy of Sciences of the United States of America*. 1997;94(5):1852-6. PMID: 20006.

80. Zoppi N, Gardella R, De Paepe A, Barlati S, Colombi M. Human fibroblasts with mutations in COL5A1 and COL3A1 genes do not organize collagens and fibronectin in the extracellular matrix, down-regulate alpha2beta1 integrin, and recruit alphavbeta3 Instead of alpha5beta1 integrin. *The Journal of biological chemistry*. 2004;279(18):18157-68.

81. Van Vliet E, Melis M, Van Ewijk W. Monoclonal antibodies to stromal cell types of the mouse thymus. *Eur J Immunol*. 1984;14(6):524-9.

82. Kaldjian EP, Gretz JE, Anderson AO, Shi Y, Shaw S. Spatial and molecular organization of lymph node T cell cortex: a labyrinthine cavity bounded by an epithelium-like monolayer of fibroblastic reticular cells anchored to basement membrane-like extracellular matrix. *Int Immunol*. 2001;13(10):1243-53.

83. Katakai T, Hara T, Lee JH, Gonda H, Sugai M, Shimizu A. A novel reticular stromal structure in lymph node cortex: an immuno-platform for interactions among dendritic cells, T cells and B cells. *Int Immunol*. 2004;16(8):1133-42.

84. Worbs T, Forster R. T cell migration dynamics within lymph nodes during steady state: an overview of extracellular and intracellular factors influencing the basal intranodal T cell motility. *Curr Top Microbiol Immunol*. 2009;334:71-105.

85. Cahalan MD, Parker I, Wei SH, Miller MJ. Two-photon tissue imaging: seeing the immune system in a fresh light. *Nature reviews Immunology*. 2002;2(11):872-80. PMID: 2749751.

86. Miller MJ, Wei SH, Cahalan MD, Parker I. Autonomous T cell trafficking examined in vivo with intravital two-photon microscopy. *Proceedings of the National Academy of Sciences of the United States of America*. 2003;100(5):2604-9. PMID: 151387.

87. Miller MJ, Wei SH, Parker I, Cahalan MD. Two-photon imaging of lymphocyte motility and antigen response in intact lymph node. *Science*. 2002;296(5574):1869-73.

88. Katakai T, Hara T, Sugai M, Gonda H, Shimizu A. Lymph node fibroblastic reticular cells construct the stromal reticulum via contact with lymphocytes. *The Journal of experimental medicine*. 2004;200(6):783-95. PMID: 2211971.

89. Link A, Hardie DL, Favre S, Britschgi MR, Adams DH, Sixt M, et al. Association of T-zone reticular networks and conduits with ectopic lymphoid tissues in mice and humans. *The American journal of pathology*. 2011;178(4):1662-75. PMID: 3070229.

90. Zeng M, Paiardini M, Engram JC, Beilman GJ, Chipman JG, Schacker TW, et al. Critical role of CD4 T cells in maintaining lymphoid tissue structure for immune cell homeostasis and reconstitution. *Blood*. 2012;120(9):1856-67. PMID: 3433090.

91. Nolte MA, Belien JA, Schadee-Eestermans I, Jansen W, Unger WW, van Rooijen N, et al. A conduit system distributes chemokines and small blood-borne molecules through the splenic white pulp. *J Exp Med*. 2003;198(3):505-12.

92. Schacker TW, Brenchley JM, Beilman GJ, Reilly C, Pambuccian SE, Taylor J, et al. Lymphatic tissue fibrosis is associated with reduced numbers of naive CD4+ T cells in human immunodeficiency virus type 1 infection. *Clin Vaccine Immunol*. 2006;13(5):556-60. PMID: 1459657.

93. Guo G, Marrero L, Rodriguez P, Del Valle L, Ochoa A, Cui Y. Trp53 inactivation in the tumor microenvironment promotes tumor progression by expanding the immunosuppressive lymphoid-like stromal network. *Cancer research*. 2013;73(6):1668-75. PMID: 3602383.

94. Van Vliet E, Melis M, Foidart JM, Van Ewijk W. Reticular fibroblasts in peripheral lymphoid organs identified by a monoclonal antibody. *J Histochem Cytochem*. 1986;34(7):883-90.

95. Prockop DJ. Marrow stromal cells as stem cells for nonhematopoietic tissues. *Science*. 1997;276(5309):71-4.
96. Noll T, Jelinek N, Schmid S, Biselli M, Wandrey C. Cultivation of hematopoietic stem and progenitor cells: biochemical engineering aspects. *Adv Biochem Eng Biotechnol*. 2002;74:111-28.
97. Krause DS, Theise ND, Collector MI, Henegariu O, Hwang S, Gardner R, et al. Multi-organ, multi-lineage engraftment by a single bone marrow-derived stem cell. *Cell*. 2001;105(3):369-77.
98. Orlic D, Kajstura J, Chimenti S, Bodine DM, Leri A, Anversa P. Bone marrow stem cells regenerate infarcted myocardium. *Pediatr Transplant*. 2003;7 Suppl 3:86-8.
99. Muller-Sieburg CE, Cho RH, Karlsson L, Huang JF, Sieburg HB. Myeloid-biased hematopoietic stem cells have extensive self-renewal capacity but generate diminished lymphoid progeny with impaired IL-7 responsiveness. *Blood*. 2004;103(11):4111-8.
100. Dominici M, Le Blanc K, Mueller I, Slaper-Cortenbach I, Marini F, Krause D, et al. Minimal criteria for defining multipotent mesenchymal stromal cells. The International Society for Cellular Therapy position statement. *Cytotherapy*. 2006;8(4):315-7.
101. Caplan AI. Mesenchymal stem cells. *Journal of orthopaedic research : official publication of the Orthopaedic Research Society*. 1991;9(5):641-50.
102. Makino S, Fukuda K, Miyoshi S, Konishi F, Kodama H, Pan J, et al. Cardiomyocytes can be generated from marrow stromal cells in vitro. *The Journal of clinical investigation*. 1999;103(5):697-705. PMCID: 408125.
103. Ortiz LA, Gambelli F, McBride C, Gaupp D, Baddoo M, Kaminski N, et al. Mesenchymal stem cell engraftment in lung is enhanced in response to bleomycin exposure and ameliorates its fibrotic effects. *Proceedings of the National Academy of Sciences of the United States of America*. 2003;100(14):8407-11. PMCID: 166242.
104. Schwartz RE, Reyes M, Koodie L, Jiang Y, Blackstad M, Lund T, et al. Multipotent adult progenitor cells from bone marrow differentiate into functional hepatocyte-like cells. *The Journal of clinical investigation*. 2002;109(10):1291-302. PMCID: 150983.
105. Fu X, Fang L, Li X, Cheng B, Sheng Z. Enhanced wound-healing quality with bone marrow mesenchymal stem cells autografting after skin injury. *Wound repair and regeneration : official publication of the Wound Healing Society [and] the European Tissue Repair Society*. 2006;14(3):325-35.

106. Friedenstein AJ, Chailakhjan RK, Lalykina KS. The development of fibroblast colonies in monolayer cultures of guinea-pig bone marrow and spleen cells. *Cell Tissue Kinet.* 1970;3(4):393-403.
107. Campagnoli C, Roberts IA, Kumar S, Bennett PR, Bellantuono I, Fisk NM. Identification of mesenchymal stem/progenitor cells in human first-trimester fetal blood, liver, and bone marrow. *Blood.* 2001;98(8):2396-402.
108. Fan CG, Tang FW, Zhang QJ, Lu SH, Liu HY, Zhao ZM, et al. Characterization and neural differentiation of fetal lung mesenchymal stem cells. *Cell Transplant.* 2005;14(5):311-21.
109. Williams JT, Southerland SS, Souza J, Calcutt AF, Cartledge RG. Cells isolated from adult human skeletal muscle capable of differentiating into multiple mesodermal phenotypes. *Am Surg.* 1999;65(1):22-6.
110. Zuk PA, Zhu M, Mizuno H, Huang J, Futrell JW, Katz AJ, et al. Multilineage cells from human adipose tissue: implications for cell-based therapies. *Tissue Eng.* 2001;7(2):211-28.
111. Peister A, Mellad JA, Larson BL, Hall BM, Gibson LF, Prockop DJ. Adult stem cells from bone marrow (MSCs) isolated from different strains of inbred mice vary in surface epitopes, rates of proliferation, and differentiation potential. *Blood.* 2004;103(5):1662-8.
112. Loi R, Beckett T, Goncz KK, Suratt BT, Weiss DJ. Limited restoration of cystic fibrosis lung epithelium in vivo with adult bone marrow-derived cells. *Am J Respir Crit Care Med.* 2006;173(2):171-9.
113. Pittenger MF, Mackay AM, Beck SC, Jaiswal RK, Douglas R, Mosca JD, et al. Multilineage potential of adult human mesenchymal stem cells. *Science.* 1999;284(5411):143-7.
114. Rafii S, Lyden D. Therapeutic stem and progenitor cell transplantation for organ vascularization and regeneration. *Nature medicine.* 2003;9(6):702-12.
115. Kawada H, Fujita J, Kinjo K, Matsuzaki Y, Tsuma M, Miyatake H, et al. Nonhematopoietic mesenchymal stem cells can be mobilized and differentiate into cardiomyocytes after myocardial infarction. *Blood.* 2004;104(12):3581-7.
116. Tormey CA, Snyder EL, Cooper DL. Mobilization, collection, and transplantation of peripheral blood hematopoietic progenitor cells in a patient with multiple myeloma and hemoglobin SC disease. *Transfusion.* 2008;48(9):1930-3.
117. Orlic D, Kajstura J, Chimenti S, Limana F, Jakoniuk I, Quaini F, et al. Mobilized bone marrow cells repair the infarcted heart, improving function and survival. *Proceedings of the National Academy of Sciences of the United States of America.* 2001;98(18):10344-9. PMID: 56963.

118. Nygren JM, Jovinge S, Breitbach M, Sawen P, Roll W, Hescheler J, et al. Bone marrow-derived hematopoietic cells generate cardiomyocytes at a low frequency through cell fusion, but not transdifferentiation. *Nature medicine*. 2004;10(5):494-501.
119. Balsam LB, Wagers AJ, Christensen JL, Kofidis T, Weissman IL, Robbins RC. Haematopoietic stem cells adopt mature haematopoietic fates in ischaemic myocardium. *Nature*. 2004;428(6983):668-73.
120. Urbich C, Dimmeler S. Endothelial progenitor cells: characterization and role in vascular biology. *Circulation research*. 2004;95(4):343-53.
121. Fox JM, Chamberlain G, Ashton BA, Middleton J. Recent advances into the understanding of mesenchymal stem cell trafficking. *British journal of haematology*. 2007;137(6):491-502.
122. Chen J, Li Y, Wang L, Zhang Z, Lu D, Lu M, et al. Therapeutic benefit of intravenous administration of bone marrow stromal cells after cerebral ischemia in rats. *Stroke; a journal of cerebral circulation*. 2001;32(4):1005-11.
123. Gussoni E, Soneoka Y, Strickland CD, Buzney EA, Khan MK, Flint AF, et al. Dystrophin expression in the mdx mouse restored by stem cell transplantation. *Nature*. 1999;401(6751):390-4.
124. Fathke C, Wilson L, Hutter J, Kapoor V, Smith A, Hocking A, et al. Contribution of bone marrow-derived cells to skin: collagen deposition and wound repair. *Stem Cells*. 2004;22(5):812-22. PMID: 1388268.
125. Badiavas EV, Abedi M, Butmarc J, Falanga V, Quesenberry P. Participation of bone marrow derived cells in cutaneous wound healing. *Journal of cellular physiology*. 2003;196(2):245-50.
126. Wang G, Bunnell BA, Painter RG, Quiniones BC, Tom S, Lanson NA, Jr., et al. Adult stem cells from bone marrow stroma differentiate into airway epithelial cells: potential therapy for cystic fibrosis. *Proceedings of the National Academy of Sciences of the United States of America*. 2005;102(1):186-91. PMID: 544045.
127. Hayakawa J, Migita M, Ueda T, Shimada T, Fukunaga Y. Generation of a chimeric mouse reconstituted with green fluorescent protein-positive bone marrow cells: a useful model for studying the behavior of bone marrow cells in regeneration in vivo. *Int J Hematol*. 2003;77(5):456-62.
128. Ishii G, Sangai T, Sugiyama K, Ito T, Hasebe T, Endoh Y, et al. In vivo characterization of bone marrow-derived fibroblasts recruited into fibrotic lesions. *Stem Cells*. 2005;23(5):699-706.

129. Brittan M, Braun KM, Reynolds LE, Conti FJ, Reynolds AR, Poulosom R, et al. Bone marrow cells engraft within the epidermis and proliferate in vivo with no evidence of cell fusion. *The Journal of pathology*. 2005;205(1):1-13.
130. Rehman J, Li J, Orschell CM, March KL. Peripheral blood "endothelial progenitor cells" are derived from monocyte/macrophages and secrete angiogenic growth factors. *Circulation*. 2003;107(8):1164-9.
131. Kinnaird T, Stabile E, Burnett MS, Lee CW, Barr S, Fuchs S, et al. Marrow-derived stromal cells express genes encoding a broad spectrum of arteriogenic cytokines and promote in vitro and in vivo arteriogenesis through paracrine mechanisms. *Circulation research*. 2004;94(5):678-85.
132. Kinnaird T, Stabile E, Burnett MS, Epstein SE. Bone-marrow-derived cells for enhancing collateral development: mechanisms, animal data, and initial clinical experiences. *Circulation research*. 2004;95(4):354-63.
133. Aoki S, Toda S, Ando T, Sugihara H. Bone marrow stromal cells, preadipocytes, and dermal fibroblasts promote epidermal regeneration in their distinctive fashions. *Molecular biology of the cell*. 2004;15(10):4647-57. PMID: 519156.
134. Nuttall ME, Patton AJ, Olivera DL, Nadeau DP, Gowen M. Human trabecular bone cells are able to express both osteoblastic and adipocytic phenotype: implications for osteopenic disorders. *J Bone Miner Res*. 1998;13(3):371-82.
135. Shih DT, Lee DC, Chen SC, Tsai RY, Huang CT, Tsai CC, et al. Isolation and characterization of neurogenic mesenchymal stem cells in human scalp tissue. *Stem Cells*. 2005;23(7):1012-20.
136. Stocum DL. *Regenerative Biology and Medicine*. 1 ed. Burlington, MA: Academic Press; 2006.
137. Fernando WA, Leininger E, Simkin J, Li N, Malcom CA, Sathymoorthi S, et al. Wound healing and blastema formation in regenerating digit tips of adult mice. *Dev Biol*. 2011;350(2):301-10. PMID: 3031655.
138. Landis WJ, Jacquet R, Hillyer J, Zhang J, Siperko L, Chubinskaya S, et al. The potential of tissue engineering in orthopedics. *Orthop Clin North Am*. 2005;36(1):97-104.
139. Colnot C, Huang S, Helms J. Analyzing the cellular contribution of bone marrow to fracture healing using bone marrow transplantation in mice. *Biochem Biophys Res Commun*. 2006;350(3):557-61.

140. Jabbarzadeh E, Starnes T, Khan YM, Jiang T, Wirtel AJ, Deng M, et al. Induction of angiogenesis in tissue-engineered scaffolds designed for bone repair: a combined gene therapy-cell transplantation approach. *Proc Natl Acad Sci U S A*. 2008;105(32):11099-104.
141. Ott HC, Matthiesen TS, Goh SK, Black LD, Kren SM, Netoff TI, et al. Perfusion-decellularized matrix: using nature's platform to engineer a bioartificial heart. *Nat Med*. 2008;14(2):213-21.
142. Bain BJ, Clark David M, Lampert IA. Bone marrow pathology. Oxford ; Boston: Blackwell scientific pub.; 1992.
143. Hocking AM, Gibran NS. Mesenchymal stem cells: paracrine signaling and differentiation during cutaneous wound repair. *Exp Cell Res*. 2010;316(14):2213-9. PMCID: 2902653.
144. Almeida-Porada G, Zanjani ED, Porada CD. Bone marrow stem cells and liver regeneration. *Exp Hematol*. 38(7):574-80.
145. Hasegawa Y, Ogiwara T, Yamada T, Ishigaki Y, Imai J, Uno K, et al. Bone marrow (BM) transplantation promotes beta-cell regeneration after acute injury through BM cell mobilization. *Endocrinology*. 2007;148(5):2006-15.
146. Hess D, Li L, Martin M, Sakano S, Hill D, Strutt B, et al. Bone marrow-derived stem cells initiate pancreatic regeneration. *Nat Biotechnol*. 2003;21(7):763-70.
147. Hocking AM, Gibran NS. Mesenchymal stem cells: paracrine signaling and differentiation during cutaneous wound repair. *Exp Cell Res*. 316(14):2213-9.
148. Smith AN, Willis E, Chan VT, Muffley LA, Isik FF, Gibran NS, et al. Mesenchymal stem cells induce dermal fibroblast responses to injury. *Exp Cell Res*. 316(1):48-54.
149. Han M, Yang X, Farrington JE, Muneoka K. Digit regeneration is regulated by Msx1 and BMP4 in fetal mice. *Development*. 2003;130(21):5123-32.
150. Han M, Yang X, Lee J, Allan CH, Muneoka K. Development and regeneration of the neonatal digit tip in mice. *Dev Biol*. 2008;315(1):125-35. PMCID: 2329911.
151. Bajenoff M, Egen JG, Koo LY, Laugier JP, Brau F, Glaichenhaus N, et al. Stromal cell networks regulate lymphocyte entry, migration, and territoriality in lymph nodes. *Immunity*. 2006;25(6):989-1001. PMCID: 2692293.
152. Link A, Vogt TK, Favre S, Britschgi MR, Acha-Orbea H, Hinz B, et al. Fibroblastic reticular cells in lymph nodes regulate the homeostasis of naive T cells. *Nat Immunol*. 2007;8(11):1255-65.

153. Mebius RE. Organogenesis of lymphoid tissues. *Nature reviews Immunology*. 2003;3(4):292-303.
154. Drayton DL, Liao S, Mounzer RH, Ruddle NH. Lymphoid organ development: from ontogeny to neogenesis. *Nature immunology*. 2006;7(4):344-53.
155. Lokmic Z, Lammermann T, Sixt M, Cardell S, Hallmann R, Sorokin L. The extracellular matrix of the spleen as a potential organizer of immune cell compartments. *Semin Immunol*. 2008;20(1):4-13.
156. Katakai T. [Lymph node stromal cells: architecture and functions]. *Seikagaku*. 2012;84(3):183-8.
157. Puchtler H, Waldrop FW. Silver impregnation methods for reticulum fibers and reticulin: a re-investigation of their origins and specificity. *Histochemistry*. 1978;57(3):177-87.
158. Repesh LA, Fitzgerald TJ, Furcht LT. Fibronectin involvement in granulation tissue and wound healing in rabbits. *The journal of histochemistry and cytochemistry : official journal of the Histochemistry Society*. 1982;30(4):351-8.
159. Gridley MF. A modification of the silver impregnation method of staining reticular fibers. *Am J Clin Pathol*. 1951;21(9):897-9.
160. Katakai T, Hara T, Lee JH, Gonda H, Sugai M, Shimizu A. A novel reticular stromal structure in lymph node cortex: an immuno-platform for interactions among dendritic cells, T cells and B cells. *Int Immunol*. 2004;16(8):1133-42.
161. Balogh P, Fisi V, Szakal AK. Fibroblastic reticular cells of the peripheral lymphoid organs: unique features of a ubiquitous cell type. *Mol Immunol*. 2008;46(1):1-7.
162. Wu Y, Wang K, Karapetyan A, Fernando WA, Simkin J, Han M, et al. Connective tissue fibroblast properties are position-dependent during mouse digit tip regeneration. *PLoS One*. 2013;8(1):e54764. PMCID: 3548775.
163. Horton JA, Hudak KE, Chung EJ, White AO, Scroggins BT, Burkeen JF, et al. Mesenchymal stem cells inhibit cutaneous radiation-induced fibrosis by suppressing chronic inflammation. *Stem Cells*. 2013.
164. Eckes B, Colucci-Guyon E, Smola H, Nodder S, Babinet C, Krieg T, et al. Impaired wound healing in embryonic and adult mice lacking vimentin. *Journal of cell science*. 2000;113 (Pt 13):2455-62.

165. Eriksson JE, Dechat T, Grin B, Helfand B, Mendez M, Pallari HM, et al. Introducing intermediate filaments: from discovery to disease. *The Journal of clinical investigation*. 2009;119(7):1763-71. PMCID: 2701876.
166. Strutz F, Okada H, Lo CW, Danoff T, Carone RL, Tomaszewski JE, et al. Identification and characterization of a fibroblast marker: FSP1. *The Journal of cell biology*. 1995;130(2):393-405. PMCID: 2199940.
167. Helfman DM, Kim EJ, Lukanidin E, Grigorian M. The metastasis associated protein S100A4: role in tumour progression and metastasis. *British journal of cancer*. 2005;92(11):1955-8. PMCID: 2361793.
168. Boye K, Maelandsmo GM. S100A4 and metastasis: a small actor playing many roles. *The American journal of pathology*. 2010;176(2):528-35. PMCID: 2808059.
169. Ambartsumian N, Klingelhofer J, Grigorian M, Christensen C, Kriaievska M, Tulchinsky E, et al. The metastasis-associated Mts1(S100A4) protein could act as an angiogenic factor. *Oncogene*. 2001;20(34):4685-95.
170. Pedersen KB, Andersen K, Fodstad O, Maelandsmo GM. Sensitization of interferon-gamma induced apoptosis in human osteosarcoma cells by extracellular S100A4. *BMC Cancer*. 2004;4:52. PMCID: 515304.
171. Takenaga K, Nakamura Y, Sakiyama S. Cellular localization of pEL98 protein, an S100-related calcium binding protein, in fibroblasts and its tissue distribution analyzed by monoclonal antibodies. *Cell Struct Funct*. 1994;19(3):133-41.
172. Cabezon T, Celis JE, Skibshoj I, Klingelhofer J, Grigorian M, Gromov P, et al. Expression of S100A4 by a variety of cell types present in the tumor microenvironment of human breast cancer. *International journal of cancer Journal international du cancer*. 2007;121(7):1433-44.
173. Semov A, Moreno MJ, Onichtchenko A, Abulrob A, Ball M, Ekiel I, et al. Metastasis-associated protein S100A4 induces angiogenesis through interaction with Annexin II and accelerated plasmin formation. *The Journal of biological chemistry*. 2005;280(21):20833-41.
174. Rudland PS, Platt-Higgins A, Renshaw C, West CR, Winstanley JH, Robertson L, et al. Prognostic significance of the metastasis-inducing protein S100A4 (p9Ka) in human breast cancer. *Cancer research*. 2000;60(6):1595-603.
175. Nose K, Saito H, Kuroki T. Isolation of a gene sequence induced later by tumor-promoting 12-O-tetradecanoylphorbol-13-acetate in mouse osteoblastic cells (MC3T3-E1) and expressed constitutively in ras-transformed cells. *Cell Growth Differ*. 1990;1(11):511-8.

176. Boucherot A, Schreiber R, Pavenstadt H, Kunzelmann K. Cloning and expression of the mouse glomerular podoplanin homologue gp38P. *Nephrology, dialysis, transplantation : official publication of the European Dialysis and Transplant Association - European Renal Association*. 2002;17(6):978-84.
177. Rishi AK, Joyce-Brady M, Fisher J, Dobbs LG, Floros J, VanderSpek J, et al. Cloning, characterization, and development expression of a rat lung alveolar type I cell gene in embryonic endodermal and neural derivatives. *Dev Biol*. 1995;167(1):294-306.
178. Farr A, Nelson A, Hosier S. Characterization of an antigenic determinant preferentially expressed by type I epithelial cells in the murine thymus. *The journal of histochemistry and cytochemistry : official journal of the Histochemistry Society*. 1992;40(5):651-64.
179. Zimmer G, Oeffner F, Von Messling V, Tschernig T, Groness HJ, Klenk HD, et al. Cloning and characterization of gp36, a human mucin-type glycoprotein preferentially expressed in vascular endothelium. *The Biochemical journal*. 1999;341 (Pt 2):277-84. PMCID: 1220357.
180. Schacht V, Ramirez MI, Hong YK, Hirakawa S, Feng D, Harvey N, et al. T1alpha/podoplanin deficiency disrupts normal lymphatic vasculature formation and causes lymphedema. *The EMBO journal*. 2003;22(14):3546-56. PMCID: 165612.
181. Zhang K, Barragan-Adjemian C, Ye L, Kotha S, Dallas M, Lu Y, et al. E11/gp38 selective expression in osteocytes: regulation by mechanical strain and role in dendrite elongation. *Molecular and cellular biology*. 2006;26(12):4539-52. PMCID: 1489126.
182. Farr AG, Berry ML, Kim A, Nelson AJ, Welch MP, Aruffo A. Characterization and cloning of a novel glycoprotein expressed by stromal cells in T-dependent areas of peripheral lymphoid tissues. *J Exp Med*. 1992;176(5):1477-82. PMCID: 2119410.
183. Balogh P, Horvath G, Szakal AK. Immunoarchitecture of distinct reticular fibroblastic domains in the white pulp of mouse spleen. *The journal of histochemistry and cytochemistry : official journal of the Histochemistry Society*. 2004;52(10):1287-98.
184. Pankov R, Yamada KM. Fibronectin at a glance. *Journal of cell science*. 2002;115(Pt 20):3861-3.
185. Mao Y, Schwarzbauer JE. Fibronectin fibrillogenesis, a cell-mediated matrix assembly process. *Matrix biology : journal of the International Society for Matrix Biology*. 2005;24(6):389-99.
186. Manabe R, Ohe N, Maeda T, Fukuda T, Sekiguchi K. Modulation of cell-adhesive activity of fibronectin by the alternatively spliced EDA segment. *The Journal of cell biology*. 1997;139(1):295-307. PMCID: 2139828.

187. Sechler JL, Schwarzbauer JE. Control of cell cycle progression by fibronectin matrix architecture. *The Journal of biological chemistry*. 1998;273(40):25533-6.
188. Rozario T, Dzamba B, Weber GF, Davidson LA, DeSimone DW. The physical state of fibronectin matrix differentially regulates morphogenetic movements in vivo. *Dev Biol*. 2009;327(2):386-98. PMCID: 2829434.
189. Tafolla E, Wang S, Wong B, Leong J, Kapila YL. JNK1 and JNK2 oppositely regulate p53 in signaling linked to apoptosis triggered by an altered fibronectin matrix: JNK links FAK and p53. *The Journal of biological chemistry*. 2005;280(20):19992-9.
190. Sottile J, Hocking DC. Fibronectin polymerization regulates the composition and stability of extracellular matrix fibrils and cell-matrix adhesions. *Molecular biology of the cell*. 2002;13(10):3546-59. PMCID: 129965.
191. McDonald JA, Kelley DG, Broekelmann TJ. Role of fibronectin in collagen deposition: Fab' to the gelatin-binding domain of fibronectin inhibits both fibronectin and collagen organization in fibroblast extracellular matrix. *The Journal of cell biology*. 1982;92(2):485-92. PMCID: 2112086.
192. Sottile J, Shi F, Rublyevska I, Chiang HY, Lust J, Chandler J. Fibronectin-dependent collagen I deposition modulates the cell response to fibronectin. *Am J Physiol Cell Physiol*. 2007;293(6):C1934-46.
193. Velling T, Risteli J, Wennerberg K, Mosher DF, Johansson S. Polymerization of type I and III collagens is dependent on fibronectin and enhanced by integrins alpha 11beta 1 and alpha 2beta 1. *The Journal of biological chemistry*. 2002;277(40):37377-81.
194. Stenman S, Vaheri A. Distribution of a major connective tissue protein, fibronectin, in normal human tissues. *The Journal of experimental medicine*. 1978;147(4):1054-64. PMCID: 2184253.
195. Fyrand O. Studies on fibronectin in the skin. I. Indirect immunofluorescence studies in normal human skin. *The British journal of dermatology*. 1979;101(3):263-70.
196. Eckes B, Zigrino P, Kessler D, Holtkotter O, Shephard P, Mauch C, et al. Fibroblast-matrix interactions in wound healing and fibrosis. *Matrix Biol*. 2000;19(4):325-32.
197. Grinnell F, Billingham RE, Burgess L. Distribution of fibronectin during wound healing in vivo. *J Invest Dermatol*. 1981;76(3):181-9.
198. Viljanto J, Penttinen R, Raekallio J. Fibronectin in early phases of wound healing in children. *Acta Chir Scand*. 1981;147(1):7-13.

199. Doillon CJ, Dunn MG, Bender E, Silver FH. Collagen fiber formation in repair tissue: development of strength and toughness. *Coll Relat Res*. 1985;5(6):481-92.
200. Parry DA, Barnes GR, Craig AS. A comparison of the size distribution of collagen fibrils in connective tissues as a function of age and a possible relation between fibril size distribution and mechanical properties. *Proc R Soc Lond B Biol Sci*. 1978;203(1152):305-21.
201. Fleischmajer R, Olsen BR, Timpl R, Perlish JS, Lovelace O. Collagen fibril formation during embryogenesis. *Proceedings of the National Academy of Sciences of the United States of America*. 1983;80(11):3354-8. PMID: 394041.
202. Gay S, Vijanto J, Raekallio J, Penttinen R. Collagen types in early phases of wound healing in children. *Acta Chir Scand*. 1978;144(4):205-11.
203. Muneoka K, Allan CH, Yang X, Lee J, Han M. Mammalian regeneration and regenerative medicine. *Birth defects research Part C, Embryo today : reviews*. 2008;84(4):265-80.
204. Reginelli AD, Wang YQ, Sassoon D, Muneoka K. Digit tip regeneration correlates with regions of *Msx1* (*Hox 7*) expression in fetal and newborn mice. *Development*. 1995;121(4):1065-76.
205. Lee J, Marrero L, Yu L, Dawson LA, Muneoka K, Han M. SDF-1 α /CXCR4 signaling mediates digit tip regeneration promoted by BMP-2. *Dev Biol*. 2013.
206. Neufeld DA, Zhao W. Bone regrowth after digit tip amputation in mice is equivalent in adults and neonates. *Wound repair and regeneration : official publication of the Wound Healing Society [and] the European Tissue Repair Society*. 1995;3(4):461-6.
207. Gretz JE, Kaldjian EP, Anderson AO, Shaw S. Sophisticated strategies for information encounter in the lymph node: the reticular network as a conduit of soluble information and a highway for cell traffic. *Journal of immunology*. 1996;157(2):495-9.
208. Sixt M, Kanazawa N, Selg M, Samson T, Roos G, Reinhardt DP, et al. The conduit system transports soluble antigens from the afferent lymph to resident dendritic cells in the T cell area of the lymph node. *Immunity*. 2005;22(1):19-29.
209. Clark RAF, Henson PM, SpringerLink (Online service). *The Molecular and Cellular Biology of Wound Repair*. Boston, MA: Springer US; 1995. Available from: <http://dx.doi.org/10.1007/978-1-4615-1795-5>.
210. Opalenik SR, Davidson JM. Fibroblast differentiation of bone marrow-derived cells during wound repair. *FASEB journal : official publication of the Federation of American Societies for Experimental Biology*. 2005;19(11):1561-3.

211. Gabelloni ML, Trevani AS, Sabatte J, Geffner J. Mechanisms regulating neutrophil survival and cell death. *Semin Immunopathol.* 2013;35(4):423-37.
212. Gilbert SF. *Developmental biology.* 9th ed. Sunderland, Mass.: Sinauer Associates; 2010.
213. Hehlhans T, Pfeffer K. The intriguing biology of the tumour necrosis factor/tumour necrosis factor receptor superfamily: players, rules and the games. *Immunology.* 2005;115(1):1-20. PMID: 1782125.
214. Hehlhans T, Muller P, Stopfer P, Mannel DN. Activation of the lymphotoxin-beta receptor induces NFkappaB-dependent interleukin-6 and MIP-2 secretion in mouse fibrosarcoma cells. *Eur Cytokine Netw.* 2003;14(2):103-7.
215. Daller B, Musch W, Rohrl J, Tumanov AV, Nedospasov SA, Mannel DN, et al. Lymphotoxin-beta receptor activation by lymphotoxin-alpha(1)beta(2) and LIGHT promotes tumor growth in an NFkappaB-dependent manner. *International journal of cancer Journal international du cancer.* 2011;128(6):1363-70.
216. Hehlhans T, Stoelcker B, Stopfer P, Muller P, Cernaianu G, Guba M, et al. Lymphotoxin-beta receptor immune interaction promotes tumor growth by inducing angiogenesis. *Cancer research.* 2002;62(14):4034-40.
217. Kahaleh MB, Smith EA, Soma Y, LeRoy EC. Effect of lymphotoxin and tumor necrosis factor on endothelial and connective tissue cell growth and function. *Clin Immunol Immunopathol.* 1988;49(2):261-72.
218. White A, Carragher D, Parnell S, Msaki A, Perkins N, Lane P, et al. Lymphotoxin a-dependent and -independent signals regulate stromal organizer cell homeostasis during lymph node organogenesis. *Blood.* 2007;110(6):1950-9.
219. Castro-Malaspina H, Gay RE, Resnick G, Kapoor N, Meyers P, Chiarieri D, et al. Characterization of human bone marrow fibroblast colony-forming cells (CFU-F) and their progeny. *Blood.* 1980;56(2):289-301.
220. Owen M. Marrow stromal stem cells. *J Cell Sci Suppl.* 1988;10:63-76.
221. Ghosh S, Hayden MS. New regulators of NF-kappaB in inflammation. *Nature reviews Immunology.* 2008;8(11):837-48.
222. Gerondakis S, Grumont R, Gugasyan R, Wong L, Isomura I, Ho W, et al. Unravelling the complexities of the NF-kappaB signalling pathway using mouse knockout and transgenic models. *Oncogene.* 2006;25(51):6781-99.

223. Al-Lamki RS, Brookes AP, Wang J, Reid MJ, Parameshwar J, Goddard MJ, et al. TNF receptors differentially signal and are differentially expressed and regulated in the human heart. *Am J Transplant*. 2009;9(12):2679-96. PMCID: 3517885.
224. Distler JH, Schett G, Gay S, Distler O. The controversial role of tumor necrosis factor alpha in fibrotic diseases. *Arthritis and rheumatism*. 2008;58(8):2228-35.
225. MacEwan DJ. TNF receptor subtype signalling: differences and cellular consequences. *Cellular signalling*. 2002;14(6):477-92.
226. Bertok S, Wilson MR, Dorr AD, Dokpesi JO, O'Dea KP, Marczin N, et al. Characterization of TNF receptor subtype expression and signaling on pulmonary endothelial cells in mice. *American journal of physiology Lung cellular and molecular physiology*. 2011;300(5):L781-9. PMCID: 3094030.
227. Thannickal VJ, Lee DY, White ES, Cui Z, Larios JM, Chacon R, et al. Myofibroblast differentiation by transforming growth factor-beta1 is dependent on cell adhesion and integrin signaling via focal adhesion kinase. *The Journal of biological chemistry*. 2003;278(14):12384-9.
228. Honda E, Yoshida K, Munakata H. Transforming growth factor-beta upregulates the expression of integrin and related proteins in MRC-5 human myofibroblasts. *The Tohoku journal of experimental medicine*. 2010;220(4):319-27.
229. Chaponnier C, Desmoulière A, Gabbiani G. Tissue repair, contraction, and the myofibroblast. Georgetown, Tex
New York: Landes Bioscience/Eurekah.com ;
Springer Science+Business Media; 2006.
230. Yannas IV, Butler CE. Regenerative medicine. Berlin ; New York: Springer; 2005.
231. Stadelmann WK, Digenis AG, Tobin GR. Physiology and healing dynamics of chronic cutaneous wounds. *Am J Surg*. 1998;176(2A Suppl):26S-38S.
232. Song G, Nguyen DT, Pietramaggiore G, Scherer S, Chen B, Zhan Q, et al. Use of the parabiotic model in studies of cutaneous wound healing to define the participation of circulating cells. *Wound Repair Regen*. 2010;18(4):426-32. PMCID: 2935287.
233. Meirelles Lda S, Nardi NB. Murine marrow-derived mesenchymal stem cell: isolation, in vitro expansion, and characterization. *British journal of haematology*. 2003;123(4):702-11.
234. Weissman IL. Translating stem and progenitor cell biology to the clinic: barriers and opportunities. *Science*. 2000;287(5457):1442-6.

235. da Silva Meirelles L, Chagastelles PC, Nardi NB. Mesenchymal stem cells reside in virtually all post-natal organs and tissues. *Journal of cell science*. 2006;119(Pt 11):2204-13.
236. Singer AJ, Clark RA. Cutaneous wound healing. *N Engl J Med*. 1999;341(10):738-46.
237. Weissman IL, Anderson DJ, Gage F. Stem and progenitor cells: origins, phenotypes, lineage commitments, and transdifferentiations. *Annu Rev Cell Dev Biol*. 2001;17:387-403.
238. Zhang J, Niu C, Ye L, Huang H, He X, Tong WG, et al. Identification of the haematopoietic stem cell niche and control of the niche size. *Nature*. 2003;425(6960):836-41.
239. Graf T. Differentiation plasticity of hematopoietic cells. *Blood*. 2002;99(9):3089-101.
240. Sata M, Saiura A, Kunisato A, Tojo A, Okada S, Tokuhiya T, et al. Hematopoietic stem cells differentiate into vascular cells that participate in the pathogenesis of atherosclerosis. *Nat Med*. 2002;8(4):403-9.
241. Bucala R, Spiegel LA, Chesney J, Hogan M, Cerami A. Circulating fibrocytes define a new leukocyte subpopulation that mediates tissue repair. *Mol Med*. 1994;1(1):71-81. PMID: 2229929.
242. Asahara T, Masuda H, Takahashi T, Kalka C, Pastore C, Silver M, et al. Bone marrow origin of endothelial progenitor cells responsible for postnatal vasculogenesis in physiological and pathological neovascularization. *Circ Res*. 1999;85(3):221-8.
243. Abe R, Donnelly SC, Peng T, Bucala R, Metz CN. Peripheral blood fibrocytes: differentiation pathway and migration to wound sites. *Journal of immunology*. 2001;166(12):7556-62.
244. Jiang Y, Jahagirdar BN, Reinhardt RL, Schwartz RE, Keene CD, Ortiz-Gonzalez XR, et al. Pluripotency of mesenchymal stem cells derived from adult marrow. *Nature*. 2002;418(6893):41-9.
245. Reyes M, Lund T, Lenvik T, Aguiar D, Koodie L, Verfaillie CM. Purification and ex vivo expansion of postnatal human marrow mesodermal progenitor cells. *Blood*. 2001;98(9):2615-25.
246. Prockop DJ. Repair of tissues by adult stem/progenitor cells (MSCs): controversies, myths, and changing paradigms. *Mol Ther*. 2009;17(6):939-46.
247. Awad HA, Butler DL, Boivin GP, Smith FN, Malaviya P, Huibregtse B, et al. Autologous mesenchymal stem cell-mediated repair of tendon. *Tissue Eng*. 1999;5(3):267-77.

248. Pereira RF, Halford KW, O'Hara MD, Leeper DB, Sokolov BP, Pollard MD, et al. Cultured adherent cells from marrow can serve as long-lasting precursor cells for bone, cartilage, and lung in irradiated mice. *Proceedings of the National Academy of Sciences of the United States of America*. 1995;92(11):4857-61. PMID: 41806.
249. Zou JP, Huang S, Peng Y, Liu HW, Cheng B, Fu XB, et al. Mesenchymal stem cells/multipotent mesenchymal stromal cells (MSCs): potential role in healing cutaneous chronic wounds. *Int J Low Extrem Wounds*. 2012;11(4):244-53.
250. Wong J, Bennett W, Ferguson MW, McGrouther DA. Microscopic and histological examination of the mouse hindpaw digit and flexor tendon arrangement with 3D reconstruction. *Journal of anatomy*. 2006;209(4):533-45. PMID: 2100351.
251. Takahashi N, Yamana H, Yoshiki S, Roodman GD, Mundy GR, Jones SJ, et al. Osteoclast-like cell formation and its regulation by osteotropic hormones in mouse bone marrow cultures. *Endocrinology*. 1988;122(4):1373-82.
252. Hermiston ML, Tan AL, Gupta VA, Majeti R, Weiss A. The juxtamembrane wedge negatively regulates CD45 function in B cells. *Immunity*. 2005;23(6):635-47.
253. Athanasou NA, Quinn J. Immunophenotypic differences between osteoclasts and macrophage polykaryons: immunohistological distinction and implications for osteoclast ontogeny and function. *J Clin Pathol*. 1990;43(12):997-1003. PMID: 502972.
254. Gerdes J, Schwab U, Lemke H, Stein H. Production of a mouse monoclonal antibody reactive with a human nuclear antigen associated with cell proliferation. *International journal of cancer Journal international du cancer*. 1983;31(1):13-20.
255. Walters J, Pop C, Scott FL, Drag M, Swartz P, Mattos C, et al. A constitutively active and uninhibitable caspase-3 zymogen efficiently induces apoptosis. *The Biochemical journal*. 2009;424(3):335-45. PMID: 2805924.
256. Dickhut A, Schwerdtfeger R, Kuklick L, Ritter M, Thiede C, Neubauer A, et al. Mesenchymal stem cells obtained after bone marrow transplantation or peripheral blood stem cell transplantation originate from host tissue. *Ann Hematol*. 2005;84(11):722-7.
257. Rieger K, Marinets O, Fietz T, Korper S, Sommer D, Mucke C, et al. Mesenchymal stem cells remain of host origin even a long time after allogeneic peripheral blood stem cell or bone marrow transplantation. *Experimental hematology*. 2005;33(5):605-11.
258. Jenkins SJ, Ruckerl D, Cook PC, Jones LH, Finkelman FD, van Rooijen N, et al. Local macrophage proliferation, rather than recruitment from the blood, is a signature of TH2 inflammation. *Science*. 2011;332(6035):1284-8. PMID: 3128495.

259. Xiao M, Inal CE, Parekh VI, Li XH, Whitnall MH. Role of NF-kappaB in hematopoietic niche function of osteoblasts after radiation injury. *Experimental hematology*. 2009;37(1):52-64.
260. Wang L, Liu Y, Kalajic Z, Jiang X, Rowe DW. Heterogeneity of engrafted bone-lining cells after systemic and local transplantation. *Blood*. 2005;106(10):3650-7. PMID: 1895047.
261. Lehoczy JA, Robert B, Tabin CJ. Mouse digit tip regeneration is mediated by fate-restricted progenitor cells. *Proceedings of the National Academy of Sciences of the United States of America*. 2011;108(51):20609-14. PMID: 3251149.
262. Rinkevich Y, Lindau P, Ueno H, Longaker MT, Weissman IL. Germ-layer and lineage-restricted stem/progenitors regenerate the mouse digit tip. *Nature*. 2011;476(7361):409-13.
263. Franz-Odenaal TA, Hall BK, Witten PE. Buried alive: how osteoblasts become osteocytes. *Dev Dyn*. 2006;235(1):176-90.
264. Montgomery RR, Gill JC. Interactions between von Willebrand factor and Factor VIII: where did they first meet. *Journal of pediatric hematology/oncology*. 2000;22(3):269-75.
265. Jaffe EA, Hoyer LW, Nachman RL. Synthesis of antihemophilic factor antigen by cultured human endothelial cells. *The Journal of clinical investigation*. 1973;52(11):2757-64. PMID: 302543.
266. Sadler JE. Biochemistry and genetics of von Willebrand factor. *Annu Rev Biochem*. 1998;67:395-424.
267. Skalli O, Ropraz P, Trzeciak A, Benzonana G, Gillesen D, Gabbiani G. A monoclonal antibody against alpha-smooth muscle actin: a new probe for smooth muscle differentiation. *The Journal of cell biology*. 1986;103(6 Pt 2):2787-96. PMID: 2114627.
268. Bergers G, Song S. The role of pericytes in blood-vessel formation and maintenance. *Neuro Oncol*. 2005;7(4):452-64. PMID: 1871727.
269. Ronnov-Jessen L, Petersen OW. A function for filamentous alpha-smooth muscle actin: retardation of motility in fibroblasts. *The Journal of cell biology*. 1996;134(1):67-80. PMID: 2120928.
270. Coen M, Gabbiani G, Bochaton-Piallat ML. Myofibroblast-mediated adventitial remodeling: an underestimated player in arterial pathology. *Arteriosclerosis, thrombosis, and vascular biology*. 2011;31(11):2391-6.
271. Martin P, D'Souza D, Martin J, Grose R, Cooper L, Maki R, et al. Wound healing in the PU.1 null mouse--tissue repair is not dependent on inflammatory cells. *Curr Biol*. 2003;13(13):1122-8.

272. Kaplan RN, Psaila B, Lyden D. Niche-to-niche migration of bone-marrow-derived cells. *Trends Mol Med*. 2007;13(2):72-81.
273. Kuter DJ, Bain B, Mufti G, Bagg A, Hasserjian RP. Bone marrow fibrosis: pathophysiology and clinical significance of increased bone marrow stromal fibres. *British journal of haematology*. 2007;139(3):351-62.
274. Mori L, Bellini A, Stacey MA, Schmidt M, Mattoli S. Fibrocytes contribute to the myofibroblast population in wounded skin and originate from the bone marrow. *Experimental cell research*. 2005;304(1):81-90.
275. Hou Z, Nguyen Q, Frenkel B, Nilsson SK, Milne M, van Wijnen AJ, et al. Osteoblast-specific gene expression after transplantation of marrow cells: implications for skeletal gene therapy. *Proc Natl Acad Sci U S A*. 1999;96(13):7294-9.
276. Choi YH, Burdick MD, Strieter RM. Human circulating fibrocytes have the capacity to differentiate osteoblasts and chondrocytes. *The international journal of biochemistry & cell biology*. 2010;42(5):662-71. PMCID: 2835809.
277. Pereira RF, O'Hara MD, Laptev AV, Halford KW, Pollard MD, Class R, et al. Marrow stromal cells as a source of progenitor cells for nonhematopoietic tissues in transgenic mice with a phenotype of osteogenesis imperfecta. *Proceedings of the National Academy of Sciences of the United States of America*. 1998;95(3):1142-7. PMCID: 18700.
278. Han X, Bolcato AL, Amar S. Identification of genes differentially expressed in cultured human osteoblasts versus human fibroblasts by DNA microarray analysis. *Connect Tissue Res*. 2002;43(1):63-75.
279. Knothe Tate ML, Adamson JR, Tami AE, Bauer TW. The osteocyte. *The international journal of biochemistry & cell biology*. 2004;36(1):1-8.
280. Gao D, Nolan DJ, Mellick AS, Bambino K, McDonnell K, Mittal V. Endothelial progenitor cells control the angiogenic switch in mouse lung metastasis. *Science*. 2008;319(5860):195-8.
281. Kerbel RS, Benezra R, Lyden DC, Hattori K, Heissig B, Nolan DJ, et al. Endothelial progenitor cells are cellular hubs essential for neoangiogenesis of certain aggressive adenocarcinomas and metastatic transition but not adenomas. *Proceedings of the National Academy of Sciences of the United States of America*. 2008;105(34):E54; author reply E5. PMCID: 2527966.
282. Purhonen S, Palm J, Rossi D, Kaskenpaa N, Rajantie I, Yla-Herttuala S, et al. Bone marrow-derived circulating endothelial precursors do not contribute to vascular endothelium and are not needed for tumor growth. *Proceedings of the National Academy of Sciences of the United States of America*. 2008;105(18):6620-5. PMCID: 2365563.

283. Hagensen MK, Raarup MK, Mortensen MB, Thim T, Nyengaard JR, Falk E, et al. Circulating endothelial progenitor cells do not contribute to regeneration of endothelium after murine arterial injury. *Cardiovascular research*. 2012;93(2):223-31.
284. Okuno Y, Nakamura-Ishizu A, Kishi K, Suda T, Kubota Y. Bone marrow-derived cells serve as proangiogenic macrophages but not endothelial cells in wound healing. *Blood*. 2011;117(19):5264-72. PMID: 3357943.
285. Carmeliet P, Jain RK. Molecular mechanisms and clinical applications of angiogenesis. *Nature*. 2011;473(7347):298-307.
286. Barcelos LS, Duplaa C, Krankel N, Graiani G, Invernici G, Katare R, et al. Human CD133+ progenitor cells promote the healing of diabetic ischemic ulcers by paracrine stimulation of angiogenesis and activation of Wnt signaling. *Circulation research*. 2009;104(9):1095-102. PMID: 2821014.
287. Hirschi KK, D'Amore PA. Pericytes in the microvasculature. *Cardiovascular research*. 1996;32(4):687-98.
288. Diaz-Flores L, Gutierrez R, Madrid JF, Varela H, Valladares F, Acosta E, et al. Pericytes. Morphofunction, interactions and pathology in a quiescent and activated mesenchymal cell niche. *Histology and histopathology*. 2009;24(7):909-69.
289. Hungerford JE, Little CD. Developmental biology of the vascular smooth muscle cell: building a multilayered vessel wall. *J Vasc Res*. 1999;36(1):2-27.
290. Majesky MW, Dong XR, Regan JN, Hoglund VJ. Vascular smooth muscle progenitor cells: building and repairing blood vessels. *Circulation research*. 2011;108(3):365-77. PMID: 3382110.
291. Kelley C, D'Amore P, Hechtman HB, Shepro D. Microvascular pericyte contractility in vitro: comparison with other cells of the vascular wall. *The Journal of cell biology*. 1987;104(3):483-90. PMID: 2114529.
292. Jain RK. Molecular regulation of vessel maturation. *Nature medicine*. 2003;9(6):685-93.
293. von Tell D, Armulik A, Betsholtz C. Pericytes and vascular stability. *Experimental cell research*. 2006;312(5):623-9.
294. Carmeliet P. Mechanisms of angiogenesis and arteriogenesis. *Nature medicine*. 2000;6(4):389-95.
295. Hellstrom M, Kalen M, Lindahl P, Abramsson A, Betsholtz C. Role of PDGF-B and PDGFR-beta in recruitment of vascular smooth muscle cells and pericytes during embryonic blood vessel formation in the mouse. *Development*. 1999;126(14):3047-55.

296. Sousa AM, Liu T, Guevara O, Stevens J, Fanburg BL, Gaestel M, et al. Smooth muscle alpha-actin expression and myofibroblast differentiation by TGFbeta are dependent upon MK2. *Journal of cellular biochemistry*. 2007;100(6):1581-92. PMID: 2586991.
297. Darby IA, Hewitson TD. Fibroblast differentiation in wound healing and fibrosis. *Int Rev Cytol*. 2007;257:143-79.
298. Bellini A, Mattoli S. The role of the fibrocyte, a bone marrow-derived mesenchymal progenitor, in reactive and reparative fibroses. *Laboratory investigation; a journal of technical methods and pathology*. 2007;87(9):858-70.
299. Uccelli A, Moretta L, Pistoia V. Mesenchymal stem cells in health and disease. *Nature reviews Immunology*. 2008;8(9):726-36.
300. Nataraj D, Ernst A, Kalluri R. Idiopathic pulmonary fibrosis is associated with endothelial to mesenchymal transition. *American journal of respiratory cell and molecular biology*. 2010;43(2):129-30.
301. Fiocchi C, Ina K, Danese S, Leite AZ, Vogel JD. Alterations of mesenchymal and endothelial cells in inflammatory bowel diseases. *Advances in experimental medicine and biology*. 2006;579:168-76.
302. Evans RA, Tian YC, Steadman R, Phillips AO. TGF-beta1-mediated fibroblast-myofibroblast terminal differentiation-the role of Smad proteins. *Experimental cell research*. 2003;282(2):90-100.
303. Goldberg MT, Han YP, Yan C, Shaw MC, Garner WL. TNF-alpha suppresses alpha-smooth muscle actin expression in human dermal fibroblasts: an implication for abnormal wound healing. *J Invest Dermatol*. 2007;127(11):2645-55. PMID: 2366884.
304. Ishiguro S, Akasaka Y, Kiguchi H, Suzuki T, Imaizumi R, Ishikawa Y, et al. Basic fibroblast growth factor induces down-regulation of alpha-smooth muscle actin and reduction of myofibroblast areas in open skin wounds. *Wound repair and regeneration : official publication of the Wound Healing Society [and] the European Tissue Repair Society*. 2009;17(4):617-25.
305. Collett G, Wood A, Alexander MY, Varnum BC, Boot-Handford RP, Ohanian V, et al. Receptor tyrosine kinase Axl modulates the osteogenic differentiation of pericytes. *Circulation research*. 2003;92(10):1123-9.
306. Doherty MJ, Ashton BA, Walsh S, Beresford JN, Grant ME, Canfield AE. Vascular pericytes express osteogenic potential in vitro and in vivo. *J Bone Miner Res*. 1998;13(5):828-38.

307. Farrington-Rock C, Crofts NJ, Doherty MJ, Ashton BA, Griffin-Jones C, Canfield AE. Chondrogenic and adipogenic potential of microvascular pericytes. *Circulation*. 2004;110(15):2226-32.
308. Papetti M, Shujath J, Riley KN, Herman IM. FGF-2 antagonizes the TGF-beta1-mediated induction of pericyte alpha-smooth muscle actin expression: a role for myf-5 and Smad-mediated signaling pathways. *Invest Ophthalmol Vis Sci*. 2003;44(11):4994-5005.
309. Lindahl P, Johansson BR, Leveen P, Betsholtz C. Pericyte loss and microaneurysm formation in PDGF-B-deficient mice. *Science*. 1997;277(5323):242-5.
310. Huang FJ, You WK, Bonaldo P, Seyfried TN, Pasquale EB, Stallcup WB. Pericyte deficiencies lead to aberrant tumor vascularization in the brain of the NG2 null mouse. *Dev Biol*. 2010;344(2):1035-46. PMID: 3197744.
311. Nehls V, Denzer K, Drenckhahn D. Pericyte involvement in capillary sprouting during angiogenesis in situ. *Cell and tissue research*. 1992;270(3):469-74.
312. Tartaglia LA, Weber RF, Figari IS, Reynolds C, Palladino MA, Jr., Goeddel DV. The two different receptors for tumor necrosis factor mediate distinct cellular responses. *Proceedings of the National Academy of Sciences of the United States of America*. 1991;88(20):9292-6. PMID: 52700.
313. Fujita M, Shannon JM, Morikawa O, Gauldie J, Hara N, Mason RJ. Overexpression of tumor necrosis factor-alpha diminishes pulmonary fibrosis induced by bleomycin or transforming growth factor-beta. *American journal of respiratory cell and molecular biology*. 2003;29(6):669-76.
314. Verrecchia F, Mauviel A. TGF-beta and TNF-alpha: antagonistic cytokines controlling type I collagen gene expression. *Cell Signal*. 2004;16(8):873-80.
315. Yamane K, Ihn H, Asano Y, Jinnin M, Tamaki K. Antagonistic effects of TNF-alpha on TGF-beta signaling through down-regulation of TGF-beta receptor type II in human dermal fibroblasts. *J Immunol*. 2003;171(7):3855-62.
316. Lygoe KA, Wall I, Stephens P, Lewis MP. Role of vitronectin and fibronectin receptors in oral mucosal and dermal myofibroblast differentiation. *Biol Cell*. 2007;99(11):601-14.

BIOGRAPHY

The author began his academic career as an undergraduate in the Division of Arts & Sciences at Tulane University in the summer of 1989 with focus on Cell and Molecular Biology and Psychology. Prior to resuming his education in the Tulane School of Science and Engineering Graduate Program, he became a board certified Histologist by the American Society of Clinical Pathologists and acquired expertise in immunohistopathology procedures, interpretation of clinical samples, and cancer prognosis at various local hospitals while serving as manager of the Laboratory Division of Anatomic Pathology. In 2001, he was appointed Director of the Morphology and Imaging Core in the Gene Therapy Program of the Department of Medicine at LSU Health Sciences Center. During his time as Core Director, he has lectured in histopathology and biomolecular imaging practice and theory; secured funding for systems involving deconvolution, confocal, multiphoton, timelapse, and *in vivo* imaging; and developed expertise in advanced analyses such as FRET, FRAP, co-localization, and second harmonic generation capture. Aside from conducting research in mammalian regeneration under the mentorship of Dr. Ken Muneoka and participating as a principal investigator in a multi-institutional project headed by Dr. Muneoka and funded by the Defense Advanced Research Projects Agency, he has led the MIC in two NIH-funded Program Projects involving vaccine development; three Louisiana Board of Regents grants based on gene therapy of neurological diseases, pathogenesis of lung infections, and *in vivo* imaging of small mammals. In addition, he has provided support for numerous private, DoD, NSF, and NIH-funded projects and is an author in dozens of manuscripts ranging from development of articular joints to oncology.